ZANCO Journal of Pure and Applied Sciences
The official scientific journal of Salahaddin University-Erbil
https://zancojournals.su.edu.krd/index.php/JPAS

ISSN (print): 2218-0230**, ISSN (online):** 2412-3986**, DOI: http://dx.doi.org/10.21271/zjpas**

RESEARCH PAPER

Theoretical Study of The Reaction of Ketene with Methanimine Using DFT Method

Haydar A. Mohammad-Salim

Department of Chemistry, Faculty of Science, University of Zakho, Duhok 42001, Kurdistan Region, Iraq

A B S T R A C T:

The Density Functional Theory (DFT) method was used to investigate the stepwise mechanism of the [2+2] cycloaddition (22CA) reaction of ketene with methanimine at the B3LYP/6-311++G(d,p) level of theory. Two modes of attack between reactants were investigated, yielding Azetidin-2-one from *path1* and Azetidin-2-one from *path2* as two possible products passing through two different transition states. The geometry of transition states and products was analysed. The study of stationary points and energetic parameters shows that the reaction mechanism is stepwise and that Azetidin-2-one **P1** is thermodynamically and kinetically more favoured than Azetidin-3-one **P2**. The analysis of the frontier molecular HOMO and LUMO orbitals shows that the Azetidin-2-one **P1** is more stable due to its higher energy gab. The global electronic flux from the strong nucleophilic ketene **R1** to the methanimine **R2** is predicted using conceptual density functional theory (CDFT) indices. Reactant's electrophilic and nucleophilic Fukui functions were also investigated.

KEY WORDS: *Stepwise mechanism; [2+2] cycloaddition; DFT; CDFT; Fukui Functions.*
DOI: http://dx.doi.org/10.21271/ZJPAS.33.4.1
ZJPAS (2021), 33(4); 1-10 .

1.INTRODUCTION :

The chemistry of heterocycles has advanced dramatically in recent years,, and This family of molecules is the basis for the majority of compounds produced in the fields of industrial pharmaceutical chemistry (King et al., 2019; H. A. Mohammad-Salim & Abdallah, 2019b; Sowmya, Lakshmi Teja, Padmaja, Kamala Prasad, & Padmavathi, 2018). It's worth noting that heterocycles make up two-thirds of all compounds mentioned in the literature (Barber et al., 2018; Glasnov, 2018; Pawlowski, Stanek, & Stodulski, 2019). Therefore, it's understandable that heterocyclic compounds have become the focus of interest of a wide group of experimental and theoretical chemists.

One of the most effective synthetic strategies that requires the formation of different membered rings is cycloddition reactions. These reactions occur when two unsaturated reactants interact. Among cycloaddition reactions, the 22CA reaction is one of the reactions used to build the four-membered ring and it is a structural unit in pharmaceutical compounds and natural occurring products (H. A. Mohammad-Salim & Abdallah, 2019a; H. A. Mohammad-Salim, Abdallah, Maiyelvaganan, Prakash, & Hochlaf, 2020; H. A. M. Salim, H. H. Abdallah, & P. Ramasami, 2018). The hetero-22CA reactions have been given attention by researchers due to their wide applications in the synthesis organic chemistry (Flores & Schmidt, 2019; Pang et al., 2018; H. M. Salim, H. H. Abdallah, & P. Ramasami, 2018). The four-membered heterocycles are the heterocyclic analogues of cyclobutane and are considered to be derived from cyclobutane by replacing a methylene group (-CH_2) with a heteroatom, usually, oxygen, sulfur or nitrogen.

* **Corresponding Author:**
Haydar Mohammad-Salim
E-mail: hayder.salim@uoz.edu.krd
Article History:
Received: 20/03/2021
Accepted: 22/04/2021
Published: 18/08 /2021

The saturated heterocycles of four-membered containing oxygen, sulfur and nitrogen are called oxetane, thietane and azetidine, respectively. The small heterocycles with two heteroatoms, e.g. oxaphosphetanes and thioanalogues prepared from Witting reaction intermediate, also attract researchers due to their reactivity (Espinosa Ferao & Streubel, 2020; A. Kyri et al., 2018; A. W. Kyri et al., 2019).

In the previous two decades, computational chemistry has been an effective method for analyzing experimentally observed selectivity and reactivity results by creating a formal description of chemical reaction mechanisms (Krylov et al., 2018). Despite the a number of modern uses of computational science in chemistry, the underlying theories of organic chemistry, since last 40 years. had not experienced major breakthrough, Domingo suggested the molecular electron density theory in 2016 to acknowledge the crucial role of electron density variations in molecular reactivity (Domingo, 2016; Ríos-Gutiérrez & Domingo, 2019). This theory has been successfully analyzing the experimental results of many cycloaddition reactions for the past four years (Domingo, Ríos-Gutiérrez, & Pérez, 2018; H. Mohammad-Salim, Hassan, Abdallah, & Oftadeh, 2020; H. A. Mohammad-Salim; H. A. Mohammad-Salim, Acharjee, & Abdallah, 2021; H. A. Mohammad-Salim, Basheer, Abdallah, Zeroual, & Jamil, 2021; Ríos-Gutiérrez & Domingo, 2019). Recently, this theory has been applied to analyse the experimental outcome of strain promoted and catalysed cycloaddition reactions and the observed chemo-, stereo- and regioselectivite synthesis of heterocyclic compounds (Abbiche et al., 2020; Acharjee, Mohammad-Salim, Chakraborty, Rao, & Ganesh; Domingo, Acharjee, & Mohammad-Salim, 2020; H. A. Mohammad-Salim, Acharjee, Domingo, & Abdallah, 2020).

Since four-membered heterocycles have industrial uses such as potential drugs, catalysts and dye-sensitized solar cells (Fuentes de Arriba, Lenci, Sonawane, Formery, & Dixon, 2017; Mathew et al., 2014; Xu, Zhang, & Luo, 2014), the analysis of these compounds is of considerable interest. Preparation of nitrogen containing heterocyclic compounds have become a major point of interest among researchers due to its biological activities and success in the involvement of cancer treatment (Tokunova et al., 2001; Willenbring & Tantillo, 2008). Therefore, the primary goal of this investigation was to study the stepwise mechanism path of 22CA of ketene **R1** with methanimine **R2** (see Scheme 1) using theoretical methods in more details.

Scheme 1. Mechanism of the 22CA reaction between ketene (**R1**) and methanimine (**R2**).

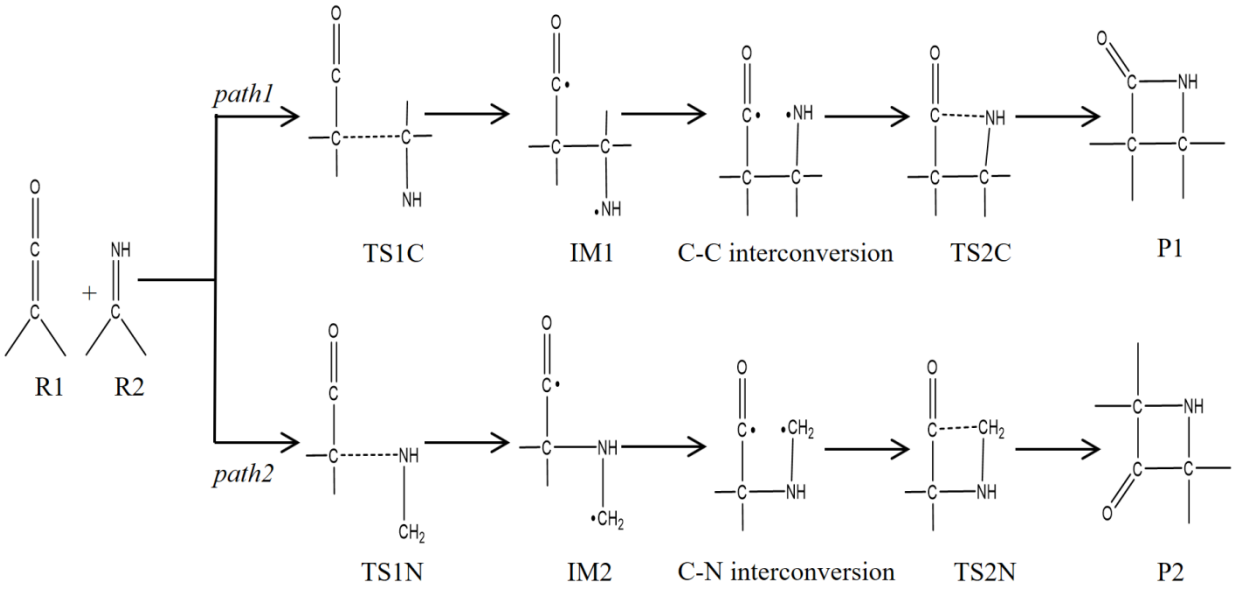

2.COMPUTATIONAL METHODS

The Gaussian 16 package was used to do all calculations under the Linux operating system (Frisch et al., 2009). The B3LYP functional in DFT method has been shown to be a suitable method for studying 22CA reactions and is used in this study (R.G. Parr & Weitao, 1989; Saha et al., 2019; Svatunek, Pemberton, Mackey, Liu, & Houk, 2020). Throughout, B3LYP functional is used in conjunction with the 6-311++G(d,p) basis set (Ditchfield, Hehre, & Pople, 1971; Lee, Yang, & Parr, 1988). Geometry optimization on geometry convergence, electron density (SCF) convergence and integration grid were carried out in default sittings.

The existence of one imaginary frequency was confirmed by frequency measurements at the optimized TSs, while in the case of the local minimum, the absence of imaginary frequency was confirmed. Intrinsic Reaction coordinate (IRC) calculations were performed using the Gonzales–Schlegal integration approach to validate the minimum energy reaction pathway linking the reactants and products through the defined TSs (Fukui, 1970; Gonzalez & Schlegel, 1991). The CDFT indices are computed using the equation discussed by Parr and co-workers (Robert G. Parr & Pearson, 1983; R.G. Parr & Weitao, 1994).

The electrophilic f_k^+ and nucleophilic f_k^- Fukui functions (Domingo, Pérez, & Sáez, 2013), which allow for the description of the nucleophilic and electrophilic centers of a reactants, were calculated via the examination of the Mulliken atomic spin density of the radical anion and the radical cation of ketene **R1** and methanimine **R2**, from the optimized neutral geometries, using single-point energy calculations.

3.RESULTS AND DISCUSSION

Two regioisomeric paths, namely the *path1* and *path2* (see Scheme 1), for these 22CA reactions are feasible, due to non-symmetry of the reactants. The *path1* reaction path is related with the formation of Azetidin-2-one (P1), while the *path2* channel with the formation of Azetidin-3-one (**P2**), passing through different transition states.

The electronic energy profile for the 22CA reaction of **R1** with **R2** is shown in Figure 1. This figure shows the all possible transition states and intermediates associate with the reaction of ketene **R1** with methanimine **R2**. The electronic energies (in kcal/mol) are relative to the energy of the two non-interacting reactants. Similarly, the relative energy for **P2** is about 22 kcal/mol above the energy of **P1**. It's worth to realize that the product **P1** is a kinetic as well as thermodynamic product. It can be noted that there are two pathways of this reaction. One of them is to obtain **IM1** intermediate passing through **TS1C** and the other is to form **IM2** intermediate passing through **TS1N**. The results of electronic energy prefer the first pathway over the other. The electronic energy of **IM2** intermediate is slightly above the most stable **IM1** intermediate.

The **IM1** and **IM2** diradical intermediates are formed via **TS1C** and **TS1N** transition states, respectively. The activation energy is higher for the **TS1N** transition structure than the transition structure **TS1C**. Therefore, the *path1* for obtaining **P1** is expected to be the rate determining step. The next step of this reaction path corresponds to a rotation of the C-C and C-N bonds through the transition states **TS2C** and **TS2N** to form the product **P1** and **P2**, respectively. The activation energy of this step is around 21 kcal/mol for **TS2C** and 30 kcal/mol for **TS2N**, respectively, such activation energies are obviously typical for the internal rotation of C-C and C-N single bond.

Table 1 lists the thermodynamic parameters for the 22CA reactions of **R1** with **R2** obtained in the gas phase with B3LYP/6-311++G(d,p) method. The first activation enthalpy for **TS1C** is 59.98 kcal/mol and for **TS1N** is 62.95 kcal/mol, while the second activation enthalpy for **TS2C** 61.89 kcal/mol while for **TS2N** is 67.85 kcal/mol. The values of Gibbs free energy for **P1** is -14.60 kcal/mol, which refers to the spontaneous reaction. However, the Gibbs free energy for **P2** is 7.61 kcal/mol that refers to the non-spontaneous reaction. The enthalpy of azetidin-2-one **P1** azetidin-3-one **P2** is negative, indicating the stability of both products. The observed data of thermodynamic parameters can be used to reach the conclusion that the product **P1** is formed faster and has negative Gibbs free energy, thus **P1** is preferred kinetically as well as thermodynamically.

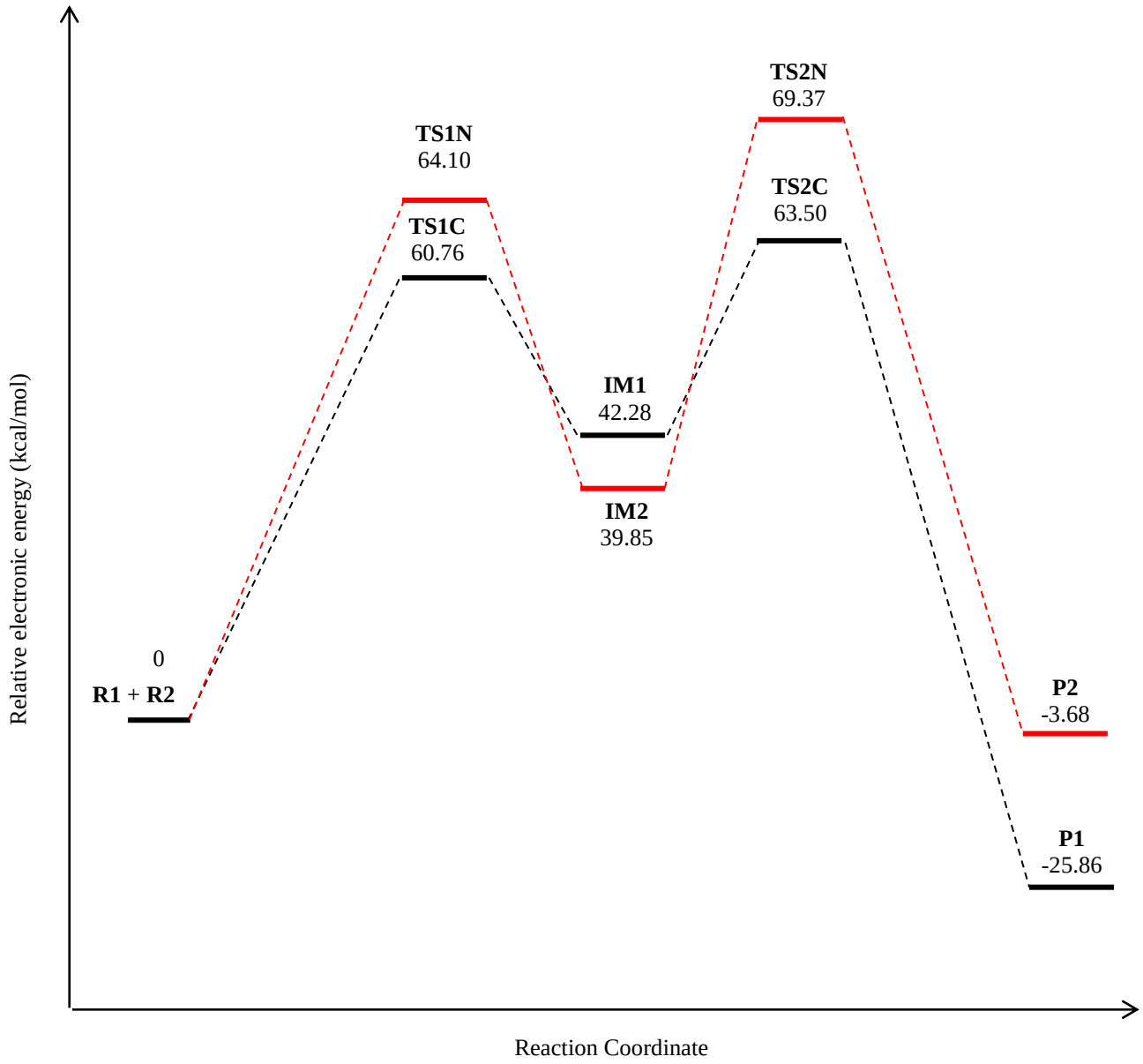

Figure 1. Relative electronic energies (ΔG) in kcal/mol of stationary points associated with the 22CA reaction of ketene with methanimine.

Table 1. Thermodynamic parameters for transition states, intermediates and products at B3LYP/6-311++G(d,p) level of theory in (kcal/mole) for ΔH and ΔG and in (cal/mol.K) for ΔS.

Species	ΔH	ΔG
TS1C	59.98	69.91
IM1	41.55	51.56

TS2C	61.89	73.94
P1	-27.53	-14.60
TS1N	62.95	74.67
IM2	39.45	48.41
TS2N	67.85	79.64
P2	-5.39	7.61

Table 2 lists the HOMO and LUMO energies in eV computed at the B3LYP level of theory for reactants and products. As shown form the results in the table, the energy gap for **R1** is lower than the energy gap for **R2**. It is worth to realize that the product **P1** has a wider energy gap than the product **P2**, indicating the stability of this product.

Table 2. HOMO energies, LUMO energies and energy gap (in eV unit) for reactants and products at B3LYP/6-311++G(d,p) level of theory.

eV	HOMO	LUMO	Enrgy Gap
R1	-7.20	-0.82	5.61
R2	-6.86	-1.75	6.69
P1	-6.70	-1.54	6.84
P2	-6.83	-1.75	5.73

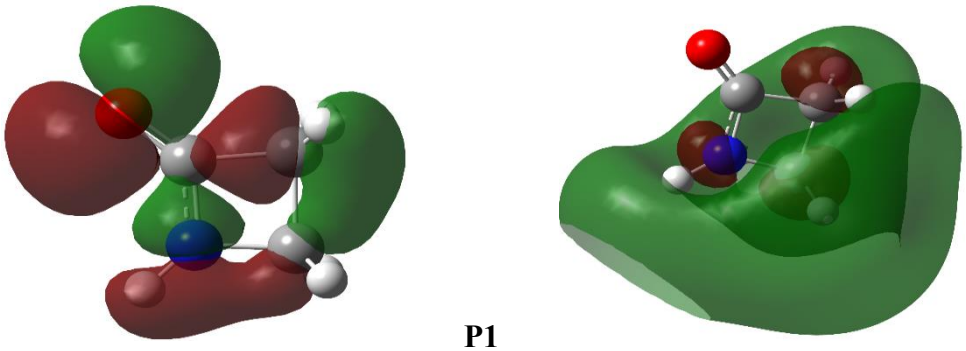

P1

HOMO **LUMO**

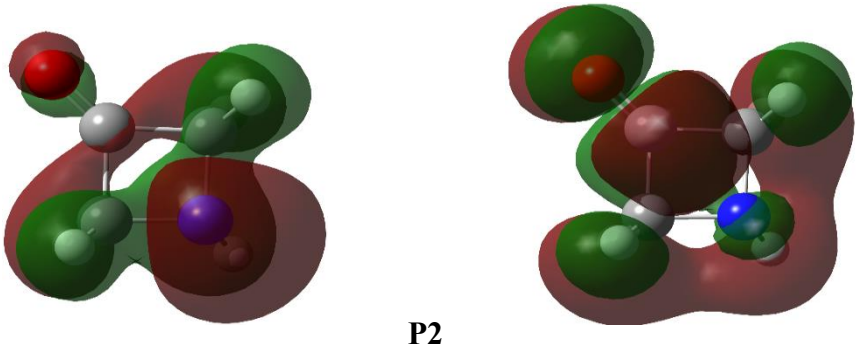

P2

HOMO **LUMO**

Figure 2. The HOMO and LUMO of the **P1** and **P2** cycloadducts at B3LYP/6-311++G(d) level of theory.

Their energies are given in Table 2.

The optimized geometries of all transition states at B3LYP/6-311++G(d,p) method are shown in Figure 3. The distances between C1 and C3, and C1 and N4 interacting centers at the transition states are: 2.15 Å at **TS1C** and 1.76 Å at **TS1N**. However, for the second part of the reaction, the distance between C1 and N4 is 1.68 Å at **TS2C**, while between C1 and C3 is 1.71 Å at **TS2N**. The C1-C3 and C1-N4 single bond distance was found to be 1.54 and 1.44 Å at the intermediates **IM1** and **IM2**, respectively. Given that the formation of C-C and C-N single bonds starts at distances of 1.50-1.60 and 1.40-1.60 Å, respectively, these geometrical parameters mean that the formation of C-C and C-N single bonds has not yet started at either of the TSs.

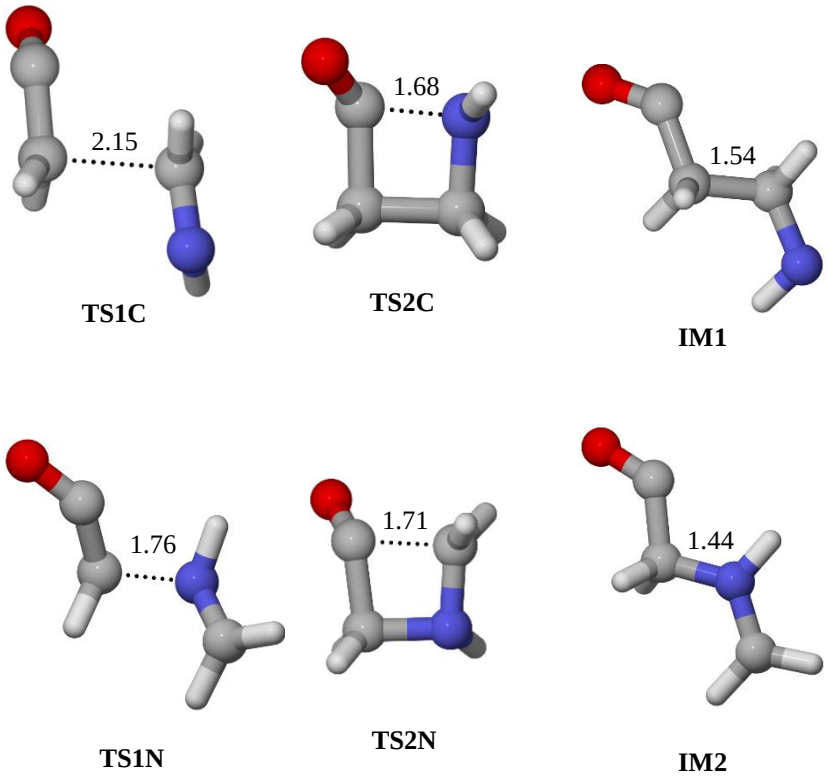

Figure 3. B3LYP/6-311++G(d,p) optimised geometries of TSs and intermediates involved in the 22CA reactions of ketene **R1** with methanimine **R2**. Bond lengths are given in Angstroms.

The reactivity in polar cycloaddition reactions can be examined using the global reactivity indices described within the conceptual DFT. The static global properties, namely, global nucleophilicity (N), chemical hardness (η), electronic chemical potential (μ) and global electrophilicity (ω) for the all reactants are listed in Table 3.

The electronic chemical potential (μ) of ketene **R1** is -4.15 eV, which is higher than the **R2** and this indicating that the global electronic flux will be from the **R1** towards the electron-deficient **R2**. The power of electrophilicity for **R1** and **R2** is 1.54 eV and 1.37, which are moderate electrophiles, while R1 has a nucleophilicity power of 2.53 eV, which places it in the high nucleophilicity range with in the nucleophilicity and electrophilicity scale (Domingo, Aurell, Pérez, & Contreras, 2002). However, the power of nucleophilicity for **R2** is 1.87 eV and it falls in the range of moderate nucleophile with in the nucleophilicity and electrophilicity scale (Domingo et al., 2002).

Table 3. The chemical hardness (η), electronic chemical potential (μ), global electrophilicity (ω) and global nucleophilicity (N) for all reactants in eV.

Reactant	η	μ	ω	N
R1	5.61	-4.15	1.54	2.53
R2	6.68	-4.27	1.37	1.87

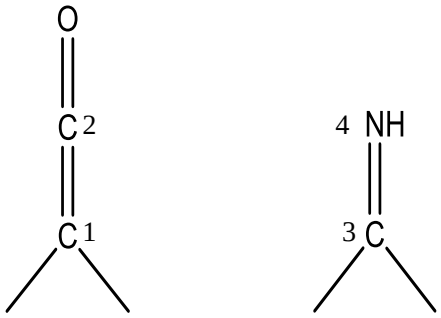

Figure 4. Schematic structures and atom numbering of reactants involved in [2+2] cycloaddition reaction.

A good explanation for the study of the regioselectivity in 22CA reactions can be computed by observing at those processes with a pronounced polar character, where the transition structure associated with the rate-determining step mostly involves the formation of one single bond between the most electrophilic and other nucleophilic sites in the 22CA pair of reactants. Table 4 lists the global and local properties of the reactants used in the 22CA reaction of **R1** with **R2**. In reactant **R1**, the nucleophilic site is the C1 carbon (see Figure 4 for atom numbering), which has the highest Fukui function value for an electrophilic attack f_k^-. Consequently, the most favourable interaction will take place between the C1 center of reactant **R1** and the C3 center of **R2**.

Table 4. Static Global and Local properties of reactants involved in [2+2] cycloaddition reactions of **R1** and **R2**.

Reactants	**site (*k*)**	f_k^-	f_k^+
R1	C1	0.54	0.33
	C2	0.06	0.16
R2	C3	0.07	0.91
	N4	0.11	0.18

To represent the charge transfer in a comparable manner, the molecular electrostatic potential (MESP) map of the transition states was obtained. Figure 5 shows the MESP maps for **TS2C** and **TS2N** transition states of two pathways *path1* and *path2*, respectively. The red and blue colors, in the MESP map, indicate the region with higher and lower electron density, respectively. Thus, due to the electrostatic attractive forces between two interacting fragments, the formation of **TS2C** is more preferable to that of **TS2N**.

Figure 5. The molecular electrostatic potential (MEP) maps of the transition states **TS2C** and **TS2N**.

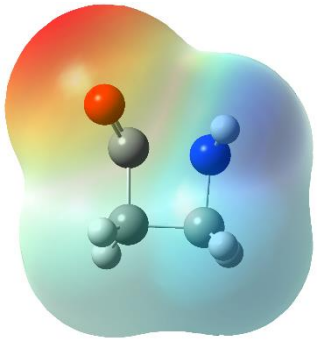

TS2C

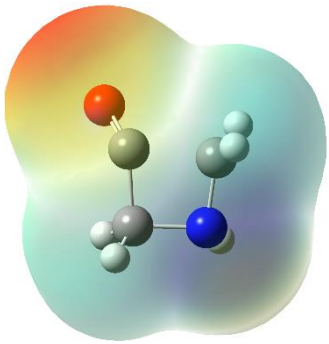

TS2N

4.CONSLUSIONS

The B3LYP/6-311++G(d) method was used to study the [2+2] cycloaddition reaction of ketene with methanimine. Two modes of attack between reactants were studied, yielding Azetidin-2-one and Azetidin-3-one as two possible products passing through two different transition states. This reaction are taking place via a stepwise mechanism. It has been noted that, on comparing the energetic results and thermodynamics parameters, the reaction path leading to the formation of Azetidin-2-one are kinetically and thermodynamically more favorable than Azetidin-3-one. The analysis of the frontier molecular HOMO and LUMO orbitals indicates that the Azetidin-2-one (**P1**) are more stable due to its wider energy gab. The global electronic flux from the ketene **R1** to the methanimine **R2** is predicted, because of the high electronic chemical potential and strong nucleophilicity of the ketene **R1** relative to the methanimine **R2**. The analysis of MESP maps for transition states indicates that the formation of **TS2C** is more preferable to that of **TS2N**. The regioselectivity of this cycloaddition is also proposed by electrophilic and nucleophilic Fukui functions.

REFERENCES

Abbiche, K., Mohammad-Salim, H., Salah, M., Mazoir, N., Zeroual, A., El Alaoui El Abdallaoui, H., . . . Hochlaf, M. 2020. Insights into the mechanism and regiochemistry of the 1,3-dipolar cycloaddition reaction between benzaldehyde and diazomethane. *Theoretical Chemistry Accounts*, *139*(9), 148. doi: https://doi.org/10.1007/s00214-020-02662-4

Acharjee, N., Mohammad-Salim, H. A., Chakraborty, M., Rao, M. P., & Ganesh, M. 2021. Unveiling the high regioselectivity and stereoselectivity within the synthesis of spirooxindolenitropyrrolidine: A molecular electron density theory perspective. *Journal of Physical Organic Chemistry*, *n/a*(n/a), e4189. doi:https://doi.org/10.1002/poc.4189

Barber, J. S., Yamano, M. M., Ramirez, M., Darzi, E. R., Knapp, R. R., Liu, F., . . . Garg, N. K. 2018. Diels–

Alder cycloadditions of strained azacyclic allenes. *Nature chemistry*, *10*(9), 953.

Ditchfield, R., Hehre, W. J., & Pople, J. A. (1971). Self-Consistent Molecular-Orbital Methods. IX. An Extended Gaussian-Type Basis for Molecular-Orbital Studies of Organic Molecules. *54*(2), 724-728. doi:10.1063/1.1674902

Domingo, L. R. 2016. Molecular electron density theory: a modern view of reactivity in organic chemistry. *Molecules*, *21*(10), 1319.

Domingo, L. R., Acharjee, N., & Mohammad-Salim, H. A. 2020. Understanding the Reactivity of Trimethylsilyldiazoalkanes Participating in [3+2] Cycloaddition Reactions towards Diethylfumarate with a Molecular Electron Density Theory Perspective. *Organics*, *1*(1), 3-18.

Domingo, L. R., Aurell, M. J., Pérez, P., & Contreras, R. 2002. Quantitative characterization of the global electrophilicity power of common diene/dienophile pairs in Diels–Alder reactions. *Tetrahedron*, *58*(22), 4417-4423. doi:https://doi.org/10.1016/S0040-4020(02)00410-6

Domingo, L. R., Pérez, P., & Sáez, J. A. 2013. Understanding the local reactivity in polar organic reactions through electrophilic and nucleophilic Parr functions. *RSC Advances*, *3*(5), 1486-1494. doi:10.1039/C2RA22886F

Domingo, L. R., Ríos-Gutiérrez, M., & Pérez, P. 2018. A Molecular Electron Density Theory Study of the Reactivity and Selectivities in [3 + 2] Cycloaddition Reactions of C,N-Dialkyl Nitrones with Ethylene Derivatives. *The Journal of Organic Chemistry*, *83*(4), 2182-2197. doi:10.1021/acs.joc.7b03093

Espinosa Ferao, A., & Streubel, R. 2020. 1, 2-Thiaphosphetanes: The Quest for Wittig-Type Ring Cleavage, Rearrangement, and Sulfur Atom Transfer. *Inorganic Chemistry*, *59*(5), 3110-3117.

Flores, D. M., & Schmidt, V. A. 2019. Intermolecular 2 + 2 Carbonyl–Olefin Photocycloadditions Enabled by Cu(I)–Norbornene MLCT. *Journal of the American Chemical Society*, *141*(22), 8741-8745. doi:10.1021/jacs.9b03775

Frisch, M. J., Trucks, G. W., Schlegel, H. B., Scuseria, G. E., Robb, M. A., Cheeseman, J. R., . . . Fox, D. J. 2009. Gaussian 09 B.01. Wallingford, CT.

Fuentes de Arriba, Á. L., Lenci, E., Sonawane, M., Formery, O., & Dixon, D. J. 2017. Iridium-Catalyzed Reductive Strecker Reaction for Late-Stage Amide and Lactam Cyanation. *Angewandte Chemie International Edition*, *56*(13), 3655-3659. doi:10.1002/anie.201612367

Fukui, K. 1970. Formulation of the reaction coordinate. *The Journal of Physical Chemistry*, *74*(23), 4161-4163. doi:10.1021/j100717a029

Glasnov, T. 2018. Photochemical Synthesis of Heterocycles: Merging Flow Processing and Metal-Catalyzed Visible Light Photoredox Transformations. In *Flow Chemistry for the Synthesis of Heterocycles* (pp. 103-132): Springer.

Gonzalez, C., & Schlegel, H. B. 1991. Improved algorithms for reaction path following: higher-order implicit algorithms. *The Journal of chemical physics*, *95*(8), 5853-5860.

King, T. A., Stewart, H. L., Mortensen, K. T., North, A. J. P., Sore, H. F., & Spring, D. R. 2019. Cycloaddition Strategies for the Synthesis of Diverse Heterocyclic Spirocycles for Fragment-Based Drug Discovery. *European Journal of Organic Chemistry*, *2019*(31-32), 5219-5229. doi:10.1002/ejoc.201900847

Krylov, A., Windus, T. L., Barnes, T., Marin-Rimoldi, E., Nash, J. A., Pritchard, B., . . . Head-Gordon, T. 2018. Perspective: Computational chemistry software and its advancement as illustrated through three grand challenge cases for molecular science. *The Journal of Chemical Physics*, *149*(18), 180901. doi:10.1063/1.5052551

Kyri, A., Gleim, F., Alcaraz, A. G., Schnakenburg, G., Ferao, A. E., & Streubel, R. 2018. "Low-coordinate" 1, 2-oxaphosphetanes–a new opportunity in coordination and main group chemistry. *Chemical Communications*, *54*(52), 7123-7126.

Kyri, A. W., Gleim, F., Becker, D., Schnakenburg, G., Ferao, A. E., & Streubel, R. 2019. Synthesis of free and ligated 1, 2-thiaphosphetanes–expanding the pool of strained P-ligands. *Chemical Communications*, *55*(11), 1615-1618.

Lee, C., Yang, W., & Parr, R. G. 1988. Development of the Colle-Salvetti correlation-energy formula into a functional of the electron density. *Physical Review B*, *37*(2), 785-789. doi:10.1103/PhysRevB.37.785

Mathew, S., Yella, A., Gao, P., Humphry-Baker, R., Curchod, B. F., Ashari-Astani, N., . . . Grätzel, M. 2014. Dye-sensitized solar cells with 13% efficiency achieved through the molecular engineering of porphyrin sensitizers. *Nature chemistry*, *6*(3), 242.

Mohammad-Salim, H., Hassan, R., Abdallah, H. H., & Oftadeh, M. 2020. The Theoretical Study on the Mechanism of [3+ 2] Cycloaddition Reactions between α, β-unsaturated Selenoaldehyde with Nitrone and with Nitrile Oxide. *Journal of the Mexican Chemical Society*, *64*(2).

Mohammad-Salim, H. A. 2021. Understanding the Reactivity of C-Cyclopropyl-N-Methylnitrone Participating in [3+ 2] Cycloaddition Reactions Towards Styrene with a Molecular Electron Density Theory Perspective. *Journal of the Mexican Chemical Society*, *65*(1).

Mohammad-Salim, H. A., & Abdallah, H. H. 2019a. Theoretical Study for the [2+ 2] Cycloaddition Reaction Mechanism of Ketenes and their Derivatives. *Oriental Journal of Chemistry*, *35*(5), 1550-1556.

Mohammad-Salim, H. A., & Abdallah, H. H. 2019b. Theoretical Study of the [4+ 2] Cycloaddition Reaction of Trifluoroethylene with Five-membered Chalcogens Heterocyclic Compounds. *ARO-THE SCIENTIFIC JOURNAL OF KOYA UNIVERSITY*, *7*(2), 69-77.

Mohammad-Salim, H. A., Abdallah, H. H., Maiyelvaganan, K. R., Prakash, M., & Hochlaf, M. 2020. Mechanistic study of the [2+2] cycloaddition reaction of cyclohexenone and its derivatives with vinyl acetate. *Theoretical Chemistry Accounts*, *139*(2), 19. doi:10.1007/s00214-019-2542-y

Mohammad-Salim, H. A., Acharjee, N., & Abdallah, H. H. 2021. Insights into the mechanism and regioselectivity of the [3 + 2] cycloaddition reactions of cyclic nitrone to nitrile functions with a molecular electron density theory perspective. *Theoretical Chemistry Accounts*, *140*(1), 1. doi:10.1007/s00214-020-02703-y

Mohammad-Salim, H. A., Acharjee, N., Domingo, L. R., & Abdallah, H. H. 2020. A molecular electron density theory study for [3 + 2] cycloaddition reactions of

1-pyrroline-1-oxide with disubstituted acetylenes leading to bicyclic 4-isoxazolines. *International Journal of Quantum Chemistry*, *n/a*(n/a), e26503. doi:https://doi.org/10.1002/qua.26503

Mohammad-Salim, H. A., Basheer, H. A., Abdallah, H. H., Zeroual, A., & Jamil, L. A. 2021. A molecular electron density theory study for [3+2] cycloaddition reactions of N-benzylcyclohexylnitrone with methyl-3-butenoate. *New Journal of Chemistry*, *45*(1), 262-267. doi:10.1039/D0NJ04049E

Pang, S., Yang, X., Cao, Z.-H., Zhang, Y.-L., Zhao, Y., & Huang, Y.-Y. 2018. Intermolecular [2 + 2] Cycloaddition/Isomerization of Allenyl Imides and Unactivated Imines for the Synthesis of 1-Azadienes Catalyzed by a Ni(ClO4)2·6H2O Lewis Acid. *ACS Catalysis*, *8*(6), 5193-5199. doi:10.1021/acscatal.8b01454

Parr, R. G., & Pearson, R. G. 1983. Absolute hardness: companion parameter to absolute electronegativity. *Journal of the American Chemical Society*, *105*(26), 7512-7516. doi:10.1021/ja00364a005

Parr, R. G., & Weitao, Y. 1989. *Density-Functional Theory of Atoms and Molecules*: Oxford University Press.

Parr, R. G., & Weitao, Y. 1994. *Density-Functional Theory of Atoms and Molecules*: Oxford University Press.

Pawlowski, R., Stanek, F., & Stodulski, M. 2019. Recent Advances on Metal-Free, Visible-Light- Induced Catalysis for Assembling Nitrogen- and Oxygen-Based Heterocyclic Scaffolds. *Molecules*, *24*(8). doi:10.3390/molecules24081533

Ríos-Gutiérrez, M., & Domingo, L. R. 2019. Unravelling the Mysteries of the [3+2] Cycloaddition Reactions. *European Journal of Organic Chemistry*, *2019*(2-3), 267-282. doi:10.1002/ejoc.201800916

Saha, R., Chatterjee, A., Mondal, S., Pal, P., Chakrabarty, K., & Das, G. K. 2019. Comparative DFT study on the platinum catalyzed [3+ 2] and [2+ 2] cycloaddition reactions between the derivatives of allene and alkene. *Computational and Theoretical Chemistry*, *1163*, 112507.

Salim, H. A. M., Abdallah, H. H., & Ramasami, P. 2018. *Stereoselectivity and Regioselectivity of the Cycloaddition Dimerization of allyl 3-(2-pyridyl) acrylate and allyl 3-(2-pyrryl) acrylate: DFT Calculations.* Paper presented at the IOP Conference Series: Materials Science and Engineering.

Salim, H. M., Abdallah, H. H., & Ramasami, P. 2018. *Mechanism and Thermodynamic Parameters of Paternò-Büchi Reaction of Benzene and Furan: DFT Study.* Paper presented at the 2018 International Conference on Advanced Science and Engineering (ICOASE).

Sowmya, D. V., Lakshmi Teja, G., Padmaja, A., Kamala Prasad, V., & Padmavathi, V. 2018. Green approach for the synthesis of thiophenyl pyrazoles and isoxazoles by adopting 1,3-dipolar cycloaddition methodology and their antimicrobial activity. *European Journal of Medicinal Chemistry*, *143*, 891-898. doi:https://doi.org/10.1016/j.ejmech.2017.11.093

Svatunek, D., Pemberton, R. P., Mackey, J. L., Liu, P., & Houk, K. 2020. Concerted [4+ 2] and Stepwise (2+ 2) Cycloadditions of Tetrafluoroethylene with Butadiene: DFT and DLPNO-UCCSD (T) Explorations. *The Journal of Organic Chemistry*, *85*(5), 3858-3864.

Tokunova, É. F., Tyurina, L. A., Nikitin, N. A., Nikitina, I. L., Klen, E. É., Khaliullin, F. A., . . . Kantor, E. A. 2001. Quantitative Structure - Activity Relationships for Microsomal Enzymatic System Modulants. Part I: Inhibitors. *Pharmaceutical Chemistry Journal*, *35*(6), 322-327. doi:10.1023/A:1012345705162

Willenbring, D., & Tantillo, D. J. 2008. Mechanistic possibilities for oxetane formation in the biosynthesis of Taxol's D ring. *Russian Journal of General Chemistry*, *78*(4), 723-731. doi:10.1134/S1070363208040336

Xu, C., Zhang, L., & Luo, S. 2014. Merging Aerobic Oxidation and Enamine Catalysis in the Asymmetric α-Amination of β-Ketocarbonyls Using N-Hydroxycarbamates as Nitrogen Sources. *Angewandte Chemie International Edition*, *53*(16), 4149-4153. doi:10.1002/anie.201400776

ZANCO Journal of Pure and Applied Sciences
The official scientific journal of Salahaddin University-Erbil
https://zancojournals.su.edu.krd/index.php/JPAS

ISSN (print): 2218-0230**, ISSN (online):** 2412-3986**, DOI: http://dx.doi.org/10.21271/zjpas**

RESEARCH PAPER

Prevalence of common bacterial etiology and antimicrobial susceptibility pattern in patients with otitis media in Duhok Province –Iraq

Zubaidah H. Mahmood Agha [1], Muna S. Al-Delaimi [2]

[1] Department of Biology, Collage of Science, University of Duhok, Kurdistan Region, Iraq

[2] Department of Biology, Collage of Science, University of Duhok, Kurdistan Region, Iraq

A B S T R A C T:

Otitis media is the most frequent type of ear infection. It is a major health problem for both children and adults but the proportion is different in different countries. The current study was designed to determine the frequency of bacterial isolates causing otitis media and their antimicrobial resistance profile to assess the incidence of multidrug-resistant (MDR), extensively drug-resistant (XDR), and pan drug resistance (PDR) among the isolated pathogens. Also, to determine the various risk factors (age, gender, type, and site of infection) associated with ear infection. A total of 200 ear discharge samples were collected from patients aged 1-77 years attending the Ear, Nose, and Throat (ENT) unit in Azadi Teaching Hospital in Duhok city from November 2018 to September 2019. The clinical samples were cultured and bacterial isolates were identified by standard microbiological methods then confirmed by VITEK® 2 Compact automated system. All gram-negative bacterial isolates were studied phenotypically for Extended Spectrum Beta Lactamase production. Out of 200 ear swabs, 95% confirmed positive culture; 85.8% were bacterial isolates. From the total bacterial isolates, 57% were gram-positive bacteria, while gram-negative bacteria were 43%; with predominant of *Pseudomonas aeruginosa*, (22%) followed by *Staphylococcus aureus* (19%) and Coagulase negative *Staphylococci* (18%). The prevalence of otitis media was not significantly affected by gender. The majority of patients belonged to the age group (1-10) years old. 64.1% of the isolates were characterized as MDR, 31.7% were XDR, with one (0.7%) as PDR. Among these, 60.7% isolates were ESBL producers, *Pseudomonas aeruginosa* was the most frequent ESBL- producing isolates (45.9%), followed by *Proteus spp* (18.9%). The *in-vitro* sensitivity results indicated that Gentamycin and Ciprofloxacin were effective antibiotics in the treatment of otitis media. Additionally, Meropenem, Imipenem, Cefepime, and Azetronam were also the most effective drug against *Pseudomonas aeruginosa*. We concluded that the drug resistant isolates were common, worryingly high, leaving only limited drugs as a treatment choice.

KEY WORDS: *Ear infection, Otitis Media, Bacterial etiology, MDR, XDR, ESBL.*
DOI: http://dx.doi.org/10.21271/ZJPAS.33.4.2
ZJPAS (2021), 33(4); 11-25 .

1.INTRODUCTION :

Otitis media is an inflammatory process of the mucosa of the inner ear with exudate production. Its consequences are hearing weakness; or even loss in adults and problems in a speech in children (Chamberlain, 2009). The most common causes of disease of the middle ear are respiratory infections producing acute or chronic otitis media. The middle ear, being connected to the respiratory tract (nasopharynx) through the Eustachian tube, is subjected to the same infections as the nose and sinuses and is frequently involved when they become inflamed (Alberti, 2001). Acute otitis media (AOM) is considered to be the initial three weeks of inflammation usually presents with ear pain. Chronic suppurative otitis media (CSOM) is characterized by chronic ear discharge through a perforated tympanic membrane for more than 6 weeks to 3 months (Lieberthal *et al*., 2013). Worldwide, around 1.23 billion people are

* **Corresponding Author:**
Zubaidah H. Mahmood Agha
E-mail: zhs_agha34@yahoo.com
Article History:
Received: 23/01/2021
Accepted: 04/05/2021
Published: 18/08 /2021

affected by otitis media; thus it is ranked as the fifth global burden of disease and the second cause of hearing loss (Tesfa *et al.,* 2020; Morris and Leach, 2009). Ear infection is caused by bacteria, viruses, and fungi. Bacteria being the most common cause (Bello *et al.,* 2011). *Staphylococcus aureus*, *Pseudomonas aeruginosa*, *Klebsiella pneumonia*, *Proteus mirabilis* and *E.coli* are the common bacteria isolated from the cases of otitis media (Al-Mosawi, 2018; Seid *et al*, 2013). The emergence of the resistance to antimicrobial agents constantly develops seriously, affecting the assessment and treatment of infections in the community and hospitals. ESBLs are enzymes that are capable of hydrolyzing the Beta lactam ring of penicillin, broad spectrum Cephalosporins, and Monobactams (Fernando *et al.,* 2017). ESBLs production is most commonly seen among gram-negative bacteria including *Klebsiella pneumonia*, *E.coli*, *Pseudomonas aeruginosa*, and *Proteus mirabilis* (Ogefere *et al.,* 2015). In addition, ESBL-producing bacteria exhibit co-resistance to other classes of antibiotics, which may limit treatment options available. Therefore, this study was carried out to determine the frequency of bacterial isolates associated with otitis media and to investigate their antimicrobial resistance profile. Also, to assess the demographic distribution of bacterial ear infection in Duhok City and to assess the prevalence of ESBL-producing bacteria.

2. Materials and Methods

2.1. Study design:

This study was carried out at Ear, Nose and Throat (ENT) unit in Azadi Teaching Hospital in Duhok city from November 2018 to September 2019. Two hundred ear discharge samples were obtained from patients, of both genders, clinically diagnosed with ear infection, their ages ranged between 1-77 years old. Only patients who didn't receive topical or systemic antibiotic treatment for two weeks were included in this study.

2.2. Sample collection

The ear discharge samples were collected immediately after clinical examination by an Otolaryngologist with caution and were taken to avoid surface contamination. The swabs were transported to the microbiology laboratory using Amies transport media (cultiplast tampon swab, Italy) for culture and antibiotics sensitivity investigation. The samples were labeled with the patient's name, identification number, age, gender, site, and type of infection, date, and time of collection. In addition, complete information was obtained directly from the patients, and a questionnaire form was used for each patient.

2.3. Culture and identification

All ear discharge samples were inoculated on the following culture media: Blood, MacConkey, Chocolate, and selective agar plates for bacterial isolation. Then, the samples were incubated aerobically and anaerobically at 37°C for 24 hours; whereas the Sabouraud dextrose agar was used as a selective media for fungi. The plates were incubated under aerobic condition for 24-48 hours at 35°C. All bacterial isolates were identified according to standard microbiological methods: cultural characteristic, gram stain and conventional biochemical tests (MacFaddin, 2000). The bacterial species were identified by VITEK® 2 Compact *(*BioMérieux, USA*)* microbiological automated system, using ID-GN(REF21341) cards specific for Gram-negative bacteria and ID-GP(REF 21342) cards for Gram-positive bacteria (Pincus, 2010).

2.4. Antimicrobial susceptibility testing

All gram-negative isolates were tested against seventeen antibiotic discs (Bioanalyse/Turkey), which include: Amikacin, Gentamycin, Netilmicin, Ertapenem, Imipenem, Meropenem, Cefuroxime, Ceftriaxone, Ceftazidime, Cefepime, Azetronam, Ampicillin, Piperacillin, Amoxicillin clavulanate, Pip-Tazobactum, Trimethoprim, and Ciprofloxacin. While twenty antibiotics were used for gram-positive bacteria which include: Gentamycin, Ampicillin, Ciprofloxacin, Tobramycin, Cefoxitin, Penicillin G, Oxacillin, Amoxicillin clavulanate, Daptomycin, Teicoplanin, Vancomycin, Clindamycin, Erythromycin, Fusidic acid, Linezolid, Fosfomycin, Levofloxacin, Rifampin, Tetracyclin, and Trimethoprim sulphamethoxazole. An antimicrobial sensitivity test was performed by the Kirby Bauer disc diffusion method on Mueller-Hinton agar (Himedia, India). The results were detected after overnight incubation at 37 ºC, by measuring the zone of inhibition according to Clinical and Laboratory Standards Institute guidelines (CLSI.,2016).

MDR, XDR, and PDR strains of pathogenic bacteria were determined according to European Center for Disease Prevention and Control (ECDC), and the Centers for Disease Control and Prevention (CDC). MDR was defined as the isolate resistant to at least one agent in three or more antimicrobial classes. Any bacterial isolate that remains sensitive to only one or two classes of antibiotics is characterized as XDR. While PDR refers to non-susceptibility to all agents in all antimicrobial classes (Magiorakos *et al*., 2012)

2.5. Extended Spectrum β-Lactamases detection methods:

2.5.1. Double Disc Synergy Test:

Double Disc Synergy Test (DDST) was performed using 3rd generation cephalosporin discs (Cefotaxime (30µg), Ceftazidime (30µg) and Ceftriaxone (30µg)), which were placed with a distance of 20mm from an Augmentin (20 µg Amoxicillin /10 µg Clavulanic acid) disc on a cultured Muller-Hinton agar then incubated overnight at 37 ºC. Extension of the inhibition zone of any type of 3rd generation cephalosporin toward the Augmentin disc was considered as a positive to the ESBL production.

2.5.2. ESBL CHROMagar™:

For the phenotypic detection of gram-negative ESBL producing bacteria, the isolates were cultured on CHROMagar™ ESBL (Conda pronadisa, Spain) after adding ESBL Supplement (CAT:6042). They then incubated at 37 ºC for 24 hours. *Klebsiella pneumoniae*, *Enterobacter* and *Serratia* produce green-blue to browny-green colonies, while *E. coli* and *Klebsiella oxytoca* produce pink to burgundy coloration colonies, *Proteus* produce dark to light brown colonies; the colorless colonies considered as ESBL producing *Pseudomonas* and *Acinetobacter*.

2.6. Statistical Analysis

All data was analyzed by SPSS version 24 and Microsoft Excel (2013). Chi-square tests ($\chi 2$) were used to test for variable categories; and probability value (P-value) of less than 0.01 was taken as being statistically highly significant.

3. Results:

Two hundred ear discharge samples were collected from patients attending ENT unit in Azadi Teaching Hospital with ear infection. Of these, 190 (95%) cases were confirmed as positive culture, while 10/200(5%) samples showed culture negative. Among the positive culture, 163/190(85.8%) were positive for bacterial isolates, and 27(14.2%) showed the growth of candida species. 160 clinical samples had single bacterial growth and 3 samples were mixed along with candida. No anaerobic bacteria were detected.

3.1. Isolated pathogens:

The current study relied on bacterial ear infection. The overall prevalence of bacterial isolates was 163/190 (85.8%) and demonstrated that the most frequent bacterial infection diagnosed was otitis media 142/163(87.1%). Out of 142 otitis media cases, 55(38.7%) were acute otitis media and 87(61.3%) were chronic suppurative otitis media. From the total bacterial isolates (142), 81(57%) were gram-positive bacteria, while gram-negative bacteria gave 61(43%). The results shown in figure (1) indicated that the most common bacteria isolated from patients with acute otitis media were: 15(10.6%) *S. aureus*; 12 (8.5%) CoNS; 11(7.7%) *P. aeruginosa*; 4(2.8%) *Kocuria;* 2(1.4%) for each *Proteus*, *Streptococcus*, *M.luteu*, *Enterobacter*, and *G.adiacense*; while *Klebsiella*, *E. faecalis*, and *S. marcescens* were 1(0.7%).

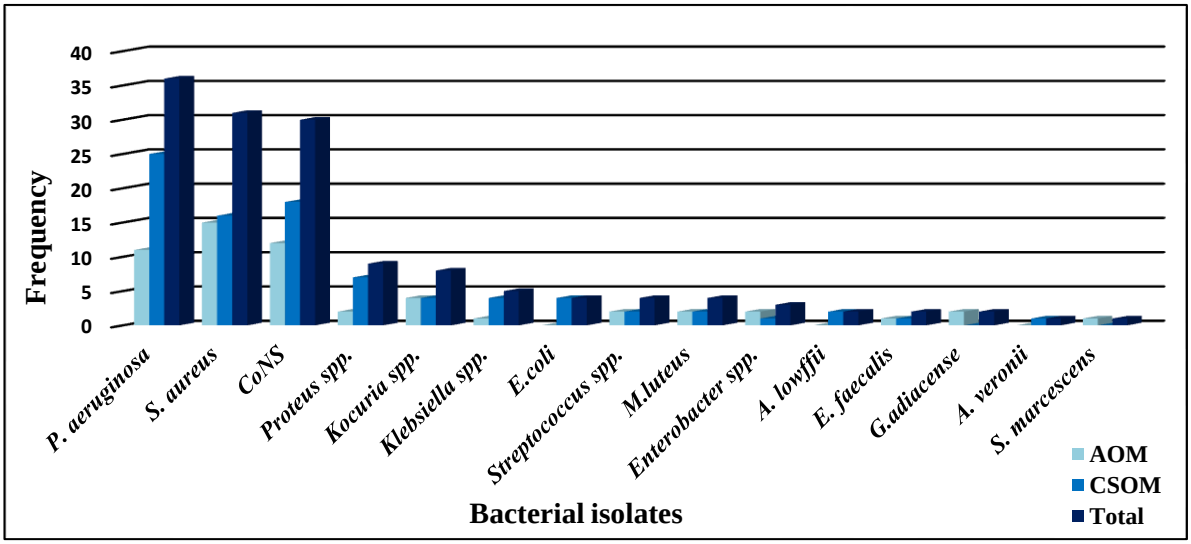

Figure (1): Frequency of bacterial isolates from patients with otitis media.

On the other hand, the same figure showed that the predominant bacteria isolated from patients with chronic suppurative otitis media, were: *P. aeruginosa* 25(17.6%); CoNS 18(12.7%); *S. aureus* 16(11.3%); *Proteus spp*. 7(4.9%); 4(2.8%) for each *Kocuria*, *Klebsiella* and *E.coli;* followed by *Streptococcus spp.*, *M.luteus* and *A. lowffii* were 2(1.4%); while the least prevalent were *Enterobacter spp.*, *E. faecalis*, and *A. veronii* 1(0.7%). The results illustrated that the distribution of various bacterial isolates was not significantly (P>0.01) associated with the types of otitis media.

3.2. Age and gender distribution:

A total of 142 patients with otitis media were enrolled in this study. The participants ages ranged from 1-77 years old, and the mean age was 27.6 (27.6 ± 19.4). Based on the results of table (1), the majority (39: 27.5%) of patients belonged to the age group of (1-10) years old. Acute otitis media was more common in this age group. Whereas chronic suppurative otitis media (19: 21.8%) was more common in the age group (45-55) years old. The chi-square test illustrated that the age groups had a statistically significant (P< 0.01) association with various types of otitis media. On the other hand, the same table showed that the males (74: 52.1%) were more infected with bacterial ear infection than female (68: 47.9%), but was statistically not significant (P>0.01).

Table (1): Distribution of otitis media according to gender and age groups of cases.

Variables		Types of otitis media			Chi-square and p- value
		AOM n(%)	CSOM n(%)	Total n(%)	
Age groups in year	1-10	25(17.6%)	14(9.9%)	39(27.5%)	Chi-square=22.554 p- value < 0.01
	11-21	8(5.6%)	17(12%)	25(17.6%)	
	22-32	8(5.6%)	13(9.2%)	21(14.8%)	
	33-44	10(7%)	12(8.5%)	22(15.5%)	
	45-55	2(1.4%)	19(13.4%)	21(14.8%)	

	>55	2(1.4%)	12(8.5%)	14(9.9%)	
Gender	Male	32(22.5%)	42(29.6%)	74(52.1%)	Chi-square=1325
	Female	23(16.2%)	45(31.7%)	68(47.9%)	p- value >0.01

3.3. Antimicrobial susceptibility testing:

3.3.1. Gram-positive bacteria:

The results in table (2) revealed that all gram-positive isolates were 100% resistant to Penicillin G, while 90% (27/30) and 75% (6/8) for CoNS and *Kocuria spp.* respectively. Regarding, Fusidic acid, all gram-positive bacteria showed high resistance (100%); and 96.8% (30/31), 93.3% (28/30) and 87.5% (7/8) for each (*S. aureus*, CoNS, and *Kocuria spp*). As for Rifampin, most isolates were found to be 100% resistant, while 86.7% (26/30) for CoNS and 75% (6/8) for *Kocuria spp.* On the other hand, the same table indicated variable sensitivity patterns for the isolates against other antibiotics.

Table (3): Pattern of susceptibility of gram-negative bacteria to various antibiotics.

Isolated bacteria		Types of Antibiotics (%)																
		AK	CN	NET	ETP	IPM	MEM	CXM	CRO	CAZ	FEP	ATM	AM	PRL	AMC	TPZ	TMP	CIP
P.aeroginosa	R	61.1%	44.4%	27.8%	86.1%	5.6%	8.3%	100%	100%	63.9%	33.3%	8.3%	100%	47.2%	100%	19.4%	100%	16.7%
	S	38.9%	55.6%	72.2%	13.9%	94.4%	91.7%	0	0	36.1%	66.7%	91.7%	0	52.8%	0	80.6%	0	83.3%
Proteus spp.	R	33.3%	44.4%	33.3%	22.2%	33.3%	11.1%	55.6%	55.6%	44.4%	33.3%	55.6%	100%	66.7%	44.4%	33.3%	77.8%	33.3%
	S	66.7%	55.6%	66.7%	77.8%	66.7%	88.9%	44.4%	44.4%	55.6%	66.7%	44.4%	0	33.3%	55.6%	66.7%	22.2%	66.7%
Klebsiella spp.	R	60%	0	0	40%	40%	20%	20%	40%	40%	0	0	100%	60%	20%	40%	40%	0
	S	40%	100%	100%	60%	60%	80%	80%	60%	60%	100%	100%	0	40%	80%	60%	60%	100%
E.coli	R	50%	25%	25%	50%	0	0	75%	75%	75%	50%	25%	100%	50%	100%	75%	50%	25%
	S	50%	75%	75%	50%	100%	100%	25%	25%	25%	50%	75%	0	50%	0	25%	50%	75%
Enterobacter spp.	R	33.3%	33.3%	0	33.3%	33.3%	0	33.3%	66.7%	33.3%	0	0	100%	0	100%	33.3%	33.3%	33.3%
	S	66.7%	66.7%	100%	66.7%	66.7%	100%	66.7%	33.3%	66.7%	100%	100%	0	100%	0	66.7%	66.7%	66.7%
A. Lowffii	R	50%	0	0	100%	0	0	50%	100%	50%	0%	100%	100%	50%	100%	0	50%	0
	S	50%	100%	100%	0	100%	100%	50%	0	50%	100%	0	0	50%	0	100%	50%	100%
A. veronii	R	100%	0	0	100%	100%	100%	0	0	0	0	0	100%	100%	100%	100%	0	0
	S	0	100%	100%	0	0	0	100%	100%	100%	100%	100%	0	0	0	0	100%	100%
S. marceses	R	0	0	0	0	0	0	100%	0	0	0	0	100%	0	100%	100%	0	0
	S	100%	100%	100%	100%	100%	100%	0	100%	100%	100%	100%	0	100%	0	0	100%	100%

*R: Resistance *S: Sensitive

3.4. Incidence of drug resistance patterns of all bacterial isolates studied:

The resistance profiles were used to recognize MDR, XDR, and PDR amongst all bacterial isolates studied which determined, out of total 142 bacterial isolates, 91 (64.1%) bacterial isolates were MDR and 45(31.7%) isolates were XDR; with one (0.7%) isolate of *Pseudomonas* was PDR. Amongst 81 gram positive pathogen isolated, 69(85.2%) and 12(14.8%) were MDR and XDR, respectively; with no PDR was detected. Out of 61 gram negative isolates, 22(36.1%) isolates were MDR, 33(54.1%) were XDR, and one isolate (1.6%) was PDR. Out of 31 *S. aureus* isolated, 26(83.9%) were MDR, and 5(16.1%) were XDR. Thirty CoNS were isolated and 27(90%) were MDR, whereas 3(10%) were XDR. *Kocuria* isolates have shown high (100%) MDR rate. Three (75%) and 1 (25%) out of 4 *Streptococcus* isolates were MDR and XDR respectively. Additionally, all four isolates of *Micrococcus* were MDR (100%). While 2 (100%) *Enterococcus* isolates were detected as XDR. Finally, of two *Granulicatella* isolates, 1(50%) was MDR, and 1 (50%) was XDR, as shown in table (4).

Table (4): Frequency of MDR, XDR, and PDR of gram-positive bacterial isolates for selected antimicrobial classes.

Isolated Bacteria (No.)	Types of Resistance		
	MDR	XDR	PDR
S .aureus (31)	26(83.9%)	5(16.1%)	-
CoNS (30)	27(90%)	3(10%)	-
Kocuria. spp (8)	8(100%)	-	-
Streptococcus .spp (4)	3(75%)	1(25%)	-
M .luteus (4)	4(100%)	-	-
E .faecalis (2)	-	2(100%)	-
G .adiacense (2)	1(50%)	1(50%)	-
Total (81)	69(85.2%)	12(14.8%)	-

Table (5) shows incidence of MDR, XDR, and PDR pathogens isolated from each species of gram negative bacterial isolates. Thirteen (36.1%), 22 (61.1%) and 1(2.8%) out of 36 *Pseudomonas* isolates were MDR, XDR, and PDR respectively. Among 9 isolates of *Proteus*, 4 (44.4%) and 5 (55.6%) were MDR and XDR respectively. Five *Klebsiella* were isolated, 1 (20%) were MDR, whereas 1 (20%) were XDR. Of four isolates *E.coli* 1 (25%) were MDR and 2 (50%) were XDR. Furthermore, out of 3 isolates of *Enterobacter* 1 (33.3%) were MDR and 1(33.3%) were XDR. Two (100%) *A. Lowffii* isolates were XDR. The overall rate of MDR among all isolates *A. veronii* and *S. marcescens* were 100%.

Table (5): Frequency of MDR, XDR, and PDR of gram-negative bacterial isolates against the antibiotics used.

Isolated Bacteria (No.)	Types of Resistance		
	MDR no.(%)	XDR no.(%)	PDR no.(%)
P. aeruginosa (36)	13 (36.1%)	22(61.1%)	1(2.8%)
Proteus.spp (9)	4(44.4%)	5(55.6%)	-
Klebsiella. spp (5)	1(20%)	1(20%)	-
E.coli (4)	1(25%)	2(50%)	-
Enterobacter. spp (3)	1(33.3%)	1(33.3%)	-
A .lowffii (2)	-	2(100%)	-
A .veronii (1)	1(100%)	-	-
S. marcescens (1)	1(100%)	-	-
Total (61)	22(36.1%)	33(54.1%)	1(1.6%)

3.5. Screening for ESBL producers:

Sixty-one gram-negative bacterial isolates obtained from patients with otitis media were studied phenotypically for ESBL production; the results indicated that 37(60.7%) isolates were ESBL producers and 24 (39.3%) isolates were non-ESBL producers. A significant correlation was observed between ESBL and non-ESBL producers and the prevalence of otitis media cases. The predominant ESBL producing isolates were *P. aeruginosa* 17/37 (45.9%), followed by *Proteus spp.* 7/37 (18.9%), *Klebsiella spp.* 5/37 (13.5%), *E.coli* 4/37 (10.8%), *Enterobacter* 3/37 (8.1%) and *S. marcescens* 1/37 (2.7%). Phenotypically, ESBL production was demonstrated by both Double Disk Synergy Test and ESBL CHROM agar methods as shown in (Fig.2 and Fig.3) respectively. Among 37 ESBL producers, 31(83.8%) isolates were detected by Double Disk Synergy Test, while ESBL CHROM agar detected 37(100%) isolates.

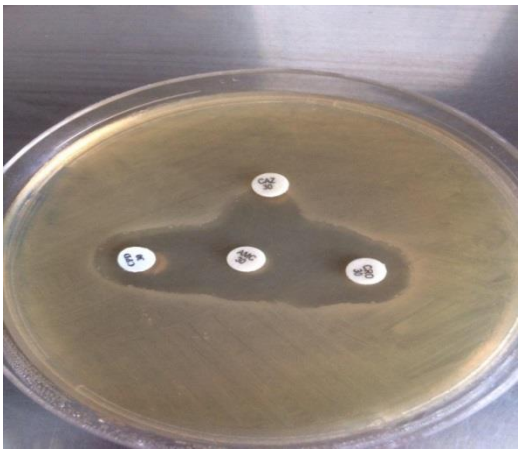

Figure (2): Double Disk Synergy Test showing positive ESBL production, when swabbed on Muller Hinton agar and incubated over night at 37°*C.*
with Cefotaxime, Ceftazidime and Ceftriaxone discs; which were placed with distance of 20mm from an Amoxicillin-clavulanic acid disc.

Figure (3): ESBL producers: colonies on CHROM agar
1- *P. aeruginosa*, 2-*Kl. pneumonia*, 3- *Kl. oxytoca* , 4-*E.coli*, 5- *Enterobacter spp.* , and 6- *S. marcescens.*

3.6. Antimicrobial susceptibility patterns of ESBL producing isolates:

The resistance profile of the ESBL and non-ESBL producing isolates was shown in table (6). It was found that all ESBL producing isolates resistant 100% to Ampicillin; other resistance rates were 78.4% Amoxicillin-clavulanic acid, 73% Ceftriaxone and Trimethoprim, and 70% Cefuroxime. Additionally, ESBL producers demonstrated high sensitivity 91.9%, 86.5%, and 83.8% for Meropenem, Azetronam and Impenem respectively. A significant difference ($p < 0.01$) in resistance pattern was observed with Gentamicin, Ertapenem, Cefuroxime, Ceftriaxone, Amoxicillin-clavulanic acid and Trimethoprim between ESBL and non ESBL isolates.

Table (6): Antibiotic susceptibility pattern of ESBL and non- ESBL producing isolates

Antibiotic	ESBL positive		ESBL negative		P-value
	Resistance	Sensitive	Resistance	Sensitive	
Amikacin	19 (51.4%)	18 (48.6%)	14 (58.3%)	10 (41.7%)	P>0.01
Gentamicin	15 (40.5%)	22 (59.5%)	7 (29.2%)	17 (70.8%)	p<0.01
Netilmicin	10 (27%)	27 (73%)	4 (16.7%)	20 (83.3%)	P>0.01
Ertapenem	20 (54.1%)	17 (45.9%)	21 (87.5%)	3 (12.5%)	p<0.01
Impenem	6 (16.2%)	31 (83.8%)	3 (12.5%)	21 (87.5%)	P>0.01
Meropenem	3 (8.1%)	34 (91.9%)	3 (12.5%)	21 (87.5%)	P>0.01
Cefuroxime	26 (70.3%)	11 (29.7%)	22 (91.7%)	2 (8.3%)	p<0.01
Ceftriaxone	27 (73%)	10 (27%)	23 (95.8%)	1 (4.2%)	p<0.01
Ceftazidim	20 (54.1%)	17 (45.9%)	14 (58.3%)	10 (41.7%)	P>0.01
Cefepime	10 (27%)	27 (73%)	7 (29.2%)	17 (70.8%)	P>0.01
Azetronam	5 (13.5%)	32 (86.5%)	6 (25%)	18 (75%)	P>0.01
Ampicillin	37 (100%)	0	24 (100%)	0	P>0.01
Pipracillin	18 (48.6%)	19 (51.4%)	12 (50%)	12 (50%)	P>0.01
Amoxicillin-clavulanic acid	29 (78.4%)	8 (21.6%)	23 (95.8%)	1 (4.2%)	p<0.01
Pip-Tazobactum	13 (35.1%)	24 (64.9%)	5 (20.8%)	19 (79.2%)	P>0.01
Trimethoprime	27 (73%)	10 (27%)	22 (91.7%)	2 (8.3%)	p<0.01
Ciprofloxacin	8 (21.6%)	29 (78.4%)	3 (12.5%)	21 (87.5%)	P>0.01

4. Discussion

Multi microbial infections are commonly reported in otitis media with mixed bacteria-bacteria, viral-bacterial and fungal-bacterial infections. Based on the present study results, the single infection was more frequent than mixed infection. The incidence of single infection was 98.2%, while it was 1.8% for mixed infection. This finding was consistent with work published by several studies (Haider, 2002; Karim, 2008; Chaudhary and Shukla, 2014**;** Balan and Viswanatha, 2017**;** Gorems *et al*., 2018). No growth was observed in 5% ear swabs, similar results were reported by (Karim, 2008; Al-Marzoqi *et al*., 2013; Gorems *et al*., 2018). This may be attributed to the possibility of viruses

(respiratory syncytial virus, influenza virus and adenovirus), chlamydia or mycoplasma as a pathogen of the otitis media (Chonmaitree, 2000; Prakash *et al*., 2013).

It was found in this study that males 52.1% more infected than females and prevalence of otitis media was not significantly affected by gender. Which was in line with other studies conducted in Iraq (Aldhaher *et al*., 2018), Nigeria (Nwokoye *et al.*, 2012), Pakistan (Javed *et al*. 2020), Ethiopia (Worku *et al.* 2014; Gorems *et al*. 2018), Uganda (Justin *et al.*, 2018), and India (Chaudhary and Shukla, 2014). But several studies showed that the infection in females were predominant (Abera *et al.*,2011; Al-Marzoqi *et al*.,2013; Akter *et al*.,2015; Jik *et al*., 2015; Basnet *et al*., 2017). Male predominance could be because life style choices, environmental effect; Kvestad *et al*., (2004) confirms that there is sufficient evidence for the presence of sex-based differences due to relative genetic effects.

The results of this study indicated that the children patients belonged age group 1-10 years had the high prevalence of otitis media. Similar to previous studies carried out by (Nwabuisi and Ologe, 2002; Nwokoye *et al.*, 2012; Saleh *et al.*, 2014; Basnet *et al*., 2017; Hassooni *et al*., 2018) and dissertation conducted by (Karim, 2008) also found similar findings. However, high children´s susceptibility to otitis media is could be attributed to their immune system; it was also shown that the Eustachian tubes were shorter, wider and more horizontal than in the adults. This position allows opportunistic organisms from noes, adenoids and sinuses pass from nasopharynx in to the sterile middle ear along the Eustachian tube "particularly during coughing, sneezing, vomiting and forced feeding commonly practiced in our environment with child´s nose blocked" (Nwabuisi and Ologe, 2002; Basnet *et al*., 2017).

Etiological agents of otitis media and their antimicrobial susceptibility varied with geographical location, age, type of infection whether acute or chronic and time (Hassan and Adeyemi, 2007). The observation in present study indicated that gram positive bacteria were the predominant isolates (57%) from patients with otitis media when compared to gram negative bacteria (43%) which was in agreement to earlier studies performed by (Al-Marzoqi *et al.* , 2013; Vaidya *et al*., 2015; Jik *et al*., 2015; Basnet *et al*., 2017; Gorems *et al*., 2018; Sah *et al.*, 2020). This, however, differs with the studies conducted by (Ogbogu *et al.*, 2013; Hassooni *et al*., 2018; Aldhaher *et al*., 2018) where gram negative bacteria were predominant. The difference might be attributed to the variation in the bacterial profile of otitis media in accordance to climate and geographical variation of the study regions. Out of 142 cases studied, 55(38.7%) were acute type of otitis media and 87 (61.3%) of chronic type in this study. Similar results were obtained from other studies (Seid *et al.*, 2013; Wasihun and Zemene, 2015**;** Vijayvargiya *et al*., 2016; Basnet *et al*., 2017; Hassooni *et al*., 2018). Low socioeconomic status, crowded living conditions, and malnutrition related to poor hygiene which is considered as risk factors for the development of chronic otitis media (Verhoeff *et al.*, 2006). In this study, patient with chronic otitis media were frequently between 45-55 years old. In contrast, Loy *et al*., (2002) showed the increased prevalence of chronic otitis media in 30-40 years old in their study. Vijayvargiya *et al*. reported high incidence in 6-68 years of age; Seid *et al.*, (2013) reported highest among 11-20 years age group. Whereas Shyamala and reddy, (2012), Nazir and Kadri (2014), and Hailu *et al*. (2016) reported that chronic otitis media was seen in first and second decade of life.

The predominant bacterial etiology of chronic otitis media was *P. aeruginosa* followed by CoNS, *S. aureus*, *Proteus* and other enteric bacteria, previous studies also found similar results (Alsaimary *et al*. 2010; Shyamala and reddy, 2012; Ogbogu *et al.*, 2013**;** Al-Marzoqi *et al*., 2013; Nazir and Kadri, 2014; Vijayvargiya *et al*., 2016; Juyal *et al*.,2017; Hassooni *et al*., 2018; Javed *et al*., 2020). While, various studies from different countries have reported that *S. aureus* is the most predominant pathogen that causes chronic otitis media (Ettehad *et al.*, 2007; Ahmad, 2013; Jakribettu *et al.* 2014; Wasihun and Zemene, 2015 ; Basnet *et al*., 2017). The dominance isolation rate of *P. aeruginosa* in this study could be related to its biofilm phenotype property which allows entry to the middle ear through the external canal. It can grow well in the environment of the ear and is difficult to eliminate. It has been suggested to damage tissues, interfere with the host defenses and inhibit antibiotic activity by enzymes and toxins (Seid *et al.*, 2013; Gellatly and Hancock 2013). Moreover, the isolation of fecal pathogens such as

K.pneumoniae and *E.coli* may indicate that individuals were at risk of infection due to low socioeconomic status related to poor hygiene. On the other hand, the most prevalent bacteria responsible for acute otitis media was *S. aureus* (10.6%), and this result was similar with previous studies (Ako-Nai *et al.* 2002; Seid *et al.*, 2013; Gorems *et al*., 2018), but differs from other investigators that indicated *Strep. pneumoniae*, *Moraxella catarrhalis* and *Haemophilus influenza* predominance (Sierra *et al.*, 2011; Qureishi *et al.* 2014;). The reason for this might be due to several factors like immunological, genetical, infectious, and environmental conditions leading to an individual´s ear infection.

Table (1) indicates that acute otitis media was more common at younger ages and the rate of acute otitis media appears to be decreasing with advancing age. The reason for this may be due to antimicrobial and immunological factors, which indicates that upper respiratory tract colonized abundantly with pathogens and the short and straight of Eustachian tube allows organisms to penetrate the middle ear. Additionally, high incidence of URTI induces middle ear bacterial infection, could be due to immature immune system (Marom *et al.*, 2012). The frequency of *S. aureus* in middle ear infections can be due to its biofilm forming organism, ubiquitous nature, and carrying of resistant strains in the external auditory canal and upper respiratory tract.

The antimicrobial susceptibility patterns of all bacterial isolates in the current study were completely variable. Gentamycin and Ciprofloxacin were effective antibiotics against more than 86% of studied isolate. These results were closely associated with many previous studies (Seid *et al.*, 2013; Gorems *et al*., 2018). Meanwhile the majority (85%-100%) of gram negative bacterial isolates showed high levels of resistance to Ampicillin and Amoxicillin-clavulanic acid in this study. Different studies reported different sensitivity patterns, in a similar study by (Ettehad *et al.*, 2007), it was found that Ciprofloxacin was an effective antibiotic for treatment of otitis media. While Alsaimary noted that Ciprofloxacin, Amoxicillin-clavulanic acid and Gentamycin were an effective for gram positive and gram negative bacteria in otitis media. Gehanno and French Study Group, 1997 found that Ciprofloxacin and Amoxicillin-clavulanic acid was more bacterial agents for many gram positive and gram negative bacteria in AOM and CSOM. These variations depend on the type of infection, type of isolate and type of antibiotic. Additionally, Meropenem, Imipenem, Cefepime and Azetronam were also found to be most effective drug against *P. aeruginosa* with less sensitive to Ceftazidime. While a study conducted by Mansoor *et al.*, (2009) showed less sensitivity to Azetronam but there was good sensitivity to Ceftazidime which contrast to our findings. On the other hand, most gram positive bacterial isolates showed highest rate of resistance to Tetracyclin, Rifampin, Erythromycin, Fusidic acid and Penicillin G. *S.aureus* was found to be highly susceptible to Fosfomycin, Gentamycin followed by Tobramycin, Levofloxacin, Trimethoprim-Sulphamethoxazole, Ciprofloxacin and Oxacillin. Sah *et al.*, (2020) showed that *S. aureus* was high susceptible to Ofloxacin followed by Ciprofloxacin, Tobramycin and Gentamycin. The reason for this variation could be due to antimicrobial susceptibility profile of isolated bacteria which differ among population according to geographical locations and prevalence of resistant bacterial strains. The drug resistant isolates in this study were common, worryingly high. Overall, 64.1% of the bacterial isolates in this study characterized as MDR pathogenic bacteria, 31.7% isolates were XDR, with one isolate (0.7%) of *P. aeruginosa* was PDR; and this detection of drug resistant isolates may limit treatment options. Hence, the prudent use of appropriate antimicrobial agent is recommended. In addition, the current results indicated high level of MDR isolates which were consistent with other studies (Seid *et al*., 2013; Muluye *et al*., 2013 Hailu *et al*., 2016; Gorems *et al*., 2018). The reason for this high drug resistance might be associated with misuse of antibiotics, inappropriate prescribing habits, and biofilm bacterial properties of common isolates (Seid *et al*., 2013).

The current study designed to detect the prevalence of ESBL production and their effect on antimicrobial susceptibility patterns using phenotypic methods (DDST and ESBL CHROM ager) in gram negative isolates from patients with otitis media. There was a significant geographical difference in the occurance of ESBL worldwide (Paterson and Bonomo, 2005; Leylabadlo *et al.*,

2017). Overall, the rate of ESBL producing isolates was 60.7% in ear study. It was lower compared to a study conducted by Sahu and Swain, (2019) 42.2%, while (Khatoon *et al.*, 2015; Mushi *et al.*, 2016; Kashyap *et al.*, 2017; Endaylalu *et al.*, 2020) reported a lower ear infection prevalence of 18.3%, 16.3%, 8.9% and 7.4% respectively. However, a study in Nigeria reported the absence of ESBL producing bacteria in ear infection (Chika *et al.*, 2013). This may attributed to variation in the ESBL detection methods, the study participants and extent of antibiotic use. Based on our results, ESBL CHROM agar method was found to be better than DDST in detection of ESBL producing bacteria. Among the total 37 ESBL producing isolates found in 83.3% by DDST and 100% by ESBL CHROM agar. This explains that this media is the most reliable for the detection of ESBL in high accuracy and rapid identification with very low false positive rates (Filius *et al.*, 2003; Uyanga *et al*., 2019)

5. References

Abera, B. and Kibret, M., 2011. Bacteriology and antimicrobial susceptibility of otitis media at dessie regional health research laboratory, Ethiopia. Ethiopian Journal of Health Development, 25(2), pp.161-167.

Ako-Nai, A.K., Oluga, F.A., Onipede, A.O., Adejuyigbe, E.A. and Amusa, Y.B., 2002. The Characterization of Bacterial Isolates from Acute Otitis Media in Ile-Ife, Southwestern Nigeria. Journal of tropical pediatrics, 48(1), pp.15-23.

Akter, S., Shamsuzzaman, S.M., Nehar, N., Siddiqui, I., Jahan, F. and Islam, S., 2015. Bacterial isolates and drug susceptibility patterns of ear discharge from patients with ear infection at Shaheed Monsur Ali Medical College. Bangladesh Journal of Medical Microbiology, 9(2), pp.20-23.

Alberti, P.W., 2001. Chapter 3: Pathology and physiology of the ear. University of Toronto, Canada Occupational exposure to noise: Evaluation, prevention, and control, https://www.who.int/occupational health/publications/noise2.pdf .

Aldhaher, Z.A., Hassan, H.F., Al-Jassim, Z.G. and Mahmood, M.A., 2018. Bacterial isolates and antibiotic susceptibility of ear infections in Iraqi patients. International Journal of Biosciences, 13(1), pp. 292-297.

Al-Marzoqi, A.H., Al-Janabi, H.S.O., Hussein, H.J., Al Taee, Z.M. and Yheea, S.K., 2013. Otitis media; etiology and antibiotics susceptibility among children under ten years old in Hillah city, Iraq. Journal of Natural Sciences Research, 3(3), pp.2224-3186.

Al-Mosawi, R.M., 2018. Microbiological study and antimicrobial susceptibility pattern of ear infections in patients with Chronic Suppurative Otitis Media (CSOM) in Basrah Province. University of Thi-Qar Journal of Science, 6(4), pp.109-116.

Alsaimary, I.E., Alabbasi, A.M. and Najim, J.M., 2010. Impact of multi drugs resistant bacteria on the pathogenesis of chronic suppurative otitis media. Afr J Microbiol Res, 4(13), pp.1373-1382.

Balan, S. and Viswanatha, B., 2017. Microbiology of chronic suppurative otitis media: a prospective study in a tertiary care hospital. J Otolaryngol ENT Res, 9(1), p.00277.

Basnet, R., Sharma, S., Rana, J.C. and Shah, P.K., 2017. Bacteriological study of otitis media and its antibiotic susceptibility pattern. Journal of Nepal Health Research Council, 15(2), pp.124-129.

Bello, R.H.,Agbo,E.B., and Olabode, H.O.K., 2011. Antibiogram of bacteria and fungal isolates associated with otitis media amongst children in Bauchi state, Nigeria. International Journal of Pharma and Bio Sciences, 2(3), pp.200-207.

Chaudhary, B.L. and Shukla, S., 2014. Bacteriological Profile and their Antibiotic Susceptibility pattern in cases of otitis media. Bulletin of Pharmaceutical and Medical Sciences (BOPAMS), 2(2).

Chika, E., Ifeanyichukwu, I., Michael, A. and Charles, E., 2013. SUSCEPTIBILITY AND DETECTION OF EXTENDED SPECTRUM [Beta]-LACTAMASE ENZYMES FROM OTITIS MEDIA PATHOGENS. American Journal of Infectious Diseases, 9(1), p.24.

Chonmaitree, T., 2000. Viral and bacterial interaction in acute otitis media. The Pediatric infectious disease journal, 19(5), pp.S24-S30.

CLSI, C., 2016. Performance standards for antimicrobial susceptibility testing. Clinical Lab Standards Institute.

Endaylalu, K., Abera, B. and Mulu, W., 2020. Extended spectrum beta lactamase producing bacteria among outpatients with ear infection at FelegeHiwot Referral Hospital, North West Ethiopia. PloS one, 15(9), p.e0238891.

Ettehad, G.H., Refahi, S., Nemmati, A., Pirzadeh, A. and Tazakori, Z., 2007. P742 Microbial and antimicrobial susceptibility patterns from patients with chronic otitis media in Ardebil,

Iran. International Journal of Antimicrobial Agents, (29), p.S183.

Fernando, M.M.P.S.C., Luke, W.A.N.V., Miththinda, J.K.N.D., Wickramasinghe, R.D.S.S., Sebastiampillai, B.S., Gunathilake, M.P.M.L., Silva, F.H.D.S. and Premaratna, R., 2017. Extended spectrum beta lactamase producing organisms causing urinary tract infections in Sri Lanka and their antibiotic susceptibility pattern–a hospital based cross sectional study. BMC infectious diseases, 17(1), p.138.

Filius, P.M.G., Van Netten, D., Roovers, P.J.E., Vulto, A.G., Gyssens, I.C., Verbrugh, H.A. and Endtz, H.P., 2003. Comparative evaluation of three chromogenic agars for detection and rapid identification of aerobic Gram-negative bacteria in the normal intestinal microflora. Clinical microbiology and infection, 9(9), pp.912-918.

Gehanno, P. and French Study Group, 1997. Multicenter study of the efficacy and safety of oral ciprofloxacin in the treatment of chronic suppurative otitis media in adults. Otolaryngology—Head and Neck Surgery, 117(1), pp.83-90.

Gellatly, S.L. and Hancock, R.E., 2013. Pseudomonas aeruginosa: new insights into pathogenesis and host defenses. Pathogens and disease, 67(3), pp.159-173.

Gorems, K., Beyene, G., Berhane, M. and Mekonnen, Z., 2018. Antimicrobial susceptibility patterns of bacteria isolated from patients with ear discharge in Jimma Town, Southwest, Ethiopia. BMC Ear, Nose and Throat Disorders, 18(1), p.17.

Haider, A., 2002. Chronic suppurative otitis media (CSOM): Bacteriological study. ORION, vol. 13.

Hailu, D., Mekonnen, D., Derbie, A., Mulu, W. and Abera, B., 2016. Pathogenic bacteria profile and antimicrobial susceptibility patterns of ear infection at Bahir Dar Regional Health Research Laboratory Center, Ethiopia. SpringerPlus, 5(1), p.466.

Hassan, O. and Adeyemi, R.E., 2007. A study of bacterial isolates in cases of otitis media in patients attending oauthc, Ile-Ife. African Journal of Clinical and Experimental Microbiology, 8(3), pp.130-136.

Hassooni, H.R., Fadhil, S.F., Hameed, R.M., Alhusseiny, A.H. and Jadoo, S.A.A., 2018. Upper respiratory tract infection and otitis media are clinically and microbiologically associated. Journal of Ideas in Health, 1(1), pp.29-33.

Jakribettu, R.P., Fysal, N., Sushanth P.S., Ahmed, S.M., Shamseer, P.T., 2014. Microbiological study of acute otitis media in children aged 2 months to 18 years. Journal of Evolution of Medical and Dental Sciences, 3(02), pp.393-398

Javed, M., Arshad, M. and Khan, M.A., 2020. 69. Pathogenic bacteria profile and antimicrobial susceptibility patterns of ear infection at Ayub Medical Complex Abbottabad, Pakistan. Pure and Applied Biology (PAB), 9(1), pp.714-719.

Jik, A., Ogundeji, E., Maxwell, I., Ogundeji, A., Samaila, J., Sunday, C., Gullek, J.S., Baso, L.A., Agbaje, A.O. and Onuoha, M.N., 2015. Identification of microorganism associated with otitis media among children in Ganawuri area of plateau state, Nigeria. IOSR J Dent Med Sci, 14(12), pp.61-67.

Justin, R., Tumweheire, G., Kajumbula, H. and Ndoleriire, C., 2018. Chronic suppurative otitis media: bacteriology, susceptibility and clinical presentation among ENT patients at Mulago Hospital, Uganda. South Sudan Medical Journal, 11(2), pp.31-35.

Juyal, D., Sharma, M., Negi, V., Prakash, R. and Sharma, N., 2017. Pseudomonas aeruginosa and its sensitivity spectrum in chronic suppurative otitis media: A study from Garhwal hills of Uttarakhand State, India. Indian Journal of Otology, 23(3), p.180.

Karim, A. 2008. Effect of Tris-EDTA and ascorbate in increasing antibiotic activity against bacteria isolated from otitis media. Doctoral dissertation, Al-Nahrain University.

Kashyap, S., Pandey, A., Thakuria, B., Saxena, A.K., Asthana, A.K. and Madan, M., 2017. Resistant microorganisms isolated from cases of chronic suppurative otitis media: a therapeutic concern. National Journal of Laboratory Medicine, 6(2), pp.M001-M006.

Khatoon, A., Rizvi, M., Sultan, A., Khan, F., Sharma, M., Shukla, I. and Khan, H.M., 2015. Chronic suppurative otitis media: a clinico-microbiological menace. Int J Res Med Sci, 3(8), pp.1932-6.

Kvestad, E., Kværner, K.J., Røysamb, E., Tambs, K., Harris, J.R. and Magnus, P., 2004. Otitis media: genetic factors and sex differences. Twin Research and Human Genetics, 7(3), pp.239-244.

Leylabadlo, H.E., Pourlak, T., Aghazadeh, M., Asgharzadeh, M. and Kafil, H.S., 2017. Extended-spectrum beta-lactamase producing gram negative bacteria In Iran: A review. African journal of infectious diseases, 11(2), pp.39-53.

Lieberthal, A.S., Carroll, A.E., Chonmaitree, T., Ganiats, T.G., Hoberman, A., Jackson, M.A., Joffe, M.D.,

Miller, D.T., Rosenfeld, R.M., Sevilla, X.D. and Schwartz, R.H., 2013. The diagnosis and management of acute otitis media. Pediatrics, 131(3),pp.e964-e999.

Loy, A.H.C., Tan, A.L. and Lu, P.K.S., 2002. Microbiology of chronic suppurative otitis media in Singapore. Singapore medical journal, 43(6), pp.296-299.

MacFaddin, J.F. 2000. Biochemical Tests for Identification of Medical Bacteria. 3rd Edition, Lippincott Williams & Wilkins, Philadelphia.

Magiorakos, A.P., Srinivasan, A., Carey, R.B., Carmeli, Y., Falagas, M.E., Giske, C.G., Harbarth, S., Hindler, J.F., Kahlmeter, G., Olsson-Liljequist, B. and Paterson, D.L. 2012. Multidrug-resistant, extensively drug-resistant and pandrug-resistant bacteria: an international expert proposal for interim standard definitions for acquired resistance, Clinical microbiology and infection, 18(3), pp.268-281.

Mansoor, T., Musani, M.A., Khalid, G. and Kamal, M., 2009. Pseudomonas aeruginosa in chronic suppurative otitis media: sensitivity spectrum against various antibiotics in Karachi. J Ayub Med Coll Abbottabad, 21(2), pp.120-3.

Marom, T., Nokso-Koivisto, J. and Chonmaitree, T., 2012. Viral–bacterial interactions in acute otitis media. Current allergy and asthma reports, 12(6), pp.551-558.

Morris, P.S. and Leach, A.J., 2009. Acute and chronic otitis media. Pediatric Clinics, 56(6), pp.1383-1399.

Muluye, D., Wondimeneh, Y., Ferede, G., Moges, F. and Nega, T., 2013. Bacterial isolates and drug susceptibility patterns of ear discharge from patients with ear infection at Gondar University Hospital, Northwest Ethiopia. BMC Ear, Nose and Throat Disorders, 13(1), p.10.

Mushi, M.F., Mwalutende, A.E., Gilyoma, J.M., Chalya, P.L., Seni, J., Mirambo, M.M. and Mshana, S.E., 2016. Predictors of disease complications and treatment outcome among patients with chronic suppurative otitis media attending a tertiary hospital, Mwanza Tanzania. BMC Ear, Nose and Throat Disorders, 16(1), p.1.

Nazir, A. and Kadri, S.M., 2014. Aerobic bacteriology of chronic suppurative otitis media: a hospital based study. Int J Res Med Sci, 2(4), pp.1521-5.

Nwabuisi, C. and Ologe, F.E., 2002. Pathogenic agents of chronic suppurative otitis media in Ilorin, Nigeria. East African medical journal, 79(4), pp.202-205.

Nwokoye, N.N., Egwari, L.O., Coker, A.O., Olubi, O.O., Ugoji, E.O. and Nwachukwu, S.C.U., 2012. Predisposing and bacteriological features of otitis media. African Journal of Microbiology Research, 6(3), pp.520-525.

Ogbogu, P.I., Eghafona, N.O. and Ogbogu, M.I., 2013. Microbiology of otitis media among children attending a tertiary hospital in Benin City, Nigeria. Journal of Public Health and Epidemiology, 5(7), pp.280-284.

Ogefere, H.O., Aigbiremwen, P.A. and Omoregie, R., 2015. Extended-spectrum beta-lactamase (ESBL)–producing Gram-negative isolates from urine and wound specimens in a tertiary health facility in southern Nigeria. Tropical Journal of Pharmaceutical Research, 14(6), pp.1089-1094. Chamberlain, N.R., 2009. Medical microbiology, chapter 11, McGraw –hill companies pp115-119.

Paterson, D.L. and Bonomo, R.A., 2005. Extended-spectrum β-lactamases: a clinical update. Clinical microbiology reviews, 18(4), pp.657-686.

Pincus, D.H. 2006. Microbial identification using the bioMérieux Vitek® 2 system, Encyclopedia of rapid microbiological methods, 1, pp.1-32.

Prakash, R., Juyal, D., Negi, V., Pal, S., Adekhandi, S., Sharma, M. and Sharma, N., 2013. Microbiology of chronic suppurative otitis media in a tertiary care setup of Uttarakhand state, India. North American journal of medical Sciences, 5(4), p.282.

Qureishi, A., Lee, Y., Belfield, K., Birchall, J.P. and Daniel, M., 2014. Update on otitis media–prevention and treatment. Infection and drug resistance, 7, p.15.

Sah, B.P., Chettri, S.T., Bhattarai, N.R., Shah, S.P., Paudel, D., Sarraf, D.P. and Mishra, S., 2020. Microbiological profile and their antibiotic sensitivity pattern in patients of chronic suppurative otitis media at eastern tertiary care center of Nepal. IP Journal of Otorhinolaryngology and Allied Science, 3(3), pp.86-90.

Sahu, M.C. and Swain, S.K., 2019. Surveillance of antibiotic sensitivity pattern in chronic suppurative otitis media of an Indian teaching hospital. World Journal of Otorhinolaryngology-Head and Neck Surgery, 5(2), pp.88-94.

Saleh, I.A., Saleh, I.A.A., Saleh, N.A.A. and Mb, M.S., 2014. Bacteria and fungi associated with Acute Otitis media. Int J Curr Eng Technol, 4(1), pp.316-318.

Seid, A., Deribe, F., Ali, K. and Kibru, G., 2013. Bacterial otitis media in all age group of patients seen at Dessie referral hospital, North East

Ethiopia. Egyptian Journal of Ear, Nose, Throat and Allied Sciences, 14(2), pp.73-78.

Shyamala, R. and Reddy, P.S., 2012. The study of bacteriological agents of chronic suppurative otitis media–aerobic culture and evaluation. J Microbiol Biotechnol Res, 2, pp.152-62.

Sierra, A., Lopez, P., Zapata, M.A., Vanegas, B., Castrejon, M.M., DeAntonio, R., Hausdorff, W.P. and Colindres, R.E., 2011. Non-typeable Haemophilus influenzae and Streptococcus pneumoniaeas primary causes of acute otitis media in colombian children: a prospective study. BMC infectious diseases, 11(1), p.4

Tesfa, T., Mitiku, H., Sisay, M., Weldegebreal, F., Ataro, Z., Motbaynor, B., Marami, D. and Teklemariam, Z., 2020. Bacterial otitis media in sub-Saharan Africa: a systematic review and meta-analysis. BMC Infectious Diseases, 20(1), pp.1-12.

Uyanga, F.Z., Ekundayo, E.O., Nwankwo, E.O. and Inimfon, A.I., 2019. Evaluation of CHROMagar ESBL and Double Disk Synergy Test (DDST) for Screening of Extended Spectrum Beta-lactamase Producing Uropathogens in South-South Nigeria. Journal of Advances in Microbiology, 17(4), pp.1-11.

Vaidya, K., Madhup, S.K., Shrestha, B.L., Gautam, A. and Tuladha, N.R., 2015. Bacteriological and mycological profile of chronic suppurative otitis media among patients visiting Dhulikhel Hospital. Annals of Clinical Chemistry and Laboratory Medicine, 1(1), pp.37-41.

Verhoeff, M., van der Veen, E.L., Rovers, M.M., Sanders, E.A. and Schilder, A.G., 2006. Chronic suppurative otitis media: a review. International journal of pediatric otorhinolaryngology, 70(1), pp.1-12

Vijayvargiya, V., Gupta, S., Goyal, J., and Kumar, U., 2016. Chronic Otitis Media- Bacteriological Spectrum and Antibiogram. IOSR Journal of Dental and Medical Sciences (IOSR-JDMS), 15(12), PP. 95-98.

Wasihun, A.G. and Zemene, Y., 2015. Bacterial profile and antimicrobial susceptibility patterns of otitis media in Ayder Teaching and Referral Hospital, Mekelle University, Northern Ethiopia. SpringerPlus, 4(1), p.701.

Worku, M. and Bekele, M., 2014. Bacterial isolate and antibacterial resistance pattern of ear infection among patients attending at Hawassa university referral Hospital, Hawassa, Ethiopia. Indian J Otol, 20(4), p.155.

ZANCO Journal of Pure and Applied Sciences
The official scientific journal of Salahaddin University-Erbil
https://zancojournals.su.edu.krd/index.php/JPAS

ISSN (print):2218-0230**, ISSN (online):** 2412-3986**, DOI: http://dx.doi.org/10.21271/zjpas**

RESEARCH PAPER

Distribution and structure of aphid and their parasitoids community in the Kurdistan Region-Iraq

Srwa K. Bandyan [1,2]*, Nawzad B. Kadir [2] , Wolfgang H. Kirchner[1]

[1] Faculty of Biology and Biotechnology, Ruhr University Bochum, Universitätsstraße 150, 44801 Bochum, Germany.
[2] Department of Plant Protection, College of Agriculture Engineering Sciences,Salahaddin University-Erbil, Kurdistan Region, Iraq.

***** Faculty of Biology and Biotechnology, Ruhr University Bochum, Universitätsstraße 150, 44801 Bochum, Germany.

*Department of Plant Protection, College of Agriculture Engineering Sciences ,Salahaddin University-Erbil, Kurdistan Region, Iraq.

A B S T R A C T

Aphids are significant pests to many host plant species throughout the world. Aphids are on the other hand parasitized by a variety of parasitoid wasps which can potentially be used as biocontrol agents. The focus of the present study is on the pattern and distribution of the aphids and their parasitoids in the Kurdistan region in the northern part of Iraq. A field study was conducted at four locations with different bio-geographic elements and climatic conditions on several different host plant species. It turned out that the highest number of aphids and parasitoids was recorded in Darbandi Gomaspan and the lowest number of aphid and parasitoids was in Choman. Number of parasitoids were generally lower than the number of aphids. The parasitoids presented in this work have been reared from 13 aphid host taxa occurring on plants sampled from different locations. Most of the species of parasitoids belonging to the families Braconidae and Aphelinidae. The results of this study can be considered as a first data on the population of aphids and their parasitoids in this region. Further research will be undertaken for promising the biological control of aphid pests in this region.

KEY WORDS: Aphid population, bio-geographical, cultivate plant, weed
DOI: http://dx.doi.org/10.21271/ZJPAS.33.4.3
ZJPAS (2021), 33(4); 26-35 .

1. INTRODUCTION

Aphids are common terrestrial pest species and can be found in everywhere in the world and exploit a large group of host plant species (Blackman and Estop, 2006; Völkl *et al*., 2007; Guerrieri and Digilio, 2008).

Due to their reproduction potential, they often give rise to large populations which are considered as good resources for many natural enemies, including hymenopteran parasitoids (Le Ralec *et al*., 2010). Hymenopteran parasitoids of aphids are found in two taxa, the sub-family Braconidae and the genus *Aphelinus* (Hymenoptera: Aphelinidae). These two taxa are

* **Corresponding Author:**
Srwa Bandyan
E-mails: Srwa.bandyan@rub.de
Article History:
Received: 26/02/2021
Accepted: 06/05/2021
Published:18/08/2021

endoparasitoid and specialized on aphids (Starý 1970,1988; Boivin *et al*., 2012). The wasps lay eggs inside the body of aphid larvae and adult aphids causing mortality of aphids at the end of the larval development of the parasitoid (O'Donnell, 1987). There are many biotic and abiotic factors that lead to dense aphid populations (Foyer *et al*., 2016). The most important factors are the host plant specialization and climatic conditions, however, these factors effect on the populations of parasitoids as well (Le Ralec *et al*., 2010). Kurdistan region is well-known with the complex biodiversity due to its climatic conditions and biogeographic area in Iraq. It is considered a significant habitat, where many herbivores with their natural enemies can be found including aphid and their parasitoids. There are few investigations that have been conducted on the aphid parasitoids in Iraq (Starý, 1969; Al-Azawi, 1970; Starý and Kaddou, 1971). So far, only one study has been carried out on aphids and their parasitoids in the Kurdistan region of Iraq (Bandyan *et al*., 2021).

Understanding of the parasitoid community associated with aphid pests and host plants in different habitat is crucial to conserve and enhance the native parasitoid populations and to develop biological control programs of aphid pests in this region. However, the knowledge on distribution and structure of the population of aphids and their parasitoids naturally active on different host plants (cultivated and non-cultivated) in different climatic conditions in this region is lacking so far. Therefore, the aim of this study was to evaluate the distribution and population of the aphids and their parasitoids covering most of the crops and non-cultivated (weed) plants around the field as well in different biogeographical areas in the Kurdistan region and to provide information about the population structure to compare their diversity in various areas and host plants as a background for further research for promising the biological control of aphid pests in this region.

2.MATERIALS AND METHODS

2.1. Study area

The field survey was carried out from April to July 2017 at four various locations within the Kurdistan region of northern Iraq (Erbil, Darbandi Gomaspan, Harir and Choman) (Figure1), which is representative different agroecosystem in the region lowland and mountainous area, covering the altitudes range from 430 to 950 meters above mean sea level.

2.2. Field collection

Fields were regularly examined twice a month for collection aphids and their parasitoids on several host plants cultivated and non-cultivated plants including *Vicia faba* L., *Solanum melongena* L., *Sorghum bicolor* L., *Capsicum annuum* L., *Citrullus lanatus* L., *Triticum aestivum* L., *Altheae sp* L., *Brassica nigra* L., *Carduus pycnocephalus* L., *Glycyrrhiza glabra* L., *Silybum marianum* L., *Sonchus asper* L., *Avena fatua* L., *Carthumus sp* L.. and *Pisum sp* L. during the study period.

2.3. Aphid collection methods

Samples from plants bearing aphid colonies consisting of living and mummified aphids were gently cut with scissors and put separately in paper bags with labels and transferred to the laboratory for processing. The aphid densities were assessed by visual assessment of samples. Around 100–125 leaves, straws and small branches were sampled in each field and around the area. The number of aphids (nymph, adult winged, adult alate) and mummies were recorded. A few live adult aphids were killed and preserved in 75% ethanol (Eastop and van Emden, 1972) for later identification. The aphids were identified to species level using the key of Blackman and Eastop (2000).

2.4. Rearing parasitoids

Parasitoids were reared from the live aphid samples and mummified aphids in the laboratory. Pieces of plants bearing aphid colonies (living aphid and mummies) were placed separately in plastic Petri dishes (Ø 9 cm × 1.5 cm) and kept at laboratory conditions (22°C, 65% relative humidity, 16:8 L:D photoperiod) to obtain emergence of adult parasitoids for at least 14 days post-collection (Kavallieratos *et al*., 2004). The

Petri dishes had a circular opening in their lid covered with muslin for ventilation in order to maintain conditions inside the Petri dishes similar to those existing in the laboratory room. The mummies were inspected daily for the emergence of adults. As soon as the adult parasitoids emerged, they were immediately captured using an aspirator and transferred into Eppendorf tubes containing 96 % ethanol and stored at -20°C (Tomanović *et al*., 2014) for later identification. The parasitoids specimens on crops were identified to species level using morphological as well as molecular traits (Bandyan *et al*. 2021). Parasitoids reared on weeds were identified morphologically on subfamily level and then classified just as morphospecies.

2.5. Data analysis

Data were analysed by one-way ANOVA in SPSS© version 21. Significant differences between host plants and date of collection according to the locations and descriptive methods were used to calculate the means and standard deviation.

3.RESULTS

3.1. Aphid and parasitoids per site

A total of 14454 aphids and 3164 parasitoid wasps were collected during the sampling survey on several different crop and weed plants. Generally, the results showed that the aphids are more abundant than their parasitoids. The highest mean number of aphids and parasitoids was collected from Darbani Gomaspan (66.7 and 17.6) respectively and lowest mean number of aphid and parasitoids was sampled from Choman (8.93 and 25.0) respectively. There was a significant difference between the populations of aphids and their parasitoids in all locations (Table1: one-way ANOVA: P< 0.001).

Table 1: Mean (±SD) aphid and parasitoids densities according to the locations in the Kurdistan Region.

Locations	Total of Aphids	Mean ±SD of aphids per plants	Parasitoids	Mean ±SD of parasitoids per plants
Erbil	3992	38.01 ± 66.46	359	3.41 ± 7.33
DarbaniGomaspan	7006	66.72 ± 123.32	1858	17.69 ± 39.82
Harir	2518	23.96 ± 54.68	682	6.49 ± 23.16
Choman	938	8.93 ± 45.10	265	2.52 ± 13.99
Kurdistan Region Total	14454	34.41 ± 81.07	3164	25.01±7.53
One way ANOVA		F (3,416) =10.30, P<0.001		F (3,416) = 8.63, P<0.001

3.2. Aphids and parasitoids per host plant

Aphids and parasitoids were collected on 15 host plant species including crop and weed plants during the survey study. In Erbil almost all host plants are attacked by aphids and parasitized by parasitoids (Figure 2a). The highest number of aphids was recorded on *Citrullus lanatus* and *Solanum melongena* 122 and 110 respectively and the mean number of parasitoids was 6.57 and 5.14 respectively. While the highest number of parasitoids was recorded on *Altheae sp.* and *Glycyrrhiza glabra* 11.7 and 11.2 respectively on which 82.8 and 76.7 aphid were recorded. In *Pisum sp.* the mean number of aphids was 4.71 but no parasitoids were recorded on the same plant. on *Carthumus sp.*, *Capsicum annuum* and *Carduus pycnocephalus* there were no specimens recorded on those plants during the study. *Vicia faba*, *Triticum aestivum*, *Sorghum bicolor*, *Silybum marianum*, *Avena fatua*, *Brassica nigra* and *Sonchus asper* the mean number of aphids were 53.1, 32.5, 47.0, 17.1, 7.71, 9.14 and 6.71 and parasitoids 6.71, 3.0, 1.0, 3.71, 0.28, 1.71 and 0.14 respectively. There is a significant difference between host plants in relation to the number of specimens in Erbil area (Figure 2a: one-way ANOVA: P< 0.001).

The maximum mean number of aphids and parasitoids recorded on *Glycyrrhiza glabra* in Darbani Gomaspan, Harir and Choman were 316, 156 and 108 and 133, 76.5 and 35.0 respectively. In Drabani Gomaspan, on *Pisum sp.* the mean number of aphids was 3.71 and no parasitoids was recorded. There were no specimens found on *Citrullus lanatus*, *Sorghum bicolor*, *Solanum melongena* and *Capsicum annuum*. The mean number of aphids and parasitoids on *Vicia faba*, *Triticum aestivum*, *Altheae sp.*, *Carthumus sp.*, *Sonchus asper*, *Silybum marianum*, *Avena fatua*, *Brassica nigra* and *Carduus pycnocephalus* were 148, 78.2, 98.5, 120, 90.2, 63.0, 17.4, 18.5 and 46.0 and 50.2, 2.8, 37.0, 8.57, 9.85, 7.85, 0.28, 3.57 and 11.4) respectively. There was a significant difference between host plants in

relation to the numbers of aphids and parasitoids in Darbandi Gomaspan. (Figure 2b: one-way ANOVA: P<0.001).

Specimens not recorded on *Vicia faba*, *Altheae sp.*, *Citrullus lanatus*, *Carthumus sp.*, *Solanum melongena*, *Silybum marianum*, *Carduus pycnocephalus* and *Pisum sp.* in Harir and Choman. As well as *Sorghum bicolor*, *Avena fatua* and *Capsicum annuum* in Choman. In Harir, the mean number of aphids and parasitoids collected on *Sorghum bicolor*, *Triticum aestivum*, *Capsicum annuum*, *Brassica nigra*, *Avena fatua* and *Sonchus asper* were 66.8, 55.8, 48.2, 19.4, 5.4, 7.85 and 5.71, 4.14, 6.57, 3.28, 0.85, 0.28 respectively. There was a significant difference between host plants and specimens in Harir (Figure 2c: one-way ANOVA: P< 0.001).
In Choman, the mean number of aphids and parasitoids on *Sonchus asper*, *Brassica nigra* and *Triticum aestivum* were 12.0, 8.57 and 4.85 and 0.57, 2.0 and 0.28 respectively. There is a significant difference between host plants and specimens in Choman (Figure 2d: one-way ANOVA: P< 0.001).

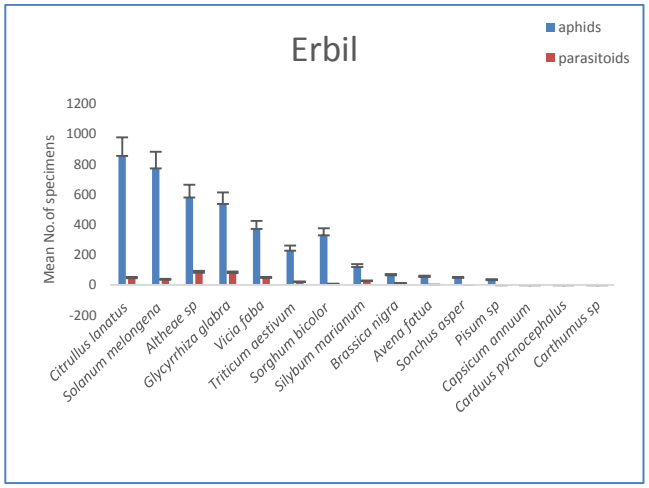

Figure 2 (a): Mean number of aphids and parasitoids on the different host plants in Erbil.

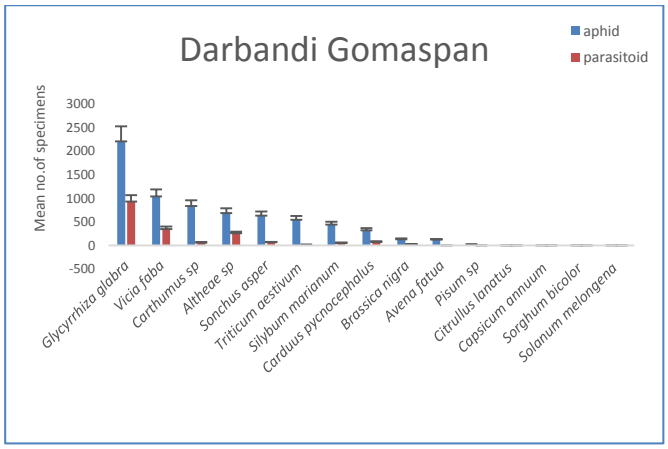

Figure 2 (b): Mean number of aphids and parasitoids on different host plants in Darbandi Gomaspan.

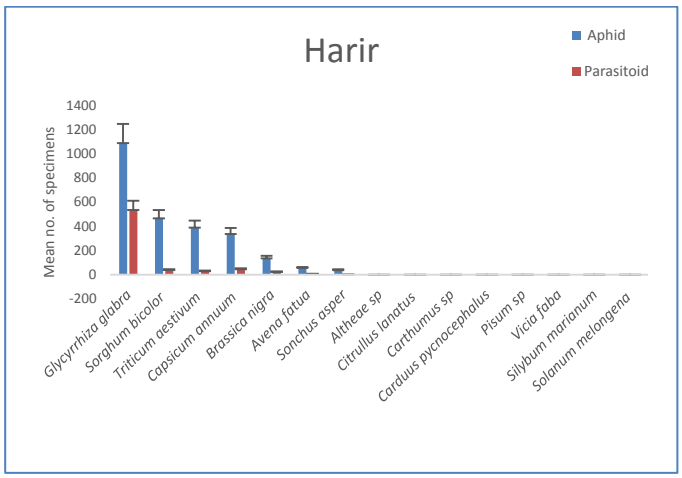

Figure 2 (c): Mean number of aphids and parasitoids on different host plants in Harir

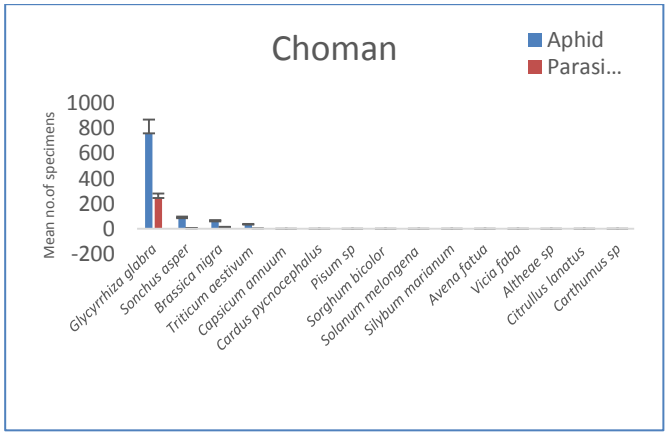

Figure 2 (d): Mean number of aphids and parasitoids on the different host plants in Choman

3.3. Aphid and parasitoids per month

The specimens were collected during cropping season from April to July 2017 in this region (Figure 3). Generally, in Erbil the mean population of aphids in the begin April was 2.13 and there were no parasitoids found. The mean number of aphids and parasitoids were dramatically increased in middle May reaching 82.3 and 6.33 respectively and the mean numbers decreased in late July to 11.8 and 1.93. In Harir, the mean number of aphids and parasitoids in begin April was 33.3 and 4.06 respectively and in middle April it decreased to 15.8 and 3.6 while the mean number of aphids increased to 31.2 in begin May and parasitoids reached to 12.2 in late May. In Darbandi Gomaspan, the mean number of aphids and parasitoids in the beginning of April was 16.1 and 12.3 respectively and then dramatically increased to 133 and 28,4 in middle May. In late July, their number decreased to 13.9 and 16.4. In Choman, there was high difference in the existed period of aphids and parasitoids compared to the previous locations, there was no specimens collected until middle May. The populations growth of aphids and parasitoids occurred in middle May 4.26 and 0.26 in this location and reached to the peak in late June 26.9 and 6.80 respectively. The number of aphid and parasitoids then decreased in late July to 9.0 and 4.0 respectively.

3.4.Parasitoids species per family

The collected parasitoids belonged to different families, two families of primary parasitoids were recorded, i.e., Braconidae and Aphelinidae, and seven families as hyperparasitoid were recorded including Eurytoimidae, Encyrtidae, Eriaporidae, Figitidae, Platygastridae, Pteromalidae and Signiphoridae. The most species were recorded in Braconidae and Aphelinidae were 7 and 4 respectively and one single species was collected for each hyperparasitoids families (Figure 4).

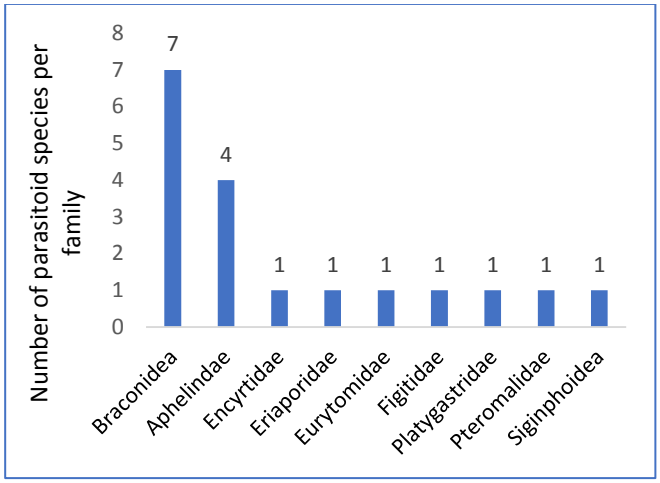

Figure 4: Parasitoids species per family

3.5. Aphid species per plant

Different aphid species were found at each host plant during the study (Figure 5). *Triticum aestivum* and *Sonchus asper* were infested by different aphid species 5 and 4 respectively, and three different aphid species were recorded on each *Carduus pycnocephalus*, *Glycyrrhiza glabra* and *Solanum melongene*. On the *Altheae sp.*, *Silybum marianum*, *Sorghum bicolor*, *Brassica nigra*, *Citrullus lanatus*, *Vicia faba*, *Carthamus sp.* and *Avena fatua* two different species were found and only one single species was found on *Pisum sp.* and *Capsicum annuum*.

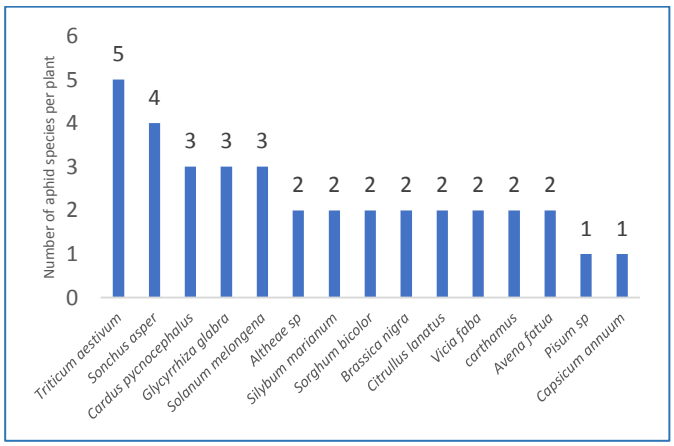

Figure 5: Aphid species per plant

4. DISCUSSION

The present study focused on the pattern of population and distribution of the aphids and their parasitoids in Kurdistan region of Iraq. Kurdistan region represents a large territory area with different bio-geographical elements and various climatic conditions.

Our assessment on the structure of population and distribution of aphid and their parasitoids indicates the most preferable climate condition and host plant species could be potentially considered to promising the biological control programs in this region.

The result of the current study indicates that abiotic factors such as climatic conditions and biogeography area are the main factor to distribution and reproduction of aphids and their parasitoids, therefore, the highest number of specimens was collected from Darbandi Gomaspan in middle and late spring, which is the suitable time for population growth and reproduction. The average temperature was 27.3 ˚C ± 1.2˚C with 55% RH and this area has favorable climatic condition and with the geographical aspect is like valley area and one side is surrounded by Safin mountain its mixture with the highland and lowland which lead to drives grow vegetation and agricultural plants. In contrast, the number of specimens were low in Choman, it is more pronoun, the climatic condition may differ considerably, the average temperature was around 20.1˚C±1.3˚C with 23% RH because it is considered the coldest area in Iraq even during the summer. According to Sigsgaard (2002) the cold weather which leads to hardly living the holocyclic aphid population and immigrating specimens to the warm area and maintaining no overwinter parasitized in this area. According to Kavallieratos *et al*. (2004) and Tomanović *et al*. (2009) in the Mediterranean climatic conditions generally favour the presence of host aphids on plants and the most suitable period for aphids infesting plant and then the parasitoids' activity is between March and June.

Aphid parasitoid species collected were mostly belonging to Aphidiinae and *Aphelinus* group which are parasitizing different aphid species on various host plants (cultivated and non-cultivated) and plants were attacked more than one aphid species during the study which is indicated that the host plant as a biotic factor has significant role to population and distribution of aphid and their parasitoids in this region. Žikić *et al.* (2017) reported that the host plants have a vital impact on the diversity of the aphids and their parasitoids. More recently, Bandyan *et al*. (2021) identified 8 species of aphids which have been parasitized by 15 species of aphid parasitoids on crops that have surveyed in this study in this region. However, it needs further study to identify the specimens that were collected on the non-cultivated plants. However, this study showed that the numerous of specimens have been collected on the non-cultivated plants for example the highest number of specimens have been collected on the *Glycyrrhiza glabra* as a non-cultivated plant that can be found around the fields and present in four locations in our study it would be preferable plant by the parasitoids this plant belonging to family Fabaceae. Considerably more work will need to be done to determine the chemical substance of this plant that might be attractive to the parasitoids. On the other hand, the high number of parasitoids on the non-cultivated plants means that the parasitoids can survive and maintain by attacking other aphid species from non-cultivated as an alternative host around the field crops. Tomanović *et al*. (2009) concluded that it is the population of large numbers of non-crop aphid hosts which leads to a build-up of many important species of parasitoids around the agroecosystems.

Additionally, Mkenda *et al*. (2019) found that field margins around fields are favorable habitats to establish a huge number of natural enemies that move to adjacent vegetable crop plants to provide biological pest control services. The current study shows that the non-cultivated plants have a significant importance to maintain the parasitoids actively in this region and support larger parasitoid populations, but aphids also profited from it, thereby counterbalancing possible biological control of aphids by parasitoids, therefore, the growers should be encouraged to avoid using herbicides and implementing agricultural practices to remove those non-cultivated plants around their fields in this region.

5. CONCLUSION

The study indicates that the Kurdistan region, as a multiple climate and geographical area and well established in local agroecosystem with the numerous of the alternative hosts that are present during the growing season which leads to grow and distribution of aphid parasitoids. The findings of this study will be taken as a basic information on the population of the aphid parasitoids in this region. In addition, this data is crucial for further study on the aphid parasitoids in more details to implement it in the biological control programs in the Kurdistan region of northern Iraq.

ACKNOWLEDGEMENTS

This study was supported by the Biology and Biotechnology Department of Ruhr University Bochum, Gremany and the Department of Plant Protection, Salahaddin University, Kurdistan Region, Iraq. We would like to thank Ali Galaly at the plant production Department, Collage of Agricultural, Kurdistan, Erbil, Iraq for their identifications of weed species. We also thank Ziwar Omer (Department of Plant Protection, Khabat Institute, Erbil Polytechnic University, Erbil, Iraq) for assistance during the study. We thank the farmers for approval to obtain the data from their fields.

RERERENCES

AL-AZAWI A.F., 1970. Some aphid parasitoids from central and south Iraq with notes on their occurrence. *Bulletin of Iraq Natural History Museum* 4,27–31.

BANDYAN S.K., PETERS R.S., KADIR N.B., FERRER-SUAY M., & KIRCHNER W.H. (2021) A survey of aphid parasitoids and hyperparasitoids (Hymenoptera) on six crops in the Kurdistan Region of Iraq. *Journal of Hymenopteran Research*,81,9-21. https://doi.org/10.3897/jhr.81.59784

BLACKMAN R.L., & EASTOP V.F. 2006. Aphids on the World's Herbaceous Plants and Shrubs. Chichester, Wiley, John Wiley and Sons, Ltd. 1439 pp.

BLACKMAN R L., & EASTOP V.F. 2000 Aphids on the World's Crops: An Identification and Information Guide (2nd edn.). Wiley, Chichester, 466 pp.

BOIVIN G., HANCE T., & BRODEUR J. 2012. Aphid parasitoids in biological control. Canadian. *Journal of Plant Science*, 92(1),1-12. https://doi.org/10.4141/cjps2011-045

EASTOP V.F, & VAN EMDEN H.F. 1972. The insect material. In: van Emden HF, Editor. Aphid technology 1-45.

FOYER C.H., RASOOL B., DAVEY J.W., & HANCOCK R.D. 2016. Cross-tolerance to biotic and abiotic stresses in plants: a focus on resistance to aphid infestation. *Journal of Experimental Botany*, 67(7), 2025–2037, https://doi.org/10.1093/jxb/erw079

GUERRIERI E., & DIGILIO M.C. 2008. 'Aphid-plant interactions: a review'. *Journal of Plant Interactions*, 3 (4), 223-232.

KAVALLIERATOS N.G., TOMANOVIĆ Z., STARÝP., ATHANASSIOU C.G., SARLIS G.P., PETROVIC O., & VERONIKI M.A., 2004. A survey of aphid parasitoids (Hymenoptera: Braconidae: Aphidiinae) of Southeastern Europe and their aphid-plant associations. *Applied Entomology and Zoology*, 39(3),527-563 https://doi.org/10.1303/aez.2004.527

LE RALEC A., ANSELME C., OUTREMAN Y., POIRIE M., VAN BAAREN J., LE LANN C., & JACQUES J.M. 2010. Evolutionary ecology of the interactions between aphids and their parasitoids. Comptes rendus biologies. 333(6-7), 554-565.

MKENDA P.A., NDAKIDEMI P.A., STEVENSON P.C., ARNOLD S.E., BELMAIN S.R., CHIDEGE M., & GURR G.M. 2019. Field margin vegetation in tropical African bean systems harbours diverse natural enemies for biological pest control in adjacent crops. Sustainability, 11(22), 6399.

O'DONNELL D.J., 1987. Larval development and the determination of the number of instars in aphid parasitoids (Hymenoptera: Aphidiidae). *International Journal of Insect Morphology and Embryology*, 16, 3-15.

SIGSGAARD L., 2002. A survey of aphids and aphid parasitoids in cereal fields in Denmark, and the parasitoids' role in biological control. *Journal of Applied Entomology* 126(2/3), 101– 107. https://doi.org/10.1046/j.1439-0418.2002.00611.x

STARÝ P., & KADDOU I.K., 1971. Fauna and distribution of aphid parasites (Hym., Aphidiidae) in Iraq. Acta Faunistica Entomologica Musei Nationalis Pragae 14,179-197.

STARÝ P., 1969. Aphids-ant-parasite relationship in Iraq. *Insectes Sociaux* 4, 269-278.

STARÝ P., 1970. Biology of Aphid Parasites (Hymenoptera: Aphidiidae) With Respect to Integrated Control. Series Entomologica 6. Junk, The Hague.

STARÝ P., 1988. Aphidiidae. in Minks AK and Harrewijn P (eds) Aphids: their Biology, Natural Enemies and Control, Volume 2B. Elsevier, New York, 171-184.

TOMANOVIĆ Z., PETROVIC A., MITROVIC M.,

KAVALLIERATOS N.G., STARÝ P., RAKHSHANI E., RAKHSHANIPOUR M., POPOVIC A., SHUKSHUK A.H., & IVANOVIC A. 2014. Molecular and morphological variability within the Aphidius colemani group with redescription of Aphidius platensis Brethes (Hymenoptera: Braconidae: Aphidiinae). *Bulletin of Entomological Research* (104), 552-565. https://doi.org/10.1017/S0007485314000327

TOMANOVIĆ Ž., KAVALLIERATOS N.G., STARÝ P., STANISAVLJEVIC L.Ž., ĆETKOVIĆ A., STAMENKOVIĆ S., & ATHANASSIOU C.G. 2009. Regional tritrophic relationship patterns of five aphid parasitoid species (Hymenoptera: Braconidae: Aphidian) in agroecosystem-dominated landscapes of south-eastern Europe. *Journal of economic Entomology*, 102(3), 836-854.

VÖLKL W., MACKAUER M., PELL J.K., & BRODEUR J. 2007. Predators, Parasitoids and Pathogens. In: van Emden H, Harrington R (Eds) Aphids as Crop Pests. CABI International, 47pp.

ŽIKIĆ V., LAZAREVIĆ M., & MILOSEVIĆ D. 2017. Host range patterning of parasitoid wasps Aphidiinae (Hymenoptera: Braconidae). Zoologischer Anzeiger 268, 75–83. https://doi.org/10.1016/j.jcz.2016.10.001

Figure 1. Study sites in Northern Iraq, Kurdistan region (Red dots).

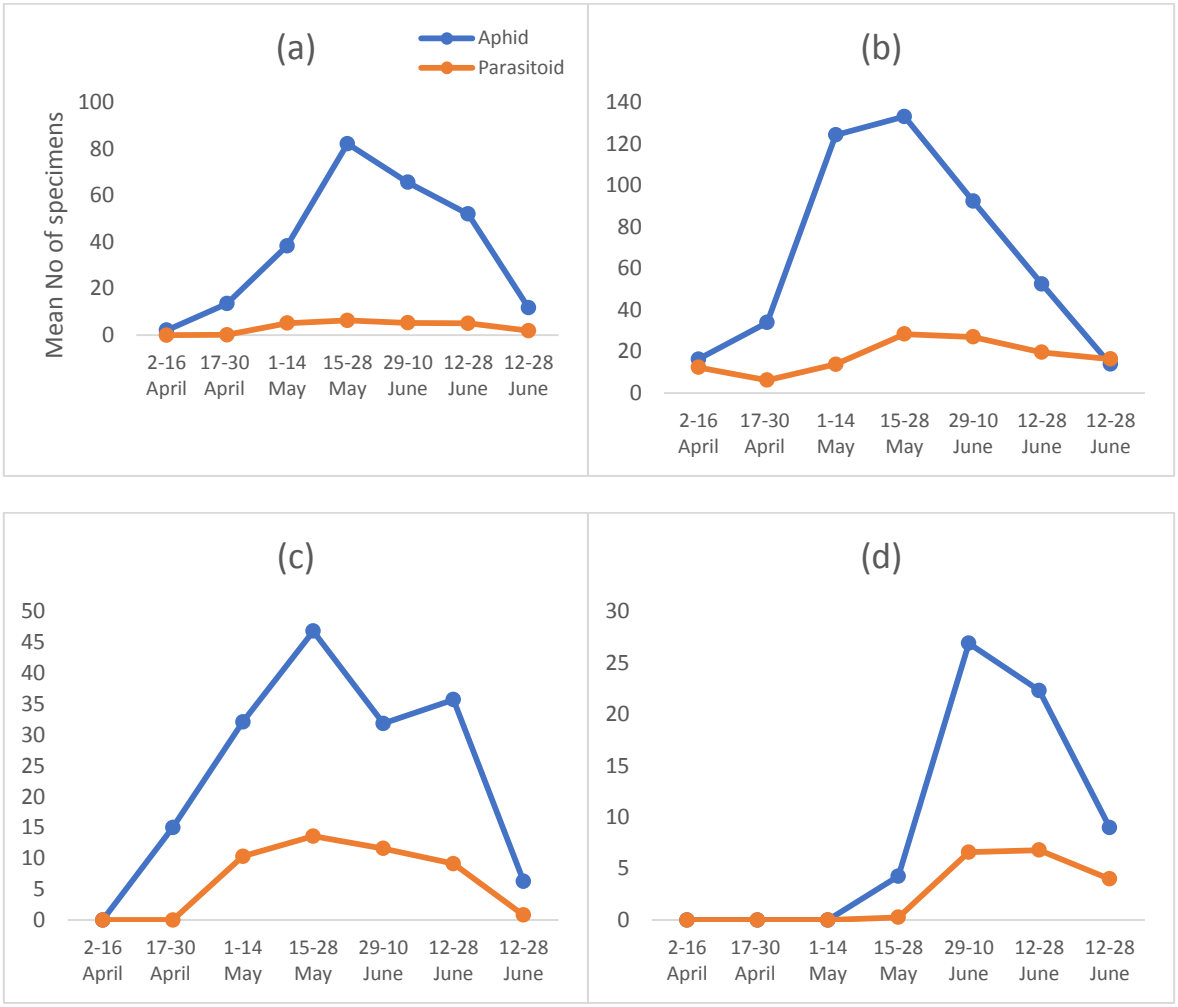

Figure 3: Mean number of aphids collection and their parasitoids during the study period in (a) Erbil, (b) Darbandi Gomaspan, (c) Harir, (d) Choman in Kurdistan Region.

ZANCO Journal of Pure and Applied Sciences
The official scientific journal of Salahaddin University-Erbil
https://zancojournals.su.edu.krd/index.php/JPAS

ISSN (print): 2218-0230**, ISSN (online):** 2412-3986**, DOI: http://dx.doi.org/10.21271/zjpas**

RESEARCH PAPER

Molecular Diagnosis of Fasciola hepatica in livestock using cox1 gene in Erbil Provence- Kurdistan Region/ Iraq

Muhammad J. Muhammad and Zuber I. Hassan
Department of Medical Laboratory Techniques, Shaqlawa Technical College, Erbil Polytechnic University, Erbil, Kurdistan Region-Iraq.

A B S T R A C T:

52 *Fasciola hepatica* worms (22 sheep, 3 goats and 27 cattle) from livers and bile ducts were collected. The prevalence rate of Fascioliasis was 7.28%, 3.37% and 10.19%, respectively. Among the three hosts regarding the sex, females of sheep and goats show a higher infection rate than males (4.3% and 2.25% versus 2.98% and 1.12%). Simultaneously, the prevalence rate was slightly higher in female cattle (5.28%) than male cattle (4.91%). Used the adult worms for DNA extraction followed by PCR amplification. The sequences of amplified products were identified under accession number (MT951586) of sheep were 99.51%, and (MT951587) of goat was 99.75% homologous to Iranian goat *Fasciola hepatica* (KF992219). Furthermore, the cattle *Fasciola hepatica* (MT951585) was 99.2% homologous with the reference of Iranian goat. Using phylogenetic tree analysis, isolated *F. hepatica* in sheep, goats, and cattle is positively related to various global *F. hepatica*.

KEY WORDS: *F.heatica, Cox1 gene, phylogenetic tree, Erbil Province* .
DOI: http://dx.doi.org/10.21271/ZJPAS.33.4.4
ZJPAS (2021), 33(4); 36-42 .

1.INTRODUCTION :

Fasciola hepatica and *Fasciola gigantica* are two liver-flukes, and it is a zoonotic parasitic disease causing Fascioliasis (Zekarias and Bassa, 2019), which is distributed worldwide infecting sheep, goats, cattle, deer, and humans as final hosts (Moazeni et al., 2012, Sah et al., 2018). *F. hepatica* is a helminths parasite of animals belong to class Trematoda (Sah et al., 2018, Munita et al., 2019). It's localized in the liver's bile duct cause mortality in domestic ruminants and lead to significant economic losses (Magaji et al., 2014). Vast numbers of infective parasite platforms can cause a highly pathogenic sub-acute presentation in lambs, characterized by hepatic haemorrhage and lesions, resulting in immediate death (Nasr et al., 2016).

Chronic fasciolosis, showing reduced weight gain, anaemia, decreased fertility, reduced milk production and reduced feed conversion efficiency (Kantzoura et al., 2011, Munita et al., 2019). As is understood, the classification of the *Fasciola species* can't be performed by clinical, pathological, or immunological techniques. Serological findings do not differentiate between these species (Amor et al., 2011, Alajmi, 2019). Different molecular methods were employed in the analysis, taxonomy, and *fasciola* studies like complete genome sequencing and single nucleotide polymorphism (Moazeni et al., 2012, Raoof et al., 2020). The PCR amplification method improves many templates for initial priming that allow the primers to anneal the known conserved regions to amplify across unknown variable regions and better diagnose species (Eman et al., 2016, Mohammed et al., 2016, Hassan, 2018). Also, the intraspecific

* **Corresponding Author:**
Muhammad J. Muhammad
E-mail: Muhamad.jamal@epu.edu.iq
Article History:
Received: 28/01/2021
Accepted: 10/05/2021
Published: 18/08 /2021

genetic variations between liver flukes may show differences in virulence, host specificity and drug susceptibility or resistance.

Some genetic variation within *F. hepatica* and *F. gigantica* sequences of the mitochondrial DNA and ribosomal regions have been described previously from Iraq (Mohammed et al., 2016, Hamoo et al., 2019), Iran (Galavani et al., 2016, Baran et al., 2017), Turkey (Erensoy et al., 2009), Saudi Arabia (Shalaby and Gherbawy, 2013) and Egypt (Dar et al., 2012). Hence, this study aimed to investigate the genetic structure of the flukes using *cox1* sequences. *Compared Fasciola* populations from the three definitive host species to find host-specific genetic structures in Erbil Province, to assess their phylogenetic analysis.

2. Materials and procedures

2.1- Parasite specimen:

The total livers of 656 slaughtered livestock (sheep (n=302), goats (n=89), and Cattle (n=265)) were carefully inspected visually (Hassan et al., 2017), and then the hepatic parenchyma was cut and squeezed directly towards the bile duct with both hands and the flukes getting out of the vents (Hamed et al., 2014). *Fasciola* specimens (n=52) were obtained from the bile duct or liver tissue of freshly slaughtered sheep, goats and cattle at regional slaughterhouses in Erbil province, Kurdistan Region-Iraq among July to November 2020. Flukes were morphologically classified as *Fasciola sp.* according to present keys and descriptions (Hamed et al., 2014, Piri et al., 2018, Hamoo et al., 2019). After collection, washed them thoroughly in Phosphate Buffer Saline (PBS), then fixed in 70 % ethanol.

2.2- Extraction of DNA and amplification of PCR

The posterior sections (without the uterus) of the samples were applied for DNA extraction, to avoid sampling sperm from another fluke (Tadayon et al., 2015). About 15 mg of adult *fasciola* worms were separated and crashed between two microscopic glass slides. The ethanol in each sample was allowed to evaporate for a few minutes and rinsed with PBS three times reference?. According to the manufacturer's directions, whole DNA was extracted utilizing the Wizard Genomic DNA Purification Kit (Promega). DNA was eluted in 100µL of elution buffer and stored at -20^{o}C till use. PCR was done according to the subsequent protocol: The fragment of *Cox1* was amplified applying the primers set Ita 8 (forward; 5`-ACGTTGGATCATAAGCGTGT-3` and Ita 9 (reverse; 5`-CCTCATCCAACATAACCTCT-3`) as explained by (Farjallah et al., 2013). Made PCR reactions (25 μl) with 3µl of DNA template, 12.5µl of (2X) Go-Tag master mix, 30 pmol (3µl) of each primers and 3.5µl nuclease-free water. Performed amplification result with the following conditions: Primary denaturation at 94^{0}C for 90 seconds was replaced by 33 cycles each at 94^{0}C for 90 seconds, annealing temperature 55^{0}C for 90 seconds, and extension at 72 for 120 seconds, the last step is the extension at 72^{0}C for 10 minutes.

2.3- Sequencing and Accession numbers:

The PCR product of all samples were loaded in 1.5% (w/v) agarose gels in tris-borate-EDTA (TBE) buffer staine with ethidium bromide. The electrophoresis is carried out for 45 min at 100 V and DNA was visualized under UV transilluminator, and the bands were visualized (figure 1) The amplified results were commercially sequenced in both directions (Macrogen Inc. South Korea). The DNA sequences undergo help analysis by applying bioinformatics tools and nucleotide alignment employing ClustalW (http://www.ebi.ac.uk/clustalw) for specific DNA sequence query (Thompson et al., 1997) and the identity matrix options of Bioedit (Hall, 1999), respectively. Saved the partial *Cox1* gene of the *F. hepatica* in the GenBank database below accession numbers MT951585- MT951587 through BLAST algorithm (http://www.ncbi.nlm.nih.gov/BLAST). The phylogenic studies of *Cox*1 sequence data were carried by maximum likelihood using MEGA6 (Tamura et al., 2013).

2.4- Data analysis and presentation

MS Excel 2010 used for data entry and statistical analysis was performed using the t-test and Chi-square (X_2) test to discover the likelihood value (p-value) applying the graph pad prism 8.0.1.

3.Results and Discussion

The infection rate of fasciolosis in sheep, goats and cattle were 7.28%, 3.37% and 10.19% respectively as shown in Table 1. The result agreed with (Kordshooli et al., 2017) in Iran, who

detected that the prevalence rate of *F. hepatica* were 5.22% of sheep, 2.15% of goat, and 11.15% of cattle. *Fasciola species* are usually found in herbivores in various parts of Iraq (Hamoo et al., 2019, Raoof et al., 2020, Abdulwahed and Al-Amery, 2019). The observation could be a return to husbandry practices and climatic variation including rain and warmth which had significant effects on the remainder of both intermediate host and the larval stages (miracidium and cercariae) of the parasite. Other factors; soil effect according to the epidemiological aspects of fasciolosis, distribute intermediate host in the environment (Kordshooli et al., 2017). In this study, The prevalence was higher in cattle, followed by sheep and goats, which may be due to free-ranged pasture grazing. But sheep and goats held either tethered or free-ranged, and the prevalence was distinctly higher in free-ranged than tethered. It may be due to exposing more further contact to the hazard factors such as the presence of metacercaria (Oryan et al., 2011, Yadav et al., 2015). The results were interpreted according to the infection rate among each host's males and females individually from the total number of all investigated livestock. Discovered the highest rate of infection in female sheep and goats 13(4.3%), 2(2.25%) as distinguished to male sheep and goats 9(2.98%), 1(1.12%), respectively. The results agreed with (Isah, 2019), who showed that female sheep and goats reported higher prevalence (44.6% and 42.6%) than males (30.7% and 30.4%) respectively; this variation could be since females stay longer in flock/herd for reproduction and breeding. Simultaneously, the prevalence rate was slightly higher in female cattle (5.28%) versus male cattle (4.91%) as revealed in table 2. Statistically, there was no significant variation (P= 0.8143) between all studied hosts. These agreed with (Yadav, 2015), who revealed that the female cattle 42 (82.3%) were more acceptable to infected in compared to the males 9 (17.7%). But the results disagreed with (Isah, 2019), who showed that the male cattle were more infected (55.3%) than female's cattle (41.3%). The potential reason may be that, sexes are travelling together for food and water and that thus the risk of infection is high for both sexes. (Magaji et al., 2014).

Table 1: prevalence of *F.hepatica* among slaughtered sheep, goat and cattle in new Erbil Slaughtered house

Hosts	Examined number	Number of infected Fasciolosis	Percentage (%)
Sheep	302	22	7.28
Goats	89	3	3.37
Cattle	265	27	10.19
Total	656	52	7.93

Table 2: The Prevalence of Fasciolosis among all slaughtered animals of both sexes

Hosts	No of slaughtered male animals	No of infected male animals	Prevalence (%)	No of slaughtered female animals	No of infected female animals	Prevalence (%)
Sheep	189	9	2.98	113	13	4.30
Goats	51	1	1.12	38	2	2.25
Cattle	187	13	4.91	78	14	5.28
Total	427	23	3.51	229	29	4.42

Statistically significant ($P < 0.05$)

In the current study, adult individuals of *Fasciola species* were found from the liver of sheep, goats, and bile ducts of infected cattle. It is subjected to confirmation with the taxonomic key (Yakhchali et al., 2015). Previously, PCR technology and DNA sequencing technologies have been facilitated to identify Trematoda species' analysis (Abdulwahed and Al-Amery, 2019), especially the partial mt genes like *Cox1* (Moazeni et al., 2012, Meshgi et al., 2017, Buathong et al., 2019). In the present study, multiple alignments compared with Trematoda references (KF992219) available in the NCBI database (Shafiei et al., 2014). The results of *Cox1* sequence analysis showed that the species of *F. hepatica* under the accession no. MT951586 in sheep was 99.51% homologous to Iranian goat *Fasciola hepatica* (KF992219) due to nucleotide substitution (T-G) at positions 254 and (A-G) at position 320. On the other hand, MT951587 of goat was 99.75% homologous to KF992219; due to nucleotide substitution (A-G) at position 320. Furthermore, the cattle *F. hepatica* (MT951585) was 99.2% homologous with the reference of Iranian goat, as shown in figure 2. The *Cox1* gene can be applied to properly identify *Fasciola species* and become a valuable tool for the specific diagnosis of the liver fluke causal factor of Fascioliasis in livestock (Simsek et al., 2011). The sequence of *Cox1* gene with only nucleotide polymorphism could be due to hybrids in our isolates, as mentioned by (Bozorgomid et al., 2020), the advantage of low substitution rate genes making it easier to interpret mixed infections (Amor et al., 2011). Figure 3 shows that the phylogenetic analysis of the *Cox1* gene sequence and the worms' species were identical to gene sequences from *F. hepatica* accession no. MK447946, LC273112, LC485089, KT893716, AB207170, AB553810 and KF992219 recovered from Iran, Egypt, Algeria, Iran and Japan, respectively. Phylogenetic analyses help understand population differentiation, species formation and ecological adaptation (Lotfy et al., 2008). Still, it was difficult to identify exactly genotype utilizing a host, suggesting that host associations are not suitable for *Fasciola* genotype classification (Tadayon et al., 2015).

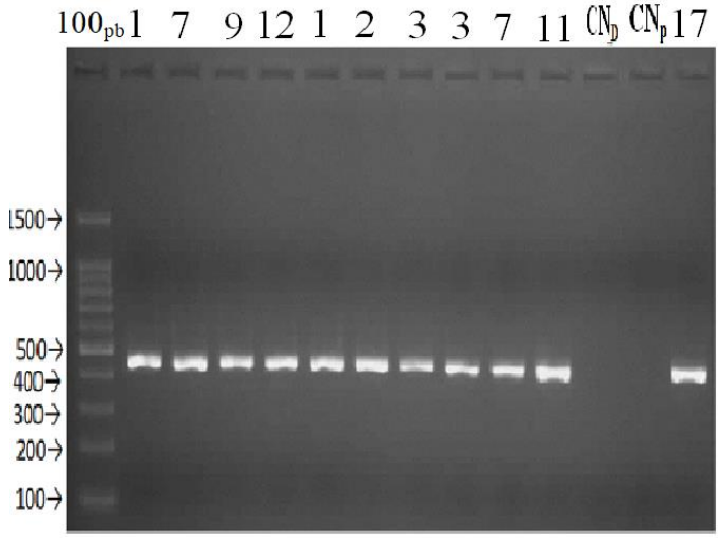

Figure 1: Amplified Cox1 region in agarose gel electrophoresis. Lanes (1,7, 9 and 12) denote sheep fluke samples, (1 to 3) denote goat fluke samples, (3,7,11 and 17) denote cattle fluke samples amplified as a single band of 425 bp; CN_D denotes DNA extraction negative control; CN_P denote PCR negative control, and 100_{bp} denote 100bp ladder molecular weight marker.

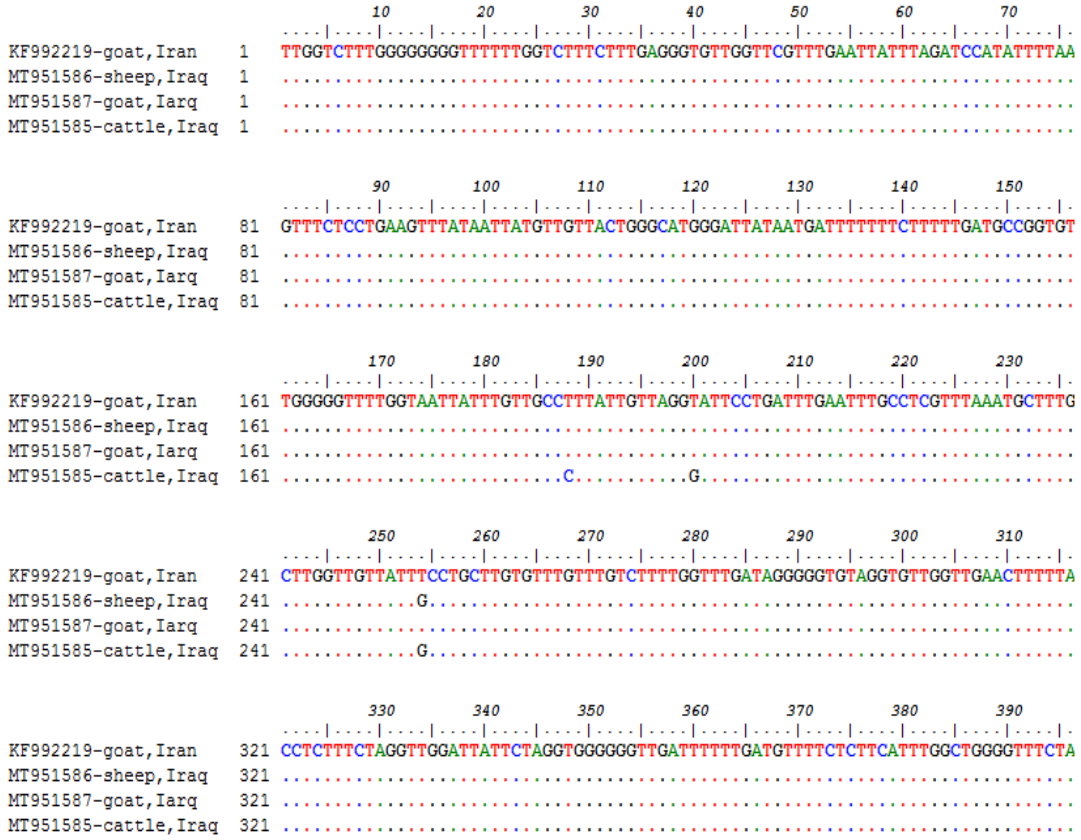

Figure 2: multiple Alignment of detected *Fasciola hepatica* with the (KF992219) (Shafiei et al., 2014). (Shafiei et al., 2014) Dots represent sequence similarities

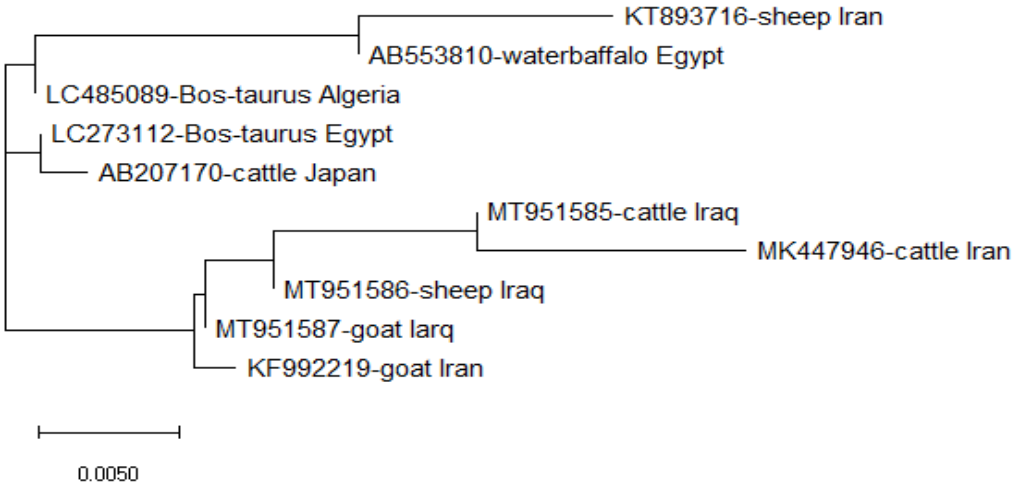

Figure 3: The nucleotide sequences of the partial *Cox1* and the adjacent procedure are a phylogenetic tree of *F. hepatica*. Molecular analysis reveals that among Iraqi *F. Hepatica* people three separate genotypes.

4.Conclusion:

According to this study, the direct inspection method is still the best approach for estimating the prevalence of liver fluids in animals. More steps are recommended to formulate appropriate control strategies to decrease diseases and financial loss due to the condemnation of infected livers in Erbil Province. The current investigation also showed that *Fasciola* isolates from domesticated animals were *F. hepatica* by using molecular methods. Classification of F. hepatica based on *cox1* genes sequencing method is an accurate, simple, quick, and available tool that can differentiate *F. hepatica* and *F. gigantica* species.

5.References:

ABDULWAHED, T. K. & AL-AMERY, A. M. 2019. Morphological and molecular study of Fasciola spp. in sheep in Alkut city. *International Journal of Biosciences (IJB),* 14**,** 121-130.

ALAJMI, R. A. 2019. Molecular characterization of Fasciola flukes using mitochondrial 28S rRNA gene in Naimi Saudi sheep. *Saudi J Biol Sci,* 26**,** 112-117.

AMOR, N., HALAJIAN, A., FARJALLAH, S., MERELLA, P., SAID, K. & BEN SLIMANE, B. 2011. Molecular characterization of Fasciola spp. from the endemic area of northern Iran based on nuclear ribosomal DNA sequences. *Exp Parasitol,* 128**,** 196-204.

BARAN, A. I., SARAY, H. C. & KATIRAEE, F. 2017. Molecular determination of Fasciola spp. Isolates from domestic ruminants fecal samples in the northwest of Iran. *Iranian Journal of Parasitology,* 12**,** 243.

BOZORGOMID, A., ROUHANI, S., HARANDI, M. F., ICHIKAWA-SEKI, M. & RAEGHI, S. 2020. Genetic diversity and distribution of Fasciola hepatica haplotypes in Iran: Molecular and phylogenetic studies. *Veterinary Parasitology: Regional Studies and Reports,* 19**,** 100359.

BUATHONG, S., WEBSTER, B. L., LEELAYOOVA, S., MUNGTHIN, M., RUANG-AREERATE, T., NAAGLOR, T., TAAMASRI, P., SUWANNAHITATORN, P., JANEKITKARN, S. & TAN-ARIYA, P. 2019. MOLECULAR CHARACTERIZATION OF FISH-BORNE TREMATODE METACERCARIAE INFECTING FRESHWATER FISH IN RICE FIELD OF CENTRAL THAILAND. *Southeast Asian Journal of Tropical Medicine and Public Health,* 50**,** 25-35.

DAR, Y., AMER, S., MERCIER, A., COURTIOUX, B. & DREYFUSS, G. 2012. Molecular identification of Fasciola spp.(digenea: Fasciolidae) in Egypt. *Parasite: journal de la Société Française de Parasitologie,* 19**,** 177.

EMAN, K., SHERIF, M. & REDA, S. 2016. Molecular characterization of Fasciola hepatica infecting cattle from Egypt based on mitochondrial and nuclear ribosomal DNA sequences. *J. Parasitol,* 11**,** 61-66.

ERENSOY, A., KUK, S. & OZDEN, M. 2009. Genetic identification of Fasciola hepatica by ITS-2 sequence of nuclear ribosomal DNA in Turkey. *Parasitology research,* 105**,** 407.

FARJALLAH, S., BEN SLIMANE, B., PIRAS, C. M., AMOR, N., GARIPPA, G. & MERELLA, P. 2013. Molecular characterization of Fasciola hepatica from Sardinia based on sequence analysis of genomic and mitochondrial gene markers. *Exp Parasitol,* 135**,** 471-8.

GALAVANI, H., GHOLIZADEH, S. & TAPPEH, K. H. 2016. Genetic characterization of Fasciola isolates from West Azerbaijan province Iran based on ITS1 and ITS2 sequence of ribosomal DNA. *Iranian journal of parasitology,* 11**,** 52.

HALL, T. A. BioEdit: a user-friendly biological sequence alignment editor and analysis program for Windows 95/98/NT. Nucleic acids symposium series, 1999. [London]: Information Retrieval Ltd., c1979-c2000., 95-98.

HAMED, N., AYADI, A. & HAMMAMI, H. 2014. Epidemiological studies on fasciolosis in northern Tunisia. *Revue Méd. Vét,* 165**,** 49-56.

HAMOO, R., AL-RUBAYE, F. & MUSTAFA, N. 2019. Molecular characterization and phylogenetic analysis of fasciola gigantica in iraqi sheep using ITS1. *Adv. Anim. Vet. Sci,* 7**,** 256-260.

HASSAN, Z. I. 2018. Molecular Characterization of Cutaneous Leishmaniasis Isolated from Human in Erbil Province-Kurdistan Region/Iraq. *Zanco Journal of Pure and Applied Sciences,* 30**,** 76-85.

HASSAN, Z. I., MEERKHAN, A. A., BOUFANA, B., HAMA, A. A., AHMED, B. D., MERO, W. M. S., ORSTEN, S., INTERISANO, M., POZIO, E. & CASULLI, A. 2017. Two haplotype clusters of Echinococcus granulosus sensu stricto in northern Iraq (Kurdistan region) support the hypothesis of a parasite cradle in the Middle East. *Acta Tropica,* 172**,** 201-207.

ISAH, U. M. 2019. Studies on the prevalence of fascioliasis among ruminant animals in northern Bauchi state, north-eastern Nigeria. *Parasite Epidemiol Control,* 5**,** e00090.

KANTZOURA, V., KOUAM, M. K., DEMIRIS, N., FEIDAS, H. & THEODOROPOULOS, G. 2011. Risk factors and geospatial modelling for the presence of Fasciola hepatica infection in sheep and goat farms in the Greek temperate Mediterranean environment. *Parasitology,* 138**,** 926-38.

KORDSHOOLI, M. S., SOLHJOO, K., ARMAND, B., DOWLATKHAH, H. & JAHROMI, M. E. 2017. A reducing trend of fasciolosis in slaughtered animals based on abattoir data in South of Iran. *Vet World,* 10**,** 418-423.

LOTFY, W. M., PERERA, V. B. V. P., LOKER, E. S., BRANT, S. V., RAJAPAKSE, R. P. V. J., LAURSEN, J. R., DEMIASZKIEWICZ, A., DEJONG, R. J. & LE, T. H. 2008. Evolutionary Origins, Diversification, and Biogeography of Liver Flukes (Digenea, Fasciolidae). *The American Journal of Tropical Medicine and Hygiene,* 79**,** 248-255.

MAGAJI, A. A., IBRAHIM, K., SALIHU, M. D., SAULAWA, M. A., MOHAMMED, A. A. & MUSAWA, A. I. 2014. Prevalence of Fascioliasis in Cattle Slaughtered in Sokoto Metropolitan Abattoir, Sokoto, Nigeria. *Advances in Epidemiology,* 2014**,** 1-5.

MESHGI, B., JAHANI, Z. & AMININIA, N. 2017. Fasciola gigantica of Ruminants: The phylogenetic analysis based on COX1 sequences. *Iranian Journal of Veterinary Medicine,* 11**,** 21-29.

MOAZENI, M., SHARIFIYAZDI, H. & IZADPANAH, A. 2012. Characterization of Fasciola hepatica

genotypes from cattle and sheep in Iran using cytochrome C oxidase gene (CO1). *Parasitology research,* 110**,** 2379-2384.

MOHAMMED, A. B., MUSTAFA, A., ISSA, A. R. & MERO, W. M. 2016. Molecular Characterization of Fasciola Spp. Isolated From the Gallbladder of Infected Cattle in Duhok Province, Kurdistan Region Iraq. *Science Journal of University of Zakho,* 4**,** 37-42.

MUNITA, M. P., REA, R., MARTINEZ-IBEAS, A. M., BYRNE, N., MCGRATH, G., MUNITA-CORBALAN, L. E., SEKIYA, M., MULCAHY, G. & SAYERS, R. G. 2019. Liver fluke in Irish sheep: prevalence and associations with management practices and co-infection with rumen fluke. *Parasit Vectors,* 12**,** 525.

NASR, S. M., BAZH, E. K. A. & FADLY, R. S. 2016. Molecular Characterization of Fasciola hepatica Infecting Cattle from Egypt Based on Mitochondrial and Nuclear Ribosomal DNA Sequences. *Research Journal of Parasitology,* 11**,** 61-66.

ORYAN, A., MANSOURIAN, M., MOAZENI, M., NIKAHVAL, B. & BARBAND, S. 2011. Liver distomatosis in cattle, sheep and goats of Northeastern Iran. *Glob Vet,* 6**,** 241-246.

PIRI, K., SAIDIJAM, M., MAGHSOOD, A., MATINI, M. & FALLAH, M. 2018. Prevalence of Animal Fasciolosis and Specification of Fasciola spp. Isolated from Sheep, Goats and Cattle by Molecular Method: Hamadan Province, West of Iran. *Iran J Parasitol,* 13**,** 524-531.

RAOOF, H. S., MARIF, H. F., RAHMAN, H. S., OMAR, M., SHEIKH, B. & SAN AHMED, A. M. 2020. Molecular characterization and phylogenetic analysis of Fasciola species in sheep and goats in Sulaymaniyah Province, Northern Iraq.

SAH, R., KHADKA, S., LAKHEY, P. J., PRADHAN, S., SHAH, N. P., SINGH, Y. P. & MAS-COMA, S. 2018. Human case of Fasciola gigantica-like infection, review of human fascioliasis reports in Nepal, and epidemiological analysis within the South Central Asia. *Acta Parasitol,* 63**,** 435-443.

SHAFIEI, R., SARKARI, B., SADJJADI, S. M., MOWLAVI, G. R. & MOSHFE, A. 2014. Molecular and Morphological Characterization of Fasciola spp. Isolated from Different Host Species in a Newly Emerging Focus of Human Fascioliasis in Iran. *Vet Med Int,* 2014**,** 405740.

SHALABY, I. & GHERBAWY, Y. 2013. Molecular Characterization of Fasciola sp. isolated from imported sheep in Taif region (Saudi Arabia). *Tropical biomedicine,* 30**,** 1-12.

SIMSEK, S., UTUK, A. & BALKAYA, I. 2011. Molecular differentiation of Turkey cattle isolates of Fasciola hepatica and Fasciola gigantica. *Helminthologia,* 48**,** 3-7.

TADAYON, S., SHARIFIYAZDI, H., MOAZENI, M. & DIVAR, M. R. 2015. Molecular differentiation of Fasciola species and characterization of genetic diversity of F. gigantica using NADH dehydrogenase I (ND1) gene in the endemic areas of Iran. *Iranian journal of parasitology,* 10**,** 9.

TAMURA, K., STECHER, G., PETERSON, D., FILIPSKI, A. & KUMAR, S. 2013. MEGA6: molecular evolutionary genetics analysis version 6.0. *Molecular biology and evolution,* 30**,** 2725-2729.

THOMPSON, J. D., GIBSON, T. J., PLEWNIAK, F., JEANMOUGIN, F. & HIGGINS, D. G. 1997. The CLUSTAL_X windows interface: flexible strategies for multiple sequence alignment aided by quality analysis tools. *Nucleic acids research,* 25**,** 4876-4882.

YADAV, S., AHADUZZAMAN, M., SARKER, S., SAYEED, M. & HOQUE, M. 2015. Epidemiological survey of fascioliasis in cattle, buffalo and goat in Mahottari and Dhanusha, Nepal. *J. Adv. Parasitol,* 2**,** 51-56.

YADAV, S. K. 2015. Epidemiological Survey of Fascioliasis in Cattle, Buffalo and Goat in Mahottari and Dhanusha, Nepal. *The Journal of Advances in Parasitology,* 2**,** 52-56.

YAKHCHALI, M., MALEKZADEH-VIAYEH, R., IMANI-BARAN, A. & MARDANI, K. 2015. Morphological and molecular discrimination of Fasciola species isolated from domestic ruminants of Urmia city, Iran. *Iranian journal of parasitology,* 10**,** 46.

ZEKARIAS, T. & BASSA, T. 2019. Prevalence of Ovine Fasciolosis in Damot Sore Woreda, Wolayta Zone, Ethiopia.

ZANCO Journal of Pure and Applied Sciences
The official scientific journal of Salahaddin University-Erbil
https://zancojournals.su.edu.krd/index.php/JPAS

ISSN (print): 2218-0230**, ISSN (online):** 2412-3986**, DOI: http://dx.doi.org/10.21271/zjpas**

RESEARCH PAPER

Q-ABSORBANCE RATIO, DERIVATIVE SPECTROPHOTOMETRIC AND H-POINT STANDARD ADDITION METHODS FOR SIMULTANEOUS DETERMINATION OF PRIDINOL MESYLATE, AND DICLOFENAC SODIUM IN PHARMACEUTICAL FORMULATION.

Hemn Khalid Qadir, Hemn Abdul Qader

Dept. of Pharmaceutical Chemistry - College of Pharmacy - Hawler Medical University,Kurdistan Region, Iraq

A B S T R A C T:

Three methods for simultaneous estimation of diclofenac sodium and pridinol mesylate have been developed. First method is the application of the Q–analysis (absorbance ratio) method, the wavelengths selected were 265nm (isosbestic point) and 285nm (λ_{max} of diclofenac sodium) with 258nm (λ_{max} of pridinol mesylate). The linearity ranges for diclofenac sodium and pridinol mesylate were 8-64 µg/ml and 14-56 µg/ml, respectively. The second technique is based on the second derivative spectrophotometric method at zero crossing wavelengths. The linearity ranges for diclofenac sodium and pridinol mesylate were (4.0-40.0) µg/ml and (4.0-30.0) µg/ml, respectively. The third method is the H-Point Standard addition method (HPSAM) depending upon the zero and second-order derivative signals for diclofenac sodium and pridinol mesylate were applied pairs of wavelengths, 250.37and 266.34 nm; with 224.18 and 235.10 nm, respectively.

The accuracy of the methods was assessed by recovery studies and was found to be 100.01 ± 0.63 and 100.64 ± 0.36 for the q-absorbance ratio method, 100.78 ±0.221 and 101.98 ±0.11 for the second derivative zero-crossing method, respectively. While for H-Point Standard addition method are 98.0±1.71, and 100.4±0.545 for zero-order HPSAM , 99.25 ±0.753, and 100.12 ± 0.35 for second derivative HPSAM for diclofenac sodium and pridinol mesylate respectively

Methods were confirmed according to the ICH guidelines; accuracy, precision, and repeatability were found to be within acceptable limits with no interferences. Finally, statistical comparisons between the proposed methods and the reported methods concerning to accuracy and precision show that no significant difference was found using Student's t-test, F-test, and one-way ANOVA.

KEY WORDS: Q-analysis, Derivative spectrophotometry, HPSAM, Diclofenac sodium, and Pridinol mesylate.
DOI: http://dx.doi.org/10.21271/ZJPAS.33.4.5
ZJPAS (2021), 33(4); 43-60 .

1.INTRODUCTION :

Pridinol mesylate (PriM) (Figure 1) is a vital anticholinergic drug, with beneficial muscle relaxant properties (Salazar-Rojas et al., 2019) and working as a myotonolytic and spasmolytic agent in antistress cure and for the treatment action of Parkinson's disease (Wongrakpanich et al., 2018, Vignaduzzo et al., 2011),

Pridinol mesylate (PriM) is most commonly formulated in link with non-steroidal anti-inflammatory drugs, containing diclofenac, meloxicam and piroxicam, for the usage and treatment of muscular contractures and low back pain (Abdel Shaheed et al., 2017) **.** Diclofenac sodium (DicNa) (2-(2,6-dichloroanilino)Phenylacetate) (Figure 2) is a non-steroidal anti-inflammatory drug (Lins et al., 2020) supported for use in painful and inflammatory rheumatic and definite non-rheumatic conditions (Moore et al., 2019, Lins et

* **Corresponding Author:**
Hemn Khalid Qadir,
E-mail:
Article History:
Received: 23/03/2021
Accepted: 31/05/2021
Published: 18/08 /2021

al., 2020), and antiarthritic source. It is suggested to decrease menstrual pain, dysmenorrhea, etc. (Anggraini and Ekawati, 2020) . Yearly intake of diclofenac is 940 tons universally with a mentioned dose of 100 mg/day (Tiwari et al., 2015).

Recently, there is a new combination consisting of DicNa, or ternary mixture combined above with cyanocobalamin (vitamin B12) have been released in the markets (Kleemann et al., 2014).

Several analytical methods have been reported for estimation of these ingredients PriM, and DicNa, separately or in combination with other compounds using HPLC(Anggraini and Ekawati, 2020, Brezovska et al., 2013, Gunji et al., 2012, Vignaduzzo et al., 2010), LC-MS (Yang et al., 2019, Chethana et al., 2012, Michopoulos et al., 2015) , UV-visible spectrophotometry (Mane et al., 2019, Darweesh et al., 2018, Dikran and Mahmood, 2017) Electrochemical methods (Kimuam et al., 2020, Afkhami et al., 2016, Robinson et al., 2014).

In the present work, Q-absorbance ratio method, zero-crossing second derivative spectrophotometric method and applied H-point standard addition method (HPSAM), second-order derivative spectra(2D-HPSAM), and the zero order derivative spectra (ZO-HPSAM), for simultaneous estimation of DicNa and PriM in bulk and pharmaceutical formulation.

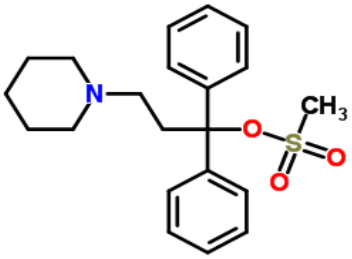

Figure (1): Chemical structure of pridinol mesylate (PriM).

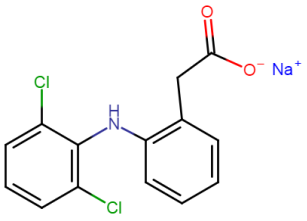

Figure (2): Chemical structure of diclofenac sodium (DicNa)

2. MATERIAL AND METHODS

2.1 Apparatus

A dual UV-Visible Spectrophotometer (Perkin Elmer Lambda 35.) was connected to identical 1.0 cm quartz cells to a computer (Wind XP), and the software used SHIMADZU UV probe data system software (2.34 ink.), using the following parameters: scan speed (240), slit width (02), delta lambda (10); Scaling factor (25), mode 2D (second derivative); The wavelength range (200-3450nm) and the digital calipers within the operating instructions (100-300mm) were used to measure height of the peaks.

2.2 Stock solutions and working solutions

Standard stock solutions of 100 µg mL^{-1} of DicNa and PriM (purchased in Glentham Life Sciences Ltd. (UK)) for binary mixture analysis were prepared by precisely weighing 100 mg of DicNa and PriM, separately into two separate 100mL volumetric flasks and then complete it to the mark with ethanol, multisolvent® HPLC grade (TDS, ET00152500) Scharlau, S.L. (Spain).

Working solutions were prepared from their own standard stock solutions diluting by ethanol into 100mL volumetric flasks containing (1.0–40.0, and 1.0–30.0, µgmL−1, DicNa and PriM), and their laboratory-prepared mixtures were prepared from their own working standard solutions in different proportions both standard stock solutions and working solutions were prepared daily.

2.3 Pharmaceutical formulation

Ten tablets of Dioxaflex® Plus (purchased from Gramón Bagó de Uruguay S.A.) weighed, powdered and mixed in a mortar for the pharmaceutical formulation solutions. 10mg of powdered drug was dissolved in 100 mL of ethanol. The solution was filtered by syringe filter 0.4µm before preparing different concentrations by serial dilution. Ethanol, multisolvent® HPLC grade (TDS, ET00152500) Scharlau, S.L. (Spain) was used as a solvent.

2.4 Condition and absorption for zero order spectra

The normal UV absorption spectra of (DicNa, and PriM) and their mixture were recorded against absolute ethanol as a solvent blank. (Figure 3) shows absorption spectrum of 20 µg/ml of DicNa solution with lambda max at 285 nm, absorption spectrum of 15 µg/mL of PriM solution with a maximum peak at 258 nm, and isosbestic point were obtained at 265 nm. The overlap spectra of DicNa and PriM at two different concentration ranges were recorded. In the absorption spectrum of the mixture shows an overlap spectrum; therefore, the simultaneous determination is very difficult due to spectral interference.

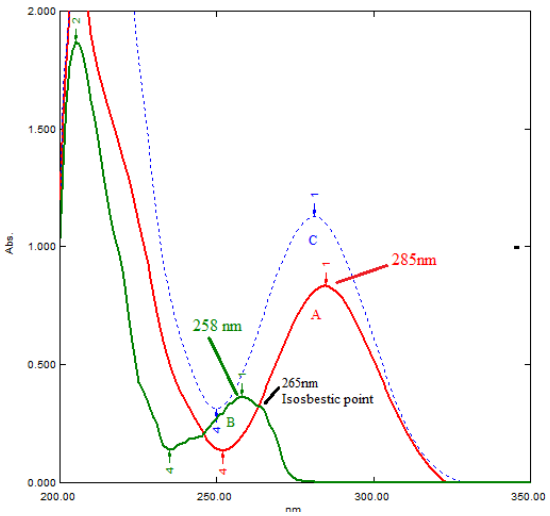

Figure (3): Zero-order spectra of (a) 20 µg/mL diclofenac sodium (DicNa), (b) 15 µg/mL pridinol mesylate (PriM), and (c) mixture of DicNa and PriM against absolute ethanol as a blank.

2.5 Q-absorbance ratio method

This method is valid to the drugs that obey Beer's law at all wavelengths and the ratio of absorbance at any two wavelengths is a constant value, (Khamar and Patel, 2012) . At wavelengths Figure 3 shows two pair wavelengths, 265nm as isosbestic point, 285nm (λmax of DicNa), and 258nm (λmax of PriM) and selected for the formation of the Q-absorbance ratio equation. The absorptivity coefficients of each compound at both wavelengths were determined. The concentration of the different components, CX (PriM)and CY (DicNa) can be planned and calculated by using the next following equations (Guideline, 2005, Patil et al., 2016).

CX = (QM-QY/QX-QY) x (A1/ax1) ……. [1]

CY = (QM-QX/QY-QX) x (A2/ay1) ……. [2]

Where, A1and A2 are absorbance of the mixture at 258 nm and 265 nm; ax1 and ay1 are absorptivity of DicNa and PriM at 258 nm; ax2 and ay2 are absorptivity of DicNa and PriM respectively at 265 nm; QM= A2 / A1, QX = ax2 / ax1 and QY = ay2 / ay1, wherever QM= (absorption ratio of isosbestic point to PriM) QX= absorptivity ratio at 258nm , and QY = absorptivity ratio at 265nm.

2.6 Condition and chosen second order derivative spectra

A set of 25 mL volumetric flasks, containing constant 20 µg/ml of DicNa and different amounts of PriM (1–30) µg/ml, while another set of 25 mL volumetric flasks, contain different amounts (1-40) µg/ml of DicNa, and PriM kept constant(15 µg/ml). The solutions were diluted with ethanol. The spectra of solutions were recorded against absolute ethanol as a solvent blank in the range of 200 –350 nm.

Considering and pending all the orders of derivative spectra of (DicNa, and PriM) from first to the fourth-order derivative, the graphical study revealed that second order of the derivative spectra as shown in (Figure 4) , was found to be simple and provide the best results for simultaneous determinations of (DicNa, and PriM) basing upon zero-crossing technique. This approach of quantitative determination allows the simultaneous guarantee of both analytes in a sample (Patel et al., 2010).

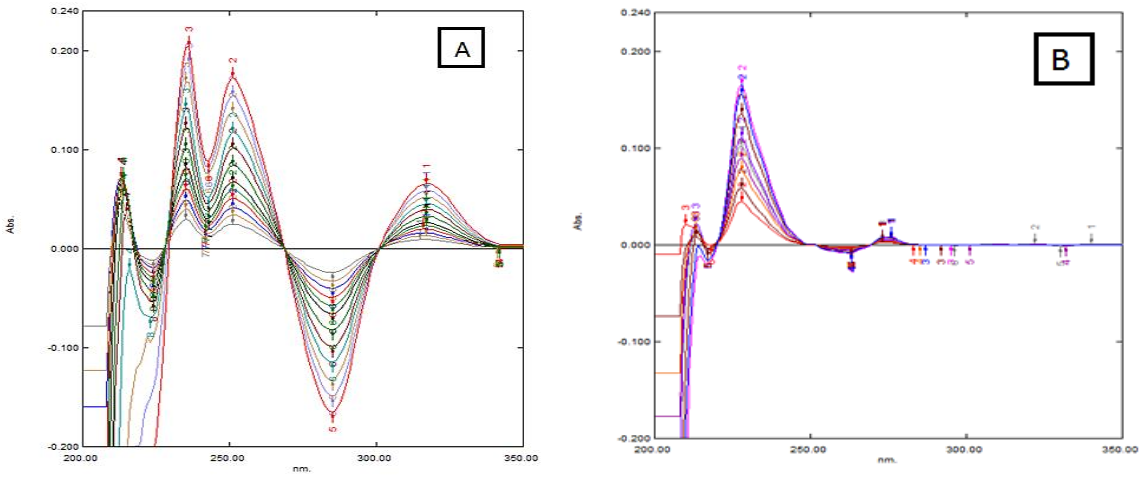

Figure (4): The overlain spectra of the second derivative of (a) 4-40 µg/mL pure DicNa and (b) 4-30 µg/mL pure PriM against absolute ethanol as a blank

2.7 Wavelength selection for HPSAM

Campins-Falco and et al. proposed an alteration and reform of the standard additions method technique known as the H-point standard additions method (HPSAM) in order to find an unbiased analyte concentration when both analyte and interferent are present in a sample. It also allowance the determination of the interferent concentration when it is known to be present (Świt et al., 2018) (Andrés et al., 1995, Reig, 1990).

To choose the suitable wavelength pair for applying of determination of DicNa and PriM in binary mixture by ZO-HPSAM and 2D-HPSAM, the following principles were applied:

1. At a selection of specific wavelengths the analyte signals necessity be linear to their concentration, and the interferent signal must remain unaffected and unchanged while varying the analyte concentration.
2. The analytical signal found from a mixture containing both analyte and the interferent should be equivalent to the sum of the specific individual or separate signals of two components.
3. The difference in the slopes of two straight lines recorded at the two selected wavelengths (λ1 and λ 2) need to be as large as possible in order to obtain decent and good sensitivity and accuracy (Andrés et al., 1995, Reig, 1990).

2.8 Condition and absorption spectra for HPSAM

The absorption spectrum of 8 µg/mL PriM, 8 µg/mL DicNa, and their mixture of PriM and DicNa were plotted against ethanol as a solvent blank on a 200 to 350 nm scale. As can be seen in (Figure 5), DicNa and PriM can be considered as an analyte and interference, respectively. In this state, and in view of these principles, the higher the slope value, the smaller the analyte concentration error, numerous pairs of wavelengths with the similar PriM absorbance were checked, the best pair of (250.37 and 266.34) nm higher slope values (Mλ1 = 0.0252, Mλ2 = 0.0114) were selected for zero-order spectra(ZO-HPSAM). Depending upon the mentioned principles the method developed by taking the second derivative mode (2D-HPSAM) instead of the normal one (Figure 6), the higher the slope value (M λ1 = 0.0581, M λ2 = 0.0294) with the best pair of (224.18 and 235.10) nm were selected.

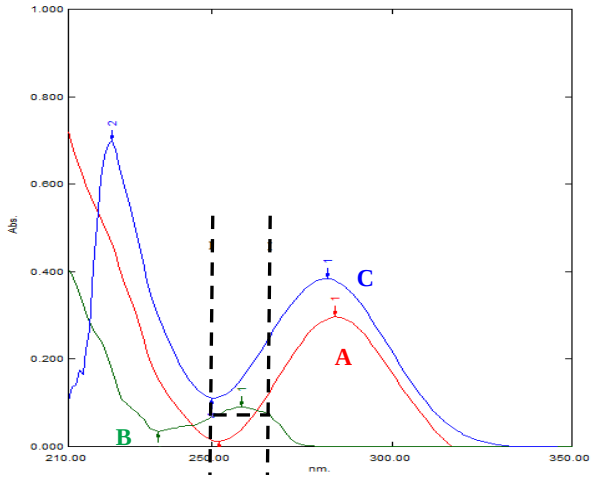

Figure (5): Overlain absorption spectra for (ZO-HPSAM) of (A) DicNa being the analyte, (B)PriM being the interference and (C) their mixture in absolute ethanol

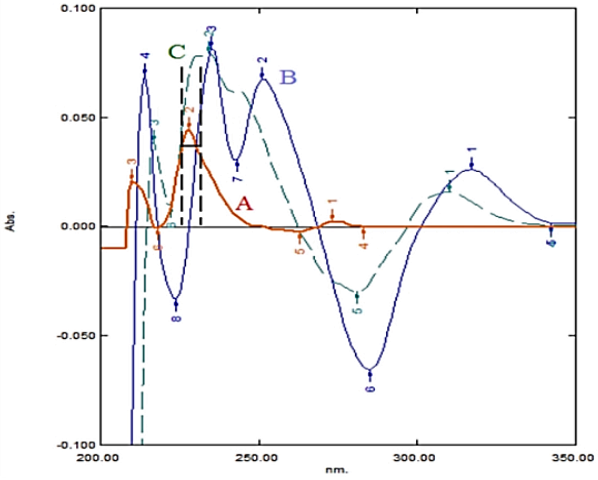

Figure (6): Overlain absorption spectra for (2D-HPSAM) of (A) DicNa being the analyte, (B)PriM being the interference and (C) their mixture in absolute ethanol

3. RESULT AND DISCUSSION

3.1 Second derivative mode study

Extremely overlapped spectra can be resolute by using derivative spectrophotometry (Kus et al., 1996). Derivative spectra can be used to resolve overlapping bands in qualitative and quantitative analysis and improve differences among spectra (O'haver and Green, 1976).

From these points of view zero-cross technique as shown in Figure 7, was used for the determination of PriM at the presence of DicNa in the solution, as follows:

Firstly at 228.2 nm DicNa undergoes zero absorption, but PriM has a positive peak. Undoubtedly at 251.69 nm and 283.98 PriM undergoes zero absorption at these points, furthermore, DicNa has a peak at positive and negative valleys respectively.Likewise, at 268.67 nm point, DicNa undergoes zero absorption, whereas PriM has a peak of negative valleys.Finally, any peak that exist after 300nm belongs to DicNa, while PriM does not have any peaks,therefore, in the present effort work, graphically studying method techniques (peak-to-baseline, height measuring, and zero-crossing) were used to contract with derivative spectra to achieve the simultaneous measurements at these points.

Figure 8 shows sets of 2nd order spectra of mixtures consist of fixed amounts of PriM (15.0 µg/mL) and in the presence of different concentrations (4-40 µg/mL) DicNa respectively.

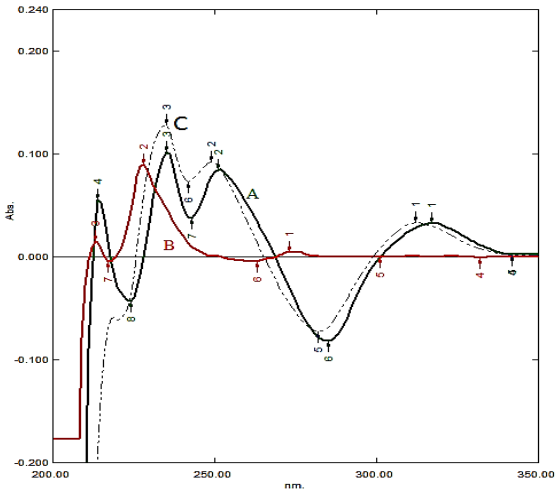

Figure (7): Second derivative spectra of: (A) 20 µg/mL DicNa,(B) 15.0 µg/mL PriM, and their mixture (C)

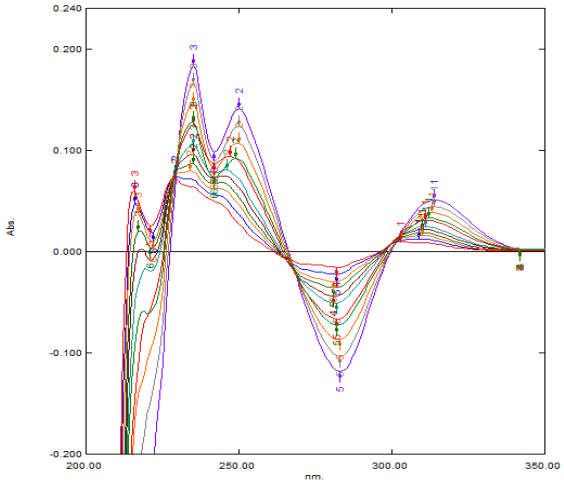

Figure (8):): The overlain spectra of the second derivative for solutions containing (4.0 – 40.0) µg/mL DicNa and fixed 15.0 µg/mL of PriM

3.2 Wavelength selection recovery for HPSAM

In the current work for (HPSAM), choosing a suitable range of the pairs of wavelengths (Table 1) known analyte quantities are sequentially new added to the mixture analyte (DicNa) and interference (PriM), and the resulting mixture absorbance was measured at the two selected wavelengths. Two straight lines were obtained and the intersection of the two linear lines is H-point (C_H, A_H), DicNa (C_H) is the analyte concentration was directly determined at the intersection of the x-axis, and (A_H) is the analytical signal by reason of the interference, resulting in high recovery percentage (99.12, and 100.12)% for (ZO-HSAM) and (2D-HPSAM) mode (Figure 9 & 10).

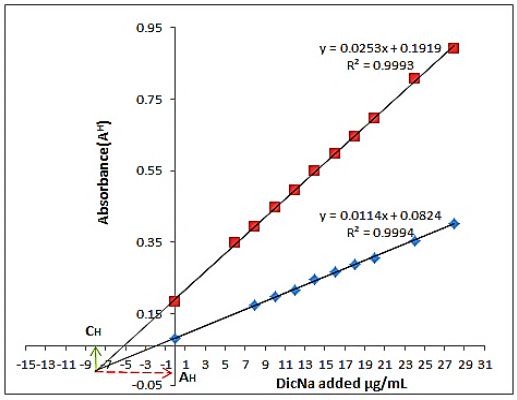

Figure (9): Plots of ZO-HPSAM method for determination of DicNa (8 µg/mL) in the presence of PriM (8 µg/mL)when different standard DicNa solutions (4-40 µg/mL) were added at the selected wavelengths 250.37 nm and 266.34 nm

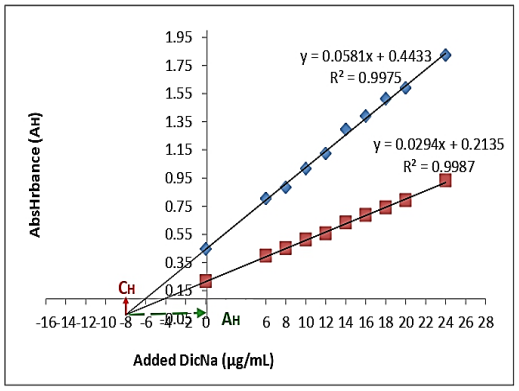

Figure (10): Figure (10): Plots of ZO-HPSAM method for determination of DicNa (8 µg/mL) in the presence of PriM (8 µg/mL) when different standard DicNa solutions (4-40 µg/mL) were added at the selected wavelengths 224.18 and 235.10 nm.

Table (1): Selection of correct wavelength for mixture analyte (DicNa) and interference (PriM) analysis

Methods	Wavelength (nm)	A-C Equation	R^2	Amount taken (µg/mL)		Amount found (µg/mL)	Recovery %	Absorbance (A_H)
				DicNa	PriM	DicNa	DicNa	PriM
ZO-HPSAM	250.37 266.34	y=0.0252x+0.1923 y=0.0114x+0.0829	0.9993 0.9994	8	8	7.93	99.12	- 0.0074
2D-HPSAM	224.18 235.10	y=0.0581x+0.4433 y=0.0294x+0.2135	0.9975 0.9987	8	8	8.01	100.12	- 0.022

3.3 Linearity studies

All methods were legalized as demonstrated by ICH guidelines (Guideline, 2005, Patil et al., 2016). The calibration curves for each one of (DicNa, and PriM) in zero-order and isosbestic point as revealed in (Figure 11 & 12) respectively, showed that the system obeyed beer's law of each component accessible linear response to the analyte concentration. For the Q-absorption ratio method way, the wavelengths designated and selected were 265nm (isosbestic point) and 285nm (λmax of DicNa) with 258nm (λmax of PriM). The absorbance at these two wavelengths for all standard solutions of both DicNa and PriM were consistent and measured, so the statistical data for these calibration curves are concise in (Table 2).

For supposed second order Derivative and zero crossing order the linearity of the methods was measured at different concentrations of DicNa, and PriM in the binary mixture in the field ranges of (4-40 and 4-30 µg/mL), respectively. Calibration graphs were constructed as shown in (Figures 13 &14). The statistical parameters are summerized in (Tables 3). All plots had an acceptable linear relationship and observed for each compound as indicated by their correlation coefficients.

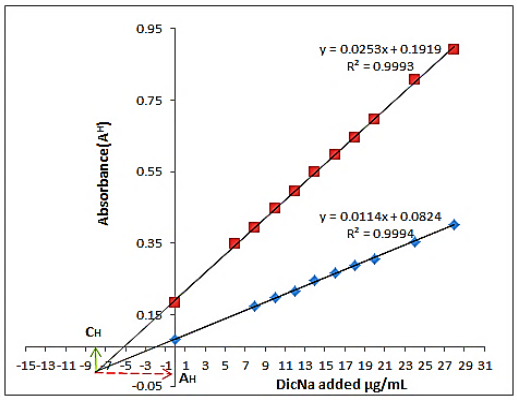

Figure (9): Plots of ZO-HPSAM method for determination of DicNa (8 µg/mL) in the presence of PriM (8 µg/mL)when different standard DicNa solutions (4-40 µg/mL) were added at the selected wavelengths 250.37 nm and 266.34 nm

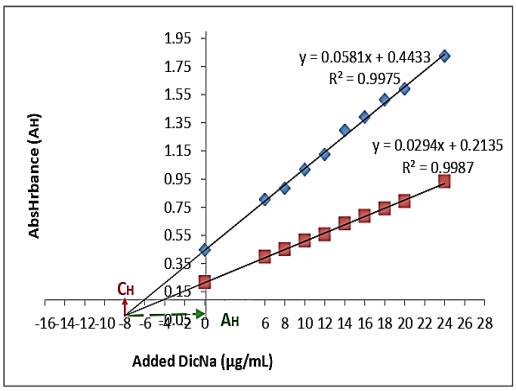

Figure (10): Figure (10): Plots of ZO-HPSAM method for determination of DicNa (8 µg/mL) in the presence of PriM (8 µg/mL) when different standard DicNa solutions (4-40 µg/mL) were added at the selected wavelengths 224.18 and 235.10 nm.

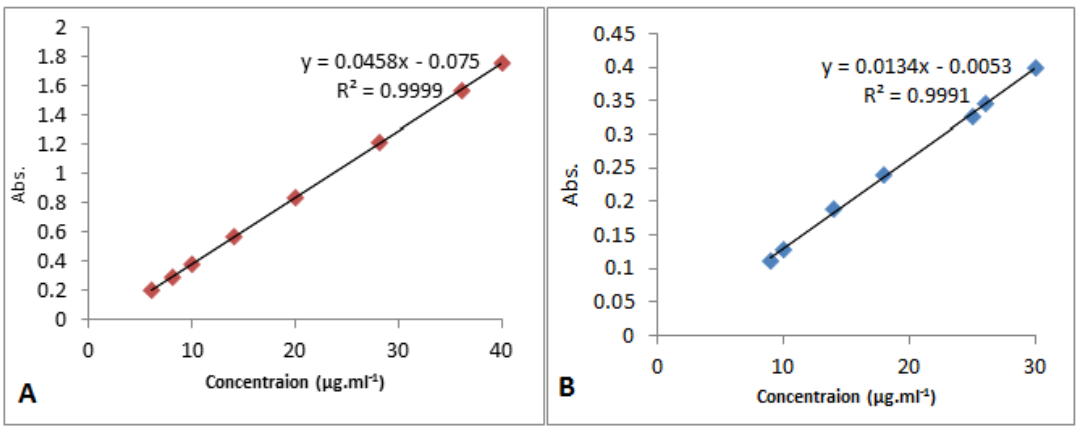

Figure (11): Linearity of zero order (A) DicNa concentration range of (4-40) µg/mL, and (B) PriM concentration range of (4-40) µg/mL

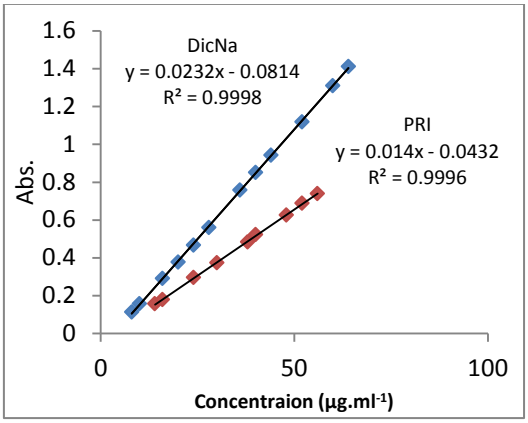

Figure (12): Linearity constructed for DicNa concentration range of (8-64) µg/mL and PriM concentration range of (14-56) µg/mL at 265nm (isosbestic point)

Table (2): Regression data of DicNa (285nm), and PriM (258nm) by Q-absorbance ratio spectrophotometric method at isosbestic point (265nm).

Parameters	Diclofenac sodium (DicNa)	Pridinol mesylate (PriM)	Q-Absorbance Ratio PriM & DicNa (isosbestic point)
λ_{max} (nm)	285	258	265
Linearity range (µg/ml)	6-40	9-30	14-56 & 8-64
Regression equation	y = 0.0458x[DicNa] - 0.075	y = 0.0134x[PriM] - 0.0053	y = 0.014x[PRI] - 0.0432 & y = 0.0232 x [DicNa] - 0.0814
Slop (L/mg.cm)	0.0458	0.0134	0.014 & 0.0232
Intercept	0.075	0.0053	0.0432 & 0.0814
Correlation coefficient (R^2)	0.9999	0.9995	0.9996 & 0.9998
LOD[a] (µg/ml)	0.6546	2.46	3.09 & 2.01
LOQ[b] (µg/ml)	1.98	7.48	9.36 & 6.10

[a] & [b]:The limit of detection (LOD) and the limit of quantification (LOQ) were derived by calculating (3.3 for LOD and 10 for LOQ) using the following equations designated by International Conference on Harmonization (ICH) guidelines. **LOD = 3.3 × σ/S…….. (3) LOQ = 10 × σ/S…… (4)** Where, σ = the standard deviation of the response and S = slope of the calibration curve.

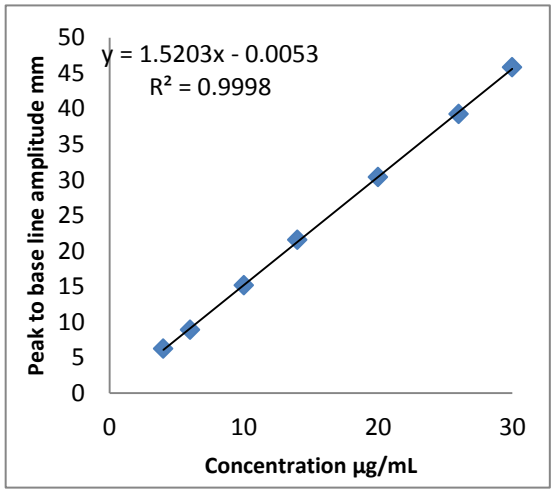

Figure (13): Calibration curve constructed under 2D proposed method for PriM in the present of fixed 20 µg/mL DicNa at 228.02nm

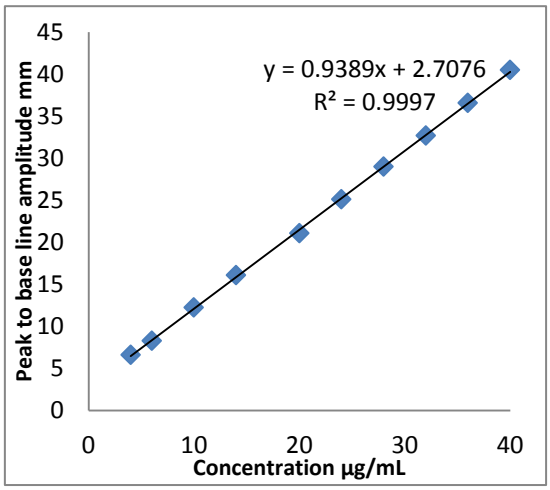

Figure (14): Calibration curves via second derivative spectra of DicNa in the present of fixed 15 µg/mL PriM at 251.69 nm.

Table (3): Statistical data of the calibration curves of the simultaneous spectrophotometric determination of DicNa, and PriM using zero-crossing technique

Compound	Methods of analysis	Linearity range (µg/mL)	Detection limit (µg/mL)	Regression equation	R^2
DicNa	Height at 251.69 nm (zero-crossing point of predinol)	4-40	1.46	Y=0.9389x+2.7076	0.9997
PriM	Height at 228.02 nm (zero-crossing point of DicNa)	4-30	0.96	y = 1.5203x - 0.0053	0.9998

3.4 Determination of unknown concentration of interference (PriM) and Analyte(DicNa) in HPSAM

In order to determine the unknown concentrations of DicNa and PriM in the mixture, it is necessary to identify the linear range which obeyed Beers law for each of them using the HPSAM method.

3.4.1 Calibration curve of the interference (PriM)

To determine the interference PriM concentration from the lineup amount of the H-point (A_H) a calibration graph is necessary. Specific DicNa concentrations were added to different mixtures of constant DicNa concentration (8 µg/mL) and different PriM concentrations (6 - 24 µg/mL). The absorbance was measured at 250.37 and 266.34 nm for (zero-order) and 224.18 and 235.10 nm for (2^{nd} order derivative) modes and plotted against added DicNa concentrations (Figure 15 & 16) separately.

A calibration curve is created by plotting the measured A_H values obtained from (Figure 14) beside the PriM concentration ranged (6.0-24.0 µg/mL) for the determination of PriM interference concentration. Calibrations are obeyed Beer's law in the UV region in the interior concentration range of (6.0-24.0) µg/mL and there was a negative deviation after 24.0 µg/mL for both (zero and second order mode) as shown in (Figure 17 & 18).

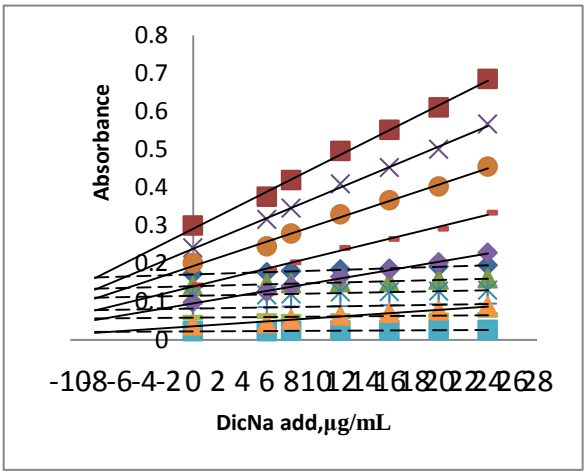

Figure (15): Plots of ZO-HPSAM for a fixed DicNa (8 µg/mL) and different concentrations of PriM at wavelengths of 250.37 and 266.34 nm

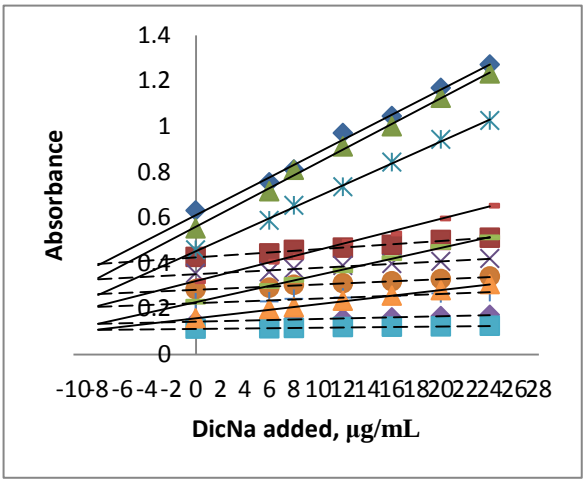

Figure (16): Plots of 2D-HPSAM for a fixed DicNa (8 µg/mL) and different PriM concentrations at wavelengths of 224.18 and λ 235.1 nm

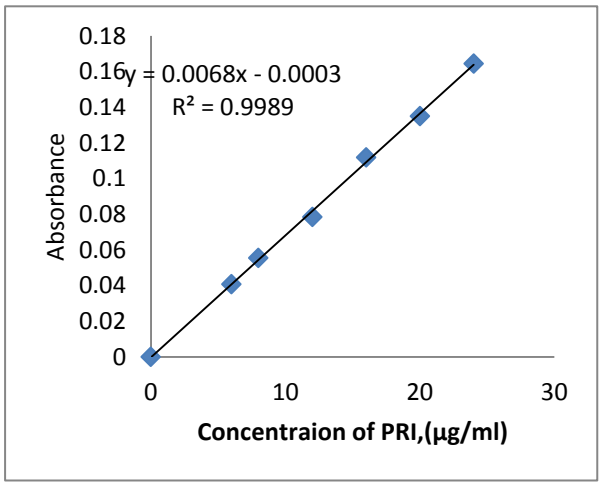

Figure (17): Calibration curve of PriM in the presence of fixed amount DicNa (8 µg/mL) for (ZO-HPSAM)

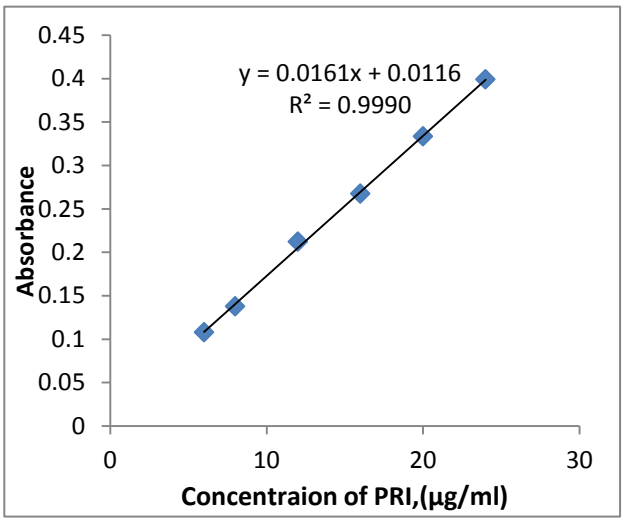

Figure (18): Calibration curve of PriM in the presence of fixed amount DicNa (8 µg/mL) for (2D-HPSAM)

3.4.2 Calibration curve of the analyte (DicNa)

To measure a quantity of the analyte DicNa, exact DicNa concentrations were added to different mixtures of constant PriM concentration (8.0 µg/mL) and variable DicNa concentrations (4.0-14.0 µg/mL). The absorbance was measured at 250.37 nm and 266.34 nm for (zero-order), and at 224.18 nm and 235.1 nm for (2^{nd} order) mode and plotted against added DicNa concentrations (Figure 19 & 20).

A calibration curve is built on plotting the founded C_H values in (Figure 16 & 22) against the DicNa concentrations ranged (4.0-14.0 µg/mL) for determination of DicNa analyte concentration. Calibration within the concentration range of (4.0-14.0) µg/mL was found to be linear and there was a positive and negative deviation after 14 µg/mL for (zero order) and (second order) modes as shown in (Figure 21 & 22) separately.

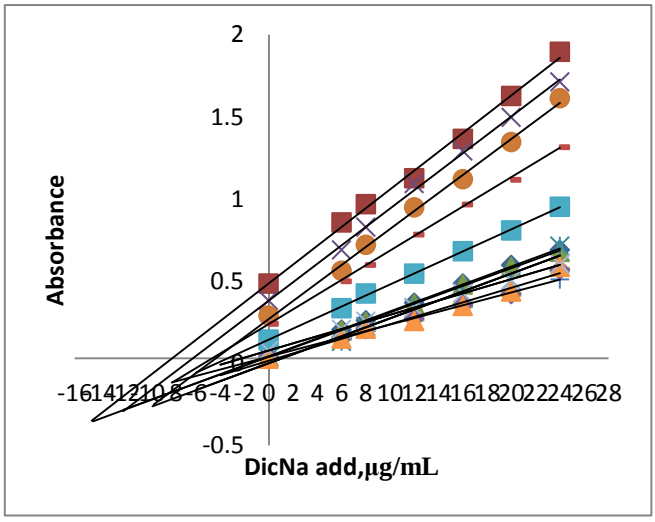

Figure (19): Plots of ZO-HPSAM curves at fixed PriM (8 µg/mL) concentration 8.0 (µg/mL) and different DicNa concentrations.

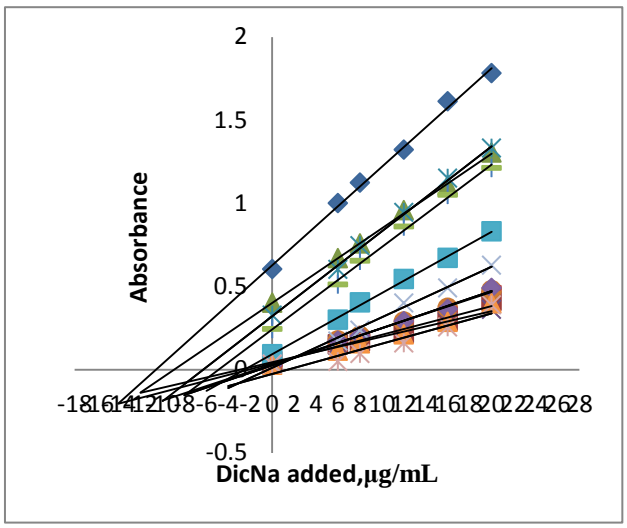

Figure (20): Plots of 2D-HPSAM curves at fixed PriM concentration (8.0 µg/mL) and different DicNa concentrations

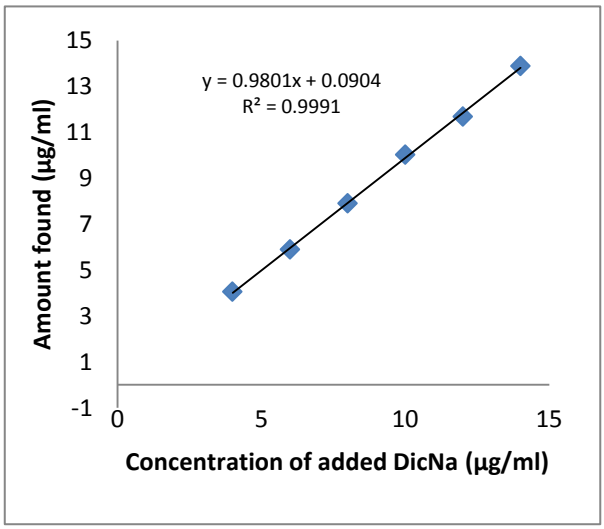

Figure (21): Calibration curve for determination of DicNa in the presence of 8 µg/mL of PriM in the mixture using ZO-HPSAM

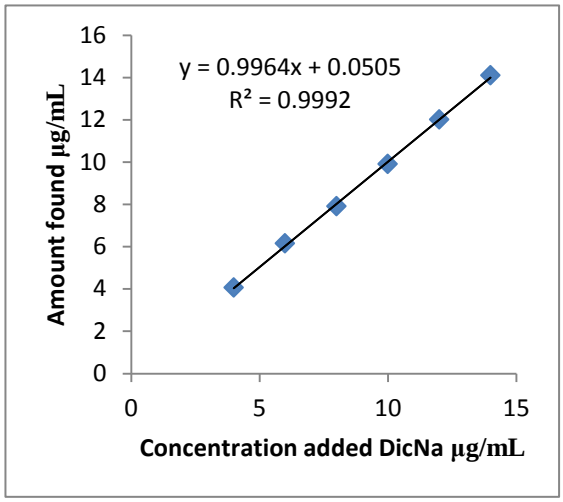

Figure (22): Calibration curve for the determination of DicNa in the presence of 8 µg/mL of PriM in the mixture using 2D-HPSAM

3.5 ACCURACY AND PRECISION

In recent years, some publications have appeared explaining several analytical titration strategies that help improve analytical accuracy (Świt et al., 2018). Both accuracy and precision of the techniques were confirmed by doing recovery studies using five replicate measurements for synthetic lab mixture and pharmaceutical formulation at three concentration levels of standard addition. The values of relative error (Error %) and relative standard deviation (RSD %) for these replicate measurements of DicNa and PriM were calculated. The results of Q-Absorption ratio and 2nd derivative spectrophotometric method zero-crossing point are tabulated in (Table 4 & 5) correspondingly.

After the determination of interference (PriM) concentration from the lineup amount of the H-point (AH) in both (ZO-HPSAM) and (2D-HPSAM,) good recovery of (97.75-102.25) percentage and (98.0-100.62) percentage (Table 6 & 7) respectively were succeeded for DicNa and PriM in the synthetic mixture, Both accuracy and precision of the method are acceptable.

(Table 8 & 9) Showed regression equations and recovery percentage for the determination of the quantity of the analyte (DicNa), a good recovery of (97.33-102.12) percent for (ZO-HPSAM) and (98.25-103.37) percent for (2D-HPSAM) were achieved for DicNa and PriM in the mixture.

Table (4): Evaluation of accuracy and precision for the determination of DicNa and PriM by Q-Absorption ratio method

Parameter	compound	λmax (nm)	Concentration (µg/mL)	Error %	RSD %
Q-Absorption ratio method	Diclofenac sodium(DicNa)	285	6	+ 3.79	+ 0.41
			20	- 4.77	+ 0.34
			40	- 1.96	+ 1.69
	Pridinol mesylate(PriM)	258	9	- 2.96	+ 4.22
			14	- 1.90	+ 4.12
			30	+ 2.91	+ 3.40
		Isosbestic point	8	- 1.40	+ 2.78
	Diclofenac sodium(DicNa)	265	32	- 4.63	+ 2.21
			64	- 4.35	+ 1.72
	Pridinol mesylate(PriM)	Isosbestic point	14	- 3.26	+ 2.65
		265	30	- 4.47	+ 2.88
			56	- 4.30	+ 4.36

Table (5): Evaluation of accuracy and precision for the determination of DicNa and PriM using 2nd derivative zero-crossings technique

Compound	Methods of analysis	Concentration (µg/mL)	Error %	RSD %
DicNa	Height at 251.69 nm (zero-crossing point PriM)	4	- 2.48	+ 2.16
		20	- 2.26	+ 3.40
		40	+ 1.75	+ 1.60
PriM	Height at 228.02 nm (zero-crossing point of DicNa)	4	+ 2.19	+ 3.46
		14	+ 3.16	+ 3.20
		30	- 0.95	+1.98

Table (6): Regression equations and recovery percentage of PriM (A_H) and a fixed concentration of DicNa (8 µg/mL) (-C_H) in (ZO-HPSAM)

A-C Equation	$\sqrt{R^2}$	Amount taken (µg/ml) DicNa	Amount taken (µg/ml) PriM	DicNa Amount found (µg/ml)	DicNa Recovery %	PriM Amount found (µg/ml)	PriM Recovery %
y=0.0021x+0.0394	0.9947	8.0	0	8.05	100.6	0	0
y=0.0001x+0.0233	0.9689						
y=0.0022x+0.0579	0.9867	8.0	6.0	7.81	97.75	6.03	100.5
y=0.0002+0.04051	0.9806						
y=0.0054x+0.0979	0.9973	8.0	8.0	7.92	99.01	8.12	101.5
y=0.0003x+0.0579	0.9731						
y=0.0078x+0.1425	0.9909	8.0	12.0	8.18	102.25	11.78	98.16
y=0.0005x+0.0826	0.9668						
y=0.0106x+0.1961	0.9952	8.0	16.0	7.95	99.37	16.27	101.68
y=0.0006x+0.1166	0.8953						
y=0.0133x+0.2412	0.9943	8.0	20.0	7.89	98.62	19.88	99.4
y=0.0008x+0.1413	0.9049						
y=0.0161x+0.2943	0.9968	8.0	24.0	8.06	100.75	24.22	100.9
y=0.001x+0.17250	0.9766						

Table (7): Regression equations and recovery percentage of PriM (A_H) and a fixed concentration of DicNa (8 µg/mL) (-C_H) in (2D-HPSAM)

A-C Equation	$\sqrt{R^2}$	Amount taken (µg/ml)		DicNa		PriM	
		DicNa	PRI	Amount found (µg/ml)	Recovery %	Amount found (µg/ml)	Recovery %
y=0.005x+0.13140	0.9985	8.0	0	7.93	99.12	0	0
y=0.0007x+0.0973	0.9975						
y=0.0062x +0.1573	0.9988	8.0	6.0	7.98	99.75	5.99	99.80
y=0.0005x+0.1118	0.9750						
y=0.0118x+0.2305	0.9980	8.0	8.0	7.86	98.25	7.84	98.0
y=0.0011x+0.1464	0.9900						
y=0.0137x+0.3208	0.9936	8.0	12.0	7.94	99.25	12.31	102.5
y=0.0019x+0.2272	0.9825						
y=0.0238x+0.4582	0.9980	8.0	16.0	8.02	100.25	15.89	99.31
y=0.0022x+0.2849	0.9929						
y=0.0292x+0.5688	0.9982	8.0	20.0	8.05	100.62	20.0	100
y=0.0027x+0.3553	0.9948						
y=0.0258x+0.6063	0.9936	8.0	24.0	8.03	100.37	24.07	100.29
y=0.0035x+0.9825	0.9825						

Table (8): Regression equations and recovery percentage of DicNa (-C_H) and a fixed concentration of PriM (8 µg/mL) (A_H) in (ZO-HPSAM)

A-C Equation	$\sqrt{R^2}$	Amount taken (µg/ml)		DicNa		PriM	
		DicNa	PriM	Amount found (µg/ml)	Recovery %	Amount found (µg/ml)	Recovery %
y=0.0415x+0.1152	0.9997	4	8	4.06	101.15	7.89	98.5
y=0.0159x+0.0112	0.9992						
y=0.0336x+0.1434	0.9994	6	8	5.9	98.3	7.95	99.37
y=0.0146x+0.0313	0.9998						
y=0.0308x+0.1875	0.9949	8	8	7.91	98.87	8.10	101.25
y=0.0144x+0.0585	0.9995						
y=0.0294x+0.2399	0.9978	10	8	10.03	100.3	8.12	101.50
y=0.0151x+0.0965	0.9862						
y=0.0287x+0.2764	0.9982	12	8	11.68	97.33	8.13	102.12
y=0.0144x+0.1106	0.9994						
y=0.0292x+0.3491	0.9925	14	8	13.89	99.21	8.08	101
y=0.014x+0.1389	0.9938						

Table (9): Regression equations and recovery percentage of DicNa (-CH) and a fixed concentration of PriM (8 µg/mL) (AH) in (2D-HPSAM)

A-C Equation	$\sqrt{R^2}$	Amount taken (µg/ml)		DicNa		PriM	
		DicNa	PriM	Amount found (µg/ml)	Recovery %	Amount found (µg/ml)	Recovery %
y=0.0323x-0.0163	0.9929	4	8	4.06	101.5	7.89	98.65
y=0.0193x-0.0676	0.9947						
y=0.0379x+0.0916	0.9964	6	8	6.15	102.5	8.06	100.75
y=0.0186x-0.0271	0.9825						
y=0.0498x+0.2422	0.9929	8	8	7.86	98.25	8.18	102.25
y=0.0221x+0.0272	0.9864						
y=0.0515x+0.3262	0.9956	10	8	9.9	99.0	8.27	10.3.37

y=0.0217x+0.0323	0.9904						
y=0.0449x+0.4016	0.9982	12	8	12.0	100.30	7.93	99.12
y=0.0153x+0.0450	0.9884						
y=0.0569x+0.6610	0.9941	14	8	14.10	100.71	8.07	100.87
y=0.0298x+0.0278	0.9881						

3.6 INTERFERENCES

The tolerance limit was describe as the concentration of the added species interference (such as lactose monohydrate, , magnesium stearate, starch, cellulose-microcrystalline, and mannitol) causing an error of more than ±5% on the analytical signal, then Before action with the analysis of the compound under study in pharmaceutical dosage forms, it was conducted to discover its effect. Samples were prepared by mixing known quantities of the investigated drugs with different quantities of mutual excipients. A good percentage recovered from the tested drugs obtained from those laboratory synthetic mixtures shows that there is no interference from these supplement additives with the methods applied. Furthermore, the accuracy of the proposed procedure has been more tested by applying the standard addition technique. The results obtained (Table 10) reveal a great degree of accuracy.

Table (10): Tolerance limit for foreign species on the determination of DicNa and PriM with the study methods

Methods	Lactose Monohydrate (850 µg/m)		Starch (850 µg/m)		Magnesium stearate (120 µg/m)		Cellulose-microcrystalline (180 µg/m)		Manitol (850 µg/m)	
	Error %	Recovery %	Error %	Recovery %	Error %	Recovery %	Error %	Recovery %	Error %	Recovery %
Q-Analysis	-3.35	103.35	+ 4.58	95.42	+ 4.52	95.48	- 4.01	104.01	95.68	+ 4.32
2D zero crossing point	+4.60	104.60	- 4.13	95.86	- 4.81	104.81	+ 4.65	104.65	103.90	- 3.90
HPSAM	+ 4.70	95.29	- 4.50	104.51	- 4.11	104.11	- 4.81	95.19	104.55	- 4.55

3.7 APPLICATION OF THE METHODS

To evaluate the analytical applicability of the planned methods, these methods and process have been applied on the pharmaceutical formulation (tab) and synthetic lab mixture, the absorbances of the sample solution i.e. A1 and A2 were noted at 258 nm (λ-max of PriM) and 265nm (Isosbestic point) respectively, and ratios of absorbance were calculated, i.e. A2/A1. The relative concentration of both two drugs in the sample was intended using equations [1] and [2]. The Q-analysis technique procedure was effectively used to determine the amounts of PriM and DicNa by repeated three times within the synthetic lab mixture and pharmaceutical formulation (Table 11), The results gotten were in good agreement with the relevant quantitative markers and labeled amount.

The suggested 2D zero-cross technique for simultaneous determination of DicNa, and PriM was effectively applied with the support and aid of standard addition method for simultaneous quantification of DicNa, and PriM in the pharmaceutical formulation. The results of the recovery study and application are potted in (Table 12 & 13) respectively. The recoveries ranged from 99.37% to 101.54 % at different drug concentrations, with % RSD < 2.

For the (ZO-HPSAM) and (2D-HPSAM) methods for the simultaneous estimation of DicNa and PriM in the synthetic mixture and pharmaceutical formulation. The results data are listed in (Table 14 & 15). The good agreement between the findings and the composition values suggested by the suppliers indicates that HPSAM is effectively applicable to the simultaneous evaluation of DicNa and PriM.

Table (11): Recovery study data of PriM and DicNa by (Q-Abbsorbance) method

Formulation	PriM	DicNa	PriM	DicNa

	(µg/ml)	(µg/ml)	Mean recovery [a] ± % RSD	Mean recovery [a] ± % RSD
Synthetic mixture	16	16	98.30 ± 1.05	101.21 ± 3.40
	28	28	99.69 ± 1.55	100.16 ± 2.70
	56	56	99.46 ± 1.05	99.75 ± 1.84
Tablet formulation [b]	24	24	100.64 ± 0.36	100.01 ± 0.63

[a] Average of 3 determination. [b] (Dioxaflex Plus)

Table (12): Determination of DicNa in pharmaceutical formulation by 2nd derivative zero-crossing method

Drug sample taken		Standard addition technique		
Name	µg/mL	Pure added	µg/mL	Mean recovery [a] ± % RSD
Tablet formulation [b]	8	DicNa	6	100.92 ± 1.2663
			12	100.32± 1.8112
			30	99.37 ± 0.4480
	10	PriM	7	99.78 ± 1.9171
			11	101.54± 1.0402
			18	100.09 ± 0.7143

[a] Average of 3 determination. [b] (Dioxaflex Plus)

Table (13): Simultaneous determination and recovery of DicNa, and PriM in tablet sample

Tablet sample	Ac	Method of analysis	Amount taken (µg/mL)	Amount found (µg/mL)	Recovery %
Tablet formulation	DicNa	2D zero-cross technique at 251.69 nm	50	50.39	100.78
	PriM	2D zero-cross technique at 228.02 nm	4	3.95	98.75

Table (14): Application of ZO-HPSAM for determination of DicNa and PriM in a synthetic lab mixture and pharmaceutical product

Formulation	A-C Equation	R^2	Amount taken (µg/ml)		DicNa		PriM	
			DicNa	PriM	Amount found (µg/ml)	Recovery %	Amount found (µg/ml)	Recovery %
Synthetic mixture	y=0.0291x+0.0807 y=0.0167x+0.0252	0.9953 0.9985	4.5	7.5	4.47	99.35	7.25	96.65
	y=0.0618x+0.3692 y=0.0206x+0.057	0.9884 0.9807	7.5	15	7.57	100.93	14.60	97.33
	y=0.0679x+0.584 y=0.0251x+0.1108	0.9895 0.9735	11	24	11.05	100.54	24.45	101.85
Tablet formulation	y=0.0095x+0.1748 y=0.0011x+0.0925	0.9969 0.9886	10	12	9.8	98.00	12.05	100.40

Table (15): Application of 2D-HPSAM for determination of DicNa and PriM in a synthetic lab mixture and pharmaceutical product

Formulation	A-C Equation	R^2	Amount taken (µg/ml)		DicNa		PriM	
			DicNa	PriM	Amount found (µg/ml)	Recovery %	Amount found (µg/ml)	Recovery %
Synthetic mixture	y=0.0317x+0.0042	0.9939	6	11	6.08	101.33	10.99	99.90
	y=0.0197x-0.0688	0.9959						
	y=0.0352x+0.1255	0.9977	12	18	12.05	100.41	17.78	98.77
	y=0.0221x-0.0323	0.9891						
	y=0.0574x+0.1963	0.9981	10	22	9.88	98.8	22.32	101.45
	y=0.0319x-0.0558	0.9944						
Tablet formulation	y=0.0293x+0.5664	0.9981	8	20	7.94	99.25	20.02	100.12
	y=0.0027x+0.3553	0.9901						

4. STATISTICAL ANALYSIS

Statistical study was achieved on the results found by the proposed ways and the stated reported method (Vignaduzzo et al., 2010), for each compound using Student's t- and F- tests at P = 0.05, with respect to both precision and accuracy; No significant difference was initiated, as shown in (Table 16). One-way ANOVA was applied to compare the alterations between the developed methods, (Table 17) showing no significant difference between the DicNa and PriM identification methods. Data analysis was performed by SPSS.

Table (16): Statistical comparison of the proposed methods with the reported one (Vignaduzzo et al., 2010) for determination of DicNa and PriM in their pharmaceutical formulation

Methods	Q-Absorption ratio method		2D- zero crossing		ZO-HPSAM		2D-HPSAM		* Reported method	
	DicNa	PriM	DicNa	PriM	DicNa	PriM	DicNa	PriM	DicNa	PriM
Mean	100.28	99.52	100.35	100.04	99.71	99.06	99.94	100.10	95.72	96.90
%RSD	0.6393	0.9664	0.6978	1.1520	1.3244	2.4988	1.1449	1.0986	0.9470	1.1976
n	4	4	4	4	4	4	4	4	4	4
Student t-test ** (2.306)	0.779	0.198	0.8037	0.5883	0.3431	0.2527	0.4664	0.5404		
F-value ** (6.38)	0.5003	0.6869	0.5969	0.9861	2.1225	4.5493	1.5940	0.8973		

* HPLC reported method (Vignaduzzo et al., 2010), the determinations were carried out on a Luna C18 analytical column (250mm ×4.6mm I.D., 5 mm particle size) thermostatted at 30°C. The mobile phase was a 48:9:43 (v/v/v) mixture of MeOH, 2-propanol and 50mM sodium phosphate (pH =5.5), pumped at 1.0 $mL.min^{-1}$. Detection wavelength was 225 nm. All samples were filtered through 0.45 mm nylon filters before injection.

** Theoretical values of t and F at (P= 0.05).

Table (17): Results of ANOVA (one-way) for comparison of the proposed methods and the reported (Vignaduzzo et al., 2010) for determination of DicNa and PriM in their pharmaceutical formulation

Variation	SS	df	MS	F	P-Value	F crit
DicNa						
Between Groups	4.6167	3	1.538906	0.287595	0.833494	3.490295
Within Groups	64.2113	12	5.350947			
Total	68.8280	15				

PriM						
Between Groups	4.5091	3	1.5030	0.347193	0.791871	3.490295
Within Groups	51.9498	12	4.3291			
Total	56.459	15				

5. CONCLUSION

Four exceptional exact mathematical treatments of spectral recorded data were successfully applied to determine two components DicNa and PriM all together in the laboratory prepared mixtures and the pharmaceutical formulations. Q-absorbance ratio, 2D- zero-crossing technique, HPSAM, were used to resolve and decide the overlapped spectra without previous separation of the mixtures, interferences were removed by choosing the most valid wavelength. Compared to the HPLC technique, these spectrophotometric methods did not need an early separation steps, and using toxic organic solvent, thus the method can be considered as an environmental friendly.

Authentication of the methods was established accuracy, precision, linearity, LOD, LOQ and selectively, the methods were confirmed to be selective, accurate, precise, cooperative, and effective for the analysis study of these compound drugs in a pharmaceutical dosage forms. The results were developed by four expected proposed methods, showing acceptable results compared with the reported methods. Based on the results gained and statistical data analysis, these methods are appropriate for the estimation and determination of these drugs without any interference of the pharmaceutical excipients present in the formulation and can be simply applied in acceptance sampling quality control lab.

ACKNOWLEDGEMENT

I would like to express my deep and sincere thankfulness to the Pharmaceutical Chemistry Department, College of Pharmacy, Hawler Medical University, and Ministry of Science & Technology (Iraq-Baghdad) for use of their research lab for UV-spectrophotometer and HPLC.

6. REFERENCES

ABDEL SHAHEED, C., MAHER, C., WILLIAMS, K. & MCLACHLAN, A. 2017. Efficacy and tolerability of muscle relaxants for low back pain: systematic review and meta-analysis. *European Journal of Pain*, 21**,** 228-237.

AFKHAMI, A., BAHIRAEI, A. & MADRAKIAN, T. 2016. Gold nanoparticle/multi-walled carbon nanotube modified glassy carbon electrode as a sensitive voltammetric sensor for the determination of diclofenac sodium. *Materials Science and Engineering: C*, 59**,** 168-176.

ANDRES, J. V., REIG, F. B. & FALCó, P. C. J. A. 1995. H-point standard additions method for analyte determination in ternary mixtures. 120**,** 299-304.

ANGGRAINI, Y. & EKAWATI, I. W. 2020. Acupressure therapy as a pain reliever for dysmenorrhea. *Enfermería Clínica*, 30**,** 84-87.

BREZOVSKA, M., JAMPILEK, J. & OPATRILOVA, R. J. C. P. A. 2013. A review of HPLC methods used for determining the presence of meloxicam. 9**,** 69-76.

CHETHANA, B., BASAVANNA, S., ARTHOBA NAIK, Y. J. I. & RESEARCH, E. C. 2012. Voltammetric determination of diclofenac sodium using tyrosine-modified carbon paste electrode. 51**,** 10287-10295.

DARWEESH, S. A., KHALAF, H. S., AL-KHALISY, R. S., YASEEN, H. M. & MAHMOOD, R. M. 2018. Advancement and validation of new Derivative spectrophotometric method for individual and simultaneous estimation of Diclofenac sodium and nicotinamide. *Oriental Journal of Chemistry*, 34**,** 1625.

DIKRAN, S. B. & MAHMOOD, R. M. 2017. Spectrophotometric Determination of Diclofenac sodium Using 2, 4-dinitrophenylhydrazine in Pure Form and Pharmaceutical Preparations. *Ibn AL-Haitham Journal For Pure and Applied Science*, 28**,** 129-141.

GUIDELINE, I. H. T. J. Q. 2005. Validation of analytical procedures: text and methodology. 1**,** 05.

GUNJI, R., NADENDLA, R. R., PONNURU, V. S. J. I. J. O. D. D. & RESEARCH 2012. Simultaneous UV-spectrophotometric determination and validation of diclofenac sodium and rabeprazole sodium using hydrotropic agents in its tablet dosage form. 4**,** 316-324.

KHAMAR, J. C. & PATEL, S. A. 2012. Q-absorbance ratio spectrophotometric method for the simultaneous estimation of rifampicin and piperine in their combined capsule dosage.

KIMUAM, K., RODTHONGKUM, N., NGAMROJANAVANICH, N., CHAILAPAKUL, O. & RUECHA, N. 2020. Single step preparation of platinum nanoflowers/reduced graphene oxide electrode as a novel platform for diclofenac sensor. *Microchemical Journal*, 155**,** 104744.

KLEEMANN, A., ENGEL, J., KUTSCHER, B., REICHERT, D., KLEEMANN, A., ENGEL, J., KUTSCHER, B. & REICHERT, D. 2014. *Pharmaceutical substances, 2009: Syntheses,*

Patents and Applications of the most relevant APIs, Georg Thieme Verlag.

KUS, S., MARCZENKO, Z. & OBARSKI, N. J. C. A. 1996. Derivative UV-VIS spectrophotometry in analytical chemistry. 41**,** 889-927.

LINS, P. V. S., HENRIQUE, D. C., IDE, A. H., DA SILVA DUARTE, J. L., DOTTO, G. L., YAZIDI, A., SELLAOUI, L., ERTO, A., E SILVA, C. L. D. P. & MEILI, L. 2020. Adsorption of a non-steroidal anti-inflammatory drug onto MgAl/LDH-activated carbon composite–Experimental investigation and statistical physics modeling. *Colloids and Surfaces A: Physicochemical and Engineering Aspects,* 586**,** 124217.

MANE, R. V., PATEL, K., SUSHMITHA, G. S. & VASANTHARAJU, S. 2019. Development and Validation of Diclofenac sodium in tablets using Simple UV Spectrophotometric method. *Research Journal of Pharmacy and Technology,* 12**,** 611-614.

MICHOPOULOS, A., FLOROU, A. B. & PRODROMIDIS, M. I. J. E. 2015. Ultrasensitive Determination of Vitamin B12 Using Disposable Graphite Screen-Printed Electrodes and Anodic Adsorptive Voltammetry. 27**,** 1876-1882.

MOORE, N., DUONG, M., GULMEZ, S. E., BLIN, P. & DROZ, C. 2019. Pharmacoepidemiology of non-steroidal anti-inflammatory drugs. *Therapies,* 74**,** 271-277.

O'HAVER, T. & GREEN, G. J. A. C. 1976. Numerical error analysis of derivative spectrometry for the quantitative analysis of mixtures. 48**,** 312-318.

PATEL, K. N., PATEL, J. K., RAJPUT, G. C. & RAJGOR, N. B. J. D. P. L. 2010. Derivative spectrometry method for chemical analysis: A review. 2**,** 139-150.

PATIL, P. A., RAJ, H. A. & SONARA, G. B. 2016. Q-absorbance ratio spectrophotometric method for simultaneous determination of atenolol and ivabradine hydrochloride in synthetic mixture. *Pharmaceutical and Biological Evaluations,* 3**,** 224-230.

REIG, B. J. A. 1990. F.; Campins Falco, P. 115**,** 111.

ROBINSON, J. W., FRAME, E. S. & FRAME II, G. M. 2014. *Undergraduate instrumental analysis*, CRC press.

SALAZAR-ROJAS, D., INTILANGELO, A., VIGNADUZZO, S. E., MAGGIO, R. M. J. J. O. P. & ANALYSIS, B. 2019. Development and validation of a green method for dissolution monitoring of pharmaceutical combinations. Meloxican and pridinol. 170**,** 228-233.

ŚWIT, P., VERDú-ANDRES, J., WIECZOREK, M., KOZAK, J., KOŚCIELNIAK, P. & CAMPíNS-FALCó, P. 2018. New calibration model: combining integrated calibration method and H-point standard addition method to detect and avoid interference effects. *Analytical Letters,* 51**,** 1194-1207.

TIWARI, D., LALHRIATPUIA, C. & LEE, S.-M. 2015. Hybrid materials in the removal of diclofenac sodium from aqueous solutions: Batch and column studies. *Journal of Industrial and Engineering Chemistry,* 30**,** 167-173.

VIGNADUZZO, S. E., CASTELLANO, P. M. & KAUFMAN, T. S. 2010. Experimentally designed, validated hplc simultaneous determination of pridinol and diclofenac in their combined pharmaceutical formulations, which allows limiting diclofenac related compound A. *Journal of liquid chromatography & related technologies,* 33**,** 1720-1732.

VIGNADUZZO, S. E., VERA-CANDIOTI, L., CASTELLANO, P. M., GOICOECHEA, H. C. & KAUFMAN, T. S. J. C. 2011. Multivariate optimization and validation of a CZE method for the analysis of pridinol mesylate and meloxicam in tablets. 74**,** 609-617.

WONGRAKPANICH, S., WONGRAKPANICH, A., MELHADO, K., RANGASWAMI, J. J. A. & DISEASE 2018. A comprehensive review of non-steroidal anti-inflammatory drug use in the elderly. 9**,** 143.

YANG, Y. J., LIU, X. W., KONG, X. J., QIN, Z., LI, S. H., JIAO, Z. H. & LI, J. Y. 2019. An LC–MS/MS method for the quantification of diclofenac sodium in dairy cow plasma and its application in pharmacokinetics studies. *Biomedical Chromatography,* 33**,** e4520.

ZANCO Journal of Pure and Applied Sciences
The official scientific journal of Salahaddin University-Erbil
https://zancojournals.su.edu.krd/index.php/JPAS

ISSN (print):2218-0230**, ISSN (online):** 2412-3986**, DOI: http://dx.doi.org/10.21271/zjpas**

REVIEW ARTICLE

The major pathways of lipids (triglyceride and cholesterol) and lipoprotein metabolism

Karzan Jalal Salih[1*]

[1]Pharmaceutical Chemistry Department, Medical and Applied Science College, Charmo University, 46023 Chamchamal-Sulaimani, Kurdistan Region, Iraq.

A B S T R A C T:
Lipids are considered as organic substances that are relatively insoluble in water while soluble in organic solvents such as alcohol and ether. Unlike carbohydrates, proteins and nucleic acids, lipids are not polymers. Further, lipids are mostly small molecules. More than 90% of the fatty acids found in plasma are in the form of fatty acid esters primarily in the form of triacylglycerol, cholesteryl esters. Lipids can be exogenously from the dietary sources and endogenously mainly from the liver. Due to insolubility of lipids, so the circulation of lipids in the blood is performed by the actions of several transport vehicles such as spherical protein complexes which is known as lipoproteins which is an assembly of lipids with proteins. There are four major types of lipoproteins are participating in transporting lipids in plasma, which are classified based on their density, these includes chylomicrons (CM), very-low-density lipoproteins (VLDL), low-density lipoproteins (LDL), and high-density lipoproteins (HDL). Different types of lipoproteins have a different set of proteins (apoprotein) on their surface, these proteins served as address tags that determine both destination and function of each lipoprotein. In this review, we summarise the pathways and metabolites that involve in lipid and lipoprotein metabolism.

KEY WORDS: Triglyceride, Fatty acid β-oxidation, Cholesterol, Chylomicron, HDL, LDL, VLDL.
DOI: http://dx.doi.org/10.21271/ZJPAS.33.4.6
ZJPAS (2021) , 33(4);61-72 .

1. INTRODUCTION:

Lipids are a large insoluble molecular complex that acts as structural components of cell membranes (Harayama and Riezman, 2018) as well as acts as an energy sources that are transported through blood within a large spherical molecule known as lipoproteins. Lipids are broadly classified into four classes based on their structure and properties, they are simple, complex, derived, and miscellaneous lipids (Fahy et al., 2011).

* **Corresponding Author:**
Karzan Jalal Salih
E-mail: Karzan.salih@charmouniversity.org
Article History:
Received: 02/04/2021
Accepted: 05/06/2021
Published: 18/08 /2021

control cellular processes (Lizardo et al., 2018), cell proliferation (Hall et al., 2020), apoptosis (Teixeira et al., 2020), metabolism and migration (Toprak, 2020). Moreover, it has been reviewed that lipid metabolism has a significant role in viral replication (Lorizate and Krausslich, 2011), as recently has shown that the lipid metabolism has a significant impact on COVID-19 virus infection and as a drug target (Abu-Farha et al., 2020), through alterations and blocking of lipid membrane composition of viruses which consequently interfere with the viral life cycle (Lorizate and Krausslich, 2011). The constituent of lipid in the body is bout 15-20%, which is mostly (90%) of the lipid is in the form of triglyceride, and the rest of them are free cholesterol, cholesteryl ester, phospholipids, glycolipids (Figure 1) (Fahy et al., 2011).

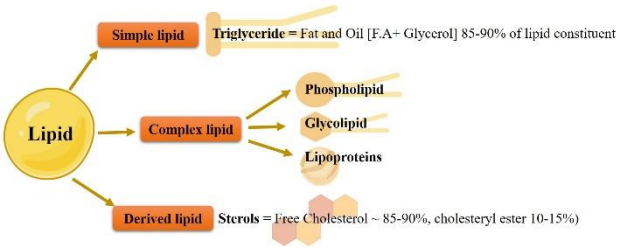

Figure 1: The composition of lipids. Most of the lipid constituents consists of triglycerides (simple lipid, while the rest of them include complex lipids (phospholipid, glycolipid, and lipoproteins), and derived lipid includes sterols.

The highest constituent of dietary lipid is Triglyceride, and its transported from the intestine to the blood via chylomicron lipoprotein (Nordestgaard, 2016) and its normal range in the blood serum is below 150 mg/dL (Kiss et al., 2018).

The esterification of three molecules of fatty acids with glycerol resulted in the formation of triglyceride. However, different types of fatty acids in triglyceride resulted in the formation of several types of triglyceride (Alvarez et al., 2002). Increasing triglyceride concentration in the blood can be either by a genetic defect (primary hyper glycemia) or due to non-genetical factors known as secondary hyperglycaemia. These include using unhealthy diet, type-II diabetes mellitus, hepatic steatosis, and nephrotic syndrome. The increase in triglyceride level in plasma is considered as an indicator of development of acute pancreatitis (AP) (Yadav and Lowenfels, 2013). Nowadays, a high-fat diet and resultant obesity are common; therefore, the prevalence of elevated serum triglyceride concentration serum triglyceride is high, affecting approximately 27% of all adults (Nordestgaard, 2016).

Beside triglyceride, cholesterol is another type of lipids which is a structural component in the cell membranes and a crucial lipid for maintaining cellular homeostasis (Gerard, 2013). Cholesterol, exclusively found in animals, is the most abundant animal sterol (Ikonen, 2008a). Cholesterol it also serves as a precursor for the synthesis of vitamin D (Prabhu et al., 2016), bile acids in the form of cholic and chenodeoxycholic acids which appear in the gut (Gerard, 2013) and variety of steroid hormones (Lyu et al., 2019, Payne and Hales, 2004), however unabsorbed dietary cholesterol which is around 200 mg/day and is added to the biliary cholesterol secretion (Gerard, 2013).

The composition of cholesterol can be present either as free form or ester form (Cholesteryl esters), which makes the structure even more hydrophobic (water insoluble) than free (unesterified) cholesterol.

Cholesterol is found as cholesterol ester in which the esterification occurs at the OH group of C3 with fatty acid. (Ikonen, 2008a). There are two major sources of cholesterol synthesis, those that are synthesized endogenously in the endoplasmic reticulum and transported through the blood via low-density lipoprotein (LDL) (Bloch, 1965). The other source is exogenously that gets from diet and absorbed from the gastrointestinal tract, where triglycerides and cholesterol are packaged to form chylomicrons with triglycerides and cholesterol in the form of chylomicrons (Ikonen, 2008b).

Lipoproteins serve as an address tag that play a significant role in transportation of cholesterol from and to tissues, thus LDL carries blood cholesterol from liver to other tissues known as bad cholesterol, inversely, HDL carries blood cholesterol from other tissues to the liver known as good cholesterol (Figure 2) (Ohkawa et al., 2020).

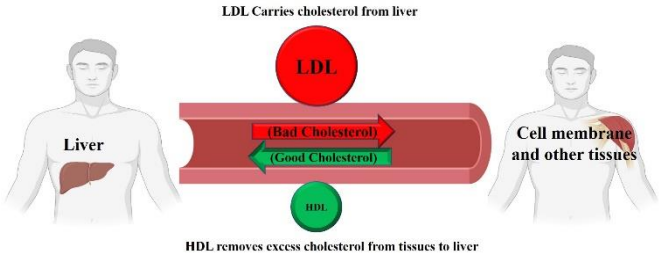

Figure 2: Mechanism of cholesterol circulation in the blood from liver to other tissues and vice versa. LDL transfer cholesterol from blood to other parts of the body known as bad cholesterol, while HDL transfer excess cholesterol after it has been used by other tissue to the liver which is called good cholesterol.

Furthermore, it has been found that different set of proteins were binding on the surface of lipoproteins which are called apolipoproteins, these proteins served as address tag, that determine both function and destination of each lipoprotein. Because the size of lipids is larger than proteins, so particles that contain more lipid are larger in size but have a lower density (Table1) (Wang et al., 2017).

Table 1: Properties of plasma lipoproteins based on their density and lipid content.

Density range (g/mL)	Lipoprotein function	Major core lipid	Apolipoproteins
d < 0.930	Chylomicrons	Exogenous Triglyceride	B-48, E, A-I, A-II, A-IV, C
0.950< d <1.006	Very-low-density lipoprotein	Exogenous Triglyceride	B-100, C-I, C-II, C-III, E
1.019 < d < 1.063	Low-density lipoprotein	Endogenous Cholesteryl esters	B-100
1.063 < d < 1.210	High-density lipoprotein	Endogenous Cholesteryl esters	A-I, A-II

2. TRIGLYCERIDE AND FATTY ACIDS:

2.1. TRIGLYCERIDE AND FATTY ACID SYNTHESIS:

Triglycerides are esters of three molecules of fatty acid and glycerol which represent the major lipid component of dietary foods including fat and oil. Here triglyceride molecules are the major storage of the lipids and transport of fatty acids in the form of chylomicron and VLDL within cells and in the plasma (Alves-Bezerra and Cohen, 2017). There are two major sources that responsible of triglyceride synthesis in the body. As can be seen in the figure 3, more than 90% of triglyceride is synthesized from exogenous sources that come from dietary source (Lowe, 2002). The dietary triglyceride is emulsified by bile acids within the intestinal lumen and enzymically degraded "digested" by pancreatic enzymes, whose secretion is hormonally controlled (Jaworski et al., 2007, Pasquier et al., 1996).

The large molecules triglyceride to be taken up efficiently therefore and break down to its constituents by the action of pancreatic lipase, which preferentially removes the fatty acids at carbons 1 and 3 (Courchesne-Loyer et al., 2017). The primary products of hydrolysis are a mixture of 2-monoacylglycerol and two molecules of free fatty acids (Lowe, 2002).

The synthesized fatty acids are stored in the muscle which undergo β-oxidation to acetyl-CoA , then the generated acetyl-CoA pass through tricarboxylic acid cycle (TCA cycle) to release energy as ATP via oxidative phosphorylation process in mitochondrion from electron transport chain (Donnelly et al., 2005). Beside β-oxidation of fatty acids, part of it combines with glycerol molecule to generate triglyceride which are stored in adipocytes (Jensen, 2002) (Figure 3a).

Triglycerides are also synthesized endogenously from fatty acid and glycerol in the liver and stored in adipose tissue for later use. To synthesise triglyceride, both fatty acids and glycerol must be activated to glycerol 3-phosphate(Alves-Bezerra and Cohen, 2017). In both liver and adipose tissue, glycerol is activated by dihydroxyacetone phosphate (DHAP) produced in glycolysis is reduced by glycerol 3-phosphate dehydrogenase to glycerol 3-phosphate, however, the enzyme of glycerol kinase, which is absent in adipose tissue serves as a precursor for glycerol 3-phosphate, then the enzyme phosphatase cleaves off phosphate of glycerol 3-phosphate to produce diacylglycerol followed by addition of acyl groups to form triglyceride (Figure 3b) (Mandal et al., 2011, Driver et al., 2017).

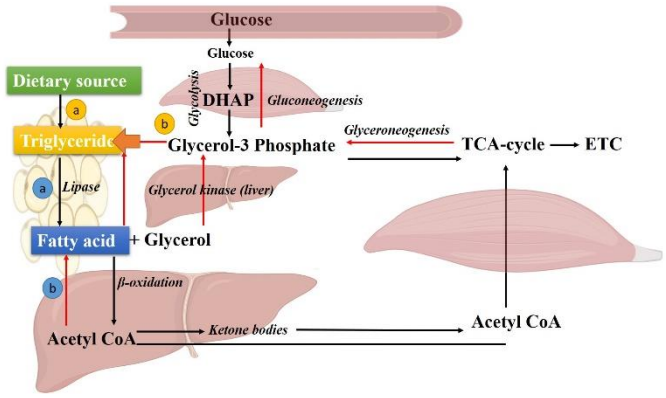

Figure 3: Triglyceride and fatty acid synthesis pathways.

a) Exogenous pathways: Triglycerides comes from the dietary sources and through lipolysis process it hydrolyzed to both fatty acids and glycerol.

b) Endogenous pathways: Triglyceride synthesized from glycerol-3-phosphate and fatty acids.

2.2. FATTY ACID β-OXIDATION:

Oxidation of fatty acids is a multi-step process that occurs in several tissues in the body including liver, skeletal muscle, and cardiac muscle for energy requirement. (Goepfert and Poirier, 2007).

Glucose and fatty acids are the three substrates for the generation of energy, however, during fasting, when blood glucose level becomes limited, fatty acid β-oxidation is importance in most tissues, except the brain. Furthermore, the liver converts fatty acids into ketone bodies that serve as an

additional energy source in most of the tissues including the brain (Dieuaide et al., 1992).

The process starts with utilizing long chain fatty acids which are activated by thiokinases or fatty acyl CoA synthetases in cytosol and convert it to fatty acyl CoA. The reaction occurs in two steps and requires ATP, coenzyme A and Mg^{2+} (Houten and Wanders, 2010). Next step is transfer fatty acyl CoA from cytosol into mitochondrion, however, the inner mitochondrial membrane is impermeable to fatty acids therefore a specialized carrier protein called carnitine carrier system reacts with fatty acyl CoA and forming acyl-carnitine which it is transported across the mitochondrion membrane to matrix of mitochondria the reaction is catalyse by carnitine acyltransferase I, once acyl-carnitine moved into mitochondrion, it converts to acyl CoA by the action of carnitine acyltransferase II and carnitine released returns to cytosol for reuse (Figure 4) (van Eunen et al., 2013, Longo et al., 2006). The process of fatty acid oxidation starts by eliminating two carbon units (acetyl CoA) from acyl CoA in a sequence of four reactions. In the first step of β-oxidation the acyl CoA undergoes dehydrogenation to form one double bond which is double bond is formed between α and β-carbons of acyl CoA resulted in the formation of trans-enoyl CoA (i.e., 2 and 3 carbons) and the reaction is catalysed by acyl CoA dehydrogenase. β -hydroxy acyl CoA dehydrogenase catalyses the third step of the reaction and convert β -hydroxy acyl CoA to β-keto acyl CoA. Finally, β-ketoacyl CoA converted to acetyl CoA and the remaining acyl CoA by the action of thiolase enzyme, and the process continues till the fatty acid is completely oxidized, and Acetyl CoA can enter citric acid (TCA) cycle and get completely oxidized to CO_2 and H_2O (Goepfert and Poirier, 2007).

Among of these four-catalysing reactions, in step one ; three FAD and NAD^+ are reduced to $FADH_2$ and $NADH+H^+$ respectively, which then pass-through tricarboxylic acid cycle (TCA) and electron transport chain (ETC) to release energy as the form of ATP, and the overall reaction for each cycle of β-oxidation can be written as follows:

C_n Acyl CoA + FAD + NAD^++ H_2O + CoASH ➔$C_{(n-2)}$ Acyl CoA+Acetyl CoA+ $FADH_2$ + NADH+ H^+.

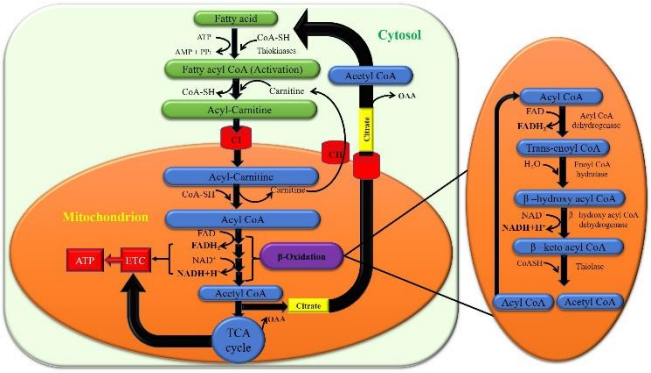

Figure 4: Fatty acid β-Oxidation Pathways. The pathway occurs in both cytoplasm (green) and mitochondrion (blue).

The most common fatty acid molecule that undergoes β-oxidation is the palmitic acid (which contain 16 carbons) that undergoes 7 cycles of β oxidation to yield 8 acetyl CoA.

Overall, fatty acid synthesis mostly occurs in cytosol and acetyl CoA is the precursor, while the process of β-oxidation occurs in mitochondria and acyl CoA is the substrate for this process. Furthermore, the synthesis of fatty acids mostly occurs after meal which the body has enough amount of carbohydrates to generate energy, however, in case, of few or no carbohydrates, fatty acid β-oxidation occurs to produce the required amount of energy (Modre-Osprian et al., 2009).

Therefore, the regulation of fatty acid synthesis and β-oxidation is important to balance the lipid contents in the body, whereas any imbalance in these two processes contribute to several diseases such as type II diabetes mellitus and obesity (Zhang et al., 2010, Boden et al., 1991, Boden, 2008).

Furthermore, it has shown that the fatty acid β-Oxidation pathway is important for decidualization or lipid metabolism in endometrial stromal cells (ESCs) in both human and mice (Tsai et al., 2014).

2.3. METABOLISM OF TRIGLYCERIDE:

2.3.1. Metabolism of Chylomicron (CM)

To begin with lipid metabolism from the dietary source, stomach push the dietary lipid that consists of about 85-90% triglycerides, and the rest are cholesterol and cholesterol ester to the small intestine (Weil et al., 2012, Xiao et al., 2011, Karpe et al., 1995).

Due to the big size of the lipid, the entero-hormone cholecystokinin which comes from main pancreatic duct stimulate the smooth muscle

around the gallbladder to contract which expel out certain substances into the cystic duct which called bile salts including both cholic acid and deoxy cholic acid (King et al., 2015, Liddle et al., 1985, Li and Chiang, 2014). Bile acids are synthesized from cholesterol metabolism in the liver and secreted into the small intestine in response to dietary fat where they enable absorption of fat-soluble vitamins and cholesterol (Hofmann et al., 2008, Li and Chiang, 2014). The amount of bile acids in the bile is about two thirds of the total weight in the human's body (Di Ciaula et al., 2017). Previously it has been shown that the concentration of bile acids is increased from 0.2-0.7 µM during a fasting situation to about 5µM after meals (Ponz De Leon et al., 1978). The synthesized bile salts transported to small intestine and combine with both glycine and taurine molecule (Di Ciaula et al., 2017) which is important for emulsification of big fat globule molecule and separate into small and little fatty droplets also known as emulation droplets (Tyor et al., 1971, Dawson et al., 2009). Due to insolubility of fat molecule, the hydrophobic part of lipid molecules interacts with the hydrophobic part of bile salt forming fat globule, while the hydrophilic portion of bile interacts with the fluid within intestine (Di Ciaula et al., 2017). The emulsified lipid is converted to small fatty droplet that contains triglyceride are digested by enzyme that secrets from the main pancreatic duct which is known as pancreatic lipase to produce two molecules of free fatty acids (FFAs) and mono acyl glycerol (MAG), which then they surround by bile salt in combination with cholesterol and fat-soluble vitamin they form a compact molecule called micelle which is about 500 times as smaller as emulsion droplet (Lo and Coschigano, 2020, Mattson and Volpenhein, 1964). Later the synthesized micelles start to move to enterocytes of the intestine which there the bile salts are recycled to the liver through the portal vein (Dawson, 2018), while both FFAs and MAG are going to a special organelle in the cell which is known as smooth endoplasmic reticulum (SER), which is there both FFAs and MAG are fused and packed together to create triglyceride (TG) (Weil et al., 2012). Here, generated TG with some of the cholesterol and cholesteryl ester combine with a special protein called apo-B_{48} protein that generated from another enterocyte's organelle which is rough endoplasmic reticulum (RER) and packed all together into a special lipoprotein molecule called nascent chylomicron (Kohan et al., 2015), however, knockout of the Apo-B_{48} resulted in the decreased secretion of TG-rich chylomicron (Lo et al., 2008). The generated chylomicron before going to the blood stream is undergo a special lymphatic circulation which is absorbed via lacteal and, eventually, they pass through the largest lymphatic vessel known as thoracic duct into the blood circulation (Dixon, 2010).

In the blood stream, beside apo-B_{48} that bounds to nascent chylomicron, there are two more apo-proteins which are donated via HDL and bound to nascent chylomicron which are known as Apo-E and Apo-CII and forming chylomicron (CM)(Lo and Coschigano, 2020).

Apo CII is important for activating a special enzyme molecule known as lipoprotein lipase (LPL) that locates in the capillary endothelial (Merkel et al., 2002). Once lipoprotein lipase is activated by apo-CII, the activated enzyme cuts triglyceride molecules which is about 85% of total lipids inside nascent chylomicron into three molecules of free fatty acids and glycerol and the apo-CII back to HDL (Havel et al., 1973, Goldberg, 1996).

The generated free fatty acids go to each of the adipocytes and muscles such as skeletal muscle and cardiac muscle which can be used to produce triglyceride by its combination with glycerol and release energy as ATP, respectively (Dixon, 2010, Lambert et al., 2012). Small amount of CM (contains uncatalyzed TG with each of cholesterol, Apo-B_{48} and Apo-E become remain called chylomicron remnants (CM remnant) start to move to the liver via binding of its Apo-E into a special receptor in liver called (LDL) (Cooper, 1997). Here, Apo-E has high affinity for a special receptor located in liver and adrenal cortex called LDL receptor related proteins which take the CM remnant into the liver, which, consequently, CM components are separated from each other to proteins, cholesterol, and small TG (Huang and Mahley, 2014). The remaining TG can be stored while cholesterol can be converted to bile salt, stored as cholesterol ester with the action of a special enzyme called Acyl-CoA: cholesterol acyltransferase (ACAT) and incorporated into a cell membrane (Xu et al., 2019).

2.3.2. Metabolism of very low density of lipoprotein (VLDL)

The endogenous lipoprotein pathway begins in the liver with the formation of VLDL. The triglycerides, cholesterol and phospholipid that come from remnant chylomicron into the liver combine with another lipoprotein molecule called Apo-B_{100} that is generated from hepatocyte cell's rough endoplasmic reticulum (RER) which is very similar to Apo-B_{48} (Hazzard et al., 1984, Hokanson and Austin, 1996). Through the combination of each of the triglycerides (from remnant chylomicron and some de novo synthesis), cholesterol and Apo-B_{100} generate another type of lipoprotein known as nascent very low-density lipoprotein (nascent VLDL) which surrounded by phospholipids (Xiao et al., 2011, Taskinen et al., 2020).

The nascent VLDL in the liver pushed out into the blood circulation, which there is nascent chylomicron. There are two more apo-proteins which are known as Apo-E and Apo-CII are donated via HDL and bind to nascent VLDL and forming very low-density lipoprotein (VLDL) (Freeman and Walford, 2016). Here, Due to activating LPL via CII as seen in CM, this activated LPL can cut TG in to both three molecules FFA and glycerol, which apoprotein CII become return to HDL, and FFA go to either muscle tissue which use as energy generator (as ATP) via its β-oxidation and pass through TCA and ETC, or go to the adipose tissue and become combine with glycerol that comes from glucose in adipocytes to make TG and store in it which gave back Apo-CII to the HDL. Small amount of VLDL become remain called (VLDL remnants or IDL) which contain cholesterol, cholesteryl ester, small amount of TG, Apo-E and apo- B_{100}. As mentioned before, Apo-E has high affinity for a special receptor called LDL receptor related proteins (LDL-R) which is located in the liver and adrenal cortex (Lillis et al., 2008). IDL can either go back to the liver and take up by the LDL-R which could be digested into different components as same fate happened in the CM remnant, or it goes to the adrenal cortex, where cholesterol taken up and utilized to make steroid hormone such as aldosterone, cortisol and sex hormones in different zones or may be stored as cholesteryl ester. However, some of the IDL molecule react by a special enzyme in the liver called hepatic TG lipase (HTG lipase) which contributes to the regulation of the level of plasma triglyceride that facilitates the clearance of TG molecule in IDL particle and send to the liver which is converted to three molecules of FFA and glycerol (Chatterjee and Sparks, 2011). The remaining IDL molecule back to the circulation and return Apo-E protein to the HDL molecule and generate another new lipoprotein molecule which contains Apo-B_{100}, small amount of TG and large amount of cholesterol and cholesteryl ester, this one known as low density lipo-protein or LDL (Warnick et al., 1990).

2.3.3. Metabolism of low density of lipoprotein (LDL)

Most of the generated LDL (60-70%) goes back to the liver, there cholesterol and triglyceride in the liver can be utilized in different sources. The remaining LDL which is about 30-40% can undergo some special tissues via LDL-receptor that is present in these tissues; and there its cholesterol can be utilized for different purposes. Some of these tissues are located in the gonads (male and female sex organs) (Lent-Schochet and Jialal, 2020) . Due to the present of LDL receptor located on these gonads, here LDL particle can go and deliver some of its cholesterol to these gonads, to create female sex hormone including progesterone and estrogen hormone if the gonad is female and generate testosterone sex hormone if the gonad is male(Wang et al., 2011). Furthermore, LDL particle can go and bind to LDL-R that located in adrenal cortex, as seen in VLDL the cholesterol molecules are taken up and can be utilized to make steroid hormones such as aldosterone (Goodfriend et al., 1995), cortisol, DHEA (Di hydro Epi aldosterone) in different zones or may be stored as cholesterol ester(Struthers and MacDonald, 2004). Finally, some of these LDL can be taken to peripheral tissues like microphages (Hannich et al., 2018). However, stay of LDL for a while in the blood resulted in its accumulation in subendothelial spaces and consequently it became undergo special oxidation reaction via reactive oxygen species (Wen and Leake, 2007).

After LDL oxidized it becomes oxidative LDL which is dangerous and causes inflammatory response. So special molecule which present in macrophage start to take up these oxidized LDL via a receptor that present in macrophage (Rosenfeld et al., 1990) called Fatty acid translocate (FAT) also called FAD/CD36 (Wang and Paigen, 2005, Nozaki et al., 1999). FAD/CD36 can take up some of the oxidized LDL-particles and become accumulated, which consequently convert the macrophage into foam cells which is dangerous to make atherosclerosis (Nozaki et al., 1999).

Here, due to the protein that is made by intestine called Apo-A1 (which is initial component of HDL molecule) comes over the macrophage (Kohan et al., 2015), which can bind into a special receptor that present on macrophage called scavenger receptor (ABCA1) and (ABCG1); which firstly bind to (ABCA1) and forming nascent HDL molecule, then taken up more cholesterol from microphage (ABCG1) (Olofsson et al., 2007). Which the cholesterol taken up into the (ABCA1) molecule and make pre or nascent HDL, after getting mole cholesterol it becomes converted to HDL3 molecule and goes to ABCG1 receptor and take up furthermore cholesterol and make HDL2 molecule. Now, there is much cholesterol in HDL molecule (Yvan-Charvet et al., 2010). These cholesterols in HDL can go over to the adrenal cortex and gonads and through its Apo-A1 protein binds to special scavenger receptor called SRB1which is present in these two organs (Bochem et al., 2014). The HDL contained cholesterol is esterified into cholesteryl ester with the action of the enzyme via lecithin-cholesterol acyltransferase (LCAT), which later it uses as a constituent of each of VLDL, IDL and LDL (Shrestha et al., 2018).

Furthermore, some of the cholesterols inside HDL particles go back to the liver via apo-A1 bind to SRB1-recepter, and then deposit their cholesterol into the liver, and decrease in size, and become immature HDL, then go back to macrophage (Feingold and Grunfeld, 2015). An overview of lipids and lipoprotein metabolism are shown in figure 5.

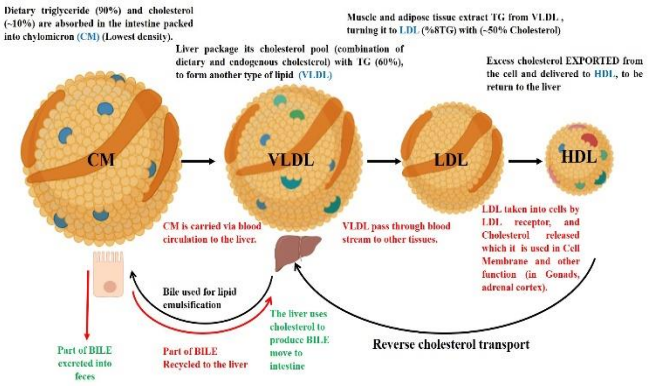

Figure 5: Overview of lipid metabolism and lipoprotein circulation. CM: Chylomicron, VLDL: Very low-density Lipoprotein, LDL: Low density lipoprotein, HDL: High density lipoprotein.

3. CHOLESTEROL METABOLISM

Cholesterol is an essential lipid for mammalian cells, it is either obtained from the dietary source or synthesized by an endogenous pathway that occurs in most cells of the body particularly in the liver. Acetyl CoA is the precursor for the synthesis of cholesterol which can be produced from glucose, fatty acids, or amino acids (Hampton et al., 1996). Beside triglyceride, cholesterol is clinically considered as a crucial part of plasma lipid. In healthy individuals the total plasma cholesterol is in the range of 150-200 mg/dl, which high cholesterol level connected to a higher risk of cardiovascular disease (Carson et al., 2020).

Cholesterol consists of four fused hydrocarbon rings (A-D) called the steroid nucleus, and it has eight carbons, branched hydrocarbon chain attached to carbon 17 of the D ring with a hydroxyl group bonded on carbon number three which present in the first ring (Tabas, 2002). Each day approximately one gram of cholesterol is synthesized via the human body, which almost 20-25% of total daily cholesterol production occurs in the liver (Russell and Setchell, 1992). Cholesterol is the precursor for the synthesis of steroid hormones like in the body (progesterone, testosterone, aldosterone, cortisol and estradiol) (Tabas, 2002), vitamin D and bile acids, it can also serve as an element of cell membrane and plasma lipoproteins particularly in low-density lipoprotein (LDL) that sent to the peripheral tissues (Hegele, 2009).

Cholesterol biosynthesis is a highly complicated process which starts with acetyl-CoA building block, followed by hydration of acetyl-CoA to convert to β-Hydroxyβ-Methyl Glutaryl CoA (HMG-CoA) (Cerqueira et al., 2016), then formation of six carbon molecule known as mevalonate, followed by decarboxylation of mevalonate to isoprenoid with five carbon units, afterward the mevalonate with several steps resulted in synthesis of thirty carbon atom called squalene and finally conversion of squalene to cholesterol with 27 carbon atoms (Russell and therapy, 1992, Cerqueira et al., 2016). In cholesterol synthesis the reducing equivalents are provided by NADPH, while ATP provides energy. Furthermore, it has shown that for the synthesis of cholesterol, beside acetyl CoA, the NADPH is required (Rohrl and Stangl, 2018).

On the other hand, during cholesterol degradation process the ring structure of cholesterol cannot be metabolized to CO_2 and H_2O as it happened in carbohydrates and proteins due to the absence of the enzymes that are crucial for degrading the ring structure of sterol (Wang et al., 2017). Therefore, beside its conversion to vitamin D, hormones, and its secretion into the bile, about 50% of cholesterol is converted to bile acids (500mg/day) and excreted in feces as an only route for disposal of cholesterol in the body (Figure 6).

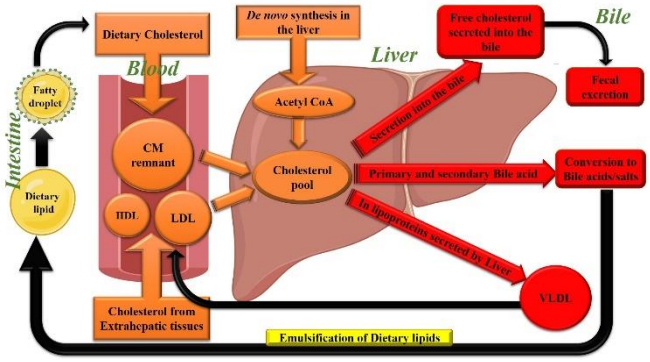

Figure 6: The diagram represents cholesterol homeostasis across the liver and shows the major sources for cholesterol entering the hepatocyte and the main pathways for its disposition from the hepatocyte. CM: Chylomicron, HDL: High Density lipoprotein, VLDL: Very low-density lipoprotein, LDL: Low density lipoprotein.

The maintenance of cholesterol homeostasis is influenced and controlled by several mechanisms. Firstly, by feedback mechanism, at which cholesterol itself participates in the decreasing the transcription of the gene responsible for producing HMG-CoA reductase (DeBose-Boyd, 2008). It has been shown that several hormones like glucagon and glucocorticoids promote the formation of inactive HMG CoA reductase, consequently decreasing cholesterol synthesis, while insulin and thyroxine increase cholesterol production by improving the formation of active HMG CoA reductase as a result increase cholesterol synthesis (Ness et al., 1994). Furthermore, certain types of drugs such as lovastatin (mevinolin) and compactin are act as a competitive inhibitor of the enzyme HMG CoA reductase and, as a result reduce cholesterol synthesis (Gb et al., 2018, Shand and West, 1995). Finally, secretion of bile salts resulted in decrease of the concentration of cholesterol due to continually conversion of cholesterol into the bile salts that facilitate intestinal absorption of lipids and fat-soluble vitamins (Li and Chiang, 2009).

4. CONCLUDING REMARKS

Lipid metabolism plays an important role for many biological functions in the cells. The most constituent part of the lipids includes triglyceride and cholesterol. Both types of lipids are synthesized from both exogenous (dietary) sources and endogenous sources particularly liver and adipose tissue. Due to their insolubility in the blood; lipids are transferred through blood circulation via a spherical molecule called lipoproteins. There are four major classes of lipoproteins at which their size and lipid contents differ from each other, they are Chylomicron, VLDL, LDL and HDL. Metabolism of both cholesterol and triglyceride has a great role in lipid homeostasis in the body. Further works are needed to focus on the enzymes that participate in catalyzing metabolism and to show how they regulate these processes.

References

ABU-FARHA, M., THANARAJ, T. A., QADDOUMI, M. G., HASHEM, A., ABUBAKER, J. & AL-MULLA, F. 2020. The Role of Lipid Metabolism in COVID-19 Virus Infection and as a Drug Target. *Int J Mol Sci*, 21.

ALVAREZ, H., STEINBÜCHEL, A. J. A. M. & BIOTECHNOLOGY 2002. Triacylglycerols in prokaryotic microorganisms. 60**,** 367-376.

ALVES-BEZERRA, M. & COHEN, D. E. 2017. Triglyceride Metabolism in the Liver. *Compr Physiol*, 8**,** 1-8.

BLOCH, K. 1965. The biological synthesis of cholesterol.

BOCHEM, A. E., HOLLEBOOM, A. G., ROMIJN, J. A., HOEKSTRA, M., DALLINGA, G. M., MOTAZACKER, M. M., HOVINGH, G. K., KUIVENHOVEN, J. A. & STROES, E. S. 2014. Adrenal Function in females with low plasma HDL-C due to mutations in ABCA1 and LCAT. *PLoS One,* 9**,** e90967.

BODEN, G. 2008. Obesity and Free Fatty Acids. *Endocrinology and Metabolism Clinics of North America,* 37**,** 635-646.

BODEN, G., JADALI, F., WHITE, J., LIANG, Y., MOZZOLI, M., CHEN, X., COLEMAN, E. & SMITH, C. 1991. Effects of fat on insulin-stimulated carbohydrate metabolism in normal men. *J Clin Invest,* 88**,** 960-6.

CARSON, J. A. S., LICHTENSTEIN, A. H., ANDERSON, C. A. M., APPEL, L. J., KRIS-ETHERTON, P. M., MEYER, K. A., PETERSEN, K., POLONSKY, T., VAN HORN, L., AMERICAN HEART ASSOCIATION NUTRITION COMMITTEE OF THE COUNCIL ON, L., CARDIOMETABOLIC, H., COUNCIL ON ARTERIOSCLEROSIS, T., VASCULAR, B., COUNCIL ON, C., STROKE, N., COUNCIL ON CLINICAL, C., COUNCIL ON PERIPHERAL VASCULAR, D. & STROKE, C. 2020. Dietary Cholesterol and Cardiovascular Risk: A Science Advisory From the American Heart Association. *Circulation,* 141**,** e39-e53.

CERQUEIRA, N. M., OLIVEIRA, E. F., GESTO, D. S., SANTOS-MARTINS, D., MOREIRA, C. T., MOORTHY, H. N., RAMOS, M. J. & FERNANDES, P. J. B. 2016. Cholesterol biosynthesis: a mechanistic overview. 55**,** 5483-5506.

CHATTERJEE, C. & SPARKS, D. L. 2011. Hepatic lipase, high density lipoproteins, and hypertriglyceridemia. *Am J Pathol,* 178**,** 1429-33.

COOPER, A. D. 1997. Hepatic uptake of chylomicron remnants. *Journal of Lipid Research,* 38**,** 2173-2192.

COURCHESNE-LOYER, A., LOWRY, C.-M., ST-PIERRE, V., VANDENBERGHE, C., FORTIER, M., CASTELLANO, C.-A., WAGNER, J. R. & CUNNANE, S. C. J. C. D. I. N. 2017. Emulsification increases the acute ketogenic effect and bioavailability of medium-chain triglycerides in humans: protein, carbohydrate, and fat metabolism. 1**,** e000851.

DAWSON, P. A., LAN, T. & RAO, A. 2009. Bile acid transporters. *J Lipid Res,* 50**,** 2340-57.

DAWSON, P. A. J. P. O. T. G. T. 2018. Bile formation and the enterohepatic circulation. 931-956.

DEBOSE-BOYD, R. A. 2008. Feedback regulation of cholesterol synthesis: sterol-accelerated ubiquitination and degradation of HMG CoA reductase. *Cell Res,* 18**,** 609-21.

DI CIAULA, A., GARRUTI, G., LUNARDI BACCETTO, R., MOLINA-MOLINA, E., BONFRATE, L., WANG, D. Q. H. & PORTINCASA, P. 2017. Bile Acid Physiology. *Annals of Hepatology,* 16**,** S4-S14.

DIEUAIDE, M., BROUQUISSE, R., PRADET, A. & RAYMOND, P. 1992. Increased Fatty Acid β-Oxidation after Glucose Starvation in Maize Root Tips. 99**,** 595-600.

DIXON, J. B. 2010. Mechanisms of chylomicron uptake into lacteals. *Ann N Y Acad Sci,* 1207 Suppl 1**,** E52-7.

DONNELLY, K. L., SMITH, C. I., SCHWARZENBERG, S. J., JESSURUN, J., BOLDT, M. D. & PARKS, E. J. 2005. Sources of fatty acids stored in liver and secreted via lipoproteins in patients with nonalcoholic fatty liver disease. *J Clin Invest,* 115**,** 1343-51.

DRIVER, T., TRIVEDI, D. K., MCINTOSH, O. A., DEAN, A. P., GOODACRE, R. & PITTMAN, J. K. 2017. Two Glycerol-3-Phosphate Dehydrogenases from Chlamydomonas Have Distinct Roles in Lipid Metabolism. *Plant Physiol,* 174**,** 2083-2097.

FAHY, E., COTTER, D., SUD, M. & SUBRAMANIAM, S. 2011. Lipid classification, structures and tools. *Biochim Biophys Acta,* 1811**,** 637-47.

FEINGOLD, K. R. & GRUNFELD, C. 2015. Introduction to lipids and lipoproteins.

FREEMAN, M. W. & WALFORD, G. A. 2016. Chapter 41 - Lipoprotein Metabolism and the Treatment of Lipid Disorders. *In:* JAMESON, J. L., DE GROOT, L. J., DE KRETSER, D. M., GIUDICE, L. C., GROSSMAN, A. B., MELMED, S., POTTS, J. T. & WEIR, G. C. (eds.) *Endocrinology: Adult and Pediatric (Seventh Edition).* Philadelphia: W.B. Saunders.

GB, R., MSAM, N. & PM, S. 2018. A Review on Anti-Cholesterol Drugs and their Mechanisms. *Journal of Medicinal Chemistry and Drug Design,* 1.

GERARD, P. 2013. Metabolism of cholesterol and bile acids by the gut microbiota. *Pathogens,* 3**,** 14-24.

GOEPFERT, S. & POIRIER, Y. 2007. Beta-oxidation in fatty acid degradation and beyond. *Curr Opin Plant Biol,* 10**,** 245-51.

GOLDBERG, I. J. J. J. O. L. R. 1996. Lipoprotein lipase and lipolysis: central roles in lipoprotein metabolism and atherogenesis. 37**,** 693-707.

GOODFRIEND, T. L., EGAN, B., STEPNIAKOWSKI, K. & BALL, D. L. 1995. Relationships Among Plasma Aldosterone, High-Density Lipoprotein Cholesterol, and Insulin in Humans. *Hypertension,* 25**,** 30-36.

HALL, Z., CHIARUGI, D., CHARIDEMOU, E., LESLIE, J., SCOTT, E., PELLEGRINET, L., ALLISON, M., MOCCIARO, G., ANSTEE, Q. M. & EVAN, G. I. J. H. 2020. Lipid Remodeling in Hepatocyte Proliferation and Hepatocellular Carcinoma.

HAMPTON, R., DIMSTER-DENK, D. & RINE, J. J. T. I. B. S. 1996. The biology of HMG-CoA reductase: the pros of contra-regulation. 21**,** 140-145.

HANNICH, M., WALLASCHOFSKI, H., NAUCK, M., REINCKE, M., ADOLF, C., VOLZKE, H., RETTIG, R. & HANNEMANN, A. 2018. Physiological Aldosterone Concentrations Are Associated with Alterations of Lipid Metabolism: Observations from the General Population. *Int J Endocrinol,* 2018**,** 4128174.

HARAYAMA, T. & RIEZMAN, H. J. N. R. M. C. B. 2018. Understanding the diversity of membrane lipid composition. 19**,** 281.

HAVEL, R. J., FIELDING, C. J., OLIVECRONA, T., SHORE, V. G., FIELDING, P. E. & EGELRUD, T. J. B. 1973. Cofactor activity of protein components of human very low density lipoproteins in the hydrolysis of triglycerides by lipoprotein lipase from different sources. 12**,** 1828-1833.

HAZZARD, W. R., KUSHWAHA, R. S., APPLEBAUM-BOWDEN, D., HAFFNER, S. M., STEINMETZ, A. & FOSTER, D. M. J. M. 1984. Chylomicron and very low-density lipoprotein apolipoprotein B metabolism: Mechanism of the response to stanozolol in a patient with severe hypertriglyceridemia. 33**,** 873-881.

HEGELE, R. A. J. N. R. G. 2009. Plasma lipoproteins: genetic influences and clinical implications. 10**,** 109-121.

HOFMANN, A. F., HAGEY, L. J. C. & SCIENCES, M. L. 2008. Bile acids: chemistry, pathochemistry, biology, pathobiology, and therapeutics. 65**,** 2461-2483.

HOKANSON, J. E. & AUSTIN, M. A. J. J. O. C. R. 1996. Plasma triglyceride level is a risk factor for cardiovascular disease independent of high-density lipoprotein cholesterol level: a metaanalysis of population-based prospective studies. 3**,** 213-219.

HOUTEN, S. M. & WANDERS, R. J. 2010. A general introduction to the biochemistry of mitochondrial fatty acid beta-oxidation. *J Inherit Metab Dis,* 33**,** 469-77.

HUANG, Y. & MAHLEY, R. W. 2014. Apolipoprotein E: structure and function in lipid metabolism, neurobiology, and Alzheimer's diseases. *Neurobiol Dis,* 72 Pt A**,** 3-12.

IKONEN, E. 2008a. Cellular cholesterol trafficking and compartmentalization. *Nat Rev Mol Cell Biol,* 9**,** 125-38.

IKONEN, E. J. N. R. M. C. B. 2008b. Cellular cholesterol trafficking and compartmentalization. 9**,** 125-138.

JAWORSKI, K., SARKADI-NAGY, E., DUNCAN, R. E., AHMADIAN, M. & SUL, H. S. 2007. Regulation of triglyceride metabolism. IV. Hormonal regulation of lipolysis in adipose tissue. *Am J Physiol Gastrointest Liver Physiol,* 293**,** G1-4.

JENSEN, M. D. J. J. O. T. R. S. O. M. 2002. Adipose tissue and fatty acid metabolism in humans. 95**,** 3.

KARPE, F., BELL, M., BJÖRKEGREN, J., HAMSTEN, A. J. A., THROMBOSIS, & BIOLOGY, V. 1995. Quantification of postprandial triglyceride-rich lipoproteins in healthy men by retinyl ester labeling and simultaneous measurement of apolipoproteins B-48 and B-100. 15**,** 199-207.

KING, A., YANG, Q., HUESMAN, S., RIDER, T. & LO, C. C. 2015. Lipid transport in cholecystokinin knockout mice. *Physiol Behav,* 151**,** 198-206.

KISS, L., FUR, G., MATRAI, P., HEGYI, P., IVANY, E., CAZACU, I. M., SZABO, I., HABON, T., ALIZADEH, H., GYONGYI, Z., VIGH, E., EROSS, B., EROS, A., OTTOFFY, M., CZAKO, L. & RAKONCZAY, Z., JR. 2018. The effect of serum triglyceride concentration on the outcome of acute pancreatitis: systematic review and meta-analysis. *Sci Rep,* 8**,** 14096.

KOHAN, A. B., WANG, F., LO, C. M., LIU, M. & TSO, P. 2015. ApoA-IV: current and emerging roles in intestinal lipid metabolism, glucose homeostasis, and satiety. *Am J Physiol Gastrointest Liver Physiol,* 308**,** G472-81.

LAMBERT, J. E., PARKS, E. J. J. B. E. B. A.-M. & LIPIDS, C. B. O. 2012. Postprandial metabolism of meal triglyceride in humans. 1821**,** 721-726.

LENT-SCHOCHET, D. & JIALAL, I. J. S. 2020. Biochemistry, lipoprotein metabolism.

LI, T. & CHIANG, J. Y. 2009. Regulation of bile acid and cholesterol metabolism by PPARs. *PPAR Res,* 2009**,** 501739.

LI, T. & CHIANG, J. Y. 2014. Bile acid signaling in metabolic disease and drug therapy. *Pharmacol Rev,* 66**,** 948-83.

LIDDLE, R. A., GOLDFINE, I. D., ROSEN, M. S., TAPLITZ, R. & WILLIAMS, J. J. T. J. O. C. I. 1985. Cholecystokinin bioactivity in human plasma. Molecular forms, responses to feeding, and relationship to gallbladder contraction. 75**,** 1144-1152.

LILLIS, A. P., VAN DUYN, L. B., MURPHY-ULLRICH, J. E. & STRICKLAND, D. K. 2008. LDL receptor-related protein 1: unique tissue-specific functions revealed by selective gene knockout studies. *Physiol Rev,* 88**,** 887-918.

LIZARDO, D. Y., PARISI, L. R., LI, N. & ATILLA-GOKCUMEN, G. E. J. B. 2018. Noncanonical roles of lipids in different cellular fates. 57**,** 22-29.

LO, C.-M., NORDSKOG, B. K., NAULI, A. M., ZHENG, S., VONLEHMDEN, S. B., YANG, Q., LEE, D., SWIFT, L. L., DAVIDSON, N. O., TSO, P. J. A. J. O. P.-G. & PHYSIOLOGY, L. 2008. Why does the gut choose apolipoprotein B48 but not B100 for chylomicron formation? 294**,** G344-G352.

LO, C. C. & COSCHIGANO, K. T. 2020. ApoB48 as an Efficient Regulator of Intestinal Lipid Transport. *Front Physiol,* 11**,** 796.

LONGO, N., AMAT DI SAN FILIPPO, C. & PASQUALI, M. 2006. Disorders of carnitine transport and the carnitine cycle. *Am J Med Genet C Semin Med Genet,* 142C**,** 77-85.

LORIZATE, M. & KRAUSSLICH, H. G. 2011. Role of lipids in virus replication. *Cold Spring Harb Perspect Biol,* 3**,** a004820.

LOWE, M. E. J. J. O. L. R. 2002. The triglyceride lipases of the pancreas. 43**,** 2007-2016.

LYU, J., YANG, E. J. & SHIM, J. S. 2019. Cholesterol Trafficking: An Emerging Therapeutic Target for Angiogenesis and Cancer. *Cells,* 8.

MANDAL, M. K., CHANDA, B., XIA, Y., YU, K., SEKINE, K. T., GAO, Q. M., SELOTE, D., KACHROO, A. & KACHROO, P. 2011. Glycerol-3-phosphate and systemic immunity. *Plant Signal Behav,* 6**,** 1871-4.

MATTSON, F. & VOLPENHEIN, R. J. J. O. B. C. 1964. The digestion and absorption of triglycerides. 239**,** 2772-2777.

MERKEL, M., ECKEL, R. H. & GOLDBERG, I. J. 2002. Lipoprotein lipase: genetics, lipid uptake, and regulation. *J Lipid Res,* 43**,** 1997-2006.

MODRE-OSPRIAN, R., OSPRIAN, I., TILG, B., SCHREIER, G., WEINBERGER, K. M. & GRABER, A. 2009. Dynamic simulations on the mitochondrial fatty acid beta-oxidation network. *BMC Syst Biol,* 3**,** 2.

NESS, G. C., ZHAO, Z. & WIGGINS, L. 1994. Insulin and glucagon modulate hepatic 3-hydroxy-3-methylglutaryl-coenzyme A reductase activity by affecting immunoreactive protein levels. *Journal of Biological Chemistry,* 269**,** 29168-29172.

NORDESTGAARD, B. G. J. C. R. 2016. Triglyceride-rich lipoproteins and atherosclerotic cardiovascular disease: new insights from epidemiology, genetics, and biology. 118**,** 547-563.

NOZAKI, S., TANAKA, T., YAMASHITA, S., SOHMIYA, K., YOSHIZUMI, T., OKAMOTO, F., KITAURA, Y., KOTAKE, C., NISHIDA, H., NAKATA, A., NAKAGAWA, T., MATSUMOTO, K., KAMEDA-TAKEMURA, K., TADOKORO, S., KURATA, Y., TOMIYAMA, Y., KAWAMURA, K. & MATSUZAWA, Y. 1999. CD36 mediates long-chain fatty acid transport in human myocardium: complete myocardial accumulation defect of radiolabeled long-chain fatty acid analog in subjects with CD36 deficiency. *Mol Cell Biochem,* 192**,** 129-35.

OHKAWA, R., LOW, H., MUKHAMEDOVA, N., FU, Y., LAI, S. J., SASAOKA, M., HARA, A., YAMAZAKI, A., KAMEDA, T., HORIUCHI, Y., MEIKLE, P. J., PERNES, G., LANCASTER, G., DITIATKOVSKI, M., NESTEL, P., VAISMAN, B., SVIRIDOV, D., MURPHY, A., REMALEY, A. T., SVIRIDOV, D. & TOZUKA, M. 2020. Cholesterol transport between red blood cells and lipoproteins contributes to cholesterol metabolism in blood. *J Lipid Res,* 61**,** 1577-1588.

OLOFSSON, S.-O., WIKLUND, O. & BORÉN, J. 2007. Apolipoproteins A-I and B: biosynthesis, role in the development of atherosclerosis and targets for intervention against cardiovascular disease. *Vascular health and risk management,* 3**,** 491-502.

PASQUIER, B., ARMAND, M., CASTELAIN, C., GUILLON, F., BOREL, P., LAFONT, H. & LAIRON, D. J. B. J. 1996. Emulsification and lipolysis of triacylglycerols are altered by viscous soluble dietary fibres in acidic gastric medium in vitro. 314**,** 269-275.

PAYNE, A. H. & HALES, D. B. 2004. Overview of steroidogenic enzymes in the pathway from cholesterol to active steroid hormones. *Endocr Rev,* 25**,** 947-70.

PONZ DE LEON, M., MURPHY, G. M. & DOWLING, R. H. 1978. Physiological factors influencing serum bile acid levels. *Gut,* 19**,** 32-9.

PRABHU, A. V., LUU, W., SHARPE, L. J. & BROWN, A. J. J. J. O. B. C. 2016. Cholesterol-mediated degradation of 7-dehydrocholesterol reductase switches the balance from cholesterol to vitamin D synthesis. 291**,** 8363-8373.

ROHRL, C. & STANGL, H. 2018. Cholesterol metabolism-physiological regulation and pathophysiological deregulation by the endoplasmic reticulum. *Wien Med Wochenschr,* 168**,** 280-285.

ROSENFELD, M. E., PALINSKI, W., YLÄ-HERTTUALA, S. & CAREW, T. E. J. T. P. 1990. Macrophages, endothelial cells, and lipoprotein oxidation in the pathogenesis of atherosclerosis. 18**,** 560-571.

RUSSELL, D. W. & SETCHELL, K. D. J. B. 1992. Bile acid biosynthesis. 31**,** 4737-4749.

RUSSELL, D. W. J. C. D. & THERAPY 1992. Cholesterol biosynthesis and metabolism. 6**,** 103-110.

SHAND, J. H. & WEST, D. W. 1995. The effects of simvastatin and cholestyramine, alone and in combination, on hepatic cholesterol metabolism in the male rat. *Lipids,* 30**,** 917-926.

SHRESTHA, S., WU, B. J., GUINEY, L., BARTER, P. J. & RYE, K. A. 2018. Cholesteryl ester transfer protein and its inhibitors. *J Lipid Res,* 59**,** 772-783.

STRUTHERS, A. D. & MACDONALD, T. M. J. C. R. 2004. Review of aldosterone-and angiotensin II-induced target organ damage and prevention. 61**,** 663-670.

TABAS, I. 2002. Cholesterol in health and disease. *J Clin Invest,* 110**,** 583-90.

TASKINEN, M. R., BJORNSON, E., KAHRI, J., SODERLUND, S., MATIKAINEN, N., PORTHAN, K., AINOLA, M., HAKKARAINEN, A., LUNDBOM, N., FERMANELLI, V., FUCHS, J., THORSELL, A., KRONENBERG, F., ANDERSSON, L., ADIELS, M., PACKARD, C. J. & BOREN, J. 2020. Effects of Evolocumab on the Postprandial Kinetics of Apo (Apolipoprotein) B100- and B48-Containing Lipoproteins in Subjects With Type 2 Diabetes. *Arterioscler Thromb Vasc Biol***,** ATVBAHA120315446.

TEIXEIRA, G. R., MENDES, L. O., VERAS, A. S. C., THORPE, H. H. A., FÁVARO, W. J., DE ALMEIDA CHUFFA, L. G., PINHEIRO, P. F. F., MARTINEZ, F. E. J. L. I. H. & DISEASE 2020. Physical resistance training-induced changes in lipids metabolism pathways and apoptosis in prostate. 19**,** 1-9.

TOPRAK, U. J. F. I. P. 2020. The role of peptide hormones in insect lipid metabolism. 11.

TSAI, J. H., CHI, M. M., SCHULTE, M. B. & MOLEY, K. H. 2014. The fatty acid beta-oxidation pathway is important for decidualization of endometrial stromal cells in both humans and mice. *Biol Reprod,* 90**,** 34.

TYOR, M. P., GARBUTT, J. T. & LACK, L. J. T. A. J. O. M. 1971. Metabolism and transport of bile salts in the intestine. 51**,** 614-626.

VAN EUNEN, K., SIMONS, S. M., GERDING, A., BLEEKER, A., DEN BESTEN, G., TOUW, C. M., HOUTEN, S. M., GROEN, B. K., KRAB, K., REIJNGOUD, D. J. & BAKKER, B. M. 2013. Biochemical competition makes fatty-acid beta-oxidation vulnerable to substrate overload. *PLoS Comput Biol,* 9**,** e1003186.

WANG, H. H., GARRUTI, G., LIU, M., PORTINCASA, P. & WANG, D. Q. H. 2017. Cholesterol and Lipoprotein Metabolism and Atherosclerosis: Recent Advances in Reverse Cholesterol Transport. *Annals of Hepatology,* 16**,** S27-S42.

WANG, X., MAGKOS, F. & MITTENDORFER, B. 2011. Sex differences in lipid and lipoprotein metabolism: it's not just about sex hormones. *J Clin Endocrinol Metab,* 96**,** 885-93.

WANG, X. & PAIGEN, B. 2005. Genetics of variation in HDL cholesterol in humans and mice. *Circ Res,* 96**,** 27-42.

WARNICK, G. R., KNOPP, R. H., FITZPATRICK, V. & BRANSON, L. 1990. Estimating low-density lipoprotein cholesterol by the Friedewald equation is adequate for classifying patients on the basis of nationally recommended cutpoints. *Clin Chem,* 36**,** 15-9.

WEIL, C., LEFÈVRE, F. & BUGEON, J. 2012. Characteristics and metabolism of different adipose tissues in fish. *Reviews in Fish Biology and Fisheries,* 23**,** 157-173.

WEN, Y. & LEAKE, D. S. 2007. Low density lipoprotein undergoes oxidation within lysosomes in cells. *Circ Res,* 100**,** 1337-43.

XIAO, C., HSIEH, J., ADELI, K. & LEWIS, G. F. 2011. Gut-liver interaction in triglyceride-rich lipoprotein metabolism. *Am J Physiol Endocrinol Metab,* 301**,** E429-46.

XU, Y., DU, X., TURNER, N., BROWN, A. J. & YANG, H. 2019. Enhanced acyl-CoA:cholesterol acyltransferase activity increases cholesterol levels on the lipid droplet surface and impairs adipocyte function. *J Biol Chem,* 294**,** 19306-19321.

YADAV, D. & LOWENFELS, A. B. J. G. 2013. The epidemiology of pancreatitis and pancreatic cancer. 144**,** 1252-1261.

YVAN-CHARVET, L., WANG, N. & TALL, A. R. 2010. Role of HDL, ABCA1, and ABCG1 transporters in cholesterol efflux and immune responses. *Arterioscler Thromb Vasc Biol,* 30**,** 139-43.

ZHANG, L., KEUNG, W., SAMOKHVALOV, V., WANG, W. & LOPASCHUK, G. D. 2010. Role of fatty acid uptake and fatty acid beta-oxidation in mediating insulin resistance in heart and skeletal muscle. *Biochim Biophys Acta,* 1801**,** 1-22.

ZANCO Journal of Pure and Applied Sciences
The official scientific journal of Salahaddin University-Erbil
https://zancojournals.su.edu.krd/index.php/JPAS

ISSN (print): 2218-0230**, ISSN (online):** 2412-3986**, DOI: http://dx.doi.org/10.21271/zjpas**

RESEARCH PAPER

Mononuclear Erbium (III) Complex with Tetradentate N2O2 Schiff Base Ligand

Kamaran Basheer Hussein
College of Education ,Chemistry Department,Salahaddin university-Erbil,Iraq.

A B S T R A C T:

The synthesis of a tetradentate Schiff-base ligand bis(salicylidene)ethylenediamine from salicylaldehyde and ethylenediamine , are important class of ligands . The results of the C.H.N study revealed the formation of a 1:1 [M:L] ratio. .$[Er(Salen)(NO_3)_2]^-$, square antiprismatic geometry, is the proposed structure of lanthanide metal complex. ^{1}H-NMR, FT-IR, UV-Visible spectral mesurements, and molar conductance were used to estimate the synthesized Schiff-base ligand and its complex.

The stoichiometry of the complex has been found to be 1:1 (Er:Salen) matching with C.H.N. analysis. After deprotonation, spectral studies revealed that the ligand was tetradentately coordinated to the metal ion (N_2O_2) through azomethine nitrogen and phenolic oxygen. The biological activities of the Schiff base (Salen , H_2L) and Er(III) complex against E.coli and Staphylococcus bacteria were examined, Schiff base ligand being less active than Erbium (III) complex.

KEY WORDS: Salen ligand , ONNO donor atoms, Er(III) , antibacterial studies
DOI: http://dx.doi.org/10.21271/ZJPAS.33.4.7
ZJPAS (2021) , 33(4);73-81

1.INTRODUCTION :

Schiff bases and their metal complexes have taken a central role in the expansion of co-ordination chemistry, the synthesis of tetradentate Schiff-base ligands from diamines and the corresponding salicylaldehyde derivative is an important reaction. Fig.1. shows the proposed structure for the known lanthanide complexes (Jadhav etal, 2017).

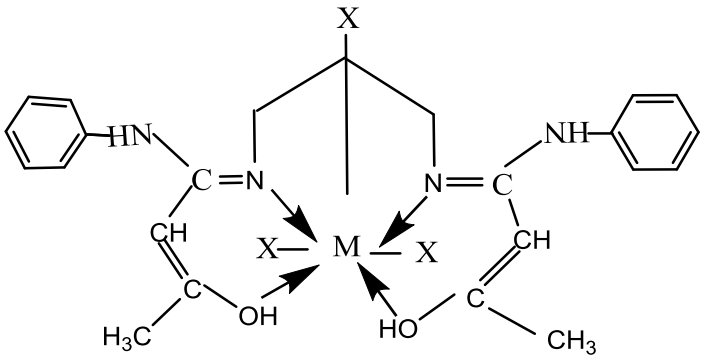

X= Cl^- , NO_3^- , NCS^-
M= Sm(III) , Gd(III) , Dy(III)

Fig.1. Proposed structure for the identified lanthanide complexes

* **Corresponding Author:**
Kamaran Basheer Hussein
E-mail: kamaran1963@gmail.com
Article History:
Received: 31/03/2021
Accepted: 10/06/2021
Published: 18/08 /2021

An comprehensive series of inquiries into the [bis(salicylidene)ethylenediamine-Erbium(III)] complex and other Complexes within this family has been performed (Holt and Post, 1971). (Lodewyckx etal.,2001) (Rao and colleagues, 2002) (Varghese and Muraleedharan, 2012) Schiff-bases are an essential class of organic compounds with many biological applications, including proteins, visual pigments, enzymic, alodolization, and decarboxylation reactions. Furthermore, some Schiff-bases and their metal ion complexes have antibacterial, antiviral, and antitumor properties. Because of the inclusion of the (-HC=N-) group (Athira et al.,2011), it is biologically important (Shelke etal, 2012) (R.V. Deun and Binnemans, 2001) (Abdel-Kader and El-Ansary, 2009) (Hayvali and Dal.H., 2004) .

Lanthanides are metals that are highly electropositive and reactive. Except for Yb(III) , their reactivity tends to be proportional to their size, with Eu having the largest metal radius being the most reactive (Greenwood, 2012). Ethylenediamine is a highly basic amine with the formula $C_2H_4(NH_2)_2$, it's a colorless liquid with an ammonia-like odor (Kotova etal.,2008). Ethylenediamine is a bidentate ligand that can bind to a variety of metal ions and form very stable complexes with lanthanide metal ions or transition metal ions. (Endale and Desalegn, 2018) (Taha etal. 2011) (T.A. Al-Diwan,2011) (Maher and Mohammed ,2015). The present study aimed to synthesis of Erbium(III) complex with tetradentate N_2O_2 Schiff -Base ligand , as possible antibacterial agents. Some authors (Acuña-Cueva, 2003) noted that salen ligand with central metal ions gives rigid compounds .

2. Experimental

2.1-Chemicals and reagents

All the chemicals used in the present work were of analytical grade. Salicylaldehyde, ethylenediamine (Sigma Aldrich), $Er(NO_3)_3.5H_2O$ as metal salt (Fluka), and solvents such as DMSO, distilled water, ethanol, methanol, and diethyl ether from Sigma Aldrich and BDH were used in this work .

2.2-Measurements

A Jenway conductivity meter 4200(0.93cell constant) (UK) was used to measure the conductivity of the complex in (DMSO). Electrothermal 9100 was used to calculate melting points (UK). In a shimadzu spectrophotometer, FT-IR spectra were registered using KBr discs in the 4000-400 cm^{-1} range. In the education college –Chemistry Department Salahaddin university – Erbil- Iraq, UV-Visible spectra were reported in DMSO on a Shimadzu 1800 UV-Visible. In Al-al-Bayt Central Labs (Jordan), 1H-NMR was performed on a Bruker ultra-shield 300MHZ with TMS as internal references. At Marash University, carbon, hydrogen, and nitrogen (C.H.N) analysis was performed using a Euro EA elemental analyzer 3000/Italy. The oxalate–oxide method was used to evaluate erbium metal (Vogel, A.I.,1963). The Erbil Medical Technical Institute of Erbil Polytechnic University in Iraq conducted biological activity studies.

2.3- Synthesis of ligand H_2L (salen)

The Schiff base ligand H_2L bis(salicylidene)ethylenediamine was synthesized by directly mixing (2mmol,0.244g) salicylaldehyde dissolved in 25ml absolute ethanol with (1mmol,0.0601g) of (en) according to a published method (Cozzi,P.G.,2004). For around 30 minutes, the reaction mixtures were cooled in an ice bath and vigorously stirred. The solution turned a bright yellow color, indicating that the Schiff base had developed. Filtration was used to extract the precipitate, which was then washed with ethanol and dried in an oven. the yields were 80% and m. p 127^oC , M.wt.268.31. The preparation Reaction for the H_2L is outlined in Scheme .1.

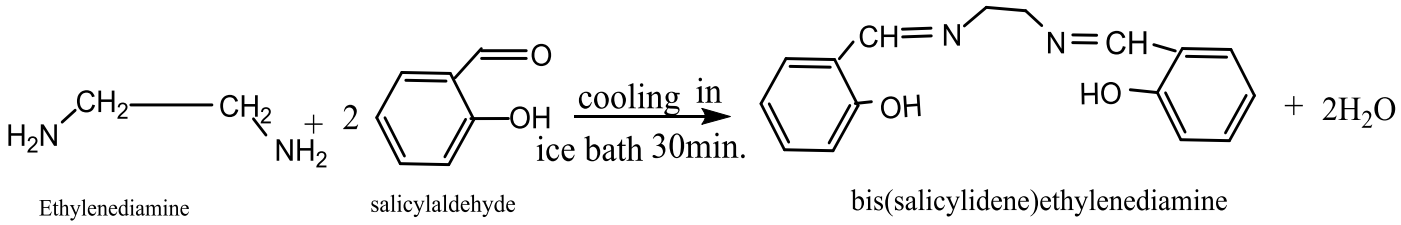

Scheme.1.Preparation reaction of (Salen) Ligand

2.4 -Synthesis of $[Er(salen)(NO_3)_2]^-$ Complex

The complex was made by dissolving [1 mmol (0.443 g)] of the metal salt Er $(NO_3)_2.5H_2O$ in 20 mL absolute ethanol and stirring it thoroughly for several minutes. [1mmol (0.268g)] H_2L dissolved in 10ml ethanol was applied to the resulting solution. The resulting mixture was heated under reflux for two hours on a magnetic stirrer, the pale brown precipitate was filtered, washed in ethanol, dried, and the m.p. was measured at 280 ^oC . In order to make complex, the metal to ligand ratio must be 1:1. The C.H.N results based on the elemental analysis data for $[Er(salen)(NO_3)_2]^-$ complex Calc.. C,34.28%, H,2.5% &, N,10 % - Found C,34.15 %, H,2.44% , N,10.11 %, and Er(III) percentage is 30% . The prepared complex in aqueous solutions and non-popular organic solvents such as ether, acetone, benzene, and carbon tetrachloride is insoluble, but it dissolves readily in DMF and DMSO. In acidic solutions, Erbium complex dissociate slowly, in acidic solution limiting their use to basic media.

3. Result and Discussion

3.1- IR Spectra

The ligand exhibits a medium intensity band at 1637cm^{-1}, which is typical of υ(C=N) stretching vibration; however, in the Erbium(III) complex, the band is shifted around 17cm^{-1} , suggesting that the azomethine nitrogen is involved in coordination to the metal ion (PalS and Pal.S,2002). The hydrogen bond package in the ligand and complex structure presence at 3186-3008 cm^{-1} . Stretching vibrations of the υ(C=C) type occur in the ligand at 1498 cm^{-1} and are moved to 1483 cm^{-1} when the erbium complex suffered bathochromic shifted. The assignable strong band in the spectrum of the ligand caused by phenolic υ(C-O) at 1284 cm^{-1} has shifted to 1280 cm^{-1} low intensity band in the spectrum of the erbium complex due to the participation of phenolic oxygen in coordination with metal ion. The presence of bands at 449cm^{-1} and 528cm^{-1} in the complex spectrum, which correspond to the stretching vibrations of the M-O and M-N bands, respectively, suggest that the salen ligand coordinated to the metal ion in the complex via a N and O atom (Toyssie P. and Charatte ,1963). The coordinated nitrate ion as a bidentate ligand is responsible for the new bands observed in the Er(III) complex at 1375-875 cm^{-1} medium bands (Agarwal etal ,2005). The I.R spectra Figures 2&3 show the Salen ligand and Er(III) complex .

3.2-^{1}H - NMR spectrum of Schiff base ligand

The ^{1}H-NMR spectrum of the Salen ligand recorded in DMSO-d_6 (Sabir et al, 2017). Fig. 4. Show the spectrum of Salen Ligand by ^{1}H-NMR. Because of the presence of the (ph-OH) proton, the ligand ^{1}H-NMR spectrum shows a signal at 13.33 ppm and at 8.4 ppm there is a sharp singlet signal for the -CH=N- proton in ligand spectrum Aromatic protons in (H_2L) appeared in multiplets ranging from 7.7 to 6.5 ppm and were unaffected by temperature.

3.3- Electronic transition spectra of ligand and its complex

In Er(III) ion 4f - orbitals do not engage in bonding because they are well protected by the $5S^2$ and $5p^6$ orbitals. The ligand has little effect on their spectroscopic and magnetic properties (Hebbink G., 2002). Fig.5. depicts the electrical

spectrum of the Er(III) metal ion. The observed wave length in the (40.000-12.500) cm^{-1} range is transitioned by 4f-4f. As a result of Er(III) absorption spectrum are usually sharp, line-like spectra, as opposed to the extensive absorption of transition metals. The 4f orbitals in lanthanides are buried deep within the atom, reducing the impact of ligand vibrations on the broadening effect (Hussein et al ,2018). Ligand to metal charge transfer bands appears as a strong band .The presence of the -CH=N- band is indicated by two maximum spectrum observed in the Er(III) complex (35.714-26.315)cm^{-1} assigned to the π - π* and n-π* transitions (Mohammed et al, 2013). Fig .6. illustrates the combined UV-Vis. spectrum of Salen ligand and Er(III) complex.

3.4- Molar conductivity - The electrical conductance measurements for the Er (III) complex indicate that it is electrolytic nature (1:1) the calculated value is 178 $\Omega^{-1}cm^{-1}mol^{-1}$.

3.5- Antibacterial activity.

The antibacterial function of the Salen ligand and Erbium(III) complex was investigated. The organization of Salen ligand and Erbium(III) complex with two bacteria species, E.coli and Staphylococcus aureus, was investigated (FI.F.H.S., 2015) (F.H. Kamel and S.S. Sabir, 2017) at 37^{o}C for 24 hours, Using (DMSO) as a solvent and a control were examined , the concentration of the compounds in this solvent was 25mg per one milliliter using disc sensitivity test and as compared with control, that the inhibition with the aid of using steel chelates is better than that of ligand . Inhibition zones were measured in millimeters . The $[Er(salen)(NO_3)_2]^-$ complex has been found to have higher antibacterial activity than the ligand. Fig.7. show the antibacterial activity of Schiff base Ligand and Er(III) complex.

Conclusion

A specific chelating Schiff base is formed when two equivalents of salicylaldehyde react with a diamine such as (en). There is a palace for two nitrate ions open to additional ligands for raising the coordination number to eight square antiprismatic geometry, salen ligand with four coordinating sites as tetradentate ligand (NOON) donor atoms sequence towards Er(III). In fact, by forming chelating complexes, Schiff bases can increase the stability of several metal ion complexes of various oxidation numbers. (N.R.Bader,2010) (Gueye,M.N.2017) Fig..8.,show the suggested structure of $[Er(salen)(NO_3)_2]^-$ is exceptional example of single ionic lanthanide complex coordinating with Schiff base ligands (Sui, Y. etal ,2015).

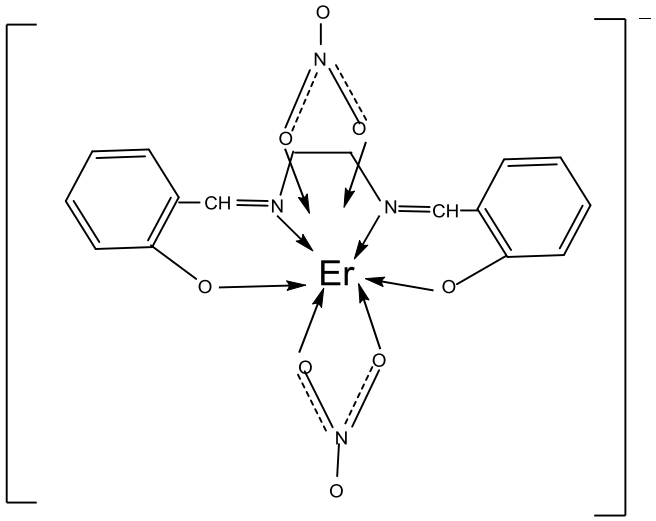

Fig. 8. Suggested structure of $[Er(salen)(NO_3)_2]^-$ complex .

Acknowledgement

Author is grateful to Mr.Sangar S. in Medical Technical Institute polytechnic University –Erbil –Iraq for providing me some chemical materials . Many thanks to the head of Chemistry department college of education – salahaddin university for providing the facilities to do the present work in their lab .

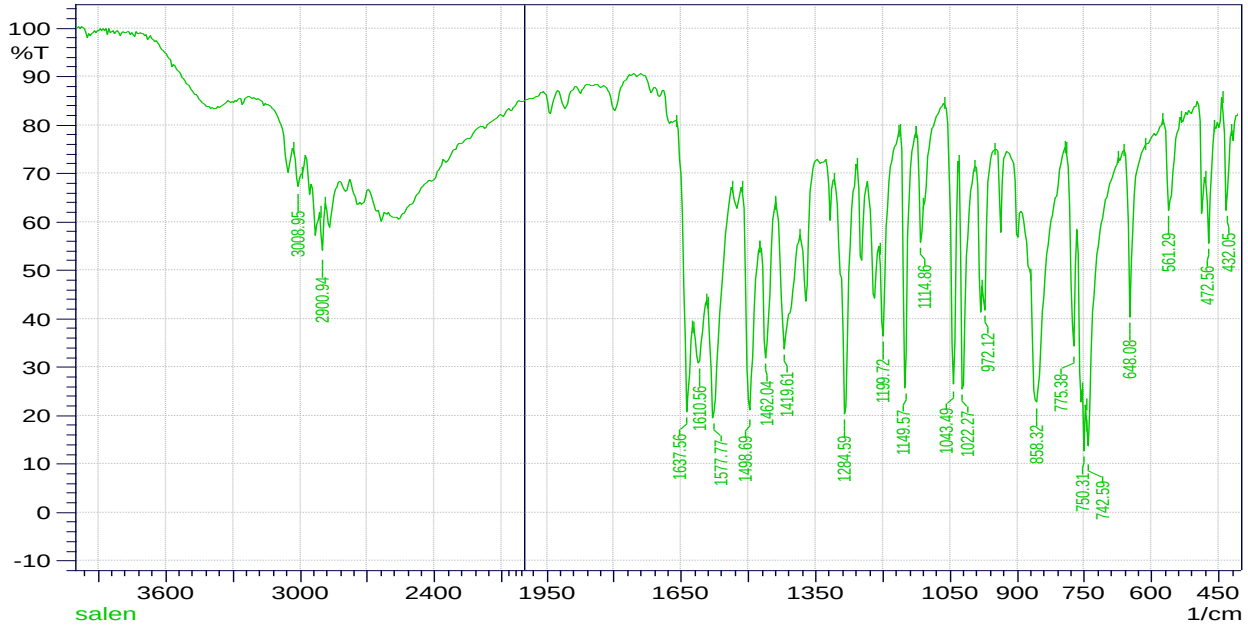

Fig.2. The IR spectrum of Salen Ligand.

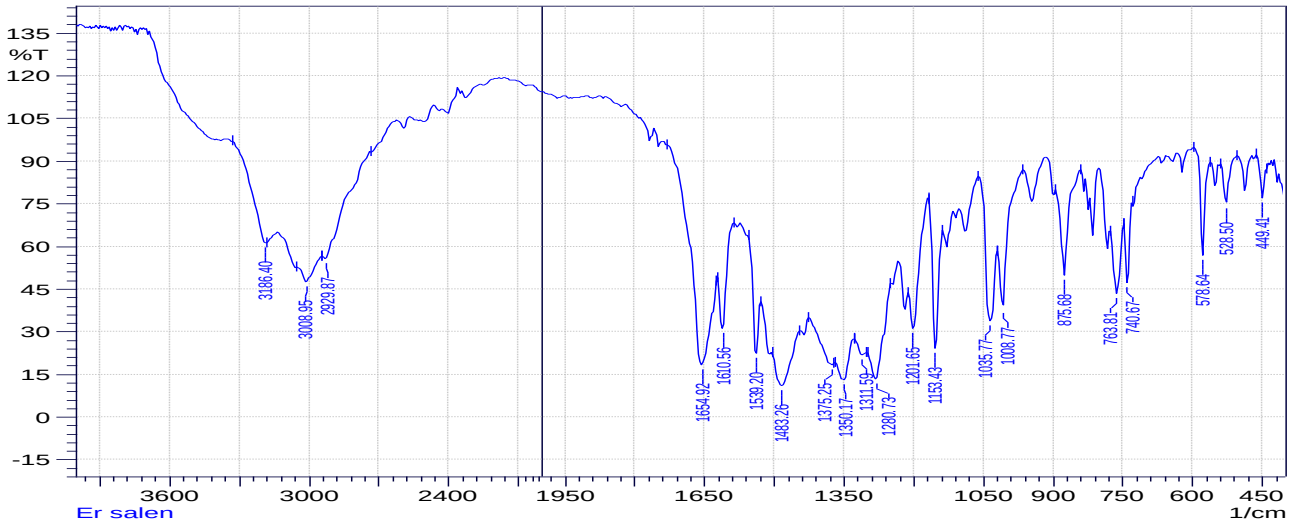

Fig.3. The IR spectrum of $[Er(salen)(NO_3)_2]^-$

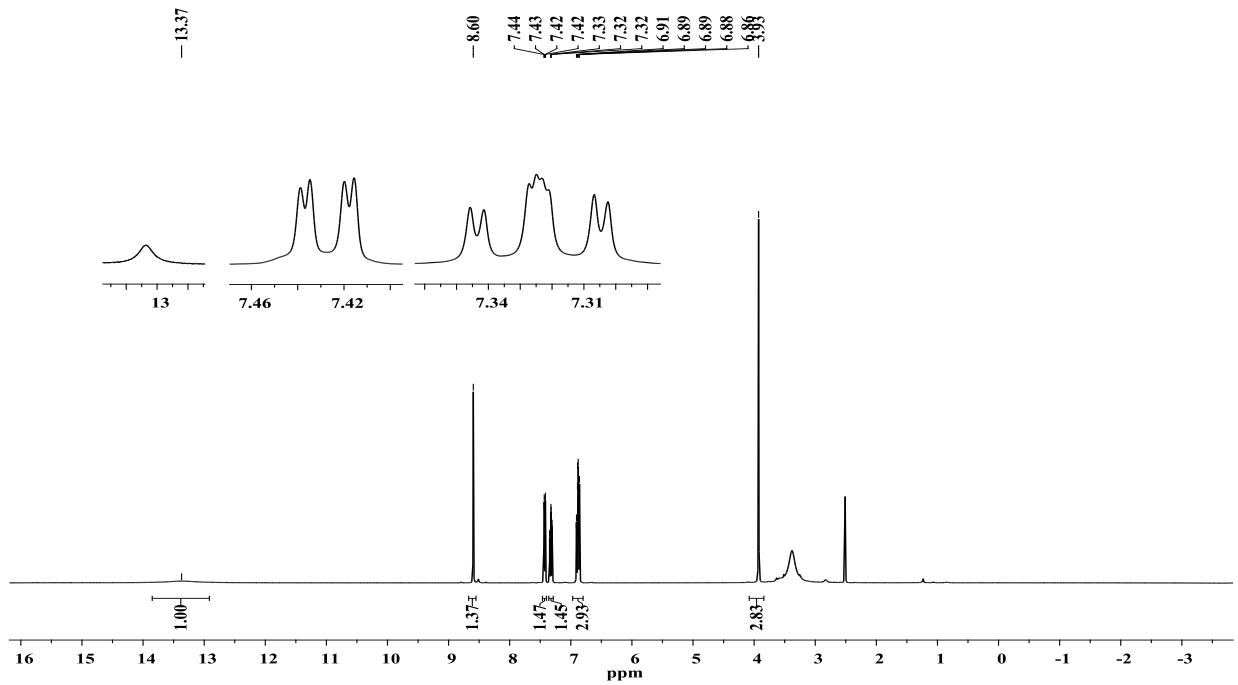

Fig.4. ^{1}H-NMR spectrum of Salen Ligand

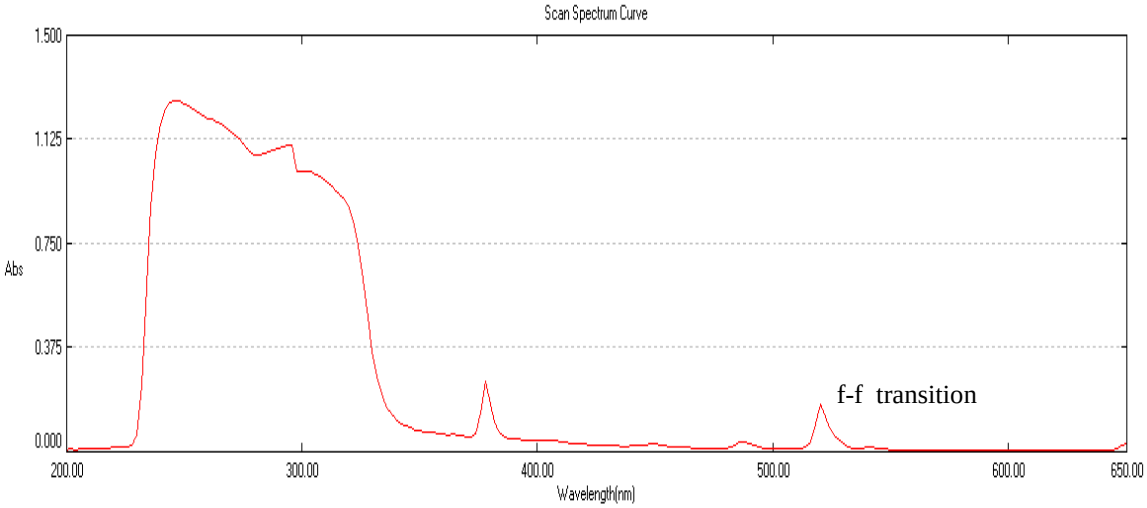

Fig.5. UV-Visible Spectrum of Er(III) Metal ion in methanol solvent .

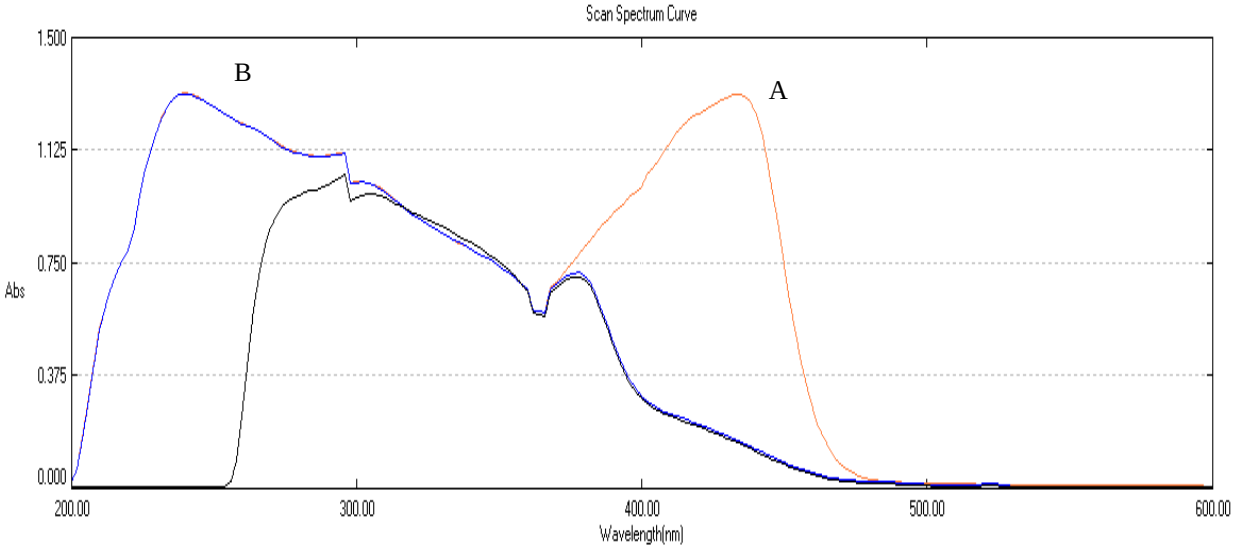

Fig.6.Combined UV-Visible Spectrum of Salen ligand (A) & Er (III) complex in DMSO solvent (B).

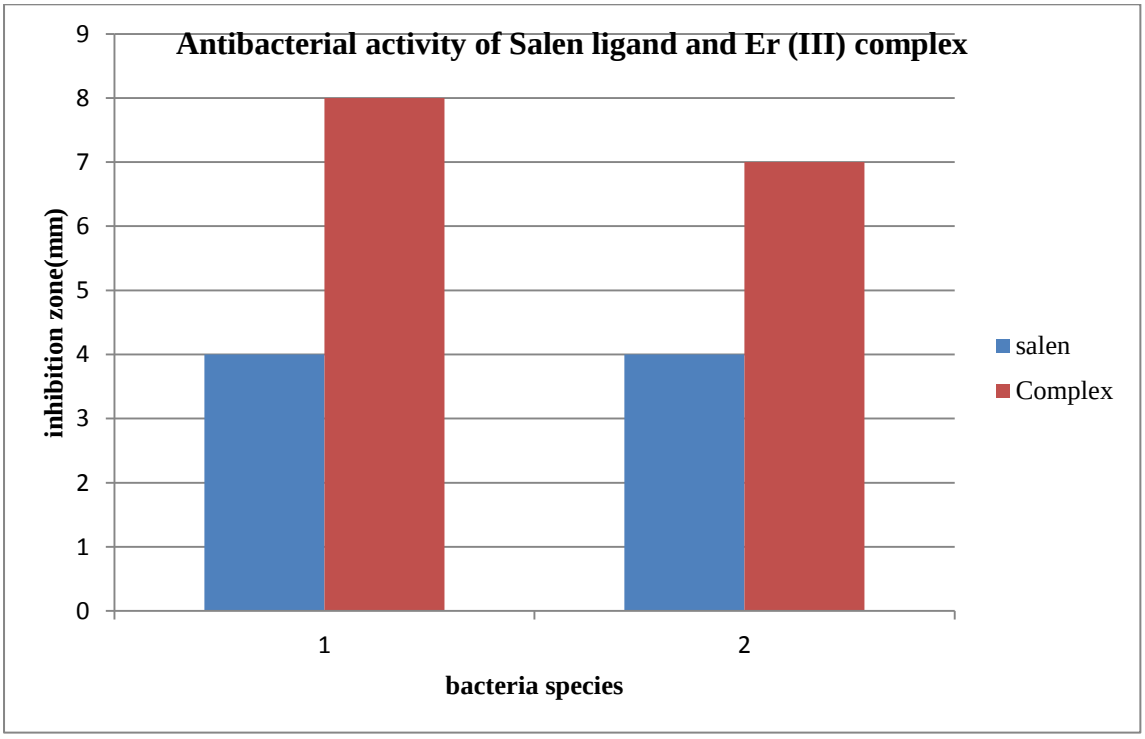

Fig.7. The antibacterial activity of Schiff base Ligand and Er (III) complex.

References

Athira, J.C., Sindhu, Y., Sujamol, S.M. and Mohanan, K., 2011. Synthesis and spectroscopic characterization of some lanthanide (III) nitrate complexes of 3-[3-carboxyethyl-4, 5-dimethylthiophene-2-yl) azo] pent-2, 4-dione. *Journal of the Serbian Chemical Society*, *76*(2), pp.249-261.

Abdel-Fattah, H., El-Ansary, A. and Abdel-Kader, N., 2009. Thermal and spectral studies on complexes derived from tetradentate Schiff bases. *Journal of thermal analysis and calorimetry*, *96*(3), pp.961-969.

Al–Diwan, T.A., 2011. Synthesis and Characterization of Some Divalent Transition Metals Complexes of Schiff Bases Derived from Salicylaldehyde Diamine Derivatives. *Al-Mustansiriyah Journal of Science*, *22*(2).

Agarwal, R.K., Garg, R.K. and Sindhu, S.K., 2005. Synthesis and magneto-spectral investigations of some six and nine coordinated complexes of lanthanides (III) derived from 4 [N-(2′-hydroxy-1′-naphthalidene) amino]

antipyrinethiosemicarbazone. *Journal of the Iranian chemical society*, *2*(3), pp.203-211.

Acuña-Cueva, E.R., Faure, R., Illán-Cabeza, N.A., Jiménez-Pulido, S.B., Moreno-Carretero, M.N. and Quirós-Olozábal, M., 2003. Synthesis and characterization of several lumazine derivative complexes of Co (II), Ni (II), Cu (II), Cd (II), Pd (II) and Pt (II). X-ray structures of a mononuclear copper complex and a dinuclear cadmium complex. *Inorganica chimica acta*, *351*, pp.356-362.

Bader, N.R., 2010. Applications of schiff's bases chelates in quantitative analysis a review. *RASAYAN j. Chem*, *3*(4), pp.660-70.

Cozzi, P.G., 2004. Metal–Salen Schiff base complexes in catalysis: practical aspects. *Chemical Society Reviews*, *33*(7), pp.410-421.

Deun, R.V. and Binnemans, K., 2001. Mesomorphism of lanthanide-containing Schiff's base complexes with dodecyl sulphate counterions. *Liquid Crystals*, *28*(4), pp.621-627.

Endale, A.T.M. and Desalegn, T., 2018. Synthesis, Characterization and Antibacterial Activity of Copper (II) and Cobalt (II) Vanillin-Aniline Schiff base Complexes. *Synthesis*, *10*(2).

FI, F.H.S., 2015. Essentials of Bacteriology. *Erbil polytechnic university/Medical Technical Institute. Edited in*, *182*.

Gueye, M.N., Dieng, M., Thiam, I.E., Lo, D., Barry, A.H., Gaye, M. and Retailleau, P., 2017. Lanthanide (III) complexes with tridentate Schiff base ligand, antioxidant activity and X-ray crystal structures of the Nd (III) and Sm (III) complexes. *South African Journal of Chemistry*, *70*, pp.8-15 .

Greenwood, N.N. and Earnshaw, A., 2012. *Chemistry of the Elements*. Elsevier.

Holt, S.L., DeIasi, R. and Post, B., 1971. Crystal structure of the oxygen-inactive form of bis (salicylaldehyde) ethylenediiminecobalt (II). *Inorganic Chemistry*, *10*(7), pp.1498-1500.

Hayvalı, Z., Hayvalı, M. and Dal, H., 2004. Synthesis and spectroscopic characterization of new Schiff bases containing the benzo-15-crown-5 moiety. *Molecules*, *9*(10), pp.860-866.

Hebbink, G., 2002. Luminescent materials based on lanthanide ions. *Basic properties and application in NIR-LEDs and optical amplifiers. 2002: Enschede. p*, *163*.

Hussein, S.S.S.K.B. and Mohamad, M.Y., 2018.Synthesis of some lanthanide complexes with (o-V2Nph. H2) Schiff-base ligand. *Polytechnic Journal, Vol.8,No.2,pp 264-276* .

Jadhav, S., Kulkarni, S. and Shujat, Q., 2017. Synthesis, Characterization and Physio-chemical and Antimicrobial Investigation of Selected Lanthanide Ions with Schiff Base. *Journal of Chemistry and Chemical Sciences*, *7*(3), pp.272-279.

Kotova, O.V., Eliseeva, S.V., Averjushkin, A.S., Lepnev, L.S., Vaschenko, A.A., Rogachev, A.Y., Vitukhnovskii, A.G. and Kuzmina, N.P., 2008. Zinc (II) complexes with Schiff bases derived from ethylenediamine and salicylaldehyde: the synthesis and photoluminescent properties. *Russian Chemical Bulletin*, *57*(9), pp.1880-1889.

Kamel, F.H., Mohammed, M.Y. and Sabir, S.S., 2017. Antibacterial activity of Pistacia khinjul fatty acids extract on some pathogenic bacteria. *Diyala Journal of Medicine*, *12*(1), pp.58-62.

Lodewyckx, K., Van Deun, R. and Binnemans, K., 2001. Lanthanide complexes of Schiff base ligands containing three aromatic rings: synthesis and thermal behaviour. *Materials Science and Engineering: C*, *18*(1-2), pp.217-221.

Maher, K.A. and Mohammed, S.R., 2015. Metal complexes of Schiff base derived from salicylaldehyde-A review. *International Journal of Current Research and Review*, *7*(2), p.6.

Mohammed, L.A., Kadhim, A.J. and Aubaid, N.H., 2013. Synthesis and Characterization of New Schiff Base Ligand with Its Some Complexes Derived from 4-Aminoantipyrine, Sulphadiazine and Acetoacetanilide; Act Chem. *Pharm. India*, *3*(2), pp.111-118.

Pal, S. and Pal, S., 2002. Ruthenium (II) complexes containing RuN 4 O 2 spheres assembled via pyridine-imine-amide coordination. Syntheses, structures, properties and protonation behaviour of coordinated amide. *Journal of the Chemical Society, Dalton Transactions*, (9), pp.2102-2108.

Rao, N.V., Paul, M.K., Rao, T.R. and Prasad, A., 2002. The synthesis of liquid crystalline lanthanide complexes of Schiff's base ligands: N-(4-n-alkoxysalicylidene)-4′-n-alkylanilines. *Liquid crystals*, *29*(9), pp.1243-1246.

Shelke, V.A., Jadhav, S.M., Patharkar, V.R., Shankarwar, S.G., Munde, A.S. and Chondhekar, T.K., 2012. Synthesis, spectroscopic characterization and thermal studies of some rare earth metal complexes of unsymmetrical tetradentate Schiff base ligand. *Arabian journal of chemistry*, *5*(4), pp.501-507.

Sabir, S.S., Hussein, K.B. and Mohamad, M.Y., 2017. Synthesis of some lanthanide complexes with Schiff-base ligand. *Polytechnic Journal*, *7*(3).

Sui, Y., Hu, R.H., Luo, Z.G., Lin, W.H. and Liu, D.S., 2015. Synthesis, Structure and Properties of an Erbium (III) Complex with Chiral Salen-type Schiff Base Ligand. *Zeitschrift für anorganische und allgemeine Chemie*, *641*(8-9), pp.1566-1570.

Taha, Z.A., Ajlouni, A.M., Al Momani, W. and Al-Ghzawi, A.A., 2011. Syntheses, characterization, biological activities and photophysical properties of lanthanides complexes with a tetradentate Schiff base ligand. *Spectrochimica Acta Part A: Molecular*

and Biomolecular Spectroscopy, *81*(1), pp.570-577.

Toyssie P . and charette . ,3,3'-(alkanediyl) bis – (2,2,2-triary-1-oxa-2-stiba-3-azabenzo[d] cyclohex-5-enes). Spectrochem.Acta, (1963) , Vol.19, pp1407-1423 .

Varghese, S. and Muraleedharan Nair, M.K., 2010. Antibacterial and antialgal studies of some lanthanide Schiff base complexes. *Int J Appl Bio Pharm Tech*, *2*, pp.608-614.

Vogel, A.I., 1963. *A text-book of quantitative inorganic analysis: including elementary instrumental analysis*.

ZANCO Journal of Pure and Applied Sciences
The official scientific journal of Salahaddin University-Erbil
https://zancojournals.su.edu.krd/index.php/JPAS

ISSN (print):2218-0230**, ISSN (online):** 2412-3986**, DOI: http://dx.doi.org/10.21271/zjpas**

REVIEW ARTICLE

Inhibitory effect of Atorvastatin on the secretion of extracellular virulence products by Methicillin resistant *Staphylococcus aureus*

Fraidoon Abdulqader Salih

Deparemrnt of Biology, College of Science, Salahaddin University – Erbil, Kurdistan Region, Iraq.

A B S T R A C T:

Statins are lipid-lowering therapeutic agents that have displayed useful anti-inflammatory and antibacterial properties. The focus of this research study was to understand the role of statins in controlling bacterial pathogenicity. Haemolysins and some other substances secreted by *S. aureus* were inhibited by Atorvastatin. It was found that Atorvastatin had a negligible effect on the growth of the bacteria at subminimal inhibitory concentrations, meanwhile it significantly reduced the secretion of haemolysins, coagulase and catalase. Thus, Atorvastatin could be used in conjunction with some antibiotics in controlling Methicillin resistant *S. aureus* MRSA infections and immunomodulation of the defense system.

KEY WORDS: MRSA, Atorvastatin, Haemolysin, α-Toxin.
DOI: http://dx.doi.org/10.21271/ZJPAS.33.4.8
ZJPAS (2021) , 33(4);82-89 .

1. INTRODUCTION:

Methicillin resistant *S. aureus* can cause serious health issues, and is responsible for both nosocomial and cosmopolitan infections (Naimi, 2003; Lakhundi and Zhang, 2018; Siddiqui and Koirala, 2020). In the past four decades considerable attention has been focused on the mechanisms of protein secretion in bacteria, numerous observations have suggested that there is a link between lipid synthesis, membrane topography, integrity, regulatory determinants and the formation and secretion of haemolysins, toxins and enzymes in *S. aureus* and other microorganisms (Altenbern, 1977; Fishman *et al.*, 1978; Caulfield *et al.*, 1979; PATON *et al.*, 1980; Engels and Kamps, 1981; MÄntsälä, 1982; Saleh and Freer, 1984; Berkeley *et al.*, 1987; Hiltunen and Söderhäll, 1992; Price *et al.*, 2001; Adhikari and Novick, 2005; Welsh *et al.*, 2009; Manalo *et al.*, 2017 A. Khan *et al.*, 2018; T. J. Khan *et al.*, 2018; Rana *et al.*, 2019).

Atorvastatin (Pfizers, lipitor) a 3- hydroxy – methylglutaryl coenzyme A reductase inhibitor which lowers serum cholesterol and lipoprotein (Ciaravino *et al.*, 1995)
(Guerin Maryse *et al.*, 2000) has also been shown to inhibit inflammatory properties of *S. aureus* and other bacteria (Pruefer Diethard *et al.*, 1999; Liu *et al.*,2005, 2008; Graziano *et al.*, 2015; Ko *et al.*, 2017). It has been shown that patients on a statin regiment manifested decreased risk of death due to bacterial infections and sepsis (Horn *et al.*, 2008, Hennessy *et al.*, 2016).

During the COVID-19 pandemic, patients on statins have been found to be more resistant to viral infections(Castiglione *et al*., 2020), they also showed a decreased risk of death due to bacterial sepsis (Horn *et al.*, 2008; Zhang *et al.*, 2020). This study attempted to evaluate the effect of atorvastatin on the secretion of virulence factors by MRSA.

* **Corresponding Author:**
Fraidoon Abdulqader Salih
E-mail: fraidoon.salih@yahoo.com
Article History:
Received: 18/02/2021
Accepted: 21/06/2021
Published: 18/08 /2021

2. Materials and Methods

2.1 Organism and growth conditions

A Methicillin resistant strain of *Staphylococcus aureus* (MRSA252, genotype EMRSA, from NARSA71, www.narsa.net) was maintained by a weekly transfer on nutrient agar plates. For cultivation, it was transferred to human blood agar plates (5%) then incubated at 37Cº overnight. Exponential phase cultures were prepared by inoculating a haemolytic colony that showed haemolysis on blood agar into 50 ml of brain heart infusion broth in a 250 ml Erlenmeyer conical flask and incubated at 37Cº on an orbital shaker (Gallenkamp UK) at 150 revolution per minute (RPM) to an optical density at 600 nm (OD 600) for 15-16 hours.

2.2 Identification

S. aureus was identified by mannitol fermentation, gram-stain, coagulase, catalase, golden colour, haemolysins production and by its resistance pattern to methicillin.

2.3 Preparation of Atorvastatin stock solution

Atorvastatin 40 mg tablets were obtained from Pfizer (Lipitor). A stock solution of Atorvastatin (40 mg tablet/ 10 ml (4000 µg/ml) in sterilized distilled water) was prepared.

From the stock solution 10, 20, 40 and 80 µl were aseptically added to 20 ml of rabbit blood agar (5%) medium in Petri dishes to reach a final concentrations of 2, 4, 8 and 16 µg/ml.

In broth culture experiments, 100 and 200 µl of Atorvastatin stock solution were added to 50 ml of brain heart infusion broth BHI in a 250 ml Erlenmeyer conical flasks to achieve final concentrations of 8 and 16 µg/ml respectively.

2.4 Inoculation of *S. aureus* onto Atorvastatin treated culture plates

Fresh cultures of *S. aureus* were subsequently subcultured onto both control and Atorvastatin treated rabbit blood agar plates. The plates were then incubated overnight at 37Cº. Zone of hemolysis around the colonies on Atorvastatin treated plates were then compared with zones around control colonies.

Coagulase production by both control and Atorvastatin treated cells were screened by emulsifying a colony of *S. aureus* in a drop of citrated rabbit plasma and observed for agglutination. Catalase production was monitored by emulsifying a colony of *S. aureus* from control and Atorvastatin treated cultures into a drop of H_2O_2 on a slide and observed for bubble formation.

2.5 Measurement of bacterial growth in control and Atorvastatin treated broth cultures

Exponential- phase cultures were prepared by inoculating a haemolytic colony into 50 ml of brain- heart infusion broth (BHI) in a 250 ml Erlenmeyer conical flask.

The flasks were incubated at 37Cº on a orbital shaker set at a speed of 150 RPM (Glallenkamp, UK). The flasks were monitored until they reached an optical density (OD) of 600 nm for $\pm$ 16 hours. An aliquot of 100 µl of this growing culture were inoculated into three 250 ml Erlenmeyer conical flasks (50 ml BHI medium), one flask was kept as control whereas the other two were treated with 8 and 16 µg/ml Atorvastatin. The experiments were performed in duplicate flasks of BHI grown at 37Cº with shaking at 150 RPM for a period of 16 hours, and repeated twice. The OD of the shaker growth was measured after an incubation period of 16 hours (Saleh and Freer, 1984).

2.6 Effect of Atorvastatin on haemolysin (alpha toxin), catalase and coagulase production during growth

The effect of Atorvastatin on haemolysins, catalase and coagulase production was monitored during growth as cited previously. Optical Density readings at 600nm were taken at 2 hour intervals. Duplicate 1 ml samples of growth cultures were taken and centrifuged at 15,000 RPM in an MSE microcentrifuge (Eisons,UK). Supernatants were assayed for haemolysins production (especially alpha haemolysin (α-toxin)) by doubling dilution titration assay against 1% v/v rabbit blood (which is highly sensitive to α- toxin) performed in phosphate buffered saline PBS in titration plates. The pellets were used for coagulase and catalase tests. To reach an optical density of 600 nm, dilutions were made in BHI broth when necessary. All experiments were repeated twice and all samples were analyzed in duplicate. To perform coagulase and catalase tests, the pellets were washed twice in PBS, centrifuged 15000 RPM, and then emulsified in 100 µl PBS.

An aliquot of 50 µl of this emulsified materal was added to a drop of citrated rabbit plasma or H_2O_2 on microscopic slides, and observed for agglutinations or bubble formations respectively.

2.7 Erythrocytes preparation and Haemolytic assay

An assay involving the lysis of rabbit erythrocytes were used to determine the presence of biologically active haemolysins (especially α-toxin of *S. aureus).* (Saleh and Freer, 1984).

Prior to use, the erythrocytes were washed three times in phosphate buffered saline (0.01 M sodium Phosphate in 0.015 M NaCl, pH 7.0, PBS). The Erythrocytes were then packed via centrifugation at 2000 RPM for 10 minutes in a Hereaus Sepatch Centrifuge (Germany)), prior to the preparation of a 1.0% v/v suspension.

Aliquots of 0.5 ml of culture supernatant were serially diluted in 0.5 ml of PBS in titration plates (Flow Laboratories, UK).

Rabbit erythrocytes (0.5 ml of 1% v/v suspension) were added to each well and the plates were incubated at 37Cº for 30 minutes. An end point at 50% haemolysis was determined visually. The point at which 50% haemolysis occurred was used to determine the haemolysins titration. This was subsequently called a ***a titre haemolytic unit per ml or HU/ml*** (Saleh and Freer, 1984).

2.9 Statistical analysis

Analysis of data was performed by using a SPSS (Version 10) Software Program. Results are expressed as mean ± SE.

3. Results

3.1 Effect of Atorvastatin on haemolysin (alpha toxin) , catalase and coagulase production by *S.aureus* grown on rabbit blood agar culture plates

Atorvastatin at concentrations of 2 and 4 µg/ml had insignificant effect on haemolysins , catalase and coagulase production, whereas, concentrations of 8 and 16 µg/ml had a significant effect on the production of haemolysins, coagulase and catalase, in fact 8 µg/ml **Atorvastatin** reduced the haemolytic zone diameters around the colonies by 50% whereas 16 µg/ml led to complete inhibition or the disappearance of haemolysins. Figure 1 represents the results, all experiments were repeated three times . **Atorvastatin** effect on catalase and coagulase production was profound since significant inhibition of coagulase and catalase were observed at 8 µg/ml , whereas complete inhibition of both enzymes were observed at 16 µg/ml of **Atorvastatin**.

The observations made via light microscopy following gram staining revealed some variations in the shape and integrity of **Atorvastatin** treated cells at a concentration of 8 and 16 µg/ml when they were compared with non-treated cell cultures. **Atorvastatin** treated cells appeared to be somehow smaller than control or non –treated cells. It was additionally observed that their grape like arrangements seemed to be distorted. These cells appeared to be more dispersed especially when involving samples taken from colonies grown on blood agar plates (some irregular clumps have been observed). It's noteworthy to mention that the grape-like arrangements were significantly affected by Atorvastatin treatment**.**

3.2 Effect of Atorvastatin **on the production of haemolysins, catalase and coagulase by *S.aureus* during growth cycle in Brain Heart Infusion broth BHI medium**

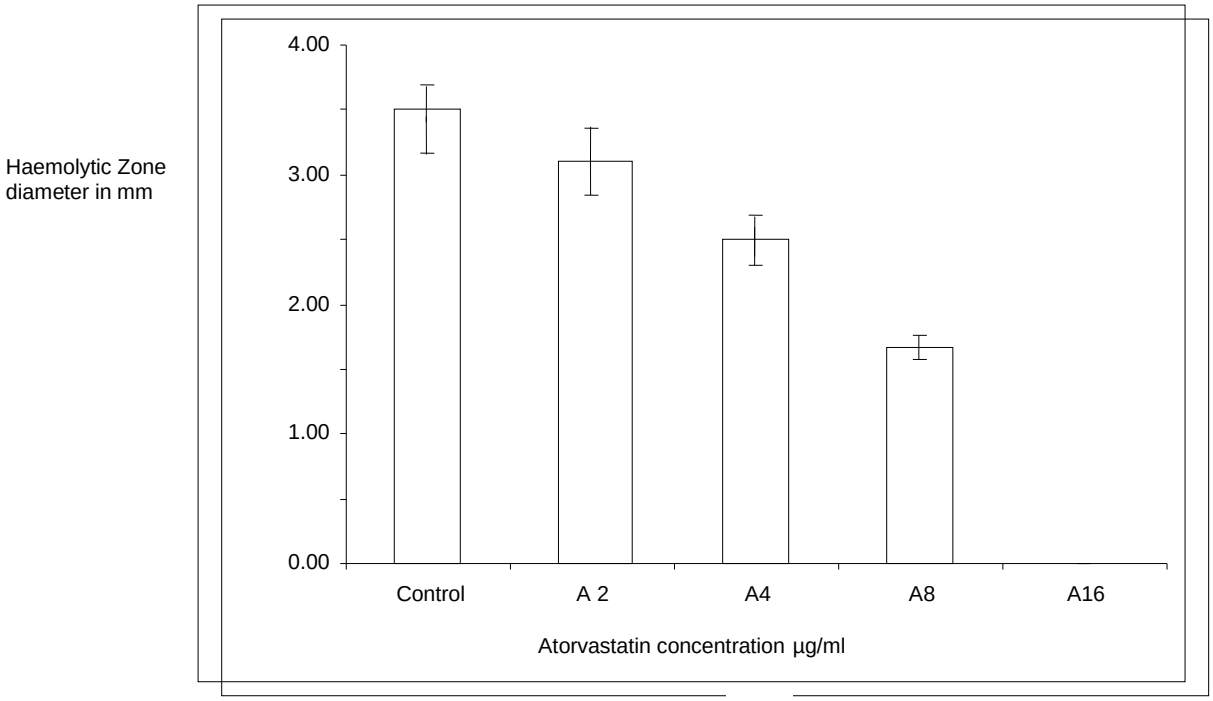

Figure 1 Means and standard errors of the effect of A2, A4, A8 and A16 µg/ml Atorvastatin on the haemolytic zones produced by MRSA grown on rabbit blood agar plates

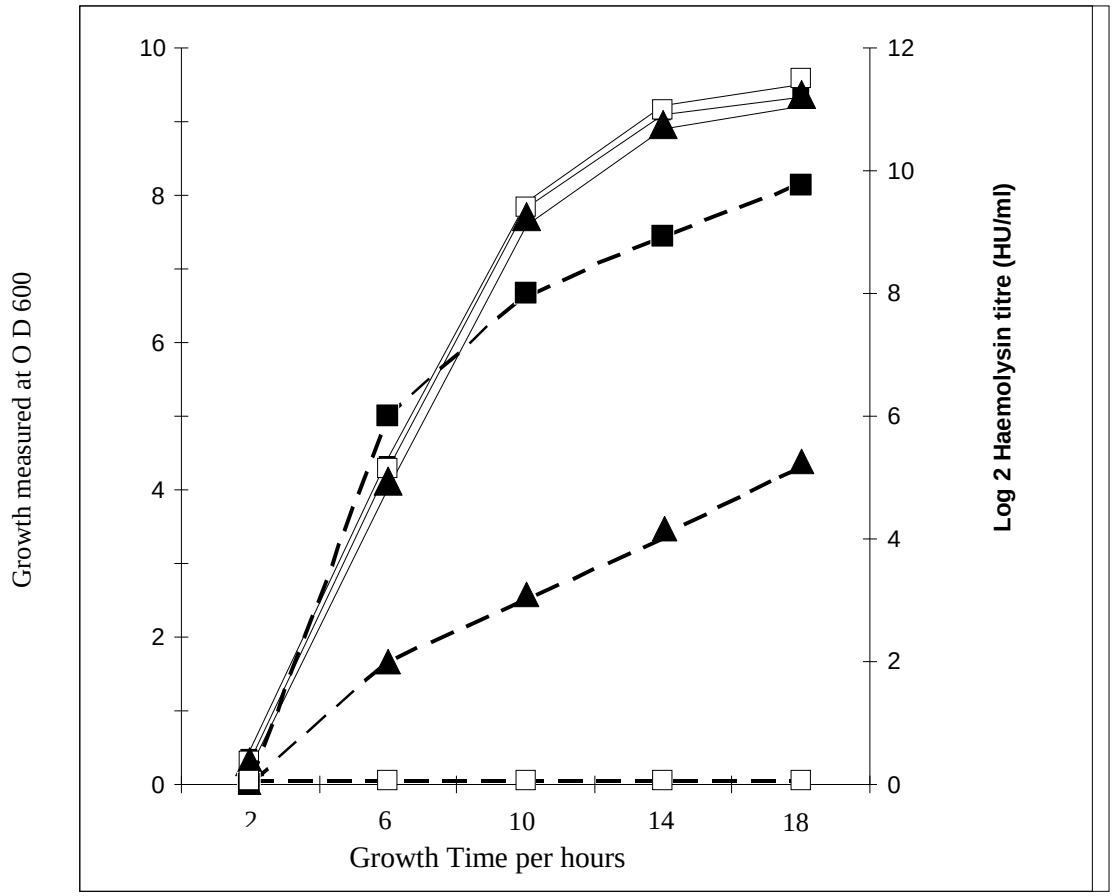

Figure 2 Effect of Atorvastatin on growth and production of haemolysins (α- toxin) by MRSA:

_____ growth measured at O D 600 ; ---------- haemolysin titre in culture supernatant ;

■ Control culture; ▲ culture containing Atorvastatin 8 µg/ml ; □ culture containing Atorvastatin 16 µg/ml

4. Discussion

The virulence characteristics and multi-drug resistance mechanisms in bacteria have been focused on for many years. Researchers have been investigating alternatives to antibiotics in order to combat this phenomenon.

The options investigated included a variety of agents among which were natural plant extracts, membrane perturbing agents, bacteriophages and lipid lowering agents. It was important to investigate the effect of lipid synthesis inhibiting agents, because they inhibit the synthesis of phospholipids in eukaryotic cells and their effects on the secretion of virulence factors by bacteria. Secretions of several exoproteins produced by several gram-position bacteria including staphylococcal enterotoxins, staphylocoagulase, penicillinase, levansucrase, α-amylase, protease, α-toxin and golden colour pigmentation in *S. aureus* have been shown to be sensitive to lipid synthesis inhibitors and membrane- perturbing agents (Altenbern, 1977; Fishman *et al.*, 1978; Caulfield *et al.*, 1979; PATON *et al.*, 1980; Engels and Kamps, 1981; MÄntsälä, 1982; Saleh and Freer, 1984; Berkeley *et al.*, 1987; Liu *et al.*, 2005, 2008; Cauz *et al.*, 2019; Chung, 2020). This investigation had focused upon evaluating the effect of Atorvastatin on the production of toxins and virulence factors by *S. aureus*.

In our research, it was found that the concentrations of Atorvastatin as high as 16 µg/ml of Atorvastatin had no significant effect on growth rate or final OD readings at 600nm, whereas it progressively inhibited the production of haemolysins especially α-toxin with the titer falling from 1024 HU/ml when compared with control cell culture. There was a complete inhibition of toxin production in the Atorvastin treated cultures at concentrations of 16µg/ml.

There also occurred a total inhibition of coagulase and catalase secretions at a concentration of 16µg/ml. The results obtained in our investigation were consistent with previous reference literature citing in this field. These earlier reports had suggested mechanisms that combined between synthesis of lipids or changes which had been induced by statins in physicochemical environments. The changes induced by statins include changes in: membrane integrity, topography or at the level of regularity determinants required for protein secretions (Petit Glatron and Chambert, 1981; Jacques, 1983; Silhavy *et al.*, 1983; Saleh and Freer, 1984; Adhikari and Novick, 2005).

The Atorvastatin effect on the shape and integrity of *S.aureus* cells may be attributed to its effect on the phospholipid and cell wall synthesis. The decrease in bacterial cell size observed in Atorvastatin treated cells may be due to a decrease in the amounts and proportion of different types of phospholipids integrated into these membranes. The dispersions of the cells could reflect the effect of Atorvastatin on the synthesis of teichoic acids which might have a role in binding or holding bacterial cells together through their role as ion chilators.

The recent literature citations associated with the emergence of MRSA have reported numerous investigations which had focused on the role of Atorvastatin in combating these hardy virulent MRSA strains (Pruefer Diethard *et al.*, 1999; Adhikari and Novick, 2005; Liu *et al.*, 2005, 2008;; DeMars *et al.*, 2020; Wang *et al.*, 2020). Recently it has also been found that statins may have a positive role in treating the symptoms of Coronavirus COVID-19 which is caused by SARS Cov-2 virus. COVID-19 supposedly enters the pulmonary cells through the action of the angiotensin converting enzyme 2 ACE2 and a common determinant CD147. The end result being an acute life threatening distress syndrome ARDS (Hirano and Murakami, 2020; Ragia and Manolopoulos, 2020).

Statins have been found to have pleiotropic effects on inflammation and antioxidative stress, which modulate immune response at different levels including immune cell adhesion, migration, antigen presenting, cytokine production and increase antioxidation (Castiglione *et al.*, 2020; Sarkeshikian *et al.*, 2020; Zhang *et al.*, 2020). In this case, Atorvastatin could have changed the lipid/protein proportion of the biological membrane which may have led to a change in the integrity and stoichemistry of ACE2 or CD receptors of SARS Cov-2 virus, therefore the virus may not be able to recognize its protein receptor. A similar scenario in our case would be explained in either of two hypotheses. Firstly, the changes that have been triggered by Atorvastatin in the biosynthesis of bacterial membrane lipids may have caused a change in the topography and stoichemistry of the membrane which may have interfered with the nascent signal protein synthesis on free ribosomes not being able to recognize their receptors. Secondly, a direct effect of Atorvastatin on the transcription of m RNA of extracellular proteins is predictable (Adhikari, R.P., Novick, R.P., 2005). Bearing these in mind, Atorvastatin may be a good tool for controlling bacterial pathogenicity.

Our investigation showed a profound effect of Atorvastatin at sub minimal inhibitory concentrations on the growth and secretion of alpha toxin, coagulase, and catalase by *S.aureus*.

Thus, we suggest that Atorvastatin could be thought of as an agent in the treatment of bacterial sepsis and infections.

This approach may provide the basis for protection at the level of the host in invasive infections by *S. aureus.* In recent years there has been increased use of statins to protect patients from arteriosclerosis.

5. Conclusion

The results obtained in our study lead us to conclude that statins, with their pleotropic and immunomodulatory characteristics and their significant effect on the secretion of virulence factors by MRSA, could be used in conjunction with other antibiotics in combating the severity of MRSA infections.

Acknowledgement

I would like to express my gratitude to Dr. Robert A. Ollar at New York Medical College for proofreading the manuscript and providing his scientific remarks.

Conflict of interest

This is an original work of the author and there is no conflict of interest to be mentioned.

References

Adhikari, R.P., Novick, R.P., 2005. Subinhibitory cerulenin inhibits staphylococcal exoprotein production by blocking transcription rather than by blocking secretion. Microbiology, 151, 3059–3069. https://doi.org/10.1099/mic.0.28102-0

Altenbern, R.A., 1977. Extreme Sensitivity of Staphylococcal Enterotoxin B and C Production to Inhibition by Cerulenin. Antimicrob. Agents Chemother. 11, 906–908. https://doi.org/10.1128/AAC.11.5.906

Berkeley, R.C.W., Pepper, E.A., Caulfield, M.P., Melling, J., 1987. The inhibition of Staphylococcus aureus enterotoxin a production by cerulenin and quinacrine; presumptive evidence for a lipid intermediate/protease release mechanism. FEMS Microbiol. Lett. 40, 103–105. https://doi.org/10.1111/j.1574-6968.1987.tb02010.x

Castiglione, V., Chiriacò, M., Emdin, M., Taddei, S., Vergaro, G., 2020. Statin therapy in COVID-19 infection. Eur. Heart J. — Cardiovasc. Pharmacother. https://doi.org/10.1093/ehjcvp/pvaa042

Caulfield, M.P., Berkeley, R.C., Pepper, E.A., Melling, J., 1979. Export of extracellular levansucrase by Bacillus subtilis: inhibition by cerulenin and quinacrine. J. Bacteriol. 138, 345–351.

Cauz, A.C.G., Carretero, G.P.B., Saraiva, G.K.V., Park, P., Mortara, L., Cuccovia, I.M., Brocchi, M., Gueiros-Filho, F.J., 2019. Violacein Targets the Cytoplasmic Membrane of Bacteria. ACS Infect. Dis. 5, 539–549. https://doi.org/10.1021/acsinfecdis.8b00245

Chung, P.Y., 2020. Novel targets of pentacyclic triterpenoids in Staphylococcus aureus: A systematic review. Phytomedicine 73, 152933. https://doi.org/10.1016/j.phymed.2019.152933

Ciaravino, V., Kropko, M.L., Rothwell, C.E., Hovey, C.A., Theiss, J.C., 1995. The genotoxicity profile of atorvastatin, a new drug in the treatment of hypercholesterolemia. Mutat. Res. Toxicol. 343, 95–107. https://doi.org/10.1016/0165-1218(95)90076-4

DeMars, Z., Singh, V.K., Bose, J.L., 2020. Exogenous Fatty Acids Remodel Staphylococcus aureus Lipid Composition through Fatty Acid Kinase. J. Bacteriol. 202. https://doi.org/10.1128/JB.00128-20

Engels, W., Kamps, M.A.F., 1981. Secretion of staphylocoagulase by Staphylococcus aureus: the role of a cell-bound intermediate. Antonie Van Leeuwenhoek 47, 509–524. https://doi.org/10.1007/BF00443238

Fishman, Y., Rottem, S., Citri, N., 1978. Evidence linking penicillinase formation and secretion to lipid metabolism in Bacillus licheniformis. J. Bacteriol. 134, 434–439.

Graziano, T.S., Cuzzullin, M.C., Franco, G.C., Schwartz-Filho, H.O., Andrade, E.D. de, Groppo, F.C., Cogo-Müller, K., 2015. Statins and Antimicrobial Effects: Simvastatin as a Potential Drug against Staphylococcus aureus Biofilm. PLOS ONE 10, e0128098. https://doi.org/10.1371/journal.pone.0128098

Guerin Maryse, Lassel Taous S., Le Goff Wilfried, Farnier Michel, Chapman M. John, 2000. Action of Atorvastatin in Combined Hyperlipidemia. Arterioscler. Thromb. Vasc. Biol. 20, 189–197. https://doi.org/10.1161/01.ATV.20.1.189

Hennessy, E., Adams, C., Reen, F.J., O'Gara, F., 2016. Is There Potential for Repurposing Statins as Novel Antimicrobials? Antimicrob. Agents Chemother. 60, 5111–5121. https://doi.org/10.1128/AAC.00192-16

Hiltunen, M., Söderhäll, K., 1992. Inhibition of polyketide synthesis in Alternaria alternata by the fatty acid synthesis inhibitor cerulenin. Appl. Environ. Microbiol. 58, 1043–1045.

Hirano, T., Murakami, M., 2020. COVID-19: A New Virus, but a Familiar Receptor and Cytokine Release Syndrome. Immunity 52, 731–733. https://doi.org/10.1016/j.immuni.2020.04.003

Horn, M.P., Knecht, S.M., Rushing, F.L., Birdsong, J., Siddall, C.P., Johnson, C.M., Abraham, T.N., Brown, A., Volk, C.B., Gammon, K., Bishop, D.L., McKillip, J.L., McDowell, S.A., 2008. Simvastatin Inhibits Staphylococcus aureus Host Cell Invasion through Modulation of Isoprenoid Intermediates. J. Pharmacol. Exp. Ther. 326, 135–143. https://doi.org/10.1124/jpet.108.137927

Jacques, N.A., 1983. Membrane Perturbation by Cerulenin Modulates Glucosyltransferase Secretion and Acetate Uptake by Streptococcus salivarius. Microbiology, 129, 3293–3302. https://doi.org/10.1099/00221287-129-11-3293

Khan, A., Wilson, B., Gould, I.M., 2018. Current and future treatment options for community-associated MRSA infection. Expert Opin. Pharmacother. 19, 457–470. https://doi.org/10.1080/14656566.2018.1442826

Khan, T.J., Ahmed, Y.M., Zamzami, M.A., Mohamed, S.A., Khan, I., Baothman, O.A.S., Mehanna, M.G., Yasir, M., 2018. Effect of atorvastatin on the gut microbiota of high fat diet-induced hypercholesterolemic rats. Sci. Rep. 8, 662. https://doi.org/10.1038/s41598-017-19013-2

Ko, H.H.T., Lareu, R.R., Dix, B.R., Hughes, J.D., 2017. Statins: antimicrobial resistance breakers or makers? PeerJ 5, e3952. https://doi.org/10.7717/peerj.3952

Lakhundi, S., Zhang, K., 2018. Methicillin-Resistant Staphylococcus aureus: Molecular Characterization, Evolution, and Epidemiology. Clin. Microbiol. Rev. 31. https://doi.org/10.1128/CMR.00020-18

Liu, C.-I., Liu, G.Y., Song, Y., Yin, F., Hensler, M.E., Jeng, W.-Y., Nizet, V., Wang, A.H.-J., Oldfield, E., 2008. A Cholesterol Biosynthesis Inhibitor Blocks Staphylococcus aureus Virulence. Science 319, 1391–1394. https://doi.org/10.1126/science.1153018

Liu, G.Y., Essex, A., Buchanan, J.T., Datta, V., Hoffman, H.M., Bastian, J.F., Fierer, J., Nizet, V., 2005. Staphylococcus aureus golden pigment impairs neutrophil killing and promotes virulence through

its antioxidant activity. J. Exp. Med. 202, 209–215. https://doi.org/10.1084/jem.20050846

Manalo, R.V.M., Josol, V.J.D., Gloriani, N.G., 2017. The differential effects of atorvastatin co-administered with ampicillin on the bacterial growth and biofilm formation of Staphylococcus aureus. Curr. Med. Res. Pract. 7, 178–183. https://doi.org/10.1016/j.cmrp.2017.08.002

MÄntsälä, P., 1982. Inhibition of Protein Secretion by Cerulenin in Bacillus subtilis. Microbiology, 128, 2967–2972. https://doi.org/10.1099/00221287-128-12-2967

Naimi, T.S., 2003. Comparison of Community- and Health Care–Associated Methicillin-Resistant Staphylococcus aureus Infection. JAMA 290, 2976. https://doi.org/10.1001/jama.290.22.2976

PATON, J.C., MAY, B.K., ELLIOTT, W.H., 1980. Cerulenin Inhibits Production of Extracellular Proteins but not Membrane Proteins in Bacillus amyloliquefaciens. Microbiology, 118, 179–187. https://doi.org/10.1099/00221287-118-1-179

Petit-Glatron, M.-F., Chambert, R., 1981. Levansucrase of Bacillus subtilis: Conclusive Evidence that Its Production and Export are Unrelated to Fatty-Acid Synthesis but Modulated by membrane-Modifying Agents. Eur. J. Biochem. 119, 603–611. https://doi.org/10.1111/j.1432-1033.1981.tb05650.x

Price, A.C., Choi, K.-H., Heath, R.J., Li, Z., White, S.W., Rock, C.O., 2001. Inhibition of β-Ketoacyl-Acyl Carrier Protein Synthases by Thiolactomycin and Cerulenin STRUCTURE AND MECHANISM. J. Biol. Chem. 276, 6551–6559. https://doi.org/10.1074/jbc.M007101200

Pruefer Diethard, Scalia Rosario, Lefer Allan M., 1999. Simvastatin Inhibits Leukocyte–Endothelial Cell Interactions and Protects Against Inflammatory Processes in Normocholesterolemic Rats. Arterioscler. Thromb. Vasc. Biol. 19, 2894–2900. https://doi.org/10.1161/01.ATV.19.12.2894

Ragia, G., Manolopoulos, V.G., 2020. Inhibition of SARS-CoV-2 entry through the ACE2/TMPRSS2 pathway: a promising approach for uncovering early COVID-19 drug therapies. Eur. J. Clin. Pharmacol. 1–8. https://doi.org/10.1007/s00228-020-02963-4

Rana, R., Sharma, R., Kumar, A., 2019. Repurposing of Existing Statin Drugs for Treatment of Microbial Infections: How Much Promising? Infect. Disord. - Drug TargetsDisorders 19, 224–237. https://doi.org/10.2174/1871526518666180806123230

Saleh, F.A.K., Freer, J.H., 1984. Inhibition of Secretion of Staphylococcal Alph Toxin by Cerulenin. J. Med. Microbiol. 18, 205–216. https://doi.org/10.1099/00222615-18-2-205

Sarkeshikian, S.S., Ghadir, M.R., Alemi, F., Jalali, S.M., Hormati, A., Mohammadbeigi, A., 2020. Atorvastatin in combination with conventional antimicrobial treatment of Helicobacter pylori eradication: A randomized controlled clinical trial. J. Gastroenterol. Hepatol. 35, 71–75. https://doi.org/10.1111/jgh.14810

Siddiqui, A.H., Koirala, J., 2020. Methicillin Resistant Staphylococcus Aureus, in: StatPearls. StatPearls Publishing, Treasure Island (FL).

Silhavy, T.J., Benson, S.A., Emr, S.D., 1983. Mechanisms of protein localization. Microbiol. Rev. 47, 313–344.

Wang, J., Ye, X., Yang, X., Cai, Y., Wang, S., Tang, J., Sachdeva, M., Qian, Y., Hu, W., Leeds, J.A., Yuan, Y., 2020. Discovery of Novel Antibiotics as Covalent Inhibitors of Fatty Acid Synthesis. ACS Chem. Biol. 15, 1826–1834. https://doi.org/10.1021/acschembio.9b00982

Welsh, A.-M., Kruger, P., Faoagali, J., 2009. Antimicrobial action of atorvastatin and rosuvastatin. Pathology (Phila.) 41, 689–691. https://doi.org/10.3109/00313020903305860

Zhang, X.-J., Qin, J.-J., Cheng, X., Shen, L., Zhao, Y.-C., Yuan, Y., Lei, F., Chen, M.-M., Yang, H., Bai, L., Song, X., Lin, L., Xia, M., Zhou, F., Zhou, J., She, Z.-G., Zhu, L., Ma, X., Xu, Q., Ye, P., Chen, G., Liu, L., Mao, W., Yan, Y., Xiao, B., Lu, Z., Peng, G., Liu, M., Yang, Jun, Yang, L., Zhang, C., Lu, H., Xia, X., Wang, D., Liao, X., Wei, X., Zhang, B.-H., Zhang, X., Yang, Juan, Zhao, G.-N., Zhang, P., Liu, P.P., Loomba, R., Ji, Y.-X., Xia, J., Wang, Y., Cai, J., Guo, J., Li, H., 2020. In-Hospital Use of Statins Is Associated with a Reduced Risk of Mortality among Individuals with COVID-19. Cell Metab. 32, 176-187.e4. https://doi.org/10.1016/j.cmet.2020.06.015

ZANCO Journal of Pure and Applied Sciences
The official scientific journal of Salahaddin University-Erbil
https://zancojournals.su.edu.krd/index.php/JPAS

ISSN (print):2218-0230**, ISSN (online):** 2412-3986**, DOI: http://dx.doi.org/10.21271/zjpas**

REVIEW ARTICLE

Effect of Foliar Application of Nano-NPK Fertilizer on Growth and Yield of Broad bean *(Vicia Faba L.)*

Bayan Rokan Aziz[1], Dilzar Basit Zrar[2]
Deparemrnt of Horticulture ,College of Agriculture, Salahaddin University – Erbil, Kurdistan Region, Iraq

A B S T R A C T:

A field research was conducted during season 2019/2020 in Gradrasha field, collage of agricultural Engineering sciences at Salahaddin University, to evaluate the effect of foliar application of Nano- NPK fertilizer at different levels (0, 30, 60, 90 and 120 mg.l^{-1}) for one and two times on growth and yield of (*Vicia faba* L.). The research was applied as foliar application of Nano-NPK at different levels (0, 30, 60, 90 and 120 mg.l^{-1}). The results shows significant effect on most studied treatment. The results indicated that number of foliar application had significant influence on most vegetative, yield and yield component parameters, the best results were obtained from twice foliar application, the best values of number of branches.plant^{-1}, chlorophyll content in leaves%, and dry matter of leaves (334.416, 5.381, 46.949 %, 22.789 % respectively) were obtained at the twice foliar application of Nano-NPK. However, the highest results of plant height, number of branches. plant^{-1}, number of leaves. plant^{-1}, leaves chlorophyll content %, dry matter in leaves and TSS in seed (131.448cm, 365.995, 6.120, 51.592%, 25.435ghighes and 16.107% respectively) were recorded from (120mg.l^{-1}) of Nano- NPK.
Moreover the foliar application of (120mg.l^{-1}) Nano-NPK for two times gave highest significant effects on vegetative growth, yield and yield component.

KEY WORDS: ***Bean, Nano-NPK fertilizer, vegetative growth, yield, chlorophyll.***
DOI: http://dx.doi.org/10.21271/ZJPAS.33.4.9
ZJPAS (2021) , 33(4);90-99 .

1. INTRODUCTION:

Broad bean (*Vicia faba* L.) is a legume member family, grown initially for edible pods and seeds. It has an upright growth that grows up to 1-2m height, it has main taproot and adventitious roots that spread to 0.90 m in width (Muehlbauer *et al.,* 1997). The broad bean can be harvested as a vegetable when the seeds are immature and green, or harvested at the maturity stage when the seeds are dry (Singh *et al.*, 2013.)

* **Corresponding Author:**
Bayan Rokan Aziz
E-mail: bayan.aziz@su.edu.krd,dilzar.zrar@su.edu.krd
Article History:
Received: 24/02/2021
Accepted: 26/04/2021
Published: 18/08 /2021

It is rich in protein that use as a source of human diet, and can be used in crop rotation to restore soil fertility and soil properties (Jasim, 2007). The top five production countries are China, Ethiopia, Australia, France and Egypt. Additionally, fresh and dry seeds of broad bean are consist of many elements like potassium, Calcium, Manganese, Iron, and Zinc (Neme *et al.*, 2015; Longobardi *et al.*, 2015; Lizarazo *et al.*, 2015).
Traditional usage of fertilizer whether organic or chemical, could be make a problem to the soil; huge quantities uses may cause ground water and soil pollution, shortage micronutrient and soil degradation, eventually lead to decrease production (Meena *et al.,* 2017). However, all kinds of fertilizer have advantage and disadvantage effects on plant growth and rate on the of soil fertility (Chen, 2008). Nano-fertilizers

provide Nano structure nutrients control and increase the availability of nutrients, reduce soil toxicity and decrease the costs for protection environment (Sekhon, 2014; Rameshaiah *et al.*, 2015). Moreover, it is requisite a new way for fertilization to increase plant product. Nanotechnology has been illustrated as concerning to materials, processes and systems which work at a size of 100nm or less, and it could be used in several stages of agricultural yields production from cultivation to storage. However, use as a source of determination plant infection and controlling disease, which is one of the most critical usage of nano technology, which enhances the capability of plants to assimilate these nutrients (Mousavi and Rezai 2011; Srilatha, 2011; Ditta 2012).

Amirnia *et al.*, (2014) indicated that foliar spraying of plant with (Fe, P, K) nano-fertilizers had significantly influence on saffron (*Crocus sativus*) growth which increased flower fresh and dry weights, stigma length and total yield. Merghany *et al.*, (2019) studied the influence of liquid nano-fertilizer (3, 4.5, 6 and 9 ml) on growth and yield cucumber which cause significant increase in number of leaves.plant^{-1}, plant height, Chlorophyll pigment, N, P, K% content in leaves, fruits and yield in comparison to control. Foliar application with nano-fertilizer-NPK in chickpea increased the yield and yield components as a result of increased growth hormone activity and improved of metabolic action, caused to rise in flowering and productivity (Drostkar *et al.*, 2016).

The current experiment was purposed to assess the impact of nano-NPK on vegetative growth, production quantity and quality and to minimize the production cost of Broad bean and attempt to participate the reducing the chemical fertilizers pollutants and preserve the environment.

2-Material and methods

2-1 Location

A research was investigated in field during the winter-spring season (1st December 2019 to 30th April 2020), at Grdarasha field, collage of agricultural Engineering sciences at Salahaddin University, Kurdistan Region. Some properties of soil (physical and chemical) of field and the metrological data during the study period are shown in tables (1) and (2) respectively.

2-2 Preparing of field experiment:

1-Horticultural Practices:

The field was prepared at November 15th 2019 and divided to three blocks each consists of (10) experimental units (plots) with two rows (100 cm in length and the distance of 50 cm between them), with five plants per row and with 20 cm interval between plants (Hussein and Badshah, 2002). The experiment was ended at April 30th 2020 by harvesting green immature seeds.

2-Preparation of Nano NPK solutions

The Nano-NPK fertilizer was prepared with five levels (0, 30, 60, 90, and 120 mg. l^{-1} distill water) and was manufactured by the Iranian company (Khazra NPK Chelated Fertilizer chemical powder (20% - 20% - 20%) of Nano NPK). Those solutions were sprayed once and twice during the experiment period starting in January 25th 2020 with 30 days interval according to their treatments.

2-3 The experiment parameters:

The following parameters were measured at the end of the study: 1- Vegetative growth parameters include; Plant height, Number of leaves and Number of branches.plant^{-1}, fresh and dry weights of vegetative growth.

2- Yield parameters which include Number of pods.plant^{-1}, Number of seed.pod^{-1}, fresh weight of individual pod, fresh weight of 100 seed (g), yield.kg.plot^{-1}, yield. kg. ha^{-1}, total soluble solid in the seeds (TSS%) (AOAC, 1990), and total chlorophyll content (SPAD) (Incesu, 2015).

2-4 Experimental design and statistical analysis:

The experiment are design as RCBD and consist three blocks each with 10 experiment unit; five concentration of Nano NPK fertilizer (0, 30, 60, 90, and 120 mg. L^{-1}) and were sprayed one and two times. All data average was compared by (Duncan's Multiple Range Test) at the level of 0.05 (Al-Rawi and Khalaf-Alla, 2000) using software program SPSS (Casanova *et al.*, 2004).

3- Results and Discussion:

3.1 Vegetative parameter:

1- Effect of number of foliar application:

The results in figure (1, a and b) show significant increase of twice foliar application of Nano-NPK in most vegetative growth parameters. Except plant plant height when the longest plant

(109.244cm) was recorded from once foliar application. However, the best values of number of leaves.plant^{-1}, number of branches.plant^{-1}, chlorophyll content in leaves%, dry matter of leaves% (334.416, 5.381, 46.949 % and 22.789 % respectively) were obtained at the twice foliar application of Nano-NPK. The results are agree with Elshamy *et al.,* (2019), and may be due to the impact of nano fertilizer which raise the available nutrient to plants which increase the the formation of chlorophyll pigment, photosynthesis process as a result enhance the vegetative growth parameter generally (Al-Juthery *et al.,* 2018).

2- Effect of Nano- NPK levels:

Results in table (3) indicated that the effects of foliar application with Nano-NPK levels had significant difference on vegetative parameter compared with control treatment. The best values of plant height number of leaves.plant^{-1}, number of branches plant^{-1}, chlorophyll content in leaves, dry matter of leaves and TSS, which are (131.448 cm, 365.995, 6.120, 51.592%, 25.435% and 16.107% respectively) were recorded from foliar application with 120 mg.l^{-1} of Nano-NPK. This finding is agreed with results mentioned previously by (Merghany *et al.,* 2019). the obtained results could be due to the physiological role of nitrogen in bimolecular compound such porphyrin that exist in metabolism process such as cytochrome and chlorophyll pigment, which the necessary in respiration and photosynthesis and coenzymes that promote by phosphorus and essential for most of enzyme and amino acid production that usage for production of protein (Espinosa *et al.,* 1999), however , potassium are responsible on enzyme activity and stable of protein (Hansch and Mendel, 2009).

3- Interaction effects of number of foliar application and Nano- NPK levels:

The present result in table (4) indicated the interaction of number of foliage spraying and levels of Nano-NPK caused significant effects on all the growth parameters when compare without spraying with Nano- NPK (control) . The highest value of plant height (142.887cm) was obtained from once foliar application of 120 mg.l^{-1}of Nano-NPK. However, the best values of number of leaves.plant^{-1}, number of branches.plant^{-1}, chlorophyll content in leaves %, dry matter of leaves and TSS % (369.670, 6.513, 52.807, 25.747 and 16.290 respectively) were recorded from twice foliar application with 120 mg.l^{-1}. These results are sympathy with those obtained by (Aziz *et al.,* 2016), this can be due to the part of Nano-fertilizer in raising the diffusion of undissolved nutrients within the soil and decrease stabilization and soil biology which cause increment effective absorption of material added (Veronica *et al.,* 2015).

3.2 Yield and Yield Parameter:

1. Effect of number of foliar application:

Figure (2, a and b) presents the effect of foliar application with Nano-NPK on yield and yield component parameters of *Vicia faba* L., it can be seen that the levels of Nano-NPK had significant effect on all parameters. The best values of number of pod.plant-1, pod length, pod weight.plant-1, pod.yield-1, number of seed.pod-1, seed yield.plant-1, seed yield.ha-1 and weight of 100 seed (10.404, 20.943cm, 29.033gm, 309.494ton, 4.340, 122.013 and 250.850g respectively) were recorded from twice foliar application. These results are corresponded with that report by Kobraee et al., (2011). The raising in vegetative growth parameter that mentioned before and thus raise the photosynthesis process efficiency by high utilization of Nano particles then lead to increasing the productivity in the source then increasing the accumulation of dry substance in sinks, and increasing of yield parameters (Liu and Lal, 2015).

2- Effect of Nano- NPK levels:

The effect of foliar application Nano- NPK concentrations on yield and yield component of *Vicia faba* L. are displays in table (5).There were significant differences in all yield and yield parameters. The best values of number of pod.plant^{-1}, pod length, individual pod weight, pod.yield^{-1}, pod yield.plant^{-1}, number of seed.pod^{-1} seed yield.plant^{-1} seed yield.ha^{-1} and weight of 100 seed (11.960, 23.412cm, 30.982g, 372.935g, 37.293 ton, 5.300, 169.725g, 16.972g and 288.200g respectively) were obtained from 120 mg.l^{-1} Nano-NPK. These results are line with discovering of Drostkar *et al.,* (2016), and the possible reason may be due to increasing the

micronutrients in plant action such as photosynthesis and enhancing the advantage function of plant hormones and caused a positive reflection on the number of flowering and seed formation which ordinary increase yield component (Quary *et al.*, 2006).

3- Interaction effects of number of foliar application and Nano- NPK levels:

The present results have indicated that yield and yield component were significantly increased by number of foliar application and levels of Nano-NPK (Table 6). The best values of number of pod.plant^{-1}, pod length, individual pod weight, pod.yield^{-1}, pod yield.plant^{-1}, number of seed.pod^{-1} seed yield.plant^{-1} seed yield.ha^{-1} and weight of 100 seed (12.780, 5.600, 201.110g, 23.510cm, 33.900g, 433.240g, 307.690g respectively). were recorded from twice foliar application and 120mg.l^{-1} of Nano-NPK. This result was similar to investigation that showed by (Mohsen *et al.*, 2020).Could be due to the effect of nitrogen which play essential role in vegetative growth, production because it is a major component of chlorophyll and protein (Sandhu *et al.*, 2014).

4- Conclusion:

The findings of this study on *Vicia faba L.* demonstrate the following conclusions:

1- Twice foliar application with Nano NPK increased the values of studied Vegetative growth and yield parameters.

2- The use of (120mg.l^{-1}) Nano- NPK. significantly promoted the most vegetative growth and yield parameters.

3- The best values of vegetative growth and yield parameter were obtained from twice foliar application and (120mg.l^{-1}) of Nano- NPK.

These findings are of great interest to use Nano-NPK fertilizer, and it can produce significantly higher yield of broad bean, and can facility to be adopted by farmers for increasing the production of green pods of this plant.

Table (1): Physical and chemical properties of field*:

Soil Texture			pH	EC (dsm^{-1})	Organic matter (%)	Total Nitrogen (%)	Total Phosphorus (%)	Total Potassium (%)
Silty Clay Loam			7.65	2.36	1.134	0.137	0.000558	0.440
Sand (%)	Silt (%)	Clay (%)						
11.7	41.8	46.5						

* Central Laboratory at College of Agricultural Engineering Sciences.

Table (2): Some metrological data recorded during experiment period*:

Months	Temperature (C◦)		Humidity (%)		Rainfall (mm)
	Min.	Max.	Min.	Max.	
Nov. 2019	10.73	23.39	20.57	49.99	45.262
Dec. 2019	7.96	16.42	46.58	82.16	47.03
Jan. 2020	5.20	13.14	45.62	82.97	50.774
Feb.2020	6.05	14.09	42.23	81.59	58.479
Mar.2020	10.70	20.54	38.50	77.00	61.175
Apr.2020	13.01	24.80	32.24	75.01	49.129
Total annual rainfall					311.849 mm

***** Ministry of Agriculture in Kurdistan region.

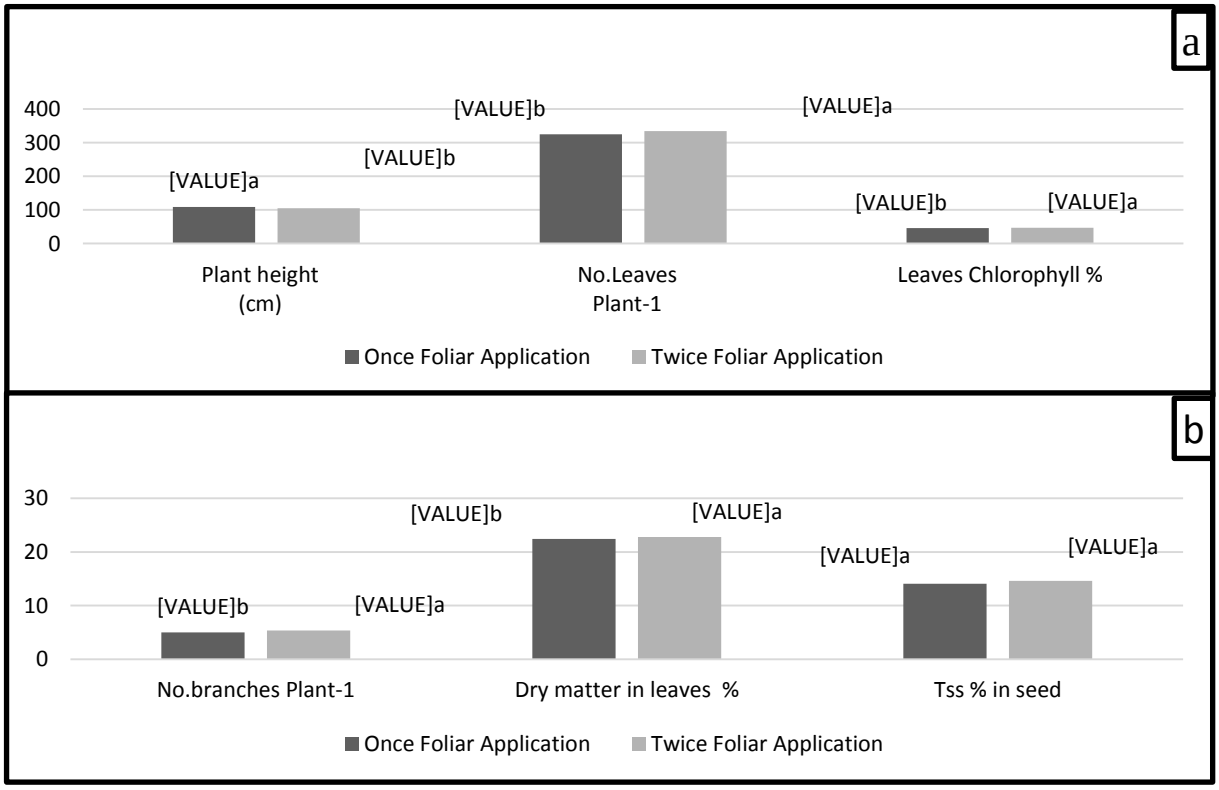

Figure (1, a and b) Effects of number of foliar application on vegetative growth parameters of *Vicia faba* L .
*(columns with the different letter are significantly different from each other depended to DMRT at 0.05 level).

Table (3) Effect of Nano NPK levels on vegetative growth parameters of *Vicia faba* L .

Con.Nano NPK mg\L	Plant.height (cm)	No.Leaves Plant^{-1}	No.branches Plant^{-1}	Chlorophyll content in leaves %	Dry matter in leaves %	Tss % in seed
0.0	90.398 c	270.788 e	4.137 e	38.855 d	21.188 c	11.055 d
30	94.920 bc	309.043 d	5.370 c	46.253 c	21.030 c	14.492 c
60	117.832 ab	355.853 b	5.817 b	48.807 b	24.708 b	15.553 b
90	100.965 bc	345.392 c	4.465 d	46.252 c	20.680 d	14.482 c
120	131.448 a	365.995 a	6.120 a	51.592 a	25.435 a	16.107 a

Data within each column followed with the different latters are indicate significantly different from each other depending to DMRT at the 0.05 level.

Table (4) Interaction effect of foliar application numbers and levels of Nano- NPK on vegetative growth parameter of *Vicia faba* L .

Application treatment	Conc. of Nano NPK	Plant.height (cm)	No.Leaves Plant^{-1}	No.branches . plant^{-1}	Chlorophyll content in leaves %	Dry matter in leaves %	TSS % in seed
Once Foliar Application	**0.0**	91.147 **b**	271.213 **g**	4.110 **f**	39.647 **f**	21.117 **e**	11.090 **g**
	30	95.583 **b**	292.597 **f**	5.120 **d**	45.070 **e**	19.980 **f**	13.983 **f**
	60	115.247 **ab**	351.677 **c**	5.633 **c**	48.377 **cd**	24.540 **c**	15.053 **c**
	90	101.367 **b**	344.257 **d**	4.323 **f**	45.303 **e**	21.380 **e**	14.333 **e**
	120	142.887 **a**	362.320 **b**	5.727 **c**	50.377 **b**	25.123 **b**	15.923 **b**
Twice Foliar Application	**0.0**	89.650 **b**	270.363 **g**	4.163 **f**	38.063 **g**	21.260 **e**	11.020 **g**
	30	94.257 **b**	325.490 **e**	5.620 **c**	47.437 **d**	22.080 **d**	15.000 **c**
	60	120.427 **ab**	360.030 **b**	6.000 **b**	49.237 **bc**	24.877 **bc**	16.053 **b**
	90	100.563 **b**	346.527 **d**	4.6107 **e**	47.200 **d**	19.980 **f**	14.630 **d**
	120	120.010 **ab**	369.670 **a**	6.513 **a**	52.807 **a**	25.747 **a**	16.290 **a**

Data within each column followed with the different latters are indicate significantly different from each other depending to DMRT at the 0.05 level.

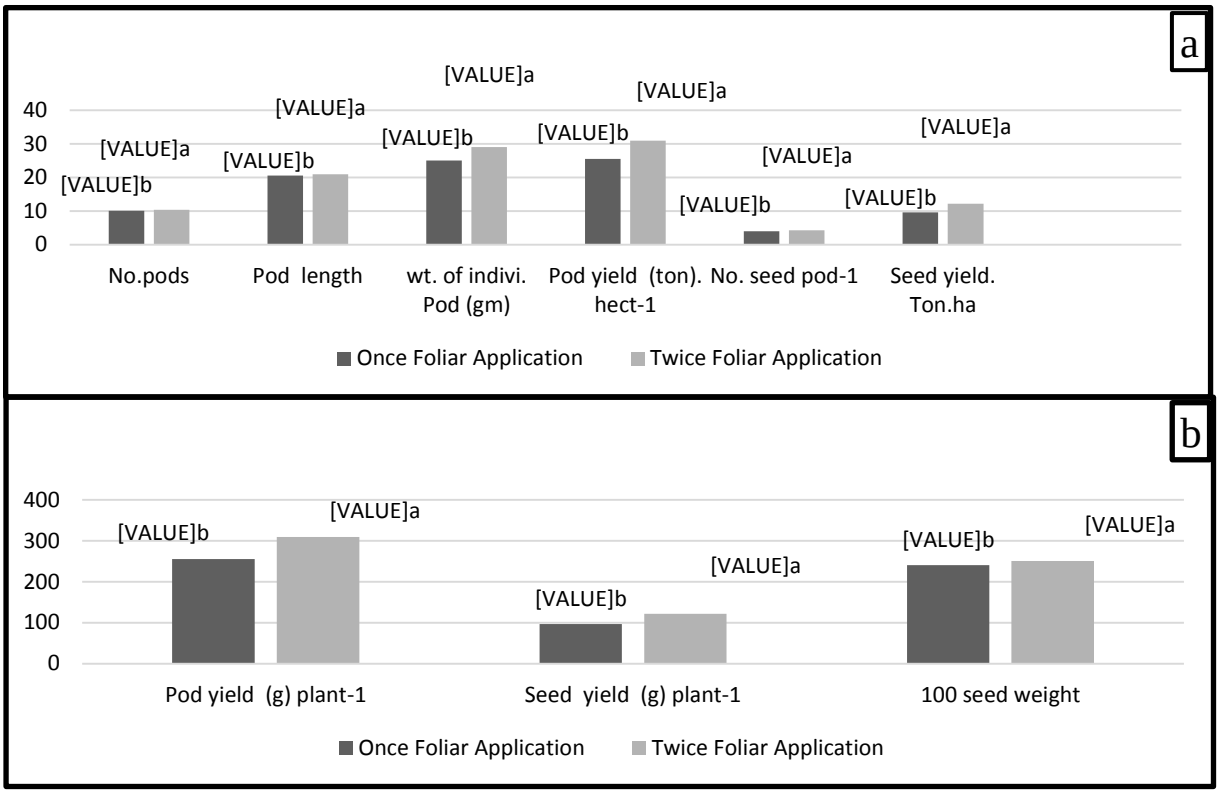

Figure (2, a and b) Effects of number of foliar application on yield and yield parameters of *Vicia faba* L .
*(columns with the different letter are significantly different from each other depended to DMRT at 0.05 level).

Table (5) Effect of Nano NPK levels on yield and yield components of *Vicia faba* L .

Con Nano.NPK mg.l^{-1}	No.pods plant^{-1}	Pod length cm	Indivi. pod weight (gm)	Pod yield (g) plant^{-1}	Pod yield (ton). hect^{-1}	No. seed pod^{-1}	Seed yield (g) plant^{-1}	Seed yield ton. ha^{-1}	100 seed weight (g)
0.0	8.585 **d**	17.108 **e**	19.383 **e**	166.007**e**	16.572 **e**	3.050 **e**	56.560 **e**	5.656e	188.892 **e**
30	9.112 **d**	19.230 **d**	24.517 **d**	223.635 **d**	22.365 **d**	3.817 **d**	84.937**d**	8.493d	232.747**d**
60	11.078 **b**	22.563 **b**	30.540 **b**	338.243 **b**	33.823 **b**	4.650 **b**	130.697 **b**	13.069b	266.260 **b**
90	10.475 **c**	21.415 **c**	29.767**c**	312.190 **c**	31.220 **c**	4.217 **c**	104.167**c**	10.416c	252.182 **c**
120	11.960 **a**	23.412 **a**	30.982 **a**	372.935 **a**	37.293 **a**	5.300**a**	169.725 **a**	16.972a	288.200 **a**

Data within each column followed with the different latters are indicate significantly different from each other depending to DMRT at the 0.05 level.

Table (6) Interaction effect of foliar application numbers and levels of Nano- NPK on yield and yield components of *Vicia faba* L .

treatment	Conc.of Nano NPK (ml.l $^{-1}$)	No.pods plant-	Pod length Cm	Pod weight (g) plant^{-1}	Pod yield (g) plant^{-1}	Pod yield (ton). hect^{-1}	No. seed pod-1	Seed yield (g) plant^{-1}	Seed yeild ton . ha^{-1}	100 seed weight (g)
Once Foliar Application	0.0	8.957 de	16.997 h	18.500 h	165.617 h	16.503 h	3.000 e	54.500 f	5.453 f	188.883 f
	30	8.950 de	18.577 g	22.833 f	204.317 g	20.433 g	3.900 d	74.560 e	7.453e	231.000 e
	60	11.080 bc	22.237 c	28.013 d	310.390 d	31.037 d	4.300 c	120.353 c	12.036c	265.333 b
	90	10.273 c	21.617 d	27.800 d	285.597 e	28.563 e	4.167 c	94.350 d	9.433 d	248.383 d
	120	11.140 b	23.313 a	28.063 d	312.630 d	31.263 d	5.000 b	138.340 b	13.836 b	268.710 b
Twice Foliar Application	0.0	8.213 e	17.220 h	20.267 g	166.397 h	16.640 h	3.100 e	58.620 f	5.860 f	188.900 f
	30	9.273 d	19.883 f	26.200 e	242.953 f	24.297 f	3.733 d	95.313 d	9.533d	234.493 e
	60	11.077 bc	22.890 b	33.067 b	366.097 b	36.610 b	5.000 b	141.040 b	14.106 b	267.187 b
	90	10.677 bc	21.213 e	31.733 c	338.783 c	33.877 c	4.267 c	113.983 c	11.403 c	255.980 c
	120	12.780 a	23.510 a	33.900 a	433.240 a	43.323 a	5.600 a	201.110 a	20.110a	307.690 a

Data within each column followed with the different latters are indicate significantly different from each other depending to DMRT at the 0.05 level.

5-References

Al-Juthery, H.W.A., Ali, N.S., Al-Taey, D.K.A. and Ali, E.A.H.M., 2018. The impact of foliar application of nanaofertilizer, seaweed and hypertonic on yield of potato. *Plant Archives*, *18*(2), pp.2207-2212.

Amirnia, R., Bayat, M. and Tajbakhsh, M., 2014. Effects of nano fertilizer application and maternal corm weight on flowering at some saffron (*Crocus sativus* L.) ecotypes. *Turkish Journal of Field Crops*, 19(2), pp.158-168.

Aziz, H.M.A., Hasaneen, M.N. and Omer, A.M., 2016. Nano chitosan-NPK fertilizer enhances the growth and productivity of wheat plants grown in sandy soil. *Spanish Journal of Agricultural Research,* 14(1), p.17.

Casanova, E, Valdes, A.E., Fernandez, B., Moysset, L. and Trillas, M.I. (2004) Levels and immune-localization of endogenous cytokinins in thidiazuron-induced shoot organogenesis in carnation. *Journal of Plant physiology,* 161(1), p. 95-104.

Chen, J.H., 2006. The combined use of chemical and organic fertilizers and/or biofertilizer for crop growth and soil fertility. International workshop on sustained management of the soil-rhizosphere system for efficient crop production and fertilizer use. 16 (20), p. 1-11.

Ditta, A., 2012. How helpful is nanotechnology in agriculture. Advances in Natural Sciences: *Nanoscience and Nanotechnology*, 3(3), p.033002.

Drostkar, E., Talebi, R. and Kanouni, H., 2016. Foliar application of Fe, Zn and NPK nano-fertilizers on seed yield and morphological traits in chickpea under rainfed condition. *Journal of Resources and Ecology*, 4, pp.221-228.

Elshamy, M.T., Husseiny, S.M. and Farroh, K.Y., 2019. Application of nano-chitosan NPK fertilizer on growth and productivity of potato plant. *Journal of Scientific Research in Science,* 36(1), pp.424-441.

Espinosa, M., Turner, B.L. and Haygarth, P.M., 1999. Preconcentration and separation of trace phosphorus compounds in soil leachate (Vol. 28, No. 5, pp. 1497-1504). American Society of Agronomy, Crop Science Society of America, and Soil Science Society of America.

FAOSTAT, 2013. FAOSTAT database. Food and Agriculture Organization of the United Nations, Rome, Italy, 1.

Hänsch, R. and Mendel, R.R., 2009. Physiological functions of mineral micronutrients (cu, Zn, Mn, Fe, Ni, Mo, B, cl). *Current opinion in plant biology*, 12(3), pp.259-266.

Jasim, A.H., 2007. Effect of foliar fertilization on growth and yield of broad bean *Vicia faba* L. *Anbar Journal of Agricultural Sciences*, 5(2), pp.177-182.

Kobraee, S., Shamsi, K. and Rasekhi, B., 2011. Effect of micronutrients application on yield and yield components of soybean. *Annals of Biological research*, 2(2), pp.476-482.

Liu, R. and Lal, R., 2015. Potentials of engineered nanoparticles as fertilizers for increasing agronomic productions. Science of the total environment, 514, pp.131-139.

Lizarazo, C.I., Lampi, A.M., Liu, J., Sontag-Strohm, T., Piironen, V. and Stoddard, F.L., 2015. Nutritive quality and protein production from grain legumes in a boreal climate. *Journal of the Science of Food and Agriculture*, 95(10), pp.2053-2064.

Longobardi, F., Sacco, D., Casiello, G., Ventrella, A. and Sacco, A., 2015. Chemical Profile of the C arpino Broad Bean by Conventional and Innovative Physicochemical Analyses. *Journal of Food Quality,* 38(4), pp.273-284.

Meena, D.S., Gautam, C., Patidar, O., Meena, P.H.M., Prakasha, G. and Vlshwa, J., 2017. NanoFertilizers are a new way to increase nutrients use efficiency in crop production. Inter. *J. of Agri. Sci.,* ISSN, pp.0975-3710.

Merghany, M., Shahein, M.M., Sliem, M.A., Abdelgawad, K.F. and Radwan, A.F., 2019. Effect of nano-fertilizers on cucumber plant growth, fruit yield and it's quality. *Plant Archives,* 19(2), pp.165-172.

Merghany, M.M., Shahein, M.M., Sliem, M.A., Abdelgawad, Mohsen, H.A., Alhhasany, A.R. and Noaema, A.H., 2020. Effect of spraying dates and concentrations with npk nanoparticles on the growth and yield of beans (*Vicia faba* L.). *Plant Archives*, 20(1), pp.335-338.

Mousavi, S.R. and Rezaei, M., 2011. Nanotechnology in agriculture and food production. *J Appl Environ Biol Sci,* 1(10), pp.414-419.

Muehlbauer, F. ; Tullu, A., 1997. *Vicia faba* L. . Purdue Univ., Cent. New Crops Plants Prod., NewCrop Factsheet.

Neme, K., Bultosa, G. and Bussa, N., 2015. Nutrient and functional properties of composite flours processed from pregelatinised barley, sprouted faba bean and carrot flours. *International journal of food science & technology*, 50(11), pp.2375-2382.

Oury, F.X., Leenhardt, F., Remesy, C., Chanliaud, E., Duperrier, B., Balfourier, F. and Charmet, G., 2006. Genetic variability and stability of grain magnesium, zinc and iron concentrations in bread wheat. *European Journal of Agronomy*, 25(2), pp.177-185.

Rameshaiah, G.N., Pallavi, J. and Shabnam, S., 2015. Nano fertilizers and nano sensors–an attempt for developing smart agriculture. *Int J Eng Res Gen Sci,* 3(1), pp.314-320.

Sandhu, A.S., Sharma, S.P., Bhutani, R.D. and Khurana, S.C., 2014. Effects of planting date and fertilizer dose on plant growth attributes and nutrient uptake of potato (*Solanum tuberosum* L.). *International Journal of Agricultural Sciences*, 4(5), pp.196-202.

Sekhon, B.S., 2014. Nanotechnology in agri-food production: an overview. *Nanotechnology, science and applications,* 7, p.31.

Srilatha B. 2011. Nanotechnology in agriculture. Journal of Nanomed. Nanotechnol. 2: 5-7

Veronica, N., Guru, T., Thatikunta, R. and Reddy, S.N., 2015. Role of Nano fertilizers in agricultural farming. *Int. J. Environ. Sci. Technol,* 1(1), pp.1-3.

ZANCO Journal of Pure and Applied Sciences
The official scientific journal of Salahaddin University-Erbil
https://zancojournals.su.edu.krd/index.php/JPAS

ISSN (print): 2218-0230**, ISSN (online):** 2412-3986**, DOI: http://dx.doi.org/10.21271/zjpas**

RESEARCH PAPER

Ecofriendly approaches for the management of rose powdery mildew (Podosphaera pannosa var. rosae)

Qasim A. Marzani[1, *], Ashna O. Mohammad [1], Othman A. Hamda[2]
[1] Department of Plant Protection, College of Agricultural Engineering Sciences, Salahaddin University-Erbil, Southern Region of Kurdistan, Iraq.
[2] Erbil Central Forest Nursery, Ministry of Agriculture and Irrigation, Erbil, Southern Region of Kurdistan, Iraq.

A B S T R A C T:

Rose and miniature rose powdery mildew caused by *Podosphaera pannosa* is the most important disease in greenhouses and outdoor plantations. The use of fungicides, as a control method, is detrimental to nature and paid public interest. This work was aimed to utilize ecofriendly methods represented with plant extracts and antagonistic fungi. Among 13 plant extracts tested *in vitro*, garlic (*Allium sativum*), ginger (*Zingiber officinale*), and rosemary (*Rosmarinus officinalis*) were the most effective bioagents that resulted in a significant reduction of conidia germination. This result is supported by the greenhouse assessment of the selected extracts, in which the powdery mildew disease was reduced by up to 88.1%. The use of the commercial product of *T. harzianum* in the greenhouse was effective as plant extracts.

KEY WORDS: *Podosphaera pannosa* var. *rosae*, Rosa, plant extracts, biological control, *Trichoderma harzianum*.DOI: DOI: http://dx.doi.org/10.21271/ZJPAS.33.4.10
ZJPAS (2021) , 33(4);100-110 .

1.INTRODUCTION :

Roses (*Rosa spp*.) are the most important ornamental horticultural crops grown throughout the world for their variety of uses in floral decoration, cut flower, medicinal, cosmetic, and industrial sectors. (Hummer and Janick, 2009).

Rose powdery mildew caused by the biotrophic ascomycete fungus *Podosphaera pannosa* var. *rosae*, is a worldwide important disease on indoor and outdoor roses. The disease reduces both plant quality and vigor; therefore, causes serious losses and becomes a limiting factor for rose producers. Distortion, curling, and premature defoliation are all severe damages caused by the pathogen (Phillips and Rix, 1988, Bélanger et al., 1994, Sangani et al., 2018).

Despite not killing the plants, the disease impairs plant growth and reduces flower production, and weakens the plants (Agrios, 2005). On the other hand, under greenhouse conditions, powdery mildew is the most important and devastating disease (Félix-Gastélum et al., 2014). The disease is favored by conditions like cool, moderate temperature, and reduced light or shade (Kumar and Chandel, 2018a, Rex and Deepika, 2020).

Several methods are practiced to control rose powdery mildew such as the traditional method which is foliar fungicide application that demonstrated to be a very effective method and could extensively reduce the impact of plant diseases. However, the chemical method which normally includes Sulphur compounds encountered public perception and it is undesired due to several negative points accompanying the method. In addition, the method is costly, needs frequent applications, causing detrimental effects to the environment and other beneficial organisms, and the emergence of fungicide

* **Corresponding Author:**
Qasim A. Marzani
E-mail: qasim.marzani@su.edu.krd
Article History:
Received: 09/02/2021
Accepted: 01/06/2021
Published: 18/08 /2021

resistance (Wheeler, 1978, Brent and Hollomon, 1995, Ribes et al., 2018). Dedication of other microorganisms antagonist to the pathogen could be an option to reduce the losses and can serve as an alternative to synthetic fungicides. In this regard, Ng et al. (1997) explored the efficacy of a naturally occurring ballistospore-forming yeast, *Tilletiopsis pallescens*, isolated from mildew-infected leaves as a bioagent against rose powdery mildew pathogen. The results from the study demonstrated the potential ability of the bioagent for biocontrol of the disease. Commercial products of *Trichoderma harzianum* have been used against grapevine foliar pathogen, *Botrytis cinerea* (O'neill et al., 1996), and in commercial greenhouses for the control of tomato and cucumber diseases (Elad and Shtienberg, 2000). In addition, potential *Trichoderma* isolates used for control of grape powdery mildew disease reduced the disease by 53.4 % (Sawant et al., 2017), squash powdery mildew (Hafez et al., 2018), and mulberry powdery mildew (Manjunatha et al., 2020).

Exploring and adopting other rational strategies as alternatives to chemicals are of imperative demand. Plant extracts may play as another alternative to synthetic chemicals and could be useful in avoiding unwanted effects of fungicides. Furthermore, plant-based compounds are natural in origin, have minimum adverse effects on the physiological processes of plants, and are easily convertible into common eco-friendly organic materials (Gnanamanickam, 2002). The antimicrobial efficacy of plant extracts, both *in vitro* and *in planta*, are as promising antifungal compounds against plant diseases (Saleem et al., 2012, Varo et al., 2017). Plants are considered the main sources of secondary metabolites, contain substances that have important antifungal bioactivities which include essential oils (EOs), phenolic compounds, flavonoids, and alkaloids among others (Fawzi et al., 2009, Mar et al., 2010, Romanazzi et al., 2012, Zaker, 2016).

Many natural products of plants have been reported to have antifungal efficacy in controlling fungal plant pathogens, for instance, extracts of neem, eucalyptus, datura, garlic, oleander, and many other plants had been used (Ćosić et al., 2010, NAShwA and Abo-ElyouSr, 2013). Grapefruit extract was investigated to control rose powdery mildew in which promising results were obtained (Wojdyła, 2001). Volatile compounds of garlic (*Allium sativum*) cloves, onion (*Allium cepa*) bulbs, and ginger (*Zingiber officinale*) rhizome volatile found to show complete inhibition of conidia germination of *Erysiphe polygoni* (Singh, 1981, Khunt et al., 2017). Compounds derived from garlic (*Allium sativum*), protected plants against *Sphaerotheca pannosa* var. rosae and *S. fuliginea*, the cause of powdery mildew of rose and cucumber, respectively (Kumar and Chandel, 2018b, Abd Elwahed et al., 2019). Phytoextracts of garlic cloves tested *in vitro* also showed more than 50% inhibitory effect on conidia germination of *Erysiphe cichoracearum*, the cause of okra powdery mildew (Jadav and Kadvani, 2019).

Keeping in view these adverse consequences of fungicides and increasing international demand to reduce the use of toxic pesticides, because of human health and environmental hazards, the present study has been undertaken to investigate the potential efficiency of plant extracts and exploiting the potential of biological control agents as eco-friendly and sound methods for the management of rose powdery mildew.

2.MATERIALS AND METHODS

2.1Preparation of plant extracts

Extracts of 13 plant species listed in table 1 were prepared following the method used by Narayana et al. (1994). Aqueous plant extracts were prepared by taking 200g fresh parts (leaves, peel, bulb, stem, root) of each plant material, washed with sterilized distilled water, and then dried by using an electric oven at 45^{o}C for one week. The dried plants ground into a fine powder using a stainless-steel grinder, placed in Erlenmeyer flasks contained 200 mL of sterilized distilled water and were then placed in a shaker for 24 hours. The material was homogenized for 5 min by a magnetic stirrer and then filtered through double-layered muslin cloth then followed by further filtration using Whatman's filter paper No.1. The extracts were concentrated by evaporation using a rotary vacuum evaporator at 40^{o} C by utilizing a water bath until dense

powder-like material was prepared. The dried extract of the total plant extracts contents, which was considered as standard stock, was placed in a refrigerator for later use.

2.2In vitro assessment

Conidia germination of *P. pannosa* was evaluated following the method described by Sadasiva and Ellingboe (1962). According to the procedure, visible powdery mildew conidia were harvested from young leaves of rose plants. To avoid the presence of old conidia, lesions were gently shaken first by a glass rod to discard any old conidia presented on such young leaves. The young conidia, which formed on conidiophores after four to six hours, were spread on dry clean glass slides previously received 0.1 ml of each one of the previously prepared plant extracts (Table 1) with the concentration of 20 % (w/v). To choose the suitable concentration for *in vitro* assays, preliminary tests were conducted using a 10-fold serial dilution constitutes 1, 10, 20, and 30 mg mL^{-1}. Glass slides prepared with sterilized distilled water only, were served as control treatment. The conidia were examined microscopically to determine the uniformity of distribution and the number of spores that had germinated in Situ. This percentage was used as a correction factor to determine the actual conidial germination. Each slide was placed on a U-shaped glass rod in a moist chamber made up of a sterile Petri plate lined with filter paper saturated with sterile distilled water. Petri plates were incubated at 25^{o}C for 24 hours after which the conidia germination on slides was examined at 400×. Five slides were used as replicates for each particular treatment. The percentage of germination and inhibition was calculated according to the following formula:

$$\text{Germination (\%)} = \frac{\text{GC}}{\text{TC}} * 100$$

Where: GC = germinated conidia, and TC = total number of measured conidia

Germination inhibition (%) = 100 – Percentage of germination

The experiment was a complete randomized design (CRD) with 5 replicates.

Table 1: Plant extracts screened for the *in vitro* efficacy against conidia growth of *P. pannosa*.

Common name	Scientific name	Family	Plant part
Rosemary	*Rosmarinus officinalis*	Lamiaceae	Leaf
Mint	*Mentha asiatica*	Lamiaceae	Leaf
Aloevera	*Aloe vera*	Asphodelaceae	Leaf
Whitetop	*Lepidium draba* L.	Brassicaceae	Stem
Eucalyptus	*Eucalyptus globulus*	Myrtaceae	Leaf
Pomegranate (sour)	*Punica granatum*	Lythraceae	Peel
Burdock	Arctium lappa	Asteraceae	Stem
Turmeric	*Curcuma longa* L.	Zingiberacea	Roots
Mandarin	*Citrus reticulata*	Rutaceae	Peel
Dodonia	*Dodonaea viscosa*	Sapindaceae	Leaf
Datura	*Datura stramonium*	Solanaceae	Leaf
Garlic	*Allium sativum*	Amaryllidaceae	Bulb
Ginger	*Zingiber officinale*	Zingiberaceae	Tuber

2.3Greenhouse experiments

Based on the results of *in vitro* assay, Rosemary, Ginger, and Garlic extracts (10 mg mL^{-1}) which showed the highest efficiency were selected for *in planta* assessment in a greenhouse. The commercial product of *Tricoderma harzianum*, Biocont-T (Dr. Rajan Laboratories, Tamil Nadu, India) at a rate of 4g L^{-1} to give a final concentration of 10^7 spore mL^{-1} (Carillo et al., 2020) and Nazole, a triazole fungicide (Propiconazole 25 EC, Syngenta, Switzerland), in the rate of 20 mL 100 mL^{-1}, were also included in the assay for comparison purposes. Two sets of one-year-old plants (roses and miniature roses), grown in pots, were spray inoculated with conidia suspension, prepared instantly from infected rose plants with powdery mildew, adjusted to 1×10^5 conidia mL^{-1} using Haemocytometer (improved Neubauer chamber, Germany). The negative controls received sterilized water only. Three plants of dog rose (*Rosa canina*), commonly known as Nasrin, were also received the inoculum and placed with other treatments as an additional control for comparisons. After the first initiation of mildew symptoms, the curative application of the treatments was applied by spraying the inoculated plants until run off with the aqueous suspension of the selected plant extracts, the spore suspension of the bioagent, *T. harzianum*, and Nazole fungicide. The plants were then placed in a plastic house provided with 90 – 100 % relative humidity (RH). After 8 days, the powdery mildew disease was assessed by measuring the disease severity on 5-6 randomly selected leaves of each plant. The disease severity index (DSI), based on white powder area on leaves, was used as criteria for disease assessment depending on the disease scale classes of 0 - 5 (Biswas et al., 1992). Where: 0 = no powdery mildew observed, 1 = 1 - 20 % of the leaf area infected, 2 = 21 - 40 % of the leaf area infected, 3 = 41 – 60 % of the leaf area infected, 4 = 61 - 80 % of the leaf area infected, 5 = 81 - 100 % of the leaf area infected.

The efficiency of the treatments was calculated according to the following formula:

$$\text{Efficiency } (\%) = \frac{\text{DC}}{\text{DT}} * 100$$

Where: DC = disease of untreated control, and DT = disease at each treatment.

2.4 Data analysis

All data were analyzed using general analysis of variance (ANOVA) and for comparisons, multiple range tests using the least significant difference (P=0.05) were made using StatGraphics Centurion software.

3.RESULTS AND DISCUSSIONS

3.1In vitro assessment

The discrimination test of thirteen plant extracts (PE) was conducted and assessed *in vitro*. The results in Figure 1 exhibits significant ($P < 0.05$) differences between the treatments. Both garlic and ginger were the most efficient PE that showed significant differences with other treatments in which the least conidia growth was noticed (14.6 and 15.5 %, respectively), followed by rosemary and datura, respectively. Other PEs were showed variable influences on conidia germination. Garlic and ginger extracts were also showed the highest inhibitory effects on conidia germination (Figure 2). The discrimination test was to select the most effective plant extracts and use them against rose and miniature rose powdery mildew *in planta*. The plant extracts with the highest inhibitory effects were chosen and decided to select them for *in planta* assessment. Garlic, ginger, and rosemary were reported to be effective against other plant pathogens. For instance, Obagwu and Korsten (2003) found that water and ethanol extracts of garlic at 0.1% v/v were most effective in inhibiting *Penicillium digitatum* and *P. italicum*, the cause of citrus green and blue mold of citrus. The broad-spectrum activity of garlic was also revealed by Curtis et al. (2004) who assessed the extracts, both *in vitro* and *in planta*. They found its efficacy against a range of pathogenic bacteria and several plant pathogenic fungi like *Alternaria brassisicola*, *Botrytis cinerea*, *Plectosphaerella cucumerina*, *Magnaporthe grisea*, and the Oomycete *Phytophthora infestans*. The inhibitory activity of garlic is referred to as the essential oil compounds in which diallyl disulfide, diallyltrisulfide, allicin, ajoene, allylmethyltrisulfide, considered the major components working against plant pathogens (Wang et al., 2019, Fufa, 2019). Ginger extracts

were found to be effective against spoilage pathogens such as *Aspergillus niger*, *Fusarium sambucinum*, *Pythium sulcatum*, and *Rhizopus stolonifera* (Mvuemba et al., 2009), anthracnose of bell pepper fruits (Alves et al., 2015), and several other important plant pathogenic fungi on tomatoes like *Alternaria solani*, and *Pythium ultimum* (Muthomi et al., 2017). It has been proved that the potential activity of ginger extract is from essential oils that are composed of monoterpenes (transcaryophyllene, camphene, geranial, eucalyptol, and neral) and sesquiterpene hydrocarbons (*α*-zingiberene, ar-curcumene, *β*-bisabolene, and *β*-sesquiphellandrene). The mode of action of these essential oils that affects both the pathogen cell's external envelope and internal structures, made them have a wide range of activities against many phytopathogens (Abdullahi et al., 2020). The antifungal activity of rosemary against plant pathogenic fungi was also evaluated by other researchers. Ribeiro et al. (2016) assessed the potential of the rosemary extract for controlling charcoal rot, *Macrophomina phaseolina*, in soybean and found to reduce the fungal growth on solid and liquid media by 44% and 74%, respectively, and the number of microsclerotia by 61%. There was a disease inhibition of 53% and 56% in the area under the disease progress curve in the first and in second assay, respectively.

It seems that the essential oils (EOs), extracted from *Allium sativum* (garlic) and *Rosmarinus officinalis* (rosemary), the most active components of the extracts. In contact and vapor assays (two *in vitro* tests that measure the minimal inhibitory concentration), Hosseini et al. (2020) found that both *A. sativum* and *R. officinalis* EOs significantly inhibited the mycelial growth and conidial germination of *Colletotrichum nymphaeae*, the cause of strawberry anthracnose. Furthermore, the EC_{50} assay indicated that garlic EO was more effective than rosemary EO against the pathogen.

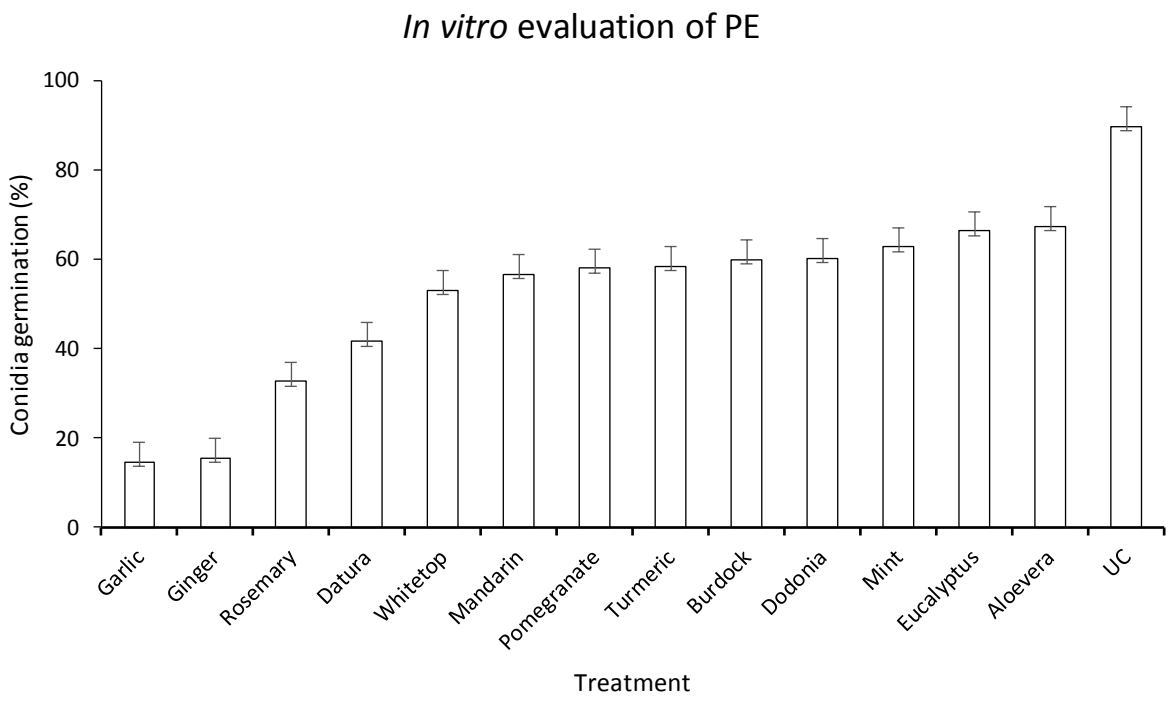

Figure 1: *in vitro* assessment of the efficacy of 13 PEs on conidia germination of *P. pannosa*.

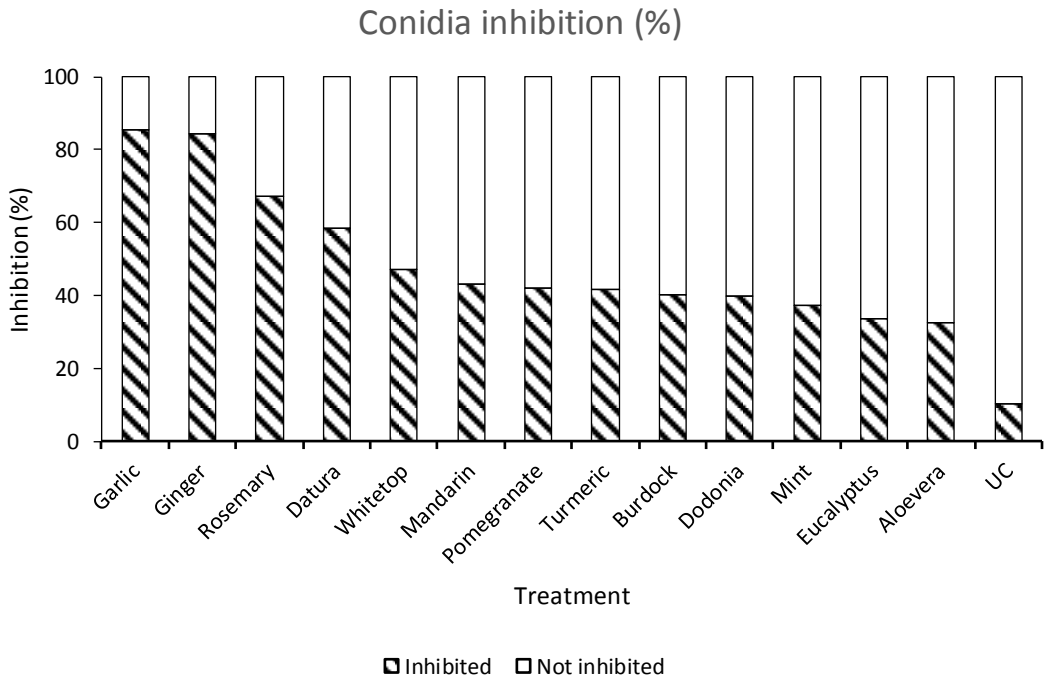

Figure 2: *in vitro* assessment of 13 PEs on % of conidia growth inhibition of *P. pannosa*.

3.2Greenhouse experiments

The results of the application of the selected plant extracts, the bioagent (*Trichoderma harzianum*) and the fungicide (Nazole), used in greenhouses, showed significant differences in DSI on roses ($P < 0.05$) and miniature roses. The results revealed that garlic, ginger, and Biocont were as effective as the Nazole fungicide, in which they retained the lowest DSI with no significant differences between them (Figure 5). However, in terms of efficiency, after the fungicide, garlic was the most efficient plant extract in reducing powdery mildew on miniature roses, followed by the bioagent (Biocont) and then ginger extract which have the efficiencies of 88.1, 86.8, and 86.5 %, respectively. Rosemary, however, didn't exhibit such good effectiveness in inhibiting the disease (Figure 6). On Roses, both garlic and ginger were the most efficient plant extracts with DSI of 7.3 and 7.5 %, respectively, in which they have not differed significantly with Nazole fungicide (6.7%). However, Rosemary extract showed less effect with DSI of 8.8% (Figure 3) and efficiency of 76.1% (Figure 4). Garlic and ginger also showed a significant efficiency in disease reduction by 86.2 and 84.2%, respectively with no significant differences with Nazole fungicide. Therefore, Nazole as a synthetic fungicide was outperformed in the efficiency which inhibited the disease by 89 %, followed by garlic and ginger with the efficiencies of 86 and 84 %, respectively (Figure 4). Nasrin plants, which were placed as an additional control for comparison, compared to roses were, showed comparatively low DSI (12%) and disease efficiency of 11.2% (Figure 3 and 4). On miniature roses, similar results were obtained in which garlic and ginger outperformed other plant extracts in both DSI and efficiency (Figures 5 and 6).

Previous studies also showed the efficacy of both garlic and ginger on *Colletotrichum nymphaeae*, the cause of strawberry anthracnose under greenhouse conditions; in which they significantly reduced the development of fruit decay and anthracnose disease incidence and severity (Hosseini et al., 2020). In an accordance with our results, Tahir et al. (2018) noticed a significant reduction of bitter melon (*Momordica charantia*), a cucurbit plant, powdery mildew

(*Sphaerntheca fuliginea*) incidence by garlic extracts, used at 5%, 10%, and 15% concentrations. Ginger was also outperformed plant extracts in the reduction of mulberry powdery mildew (*Phyllactinia corylea*) in which it reduced the disease to 60.31% (Manjunatha et al., 2020).

The antagonistic fungus, *Trichoderma harzianum* retained significant control capability *in planta* and was successful in reducing DSI and increases in disease inhibition percentage. On Roses, *Trichoderma* showed a significant disease reduction expressed as DSI (8.87%) and efficiency (75.7%) which has not differed significantly from that of ginger and rosemary plant extracts (Figure 3 and 4). On miniature rose, the bioagent, *Trichoderma*, not differed significantly in both DSI (7.3%) and disease inhibition (86.8%) with Nazole fungicide and the foremost plant extracts, ginger and garlic (Figure 5 and 6). Species of *Trichoderma* have been used against a wide range of plant pathogenic fungi including powdery mildew fungi. Several previous studies have revealed the capability of *Trichoderma* species in reducing powdery mildew disease on roses and other different plant species. On greenhouse cucumber, powdery mildew (*Podosphaera fuliginea* also known as *Podosphaera xanthii)*) reduction up to 97 % was achieved on young leaves by the commercial product of *T. harzianum*, TRICHODEX (Elad et al., 1998). Similar to our finding, Picton and Hummer (2003) stated that the incidence and the severity of gooseberry powdery mildew on young leaves and stems were reduced significantly by *T. harzianum* combined with mineral oils when applied to plants in 2-week intervals in potted plants in the greenhouse. Additionally, its ability in disease reduction was as good as Thiophanate fungicide used in the trial, enabling it to be a commercially acceptable product. The commercial formulations of the bioagent, either in the organic or inorganic carriers, have been used for seed treatment, seed bio-priming, seedling dip, soil application, and foliar spray for the management of plant diseases.

The mechanism of mycoparasitism of *T. harzianum* involves nutrient competition, hyperparasitism, antibiosis, space and cell wall degrading enzymes (Chet et al., 1997, Ghorbanpour et al., 2018).

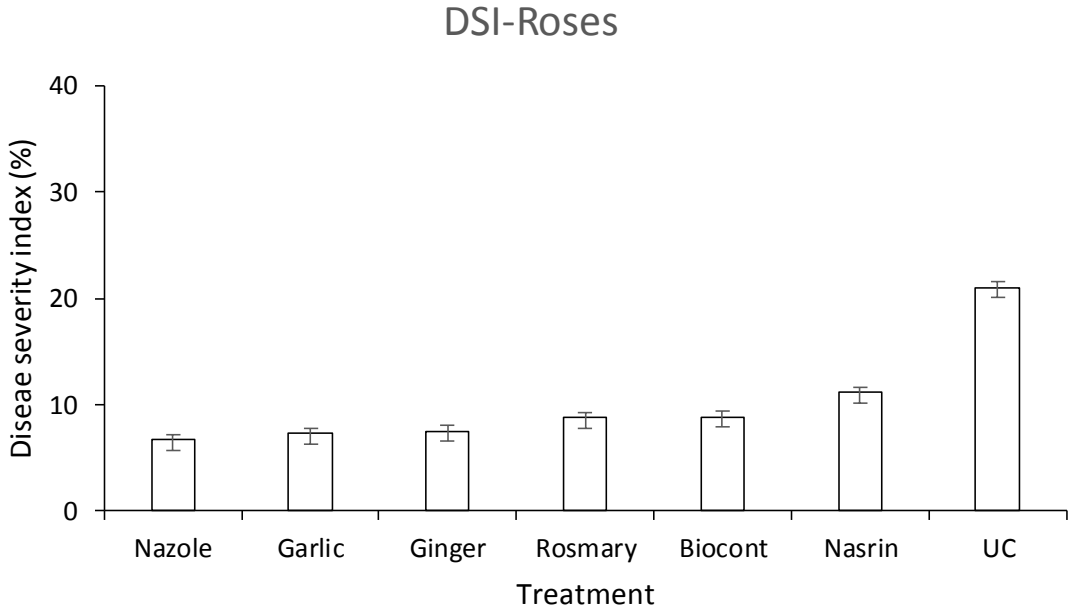

Figure 3: *in planta* activity of 3 selected plant extracts, one bioagent, and a synthetic fungicide on DSI of rose powdery mildew.

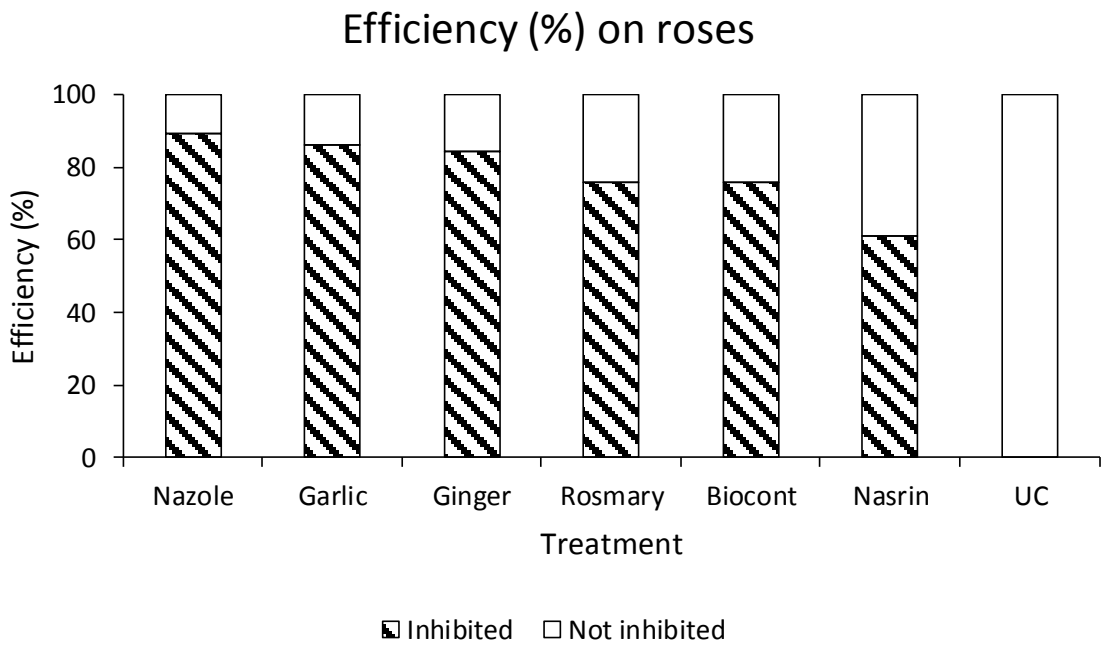

Figure 4: *in planta* efficiency of 3 selected plant extracts, one bioagent, and a synthetic fungicide on rose powdery mildew.

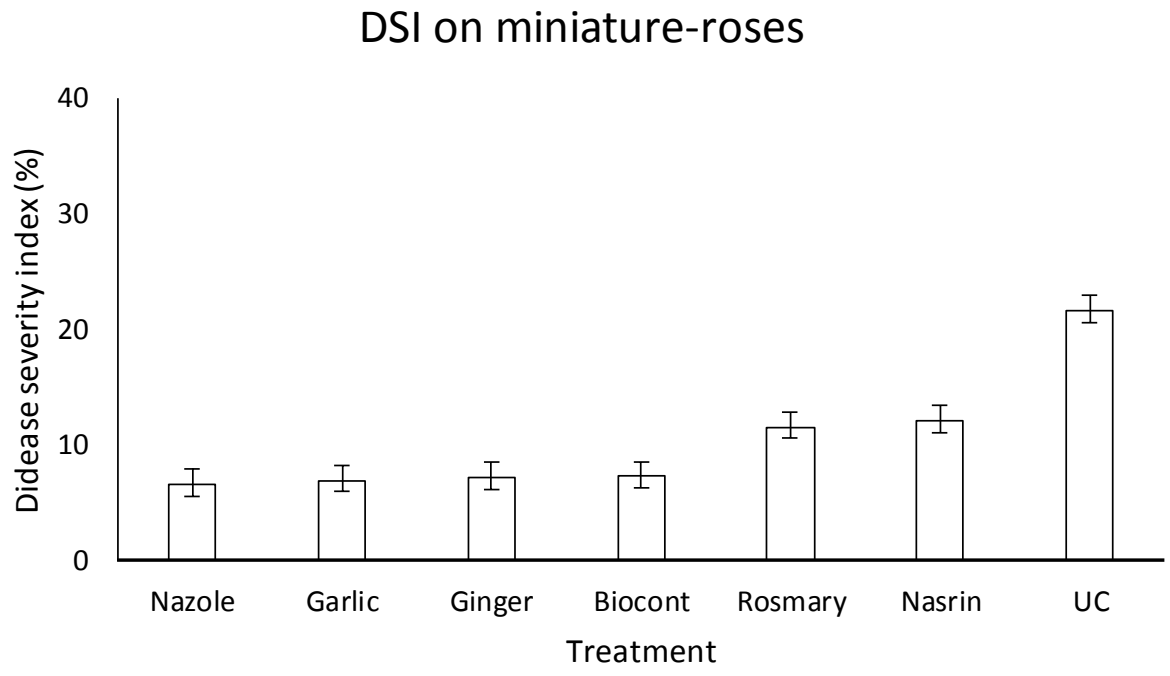

Figure 5: *in planta* activity of 3 selected plant extracts, one bioagent, and a synthetic fungicide on DSI of miniature-rose powdery mildew.

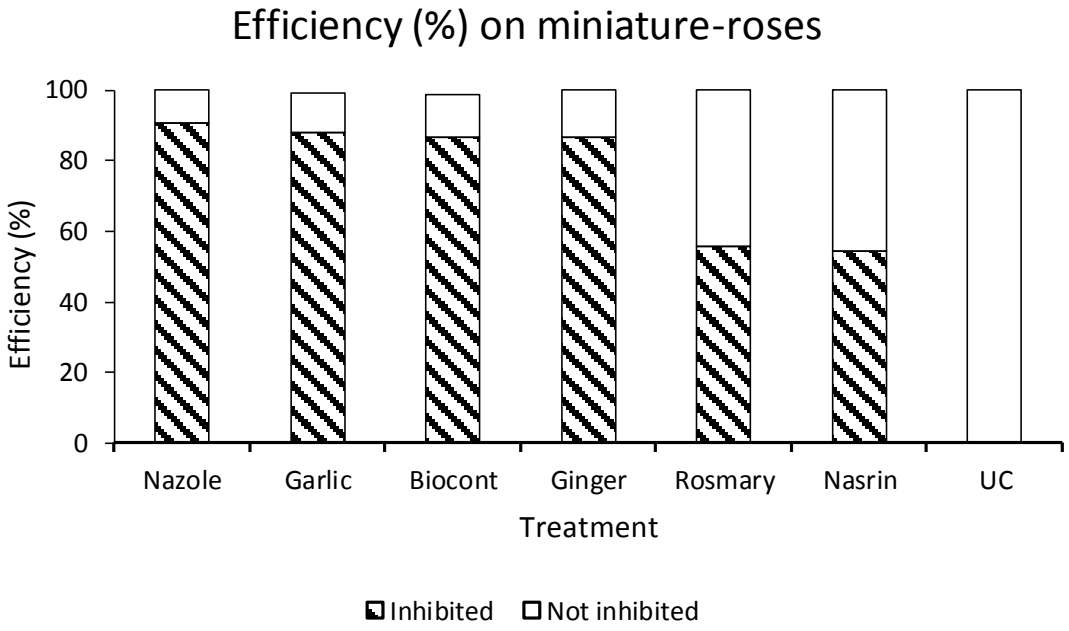

Figure 6: *in planta* efficiency of 3 selected plant extracts, one bioagent, and a synthetic fungicide on miniature-rose powdery mildew.

4.CONCLUSIONS

In conclusion, plant extracts as biofungicides, may work efficiently against a range of fungal pathogens including powdery mildew fungi. This work found that extracts of garlic, ginger, and rosemary are the most efficient plants that contain components that work as an antifungal against rose and miniature rose powdery mildew. The fungal bioagent, *T. harzianum*, on the other hand, also works effectively in disease reduction. Both plant extracts and the bioagent could be used as ecofriendly approaches to combat plant powdery mildew and play as alternatives to the deleterious impacts of synthetic inorganic chemicals. It is also concluded that dog rose (*Rosa canina*), commonly known as Nasrin, were generally less sensitive to rose powdery mildew.

REFERENCES

ABD ELWAHED, M. S., MAHDY, H. A., EL-SAEID, H. M. & ABOUZIENA, H. F. 2019. Effect of some bio-regulators on yield quantity and quality of garlic plants (Allium Sativum L.). *Middle East Journal of Applied Sciences,* 9**,** 17-24.

ABDULLAHI, A., AHMAD, K., ISMAIL, I. S., ASIB, N., AHMED, O. H., ABUBAKAR, A. I., SIDDIQUI, Y. & ISMAIL, M. R. 2020. Potential of Using Ginger Essential Oils-Based Nanotechnology to Control Tropical Plant Diseases. *The plant pathology journal,* 36**,** 515.

AGRIOS, G. N. 2005. Plant diseases caused by fungi. *Plant pathology*. Elsevier academic press, Amsterdam. pp451-452.

ALVES, K. F., LARANJEIRA, D., CÂMARA, M. P., CÂMARA, C. A. & MICHEREFF, S. J. 2015. Efficacy of plant extracts for anthracnose control in bell pepper fruits under controlled conditions. *Horticultura Brasileira,* 33**,** 332-338.

BÉLANGER, R., LABBÉ, C. & JARVIS, W. 1994. Commercial-scale control of rose powdery mildew with a fungal antagonist. *Plant Disease,* 78**,** 420-424.

BISWAS, S., TEOTIA, R. & MANIL, S. 1992. Some field observations on the severity of powdery mildew (Phyllactinia corylea) in mulberry. *Indian J. Seric,* 31**,** 67-69.

BRENT, K. J. & HOLLOMON, D. W. 1995. *Fungicide resistance in crop pathogens: how can it be managed?*, Citeseer.

CARILLO, P., WOO, S. L., COMITE, E., EL-NAKHEL, C., ROUPHAEL, Y., FUSCO, G. M., BORZACCHIELLO, A., LANZUISE, S. & VINALE, F. 2020. Application of Trichoderma harzianum, 6-pentyl-α-pyrone and plant biopolymer formulations modulate plant metabolism and fruit quality of plum tomatoes. *Plants,* 9**,** 771.

CHET, I., INBAR, J. & HADAR, I. 1997. Fungal antagonists and mycoparasites. *The mycota IV: environmental and microbial relationships. Springer-Verlag, Berlin***,** 165-184.

ĆOSIĆ, J., VRANDEČIĆ, K., POŠTIĆ, J., JURKOVIĆ, D. & RAVLIĆ, M. 2010. In vitro antifungal activity of

essential oils on growth of phytopathogenic fungi. *Poljoprivreda (Osijek)*, 16**,** 25.

CURTIS, H., NOLL, U., STÖRMANN, J. & SLUSARENKO, A. J. 2004. Broad-spectrum activity of the volatile phytoanticipin allicin in extracts of garlic (Allium sativum L.) against plant pathogenic bacteria, fungi and Oomycetes. *Physiological and molecular plant pathology,* 65**,** 79-89.

ELAD, Y., KIRSHNER, B., YEHUDA, N. & SZTEJNBERG, A. 1998. Management of powdery mildew and gray mold of cucumber by *Trichoderma harzianum* T39 and Ampelomyces quisqualis AQ10. *BioControl,* 43**,** 241-251.

ELAD, Y. & SHTIENBERG, D. 2000. Management of humidity-promoted diseases in non-heated greenhouses by means of fenhexamide, *Trichoderma harzianum* T39 and integrated control according to GREENMAN. *PXanzenschutz-Nachrichen Bayer*.

FAWZI, E., KHALIL, A. & AFIFI, A. 2009. Antifungal effect of some plant extracts on Alternaria alternata and *Fusarium oxysporum*. *African Journal of Biotechnology,* 8.

FÉLIX-GASTÉLUM, R., HERRERA-RODRÍGUEZ, G., MARTÍNEZ-VALENZUELA, C., MALDONADO-MENDOZA, I. E., QUIROZ-FIGUEROA, F. R., BRITO-VEGA, H. & ESPINOSA-MATÍAS, S. 2014. First report of powdery mildew (Podosphaera pannosa) of roses in Sinaloa, Mexico. *Plant Disease,* 98**,** 1442-1442.

FUFA, B. K. 2019. Anti-bacterial and anti-fungal properties of garlic extract (Allium sativum): A review. *Microbiology Research Journal International***,** 1-5.

GHORBANPOUR, M., OMIDVARI, M., ABBASZADEH-DAHAJI, P., OMIDVAR, R. & KARIMAN, K. 2018. Mechanisms underlying the protective effects of beneficial fungi against plant diseases. *Biological Control,* 117**,** 147-157.

GNANAMANICKAM, S. S. 2002. *Biological control of crop diseases*, CRC Press.

HAFEZ, Y. M., EL-NAGAR, A. S., ELZAAWELY, A. A., KAMEL, S. & MASWADA, H. F. 2018. Biological control of *Podosphaera xanthii* the causal agent of squash powdery mildew disease by upregulation of defense-related enzymes. *Egyptian Journal of Biological Pest Control,* 28**,** 1-8.

HOSSEINI, S., AMINI, J., SABA, M. K., KARIMI, K. & PERTOT, I. 2020. Preharvest and Postharvest Application of Garlic and Rosemary Essential Oils for Controlling Anthracnose and Quality Assessment of Strawberry Fruit During Cold Storage. *Frontiers in Microbiology,* 11**,** 1855.

HUMMER, K. E. & JANICK, J. 2009. Rosaceae: taxonomy, economic importance, genomics. *Genetics and genomics of Rosaceae*. Springer.

JADAV, A. & KADVANI, D. 2019. Efficacy of different phytoextracts against *Erysiphe cichoracearum* dc causing powdery mildew of okra. *Journal of Pharmacognosy and Phytochemistry,* 8**,** 538-540.

KHUNT, A., AKBARI, L., BHALIYA, C. & GOSWAMI, G. 2017. Efficacy of Different Phytoextracts against *Erysiphe polygoni* DC Causing Powdery Mildew of Cumin. *Trends in Biosciences,* 10**,** 1096-1098.

KUMAR, V. & CHANDEL, S. 2018a. Effect of epidemiological factors on percent disease index of rose powdery mildew caused by *Podosphaera pannosa* (Wallr.) de Bary. *Journal of Crop and Weed,* 14**,** 137-142.

KUMAR, V. & CHANDEL, S. 2018b. Management of rose powdery mildew (*Podosphaera pannosa*) through ecofriendly approaches. *Indian Phytopathology,* 71**,** 393-397.

MANJUNATHA, S., KUMAR, V. S., RAJEGOWDA, N. & RAJU, M. 2020. Assortment for host resistance and eco-friendly management of mulberry powdery mildew caused by Phyllactinia corylea (Pers.) Karst. *Journal of Pharmacognosy and Phytochemistry,* 9**,** 2159-2162.

MAR, R. J., HASSANI, A., GHOSTA, Y., ABDOLLAHI, A., PIRZAD, A. & SEFIDKON, F. 2010. *Thymus kotschyanus* and *Carum copticum* essential oils as botanical preservatives for table grape. *Journal of Medicinal Plants Research,* 4**,** 2424-2430.

MUTHOMI, J. W., LENGAI, G. M., WAGACHA, M. J. & NARLA, R. D. 2017. In'vitro'activity of plant extracts against some important plant pathogenic fungi of tomato. *Australian Journal of Crop Science,* 11**,** 683.

MVUEMBA, H., GREEN, S., TSOPMO, A. & AVIS, T. 2009. Antimicrobial efficacy of cinnamon, ginger, horseradish and nutmeg extracts against spoilage pathogens. *Phytoprotection,* 90**,** 65-70.

NARAYANA, B., SIVAPRAKAKASAM, M. & JEYARAJAN, R. 1994. Antifungal activity of some plant extracts. *Indian Journal of Forestry,* 17**,** 10-14.

NASHWA, S. M. & ABO-ELYOUSR, K. A. 2013. Evaluation of various plant extracts against the early blight disease of tomato plants under greenhouse and field conditions. *Plant Protection Science,* 48**,** 74-79.

NG, K. K., MACDONALD, L. & PUNJA, Z. K. 1997. Biological control of rose powdery mildew with the antagonist yeast *Tilletiopsis pallescens*. *HortScience,* 32**,** 262-266.

O'NEILL, T., ELAD, Y., SHTIENBERG, D. & COHEN, A. 1996. Control of grapevine grey mould with Trichoderma harzianum T39. *Biocontrol Science and Technology,* 6**,** 139-146.

OBAGWU, J. & KORSTEN, L. 2003. Control of citrus green and blue molds with garlic extracts. *European Journal of Plant Pathology,* 109**,** 221-225.

PHILLIPS, R. & RIX, M. 1988. *The Random House book of roses*, Random House.

PICTON, D. D. & HUMMER, K. E. 2003. Control of powdery mildew on leaves and stems of Gooseberry. *HortTechnology,* 13**,** 365-367.

REX, B. & DEEPIKA, V. 2020. Diseases of Rose and its Management. *Biotica Research Today,* 2**,** 221-222.

RIBEIRO, A., CALEJA, C., BARROS, L., SANTOS-BUELGA, C., BARREIRO, M. F. & FERREIRA,

I. C. 2016. Rosemary extracts in functional foods: extraction, chemical characterization and incorporation of free and microencapsulated forms in cottage cheese. *Food & function,* 7**,** 2185-2196.

RIBES, S., FUENTES, A., TALENS, P. & BARAT, J. M. 2018. Prevention of fungal spoilage in food products using natural compounds: a review. *Critical reviews in food science and nutrition,* 58**,** 2002-2016.

ROMANAZZI, G., LICHTER, A., GABLER, F. M. & SMILANICK, J. L. 2012. Recent advances on the use of natural and safe alternatives to conventional methods to control postharvest gray mold of table grapes. *Postharvest Biology and Technology,* 63**,** 141-147.

SADASIVA, K. R. & ELLINGBOE, A. H. METHOD OF CONTROLLED INOCULATIONS WITH CONIDIOSPORES OF ERYSIPHE-GRAMINIS-VAR-TRITICI. Phytopathology, 1962. AMER PHYTOPATHOLOGICAL SOC 3340 PILOT KNOB ROAD, ST PAUL, MN 55121, 714-&.

SALEEM, A., EL-SAID, A., MOHARRAM, A. & HAMED, A. 2012. Cellulose decomposing fungi and cellulase activity as affected by amistar and moncut fungicides. *African Journal of Microbiology Research,* 6**,** 4457-4470.

SANGANI, M., LFAKBARI, S. & SHEKHDA, M. 2018. Investigation on different systemic fungicides against *Leveillula taurica* causing powdery mildew of cluster bean in vitro. *IJCS,* 6**,** 2339-2341.

SAWANT, I. S., WADKAR, P. N., GHULE, S. B., RAJGURU, Y. R., SALUNKHE, V. P. & SAWANT, S. D. 2017. Enhanced biological control of powdery mildew in vineyards by integrating a strain of *Trichoderma harzianum* with sulphur. *Biological Control,* 114**,** 133-143.

SINGH, H. 1981. Effect of volatiles of some plant extracts and their oils on conidia of Erysiphe polygoni DC.

TAHIR, A., SATTAR, S., SAIF, R., TAHIR, S., QADIR, M. & SULTANA, R. 2018. Biological control of powdery mildew of bitter gourd. *International Journal of Biological Research,* 1**,** 66-98.

VARO, A., MULERO-APARICIO, A., ADEM, M., ROCA, L., RAYA-ORTEGA, M., LÓPEZ-ESCUDERO, F. & TRAPERO, A. 2017. Screening water extracts and essential oils from Mediterranean plants against Verticillium dahliae in olive. *Crop Protection,* 92**,** 168-175.

WANG, Y., WEI, K., HAN, X., ZHAO, D., ZHENG, Y., CHAO, J., GOU, J., KONG, F. & ZHANG, C.-S. 2019. The antifungal effect of garlic essential oil on Phytophthora nicotianae and the inhibitory component Involved. *Biomolecules,* 9**,** 632.

WHEELER, B. 1978. Powdery mildews of ornamentals. *The powdery mildews***,** 411-445.

WOJDYŁA, A. 2001. Grapefruit extract activity in the control of rose powdery mildew and black spot. *Mededelingen (Rijksuniversiteit te Gent. Fakulteit van de Landbouwkundige en Toegepaste Biologische Wetenschappen),* 66**,** 167-177.

ZAKER, M. 2016. Natural plant products as eco-friendly fungicides for plant diseases control-A Review. *The Agriculturists,* 14**,** 134-141.

ZANCO Journal of Pure and Applied Sciences
The official scientific journal of Salahaddin University-Erbil
https://zancojournals.su.edu.krd/index.php/JPAS

ISSN (print):2218-0230**, ISSN (online):** 2412-3986**, DOI: http://dx.doi.org/10.21271/zjpas**

RESEARCH PAPER

Use of Isotope Technique in Groundwater Investigation around Erbil City- Northern Iraq

Dana K. Mawlood[1], Bruska S. Mamand[2]
[1]Department of Civil Engineering, College of Engineering, Salahaddin University- Erbil, Kurdistan Region, Iraq
[2]Department of Water Resources Engineering, College of Engineering, Salahaddin University- Erbil, Kurdistan Region, Iraq

A B S T R A C T:
The fundamental characteristics of environmental isotopes in water resources management is dependable on the nature of geographical region of the catchment boundaries. The method of applying different isotopes has a main character in quantity and quality estimations of water resources that sometimes cannot be achieved by old techniques. Nowadays the detailed inquiry of surface water or groundwater difficulties can practically have been explained against the support of performing the isotopes. In this study, the environmental isotopes were measured and are used to predict the residence time (age) of groundwater in the areas around Erbil city in Kurdistan region- Iraq. Or to predict some of ground water characteristics. A total of 22 (10 wells and 12 springs) samples of water were taken at different places starting from Haji-Omran to Barzan. The samples collected through a glass bottles and covered to prevent the evaporation then transported to the laboratory in Vienna for the purpose of measuring the isotope contents in water molecule. The results show that, groundwater saves the ^{18}O and deuterium (D) content out of which they were formed. The isotope content includes high degree in deuterium surplus (d) is about 20‰ which is representative for the areas having high elevation. also, the high concentration of isotopes was taken place at Haji-Omran and Jundian w that about 8.93 and 8.37 degrees respectively. The water in the well from Per-Daud has a ^{3}H content of 0.8 TU which means that is an old water and its age is more than 40 years. Whereas, the tritium content of water taken from Haji-Omran was 13.4 TU that can be accounted as young water due to quickly recharge rate and the effects of precipitation at this location.

KEY WORDS: Isotope technique, Groundwater dating, Erbil city.
DOI: http://dx.doi.org/10.21271/ZJPAS.33.4.11
ZJPAS (2021), 33(4);111-116.

1. INTRODUCTION:

An isotope has exerting a great force in the field of engineering hydrology based on the natural water cycle. The environmental isotope either related to natural (stable isotopes) or they are artificial and unstable (radioactive isotopes). Water molecules carry unequaled isotopic fingerprints, based in part on differing ratios of the oxygen and hydrogen isotopes that establish the water molecule. isotopes include ^{1}H which is common hydrogen having only one proton,^{2}H which is deuterium (D) which is heavy stable hydrogen and produced from addition of one and two neutrons. The frequent isotopes processed in hydrology are the natural isotopes of the water molecule (^{1}H, ^{2}H, ^{16}O, and ^{18}O). Other stable isotopes, such as ^{13}C and ^{15}N were greatly applied to find origination of water pollution, recharge rate and recharge mechanism, determination of flow velocity and its direction, separation of groundwater flow and baseflow with stream flow, the interconnections between aquifers, some aquifer characteristics and source of salinity.

Natural isotopes have applicability in many fields used for solving several problems in the environment. This means that this technique is not bounded only to engineering hydrology but also apply to other areas such as meteorology, oceanography, archaeology, animal migration, forensic and health studies.

2. LITERATURE REVIEW:

* **Corresponding Author:**
Bruska Sardar Mamand
E-mail: bruska.mamand@su.edu.krd
Article History:
Received: 23/01/2021
Accepted: 28/04/2021
Published: 18/08 /2021`

2.1 Modifications of tritium (T) and oxygen-18 of different types of precipitation in Czechoslovakia:

Dencer and Martinic,1965 studied the variation of tritium (T) and oxygen-18 in precipitation, snowmelt and snowpack during the winter in a small mountain basin in northern Czechoslovakia. The results show that a significant altitude effect exists for oxygen-18 when the precipitation is not in the solid form. Evolution of the isotopic composition of the snowpack reflects the movement of water resulting from melted snow in the snowpack and its relation to the thermal conditions in the snowpack.

2.2 Distribution of deuterium (D) isotope in Canadian waters:

Brown,1970 investigated on the distribution of hydrogen isotope (especially deuterium) in Canadian waters like precipitation and surface water. In this investigation, the change in concentration of deuterium (D) and tritium (T) was determined. High concentration of deuterium and low concentration of tritium taken place near the land along the sea which absorb the first condensate from oceanic vapour due to reduction in temperature, recycle of surface water by evaporation, and resumed the involvement of atmospheric tritium. Storm-to-storm fluctuations in isotope content of precipitation at Ottawa reflect a variability in the origin of precipitating moisture. Seasonal variation of tritium, due to late spring feed-in from the stratosphere, has been particularly prominent and regular at Canadian latitudes. Declining annual peak concentrations since 1963 indicate depletion of the stratospheric reservoir with a half-time of 1.2 years.

2.3 Dating of young groundwater:

Plummer, 2003 In America investigated that the age of young groundwater is depends on the time elapse since recharge and the groundwater concentration, while different methods achieved that the age of young groundwater is ranged between (0-50 years). Base on this investigation the groundwater dating is related to three main processes:

a. Initial concentration of the radionuclide is recreated from the measured concentrations of the parent and daughter isotopes and then the groundwater age is illustrated from the decay equation.
b. Initial concentration of the radionuclide loaded again to the aquifer, and then the dating of groundwater is estimated from the measured concentration.
c. Age information is reasoning the atmospheric input function of an anthropogenic gas, its capability to soluble in water, and the measured concentration in the water sample.

Each technique has advantages and limitations therefore, a multi-tracer concept is proposed.

2.4 Radiocarbon dating of old groundwater:

Geyh, 2003 in Germany explained that, ^{14}C is the method that recognized to dating of groundwater based on estimations of geo-hydraulic characteristics of aquifers and aquitards. In aired and semi-aired zones, the age of groundwater changes due to renewability and non-renewability of its source.

2.5 Compound specific stable isotope analysis:

Lollar et. al., 2007 Charecterized the compound stable isotopes to evaluation the contamination dissolved in groundwater. The multi-isotopes of carbon and hydrogen was used and the results of this study found that stable isotope identified the source of contamination in groundwater.

2.6 Groundwater management strategies under semi-aired area in Morocco:

Mohammed et. al., 2015 investigated the groundwater under semi-aired catchment for the wadi ouazzi basin in morocco city. Results of isotope content in water molecule illustrates that there is low evaporation of precipitation during the infiltration process. Tritium value in the groundwater of the Ouazzi Basin are below 1.5 tritium unit (<1.5 TU).

2.7 Use of radioactive tritium (^{3}H) and radiocarbon (^{14}C) isotope hydrology in water resources:

Samie et. al., 2018 used the radioactive tritium (^{3}H) and radiocarbon (^{14}C) as a dating tools to determine the age of groundwater, residence time, and thus refreshing the groundwater. Isotope tracers in catchment analysis known as tracing concept such as chlorofluorocarbons, Freon (CFCs) and Sulfur hexafluoride (SF6), are used for dating young groundwater, whereas noble gases ($T/^{3}He$) are used for determining the age and the water temperature during groundwater recharge, and consequently mean elevation of groundwater recharge.

2.8 Futuristic isotope hydrology in the Gulf region:

Kumar and Hadi, 2018, used the isotope technique in applications of groundwater management at Arabian Gulf region. this investigation focused on the evaluation of aquifer storage and recharge with its recovery system. The results explained that in this region the quantity of groundwater includes the hydrocarbon pollution and the solute movement of water was in unsaturated zone.

3. METHODOLOGY OF THE STUDY:

The mass spectrometer is an analytical method used for measuring mass to charge ratio of ions, the spectra are used to find an isotopic fingerprint of each sample were taken. The details of this test are that the groundwater sample molecules break up t the positively charged ions or without ions. Then the ions will separate based on their mass to charge ratio that becomes a spectrum of the signal intensity of detected ions as a function of the mass-to-charge ratio. For the aim of this investigation, samples of groundwater between July 30th 2001 and August 24th 2001, 22 from springs and wells from the northern Iraq (Erbil city) were drawn by (Dana, 2003), to make ^{2}H, ^{3}H and ^{18}O measurements. The isotopic composition of water, determined by mass spectrometry device as explained earlier, it is expressed in per mil (‰) deviations from the standard mean ocean water (SMOW).

3.1 Sampling points:

Natural springs are usually ideal sites for drawing samples of groundwater and its dissolved components representing a continuous outflow. One must be careful and make sure that the sample was drawn as close to the spring discharge as possible in order to minimize the effects of atmospheric pollution and decarburization. Drill mixture can be deposited on the walls of the well or it can penetrate the aquifer due to hydraulic pressure. The zone from where the samples drawn was defined and the contingents from other zones excluded then wells rinsed thoroughly before drawing the samples.

a. Isotope analysis:

As shown in table 1, Samples at different locations taken for analysis of Deuterium (D) ^{2}H and ^{18}O is proportionality simple because none of two isotopes measured for chemical and biological processes. During the sampling, the evaporation caused by permeable bottle caps or by partly filled bottles were prevented because it could represent problem when the heavy isotopes can be enriched in the residual water. Also, the samples containing elusive organic components was marked and pre-treated in the laboratory because gasses made a problem during the mass spectrometry measurement. The volume of 100 ml (minimum 10 ml) was taken through a glass bottle that tightly closed to avoid evaporation as explained earlier the isotopes of Deuterium (D) and ^{18}O identified with isotope ration mass spectrometer. The samples drawn for tritium (^{3}H) measurements in the direct analysis method one can use 50-125 ml (50 ml is taken for this investigation) bottle for all three isotope determinations without being the need of filter method or any special conservation method. Whereas, in electrolytic enrichment method usually 1 liter is necessary.

Table 1: Summary of the sampling points for isotope measuring data within the time interval between July 30th 2001 and August 24th 2001.

No	Location	Type	Water Level (m)	Date	Altitude (m)	$\delta^{2}H$ ‰	$\delta^{18}O$ ‰	^{3}H (TU)
1	Haji-Omran	Spring	-	17.08.2001	1673	-51.1	-8.93	13.4
2	Rayat	Spring	-	17.08.2001	1480	-45.8	-8.11	8.6
3	Chuman	Spring	-	17.08.2001	1140	-44.2	-7.82	9.3
4	Rezanok	Spring	-	17.08.2001	750	-40.9	-7.34	9.5
5	Piera-sawed	Spring	-	17.08.2001	1050	44.6	-7.98	11.7
6	Jundijan	Wells	8-15	17.08.2001	570	-47.4	-8.37	10.8
7	Diana	Spring	-	17.08.2001	720	-44.6	-7.79	12.8
8	Gali-Ali-Bag	Spring	-	17.08.2001	670	-43.8	-8.01	9.1
9	Bekhal	Spring1	-	17.08.2001	640	-44.5	-7.98	10.7
10	Bekhal	Spring2	-	17.08.2001	644	-43.8	-7.99	11.0
11	Harir	Spring	-	17.08.2001	740	-39.9	-7.28	10.2
12	Mirawa	Wells	19-22	17.08.2001	775	-31.7	-5.79	7.4
13	Betrma	Wells	65-70	24.08.2001	845	-37.9	-7.15	13.9
14	Shaqlawa	Wells	60-70	24.08.2001	840	-39.0	-7.28	12.0
15	Kawanjan	Wells	50-60	24.08.2001	950	-36.8	-6.85	10.8
16	Hirjan	Spring	-	24.08.2001	840	-36.8	-6.87	12.8
17	Kore	Wells	19-22	24.08.2001	600	-36.8	-6.83	6.8
18	Malla-Omar	Wells	15-20	24.08.2001	550	-33.2	-5.93	3.5
19	Per-Daud	Wells	30	24.08.2001	400	-29.5	-5.28	0.8
20	Kasnazan	Wells	15-20	30.07.2001	420	-29.1	-5.17	4.9
21	Bila	Wells	30-40	30.07.2001	700	-38.4	-7.27	11.2
22	Barzan	Spring	-	30.07.2001	720	-39.0	-7.30	9.9

Where:

- □: the value of isotope content, referred to a standard.
- □ ^{18}O: □ value calculated from the oxygen isotope ration ($^{18}O/^{16}O$) and referred to Vienna V-SMOW standard. The absolute isotope ratio ($^{18}O/^{16}O$) ranges from 1:490 to 1:530.
- V-SMOW: Vienna Standard Mean Ocean Water, isotope standard for the determination of both □ ^{18}O and □ ^{2}H values of water and ice. It is submitted by IAEA (international atomic

energy agency in Vienna).

- $\delta\ ^{2}H$: δ value calculated from the hydrogen isotope ration ($^{2}H/^{1}H$) and referred to Vienna V-SMOW standard. The stable isotope ^{2}H is also named as Deuterium (D). The absolute isotope ratio ($^{2}H/^{1}H$) in groundwater ranges from 1:5800 to 1:10000.
- ^{3}H: is the tritium isotope and also named as (T).
- TU: is the tritium unit. 1 TU= 1 tritium atom per 10^{18} hydrogen atoms.

3.3 Transporting the samples to the laboratory:

The samples were transported to the (Arzinal) laboratory in Vienna/Namsa inside the suitable bottles. All samples from the province Erbil were drawn by trustworthy persons, Unfortunately, due to the political situation within this study, it had been impractical to personally access the sampling points of the springs and there is also no hydrological information about the sampled springs within the available technical literature. The subsequent description of the sampling points will therefore be considered provisional, and must be completed for further research by exact interpretation of the isotopic data.

4. Results and discussion:

4.1 Calculation of isotope measurements:

According to the equation that mentioned by (Dana,2003) the calculation was done. in column six in table (2), the Deuterium isotope ($\delta^{2}H$) according to eastern Mediterranean meteoric water line (EMWL) founded by equation (1) as follow:

$\delta D= 8\ \delta\ ^{18}O +22$ …….. (1)

whereas the global meteoric water line (GMWL) used the following equation to calculate $\delta\ ^{2}H$ in column seven:

$\delta D= 8\ \delta\ ^{18}O +10$ …….. (2)

and the local meteoric water line (LMWL) equation for the northern Iraq based on the isotope data of the groundwater, equation (3) is applicable for column eight.

$\delta D= 8\ \delta\ ^{18}O +20$ …….. (3)

This equation defines the Kurdish meteoric water line (northern Iraq, Erbil city and the surrounding region).

Finally, in the last column, the Deuterium surplus was defined by equation (4):

$d= \delta D - 8\ \delta\ ^{18}O$ …….. (4)

Table 2: calculated results of the sampling points for isotope measuring data.

No	Location	Measurements			Eq. (1)	Eq. (2)	Eq. (3)	Eq. (4)
		$\delta^{18}O$ ‰	$\delta^{2}H$	^{3}H (TU)	$\delta^{2}H$ ‰	$\delta^{2}H$ ‰	$\delta^{2}H$ ‰	d ‰
1	Haji-Omran	-8.93	-51.1	13.4	-49.44	-61.44	-51.44	20.34
2	Rayat	-8.11	-45.8	8.6	-42.88	-54.88	-44.88	19.08
3	Chuman	-7.82	-44.2	9.3	-40.56	-52.56	-42.56	18.36
4	Rezanok	-7.34	-40.9	9.5	-36.72	-48.72	-38.72	17.82
5	Piera-sawir	-7.98	-44.6	11.7	-41.84	-53.84	-43.84	19.24
6	Jundijan	-8.37	-47.4	10.8	-44.96	-56.96	-46.96	19.56
7	Diana	-7.79	-44.6	12.8	-40.32	-52.32	-42.32	17.72
8	Gali-Ali-Bag	-8.01	-43.8	9.1	-42.08	-54.08	-44.08	20.28
9	Bekhal	-7.98	-44.5	10.7	-41.84	-53.84	-43.84	19.34
10	Bekhal	-7.99	-43.8	11	-41.92	-53.92	-43.92	20.12
11	Harir	-7.28	-39.9	10.2	-36.24	-48.24	-38.24	18.34
12	Mirawa	-5.79	-31.7	7.4	-24.32	-36.32	-26.32	14.62
13	Betrma	-7.15	-37.9	13.9	-35.2	-47.2	-37.2	19.3
14	Shaqlawa	-7.28	-39	12	-36.24	-48.24	-38.24	19.24
15	Kawanjan	-6.85	-36.8	10.8	-32.8	-44.8	-34.8	18
16	Hirjan	-6.87	-36.8	12.8	-32.96	-44.96	-34.96	18.16
17	Kore	-6.83	-36.8	6.8	-32.64	-44.64	-34.64	17.84
18	Malla-Omar	-5.93	-33.2	3.5	-25.44	-37.44	-27.44	14.24
19	Per-Daud	-5.28	-29.5	0.8	-20.24	-32.24	-22.24	12.74
20	Kasnazan	-5.17	-29.1	4.9	-19.36	-31.36	-21.36	12.26
21	Bila	-7.27	-38.4	11.2	-36.16	-48.16	-38.16	19.76
22	Barzan	-7.3	-39	9.9	-36.4	-48.4	-38.4	19.4

4.2-Comparison of measured readings with Mediterranean and global meteoric water line:

As calculated in Table 1, the value of deuterium surplus (d) are mainly higher than 10, this finding was also determined by (Craig, 1961 cited in Dana, 2003) for a large number of measuring stations all around the world. This relatively high deuterium surplus is typical for the Mediterranean Sea region. The highest deuterium surplus in the research area is thus attributed to the humidity coming from the Mediterranean Sea. The cause of this surplus is the low relative air humidity prevailing in the Mediterranean Sea region. as shown in figure (1), most of the measure values from this study remain close to the Eastern Mediterranean Meteoric Water Line (EMWL) and others present some variations.

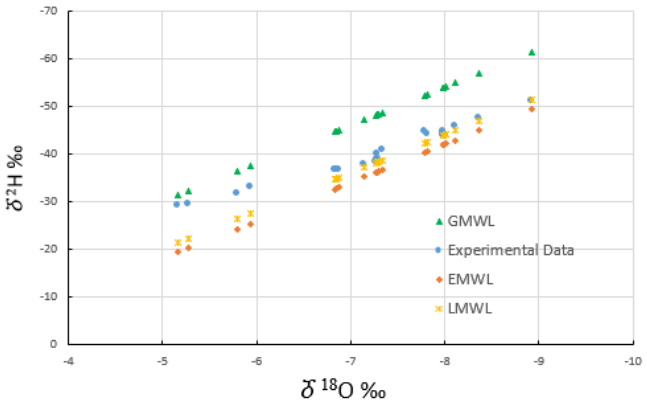

Figure (1). Relation between ^{2}H ‰ and ^{18}O ‰ and comparing it with different standards.

4.3 Constitution of ^{2}H and ^{18}O in groundwater:

The isotope composition of groundwater samples from ten wells and twelve springs. Usually the isotope composition of groundwater presents a large range as a result of influencing variables such as altitude, temperature, quantity of precipitation, and evaporation because the samples were taken in summer. Besides, it is assumed that groundwater systems store the ^{18}O and deuterium (D) content.

4.4 Deuterium excess (d):

The value of deuterium excess (d) was changed with climate, the warmer places have greater (d). it was lower than 15‰ are from Mirawa, Malla-Omar, Per-Daud, Kasnazan. These findings can probably be attributed to an isotopic enrichment due to the evaporation influences. The highest deuterium excess is about 20‰ was determined at sampling points at high altitude.

4.5 Concentration of heavy isotope (^{18}O):

The concentration of heavy isotopes was at points from Haji-Omran, and Jundian which are -8.93 and -8.37 respectively. Both sampling points were the lowest values lie in higher catchment basins. From the point of view of the measured accuracy, Bekhal 1 and Bekhal 2 was -7.98 and – 7.99 respectively are presents no differences in their isotope ratio.

4.6 Tritium (^{3}H) content in spring water and groundwater:

Tritium is the only isotope that is part of water molecule. Its half-life is 12.32 years (Terwey, 1984). The tritium is important to allow the determination of groundwater dwell time up to 100 years. As shown in table 3, the tritium content was varied at different catchments in Kurdistan region. Its highest value was recorded in the groundwater from the mountain regions, while the lowest value was seen in the plain basin near Erbil city. Table 3 illustrates that the water age results from the law of the radioactive decomposition.

Table 3. Age of water with different TU (Dana, 2003).

^{3}H (TU)	10	5.7	3.3	1.9	1.1	0.6	0.4
Age (year)	0	10	20	30	40	50	60

As explained in table 4, the interpolating measurement values listed in table 2 with values in table 3 shows the water age at each position.

Table 4. Groundwater age at different location in Erbil city.

Location No.	Location	^{3}H (TU)	Interpolated age of water (Year)
1	Haji-Omran	13.4	0
2	Rayat	8.6	3.26
3	Chuman	9.3	1.63
4	Rezanok	9.5	1.16
5	Piera-sawir	11.7	0
6	Jundijan	10.8	0
7	Diana	12.8	0
8	Gali-Ali-Bag	9.1	2.09
9	Bekhal	10.7	0
10	Bekhal	11	0
11	Harir	10.2	0
12	Mirawa	7.4	6.04
13	Betrma	13.9	0
14	Shaqlawa	12	0
15	Kawanian	10.8	0
16	Hirjan	12.8	0
17	Kore	6.8	7.44
18	Malla-Omar	3.5	19.17
19	Per-Daud	0.8	46
20	Kasnazan	4.9	13.33
21	Bila	11.2	0
22	Barzan	9.9	0.23

the water in the well from Per-Daud has a ^{3}H content of less than 1 TU (0.8 TU) which allows the discussion that the water is older than 40 years

(about 46 years). Also, for sampling point at Malla-Omar, the tritium content was measured as 3.5 TU which means that the age of water at this location is older than 10 years (about 19 years). In case of this proportionally long retention time of groundwater, there is a danger of a lake of balance between the natural supply and the extraction from the wells.

5. **Conclusions**:

The investigation of Appling an isotope technique on the groundwater in northern Iraq was the first step of determination the origin and dwell time of the respected water. this could be of great help for the further development of the region especially for the population, agriculture, industry and economy. The main key points of this investigation were summarized in the following points:

- The comparison of measured readings with Mediterranean and global meteoric water line has a slight difference that can be ignored due to the local climate at our region.
- The groundwater systems store the ^{18}O and deuterium (D) content out of which they were formed.
- From Mirawa, Malla-Omar, Per-Daud, Kasnazan, the value of deuterium excess (d) was smaller than 15 per mil due to the effect of evaporation at these places.
- The heavy concentration of $\delta^{18}O$ isotope were -8.93 and 8.37 per mil were from Haji-Omran and Jundian respectively.
- The tritium (^{3}H) content from Per-Daud was 0.8 TU, the dwell time of water was older than 40 years.

6. References:

Brown R.,1970, ″Distribution of hydrogen isotopes in Canadian waters″, calk river nuclier laboratories, IAEA-SM-129/1, international atomic energy agency, vienna,1970.

Dana K., 2003, ″Application of isotope hydrology studies considering the specific collimation, hydrological and geological conditions in order to research under-groundwater resources in a specific area in the near east″, PhD doctor technic in Vienna university of technology-Austria.

Dencer T. and Martinic J.,1965, ″Variation of tritium and oxygen-18 content in precipitation and snowpack in a representative basin in czechoslovakia″,IAEA-SM-129/3, international atomic energy agency, vienna,1970.

Geyh M., 2003, ″ Radiocarbon dating ^{14}C of old groundwater, history, potential, limits and future″, IAEA-CN-104/148, International Symposium held in Vienna, 19–23 May 2003 IN book: Isotope Hydrology and Integrated Water Resources Management.

Kumar U. and Hadi K., 2018, ″Futuristic isotope hydrology in the Gulf region″, J. Applied Water Science, No. 25, available at: https://doi.org/10.1007/s13201-018-0647-4.

Lollar B., Chartrand M., Hirschorn S., Hawlett M., Bedliman T., Jantunen L., Mancini S., Mckelvae J., Couloume G., Edwards E., 2007, ″compound specific stable isotope analysis: research frontiers in isotope hydrology and water resources management″, IAEA–CN–151/156, http://www.iaea.org/books.

Mohammed B., Achid E., Carreira P., 2015, ″ isotopic and geochemical methods for groundwater management strategies under semi-arid area: case of the wadi ouazzi basin (morocco) ″, IAEA-CN-225 water resources program.

Plummer L.,2003, ″Dating of young groundwater″ , IAEA-CN-104/153, International Symposium held in Vienna, 19–23 May 2003 IN BOOK: Isotope Hydrology and Integrated Water Resources Management.

Samie S., Murillo R., Marah H., Akech N., Tindimugaya C., Zouari K., 2018, "Enhancing the Use of Isotope Hydrology in Planning, Management, and Development of Water Resources", J. African Regional Cooperative Agreement for Research, Developing, and Planning Related to Nuclear Science and Technology (AFRA), RAF 7013.

Terwey J., 1984, ″Isotopes in groundwater hydrology″, Challenges in African Hydrology and Water Resources (Proceedings of the Harare Symposium, July 1984). IAHS Publ. no. 144, PP. 144-160.

ZANCO Journal of Pure and Applied Sciences
The official scientific journal of Salahaddin University-Erbil
https://zancojournals.su.edu.krd/index.php/JPAS

ISSN (print):2218-0230**, ISSN (online):** 2412-3986**, DOI: http://dx.doi.org/10.21271/zjpas**

RESEARCH PAPER

Application of Binary Logistic Regression Model to Cancer Patients: a case study of data from Erbil in Kurdistan region of Iraq.

Khwazbeen Saida Fatah [1], Zhyan Rafaat Ali Alkaki [2]

[1] Department of Mathematics, College of Science, Salahaddin University-Erbil, Kurdistan Region, Iraq.
[2] Department of Mathematics, College of Basic Education, Salahaddin University-Erbil, Kurdistan Region, Iraq.

A B S T R A C T:

In this paper, Binary Logistic Regression technique for fitting the best model for analyzing cancer diseases data is introduced using SPSS software based on forward stepwise procedures using different tests. The main objective is to investigate the last status of patients suffer from various types of cancer in Kurdistan Region of Iraq for the period 2010-2019 based on the main factors that contribute significantly to their last situation. A random sample of size 821 cancer patients from two main public hospitals (Rzgari and Nankali) in Erbil, where the patients take permanent and appropriate treatment, is selected of 619 alive and 202 dead. The results of the study showed that binary logistic regression is an appropriate technique to identify statistically significant predictor variables such as gender, age, cancer site and region to predict the probability of the last status (alive or dead) for each cancer patients. Moreover, it is deduced that despite the higher rate of cancer for female patients than the male; the chance for female cancer patients to be alive is more than male patients.

KEY WORDS: Binary Logistic Regression, Odds Ratio, Probability, and Hosmer and Lemeshow Test.
DOI: http://dx.doi.org/10.21271/ZJPAS.33.4.12
ZJPAS (2021), 33(4);117-128.

1. INTRODUCTION:

Logistic Regression Models analyze the relationship between a response (dependent) variable and a set of predictors (independent) variables. The main purpose for designing these models is to analyze the existence of the association between a nominal dependent variable and a group of independent (continuous or categorical) variables. With this model, instead of predicting the value of the response variable directly, the logistic regression equation predicts the odds of the event of interest occurring; this enables the approach to become a widely used statistical technique in medical research studies particularly over the last two decades in which the majority of the medical investigations are published (Yusuff, et al.,2012; Abdalrada, et al., 2019; Yuri, et al., 2016; Nankani, et al., 2019).

Binary Logistic Regression (BLR) , which studies the association between a binary response variable with only two categories and a set of predictors, is the most common used statistical model for the analysis of binary data in various applications such as physical, biomedical and health sciences, in which BLR model can be implemented for many applications in which data analysis comprise predicting the value of the outcome variable (Vupa and Çelikoğlu, 2006). This approach is particularly appropriate for models in which the dependent variable represents disease state (diseased or healthy) or patient status (dead or alive) for patients suffering from a certain disease (Sweet and Martin, 2011; Osborne, 2012; Mabula, 2015; Neupane, et al., 2002; Şirin, and Şahin, 2020; Bozpolat, 2016; Bahadır, 2016; Huang, and Moon, 2013). In situations when the response variable takes more than two categories it is then referred to as multinomial logistic regression (El-Habil, 2012).

* **Corresponding Author:**
Khwazbeen Saida Fatah
E-mail: khwazbeen.fatah@su.edu.krd
Article History:
Received: 15/03/2021
Accepted: 19/05/2021
Published: 18/08 /2021`

However, cancer is one of the diseases that causes major health problems with millions of human deaths in the world with numerous of new cancer cases arising each year and millions of cancer-related deaths with many factors that affect the increase or presence of this disease. The report by WHO (World Health Organization, 2021) on 5th March 2021, stated that the second leading cause of worldwide deaths is cancer; it is responsible for about 10 million deaths per year. Moreover, the report indicated that in low- and middle-income countries approximately 70% of deaths are due to cancer and that the most popular types of cancers are: Lung, Breast, Colorectal, Prostate, Skin cancer (non-melanoma); while Lung; Colorectal; Stomach; Liver and Breast cancer are the major causes of cancer .

Therefore, the aim of this study is to apply BLR model to analyze cancer patient's data for both genders male and female and then identify the predictor variables associated with the last status for all cancer patients in Kurdistan Region of Iraq and hence, based on these factors, determine the chance of being alive of both male and female patients.

2.Logistic Regression Model (LRM)

LRM analyzes the relationship between a response (categorical) variable, which is measured on a nominal scale, and a set of predictors (explanatory) variables. This model, which sometimes is called the logistic or logit model, estimates the probability of an event occurring by using a logistic curve. Logistic regression (LR) works very similar to linear regression except that in case of binary response variable the assumption of normality fails. The model is mathematically flexible; the interest in using this method has been increased due to not having any assumption limitations (Pregibon, 1981; Santner and Duffy, 1986; Abaye, 2019).

2.1Binary logistic regression model (BLRM)

The BLRM, which has begun to be a widely used model especially in medical research studies in which the dependent variable is dichotomous, for example: live/die; disease/no disease, can be considered as a statistical tool for predicting the association between the explanatory variables (predictors) and a binary (dichotomous) dependent or response variable with only two categories. With this model, the probability that an event falls into one of the two categories of the response variable is predicted by using one or more independent variable (continuous or categorical).

2.1.1 The Logistic Curve

In the BLRM, the variable representing the response categories takes values of 0 or 1 and the resulted value for the event of interest, the probability of the event occurring, should be in [0,1]. Hence, LRM uses the logistic curve to express the association between the predictors and the response variable. At a very low level of the predictor, the probability approximates to 0, but never becomes 0. While when the predictor variable increases the predicted value increase too; it approaches 1 but never equal to 1 (Nelder, 1961).

2.1.2 Transforming a Probability into Odds and Logit Values

Probability and odds both measures how likely it is that something will occur. The transformation of the logistic curve ensures that the predicted values fall inside the range of 0 and 1; this is obtained when the probability is measured as odds. Odds is defined as the ratio of the probability of the event occurring to the probability of the event does not occurring.

$$Odds\ (OR) = (probability\ of\ an\ event\ occuring)/(probability\ of\ event\ not\ occuring)$$

Then, to ensure that the odds values do not go below 0 which is the lower limit (there is no upper limit) the logit value is computed; it is obtained by taking the logarithm of the odds. Then, the odds value can be converted back into a probability; thus,

$$\text{Probability (event)} = \frac{\text{odds(event)}}{1+odds(event)} \qquad (1)$$

When there is an increase of one unit change in one of the independent variables, while the other predictors remain constant, there will be an increase in the odds of the response variable measured by a factor $exp(\beta_i)$; this factor is called the Odds Ratio (OR) and its value is greater than zero. This is a measure of the relative quantity by which the odds of the response variable increase (OR > 1) or decrease (OR < 1) when the value of the corresponding predictor increases by one (1) unit. Therefore, OR is a measure of association which is easy to be calculated and interpreted; it is a ratio of two odds measured by the odds of an event occurring in one category to the odds of that event when occurring in the other category.

2.2 Model building

In BL function, the likelihood or chance of an outcome based on individual characteristics is modeled. Because chance is a ratio, the BLRM applies a transformation called a logit to the probabilities to ensure its boundaries. The logit is defined as the logarithm of the OR; it is given by

$$logit(\pi) = \ln\left(\frac{\pi}{1-\pi}\right) \quad (2)$$

In equation (2), π is the probability of an event occurring; the mean of a binary variable is π, given the values of the predictor variables; Or the BLRM relates the log odds $[\ln(\pi/1-\pi)]$ in a linear way to the variation in the predictor variables with $\pi = \Pr(Y = 1|X = x)$ and the information of $0 \leq \pi \leq 1$ can be transformed into information of $-\infty \leq logit(\pi) \leq \infty$.

Variables are explained as follows:
Variable Y is a binary response with two categories:
$Y_i = 1$ if the event occurs in observation i
$Y_i = 0$ if the event does not occur in observation i
and variable $X = (X_1, X_2, \ldots, X_k)$ is a set of predictors that can be discrete, continuous, or a combination of both with x_i, the observed value of the predictors for observation i.

$$\pi_i = \Pr(Y_i = 1|X_i = x_i) = \frac{\exp(\beta_0 + \beta_1 x_i)}{1 + \exp(\beta_0 + \beta_1 x_i)} \quad (3)$$

Hence, $\text{logit}(\pi_i) = \ln(\pi_i/(1-\pi_i)) = \ln[\exp(\beta_0 + \beta_1 x_{i1} + \ldots. + \beta_k x_{ik})]$. (4)

Therefore, when the logits is defined as a linear relationship which takes the following form:

$$\text{logit}(\pi_i) = \beta_0 + \beta_1 x_{i1} + \ldots. + \beta_k x_{ik} \quad (5)$$

The Main assumptions for constructing the model:

- The data $Y_1, Y_2, \ldots, Y_n$ are identically independently distributed with binomial distribution $Bin(n_i, \pi_i)$, does not need to be normally distributed.
- There is no linear relationship between the outcome variable and the explanatory variables, but the linearity is between the logit of the response and the predictor variables; $\text{logit}(\pi_i) = \beta_0 + \beta_1 x_i$, so that changing an input variable multiplies the probability of the event of interest (output variable) by a fixed amount.
- The homogeneity of variance, which is not even possible in many cases, does not satisfy. The error terms are independent but normally do not satisfied. For parameter estimation the maximum likelihood estimation (MLE) is used instead of ordinary least squares (OLS), and thus relies on large-sample approximations. Goodness-of-fit measures rely on sufficiently large samples.

2.2.1 The Stepwise LRM

In model building, the stepwise LR is a widely used method specifically when the outcome variable being studied is relatively new (AIDS, some cancer types…) or the major predictors may not be identified and their relationship with the response variable may not be well defined. For these cases, stepwise procedures are used as a useful and effective tool to study a large number of such variables and fit a number of logistic regression equations. The technique for these procedures is to consider an initial model and then implement certain rules for selecting variables to

arrive at a final model (Cristensen, 1997). There are two techniques in stepwise LRM: the first one is the forward selection, which sequentially adds different predictor variables to the model and then at each stage, the variables that give largest improvement in the fit are chosen until there is no improvement in the fit. The main criterion for this process is the maximum p-value for the final model. The second approach is the backward elimination process which starts by a complicated model and then sequentially eliminates variables; variables with minimum effect on the model are removed at each stage.

2.2.2 Likelihood Ratio Test (LRT)

The LRT, which is sometimes called the chi-square test, is a practical test applied to check the variation between the likelihood ratios L_1, L_2 for two models, the null model, which is with only a constant, and the one with predictor variables respectively. This test checks the contribution of each effect to the model based on the value $-2\log(L_1/L_2)$, which is the ratio between the log-likelihood of the null model (L_1) to the log-likelihood (L_2) for the model with more predictors. The model is significance at the level of $\alpha = 0.05$ or less means that the model including the predictors is significantly different from that one with the constant only or null model (all 'β' coefficients are zero). Otherwise, when the probability unable to reach the value 0.05 means that predictors has no influences on response variable then they are to be rejected. (Burns and Burns, 2008).

2.3 Measures of Goodness of Fit Test

Goodness of fit is a test used to see if the sample data fits a distribution or shows how effectively the model describes the variables. In linear regression method, the coefficient of determination R^2 is employed to measure the goodness of fit or the variation ratio explained by the model but with LR there is no such measure to test the goodness of fit, and therefore other statistics similar to R^2 such as Cox and Snell, Nagelkerke R Square and Hosmer and Lemeshow (Hosmer and Lemeshow, 1989) test are applied; the value of each test statistic is used to test the hypothesis of the model. The following hypotheses are considered:

H_0: The modified model fits the data well.

H_1: The modified model does not fit the data well.

When the test is applied, at a standard level of significance $\alpha = 0.05$, the determined p-value is compared with α and H_0 will be rejected if its value is less or equal to α otherwise H_0 cannot be rejected.

2.4 Statistical Significant Test

Statistical significant test is applied to ensure the real contribution of the predictors in the model building and the prediction of the outcome. Wald test is one of these tests used to verify specifically whether the coefficient of predictor variables is significantly different from zero. Wald test, which is similar to the t-test performed on the coefficients of regression in a linear regression, is used to evaluate the fit of a logistic regression model; the larger value for this measure is an indication for the significance (Kleinbaum, and Klein, 2010).

2.5 Odds Ratios (OR) with 95% Confidence Interval (CI)

To estimate the accuracy of the OR, which is a measure of association, the 95% confidence interval (CI) is used. It is unlike the p-value, the 95% confidence does not refer to the statistical significance for the measure, but it is often used as a representative for the presence of the significance. A large CI indicates a low level of accuracy of the OR, while a small CI indicates a higher accuracy for the OR (Morris, and Gardner, 1988).

3.Methodology

3.1 Data collection and representation

The aim of the study is to analyze cancer patients data in Kurdistan Region of Iraq (with population approximately 6.5 million) where, over the years, health authorities have recorded annually thousands of patients who suffer from different types of cancer. The focus is specifically on Erbil city, the capital of Kurdistan Region, where cancer patients take permanent and appropriate treatment in two main public hospitals (Rzgari and Nankali). The patients involved in this study are

those who suffer from different types of cancer and get treatment from Erbil hospitals; they are from two different parts of Iraq, Erbil city and others, who come from different places in Kurdistan Region and all over Iraq. The analysis for cancer patients treated at two the public hospitals (Rzgari) and (Nankali) in Erbil city covered the period 2010-2019. A sample of 821 cancer patients data was provided by the General Directorate for Health in Erbil; they confirmed that it represents 10% of total number of patients for that period; this sample consists of 619 survived patients of which 357 females and 262 males and 202 died including 87 females and 115 males. The main variables for this study are described by Table 1:

The predictor variables are: the time period, Year variable, for the investigation, from 2010-2019 which is divided into three classes; the first class is from 2010 - 2012 which covers 11.5% of all cases, and the second class is 2013-2015 which represents 37.2%, finally the last class is 2016-2019 with 51.3% of all cases; it is the major class of the study.

The second predictor is the patient's age; it is divided into five groups: 0-20 which represents 2.5%; 21-40 represents 15.5%; 41-60 as 39.8%; 61-80 with 38%; finally 81 and above which covers only 4.1% . Then the Gender is another predictor which is either male or female.

Another important predictor is Cancer Site which is divided into four main groups; they are G1 group the breast cancer with 21.5%; the G2 group (Stomach, brain, lung, pancreas and liver) which represents 31.2%, and the G3 group (Prostate, colon, bladder and ovary) covers 17.5% and finally the G4 group (bone, skin, thyroid gland, hypo pharynx, other parts of tongue, ear, small intestine, parts of mouth, palate, tonsil, ureter) which covers 29.9% of all cases.

Finally, the region of residence is classified in to Erbil state with 73.4% and the others, who are from other parts of Iraq but treated in Erbil, 26.6% of all cases.

While the response variable in this study is the patient's last status (dead, alive) represented by values (0, 1).

In this study, the Statistical Package for Social Sciences (SPSS) software has been used for data analysis for the main variables and the results are shown by the following tables:

Table 2 shows that theme an alive percentage is equal to 75.4 since no independent variable has yet been entered.

Table 3 shows the intercept-only model where no variable contributes the prediction. It is shown that $B = 1.120$, if the exponential function is taken for both sides of this expression then the predicted odds is $EXP(B) = 3.064$, which explains that the predicted odds for being alive equals 3.064. Since 619 of all patients are alive while 202 are dead then the observed odds are $619/202 = 3.064$.

In classification table, Table 4, for the model with predictors, it is shown that the predicted number of dead patients is 27 out of 619, and from 202 only 139 are alive, and the percentage can be calculated as follows: $\frac{63}{202} \times 100 = 31.2\%$ dead, $\frac{592}{619} \times 100 = 95.6\%$ alive.

And the overall percentage equals: $\frac{619}{821} \times 95.6 + \frac{202}{821} \times 31.2 = 79.8$

It also shows that introducing independent variables to the model will improve the model in the ratio from 75.4% to 79.8%.

In Table 5, it is shown that all predictor variables are significant depending on P-value; this means that introducing each of the independent variables is significant to improve the model.

It is noted that in fitting a linear regression model, the amount of variance in the output variable associated with the independent variables is determined by the coefficient of determination, R^2. Large value for R^2 indicates that most of the variation is explained by the model, to a maximum of 1. While for LRMs, in which the dependent variable is categorical, it is not possible to determine a value for R^2; instead there are various ways to determine an R^2 for LR and no consensus on which one is the best; the following are three measures of fit:

- Cox and Snell's R^2 : for this measure, which is proposed by Cox and Snell, the log likelihood for the model is compared with the log likelihood for a baseline or the null model, the model with no

predictor; it has a theoretical maximum value of less than 1, even for a "perfect" model.

- Nagelkerke's R^2 is an adjusted version of the Cox & Snell *R*-square that modifies the scale of the measure in order to cover the full range from 0 to 1.
- Hosmer and Lemeshow Chi-square test of goodness of fit for logistic regression tells how well the data fits the model. This test determines if the observed and expected data are matched.

These tests, which show how R^2 are calculated, are explained by table 6.

Table 6, for each model $(-2LL)$ is determined, it is an estimate of a model's suitability for the data which is often used to see if adding additional variables to the model results in a significant reduction.

The results indicate that the hypothesis H_0 is rejected if the p-value (sig.) for the overall model is less than 0.05; this concludes that there is evidence that at least one of the independent variable contributes to the prediction of the outcome. In addition, the results explains that adding any variable to the model, the value of $(-2LL)$ will be decreased.

Furthermore, Cox and Snell's R^2 is determined. This value indicates that the probability ratio of the variance in the response variable is explained by the predictor variable which is assumed to be good enough. However, Nagelkerke's R^2 is an adjusted version of the Cox & Snell R^2 statistic.

In Table 7, the Forward Stepwise (Wald) method, which is a method for finding the best model among others, is applied; it selects the largest significant value. In Step 4, the model is with highest significance; hence it will be the preferred one among the others.

The table 8 shows how the BLR, including all variables, is implemented and then different tests are applied.

Table 8 displays data analysis for different models with their accuracy within some intervals; it shows that all predictors are significant and that the fourth model is the best model based on the value of the tests. Therefore, the model identified as the fourth model is supposed to be the best one with exclusion of gender variable; the logit function it is defined as:

$$\log\left[\frac{\pi}{1-\pi}\right] = -1.747 - 0.529\ \text{age} + 1.034\ \text{year} + 1.421\ \text{region} + 0.225\ \text{cancer site}$$

However, the gender variable has been considered as a major predictor for identifying the last status, the gender variable is taken into consideration and the last model, with inclusion of gender is proposed. It is noted that data analysis shows that females have more chance to get cancer than males, but males have chance to die more than females. The following table is with Gender included.

In the table 9, the predictor variable Gender has been added to the overall model and the logit function it is defined as:

$$\mathbf{\log\left[\frac{\pi}{1-\pi}\right] = -3.124 - 0.464\ age + 0.651\ gender + 1.01\ year + 1.447\ region + 0.305\ cancer\ site}$$

In this model, for example, if a male patient is selected who is from the second age group with breast cancer (G1) and from first category period in Erbil Region then the chance of being alive will be given by:

OR = $e^{-3.124-0.464\,(2)+0.651(\,1)+1.01\,(1)+1.447(1)+0.305(1)} = 0.52782$ with probability calculated from $\frac{\text{OR}}{1+\text{OR}} = \frac{0.52782}{1+0.52782} = 0.35$.

But if another a female patient from the same groups is selected then the chance of being alive is OR= $e^{-3.124-0.464\,(2)+0.651(\,2)+1.01\,(1)+1.447(1)+0.305(1)} = 1.012072$ with probability $= \frac{\text{OR}}{1+\text{OR}} = \frac{1.012072}{1+1.012072} = 0.5$.

While, if a male patient is selected from the second age group and from first category period in Erbil Region but with cancer of G2 group, then the chance of being alive is

$OR=e^{-3.124-0.464\,(2)+0.651(\,1)+1.01\,(1)+1.447(1)+0.305(2)} = 0.716054$ with probability$= \frac{OR}{1+OR} = \frac{0.716054}{1+0.716054} = 0.42$.

But if the patient is a female and from the same groups then the chance of being alive is $OR = e^{-3.124-0.464\,(2)+0.651(\,2)+1.01\,(1)+1.447(1)+0.305(2)} = 1.373003$ with probability $= \frac{OR}{1+OR} = \frac{1.373003}{1+1.373003} = 0.58$.

Table 1: categories and levels of variables included in the study

Category	Level
Years	2010-2012, 2013-2015, 2016-2019
Age	0-20, 21-40, 41-60, 61-80, 81-
Gender	Male, Female
Cancer Site	G1, G2, G3, and G4
Region	Erbil, others
Patients last status	Alive, dead (binary variable)

Table 2: Classification Table

			Predicted		
			Situation		Percentage Correct
	Observed		Dead	Alive	
Step 0	Situation	Dead	0	202	.0
		Alive	0	619	100.0
	Overall Percentage				75.4

Table 3: Variables in the Equation

		B	S.E.	Wald	Df	Sig.	Exp(B)
Step 0	Constant	1.120	.081	190.989	1	.000	3.064

Table 4: Classification Table

			Predicted		
			Situation		Percentage Correct
	Observed		dead	Alive	
Step 1	Situation	Dead	63	139	31.2
		Alive	27	592	95.6
	Overall Percentage				79.8

Table 5: Variables not in the Equation

			Score	df	Sig.
Step 0	Variables	Age	25.119	1	.000
		Gender	13.081	1	.000
		Year	75.597	1	.000
		Region	34.125	1	.000
		Cancer site	9.496	1	.002
	Overall Statistics		147.558	5	.000

Table 6: Forward Stepwise (Wald) method

Model Summary				Hosmer and Lemeshow Test		
Step	-2 Log likelihood (-2LL)	Cox & Snell R Square	Nagelkerke R^2	Chi-square	df	Sig.
1	843.039[a]	.085	.127	27.875	1	.000
2	802.552[b]	.129	.192	32.326	4	.000
3	778.462[b]	.154	.230	22.408	8	.004
4	771.092[b]	.162	.241	11.080	8	.197
5	759.260[b]	.174	.259	17.596	8	.024

Table 7: Forward Stepwise (Wald) method, Likelihood ratio test

Omnibus Tests of Model Coefficients

		Chi-square	Df	Sig.
Step 1	Step	73.105	1	.000
	Block	73.105	1	.000
	Model	73.105	1	.000
Step 2	Step	40.487	1	.000
	Block	113.592	2	.000
	Model	113.592	2	.000
Step 3	Step	24.091	1	.000
	Block	137.683	3	.000
	Model	137.683	3	.000
Step 4	Step	7.370	1	.007
	Block	145.053	4	.000
	Model	145.053	4	.000
Step 5	Step	11.832	1	.001
	Block	156.884	5	.000

Model	**156.884**	**5**	**.000**

Table 8: Binary Logistic Regression Models using (Forward Stepwise (Wald) method)
Variables in the Equation

		B	S.E.	Wald	Df	Sig.	Exp(B)	95% C.I.for EXP(B)	
								Lower	Upper
Step 1[a]	Year	1.003	.121	68.587	1	.000	2.726	2.150	3.456
	Constant	-1.176	.279	17.763	1	.000	.309		
Step 2[b]	Year	1.036	.125	69.225	1	.000	2.818	2.208	3.597
	Region	1.423	.250	32.322	1	.000	4.150	2.541	6.779
	Constant	-2.964	.425	48.742	1	.000	.052		
Step 3[c]	Age	-.527	.111	22.439	1	.000	.590	.475	.734
	Year	1.068	.127	70.190	1	.000	2.909	2.266	3.735
	Region	1.376	.254	29.405	1	.000	3.960	2.408	6.513
	Constant	-1.218	.557	4.784	1	.029	.296		
Step 4[d]	Age	-.529	.113	21.998	1	.000	.589	.472	.735
	Year	1.034	.128	65.116	1	.000	2.811	2.187	3.613
	Region	1.421	.255	31.006	1	.000	4.140	2.511	6.827
	Cancer site	.225	.084	7.270	1	.007	1.253	1.063	1.475
	Constant	-1.747	.595	8.615	1	.003	.174		
Step 5[e]	Age	-.464	.114	16.469	1	.000	.629	.502	.787
	Gender	.651	.191	11.626	1	.001	1.918	1.319	2.789
	Year	1.010	.129	61.111	1	.000	2.745	2.131	3.535
	Region	1.447	.256	31.942	1	.000	4.252	2.574	7.023
	Cancer site	.305	.090	11.625	1	.001	1.357	1.139	1.617
	Constant	-3.124	.731	18.251	1	.000	.044		

Table 9: Variables in the Equation

		B	S.E.	Wald	Df	Sig.	Exp(B)	95% C.I.for EXP(B)	
								Lower	Upper
Step 5[e]	Age	-.464	.114	16.469	1	.000	.629	.502	.787
	Gender	.651	.191	11.626	1	.001	1.918	1.319	2.789
	Year	1.010	.129	61.111	1	.000	2.745	2.131	3.535
	Region	1.447	.256	31.942	1	.000	4.252	2.574	7.023
	Cancer site	.305	.090	11.625	1	.001	1.357	1.139	1.617
	Constant	-3.124	.731	18.251	1	.000	.044		

3.2 Final Model

When the model is fitted, the following table explains how the data is analyzed and then how the most significant predictors are selected.

Table 10 explains that with the best model, which is the fifth one, all variables are significant except the first and third age categories with third cancer site category (significance is greater than 0.05).

In Table 11, the Wald Chi-Square test statistic is calculated; it shows the unique contribution of each predictor, holding the other predictors constant, wherefore each variable group the comparison is with final category. For example, for cancer site, where each group is compared with $G4$, predictors meets the conventional .05 standard for statistical significance, except for variable $G1(1)$. It is explained that for a patient whose in the second cancer site category, his chance to be alive decreases by the OR which is $EXP(\beta) = 0.159$ with probability 0.14 while if that patient is in third category then the chance will be reduced by $EXP(\beta) = 0.348$ with probability 0.26.

Table 10: Variables not in the Equation

			Score	Df	Sig.
Step 0	Variables	Age	26.698	4	.000
		0-20(1)	1.237	1	.266
		21-40(2)	13.255	1	.000
		41-60(3)	1.523	1	.217
		61-80(4)	10.311	1	.001
		Gender male(1)	13.081	1	.000
		Years	120.043	2	.000
		2010-2012(1)	119.035	1	.000
		2013-2015(2)	4.241	1	.039
		Region Erbil(1)	34.125	1	.000
		Cancer site	112.332	3	.000
		G1(1)	23.027	1	.000
		G2(2)	92.605	1	.000
		G3(3)	1.544	1	.214
	Overall Statistics		225.037	11	.000

Table 11: Binary Logistic Regression model fitted to Classes and Levels of the Variables Included (final model)

Variables in the Equation

		B	S.E.	Wald	df	Sig.	Exp(B)	95% C.I.for EXP(B)	
								Lower	Upper
Step 1[a]	Age			10.362	4	.035			
	0-20(1)	.843	.856	.969	1	.325	2.322	.434	12.427
	21-40(2)	1.504	.511	8.672	1	.003	4.501	1.654	12.249
	41-60(3)	.748	.431	3.006	1	.083	2.113	.907	4.922
	61-80(4)	.564	.425	1.762	1	.184	1.758	.764	4.042
	Gender male(1)	.049	.214	.052	1	.820	1.050	.690	1.598
	Years			65.495	2	.000			
	2010-2012(1)	-2.376	.296	64.372	1	.000	.093	.052	.166
	2013-2015(2)	-.350	.211	2.749	1	.097	.705	.466	1.066
	Region Erbil(1)	-1.431	.275	27.157	1	.000	.239	.140	.410
	Cancer site			59.401	3	.000			
	G1(1)	-.023	.368	.004	1	.951	.977	.475	2.009
	G2(2)	-1.840	.274	45.210	1	.000	.159	.093	.271
	G3(3)	-1.055	.306	11.845	1	.001	.348	.191	.635
	Constant	2.947	.539	29.851	1	.000	19.057		

a. Variable(s) entered on step 1: age, gender, year, region, cancer site.

4.Conclusion

BLR provides an effective tool for modeling the dependence of a binary output variable on one or more predictors that can be either categorical or continuous variables. In this study, a BLRM is fitted to data obtained from a case study concerns an investigation on the last status for patients suffer from different types of cancer treated in Erbil in Kurdistan Region of Iraq for the period of 2010-2019.

According to the results obtained from the analysis of data, using SPSS software, by implementing various procedures based on forward stepwise and applying different tests, the best model for all cancer patients, male and female patients with the response variable as the patient's last status, can be obtained. The model can easily identify the factors or predictors that will affect the response variable, which is the patient's last status (alive or dead). It is concluded that the main predictors contribute the chance of the cancer patients to be alive or dead are each of variables, age, gender, cancer site and the region. When predictor variables are included in the model, the results show improvement for the model by the ratio from 75.4% to 79.8%. In addition, when Forward Stepwise (Wald) methods are applied for each model, it is shown that the value for $-2LL$ is decreased. All other tests showed that the model is improved by adding a new influence predictor. Moreover, it is concluded that despite the rate of female patients who suffer from cancer is higher than the male patients; the rate of death for male patients is higher than for female. Finally, by applying the best model, if one patient (male or female) is randomly sampled and

all information for the factors in the model is identified then the status of that patient can easily be predicted through the estimated logit value.

References

Abaye**,** D. 2019. A Review of the Logistic Regression Model with Emphasis on Medical Research. *Journal of data analysis and information processing*, 7(4), 190-207.

Abdalrada, A., Yahya, O., Alaidi, H., Hussein, N., Alrikabi, H., and Al-Quraishi, T. 2019. A Predictive Model For Liver Disease Progression Based On Logistic Regression Algorithm. *Periodicals of Engineering and Natural Sciences*, 7(3), 1255-1264.

Abadi, A., hajizadeh, E., Pourhoseingholi, M. and Mojarad, E. 2019. Comparison of Random Forest and Logistic Regression Methods in Predicting Mortality in Colorectal Cancer Patients and Its Related Factors. *Iranian Journal of Epidemiology*, 14(4), 375-383.

Bahadır, E. 2016. Using Neural Network and Logistic Regression Analysis to Predict Prospective Mathematics Teachers's Academic Success upon Entering Graduate Education. *Educational Sciences: Theory & Practice*, 16(3), 943-964.

Bozpolat, E. 2016. Investigation of the Self-Regulated Learning Strategies of Students from the Faculty of Education Using Ordinal Logistic Regression Analysis. *Educational Sciences: Theory & Practice*, 16(1), 301-318.

Burns, R. and Burns, R. 2008. *Business Research Methods and Statistics Using SPSS*.

Cristensen, R. 1997. *Log-Linear Models and Logistic Regression*. 2nd edition, Springer-Verlag, New York.

El-Habil, A. M. 2012. An Application on Multinomial Logistic Regression Model. *Journal of Statistics and Operation Research*, 8(2), 271-291.

Hosmer, W. and Lemeshow, S. 1989. *Applied Logistic Regression.* Second Edition, Canada.

Huang, L. and Moon, R. 2013. What Are the Odds of That? A Primer on Understanding Logistic Regression. *Gifted Child Quarterly*, 57(3), 197–204.

Kleinbaum, D. and Klein, M. 2010. *Introduction to Logistic Regression*. Springer Science+Business Media. LLC

Mabula, S. 2015. Modeling Student Performance in Mathematics Using Binary Logistic Regression at Selected Secondary Schools A Case Study of Mtwara Municipality and Ilemela District. *Journal of Education and Practice*, 6(36), 96-103.

Morris, A. and Gardner, J. 1988. Calculating confidence intervals for relative risks (odds ratios) and standardized ratios and rates. *British Medical Journal (Clinical Research Ed.)*, 296(6632), 1313-1316

Nankani, H,; Gupta, S., Singh, S., Ramesh, S. S. S. 2019. Detection Analysis of Various Types of Cancer by Logistic Regression using Machine Learning. *International Journal of Engineering and Advanced Technology (IJEAT)*, 9(1), 99-104.

Nelder, J. A. 1961. The Fitting of A Generalization of the Logistic Curve. *International Biometric Society*, 17(1), 89-110.

Neupane, R. P., Sharma, K. R., and Thapa, G. B. 2002. Adoption of agroforestry in the hills of Nepal: a logistic regression analysis. *Agricultural Systems*, 72(3), 177–196.

Osborne, J. W. 2012. Logits and Tigers and Bears, oh my! A Brief Look At The Simple Math Of Logistic Regression And How It Can Improve Dissemination Of Results. *Practical Assessment, Research, and Evaluation*, 17(11), 1-10.

Pregibon, D. 1981. Logistic Regression Diagnostics. Annals of Statistics. *The Annals of Statistics*, 9(4), 705-724.

Santner, T. J., and Duffy, E. D. 1986. A Note on A. Albert and J.A. Anderson's Conditions for the Existence of Maximum Likelihood Estimates in Logistic Regression Models. *Oxford University Press on behalf of Biometrika Trust*, 73(3), 755-758.

Şirin, Y. E., and Şahin, M. 2020. Investigation of Factors Affecting the Achievement of University Students with Logistic Regression Analysis: School of Physical Education and Sport Example. *SAGE Open*, 10, 1-9.

Sweet, S. A., and Martin, K. G. 2011. *Data Analysis with SPSS + Mysearchlab with Etext: A First Course in Applied Statistics*. Pearson College Division.

Vupa, Ö. and Çelikoğlu, C. 2006. Model Building in Logistic Regression Models About LUNG CANCER DATA. *Anadolu University Journal of Science and Technology*, 7(1), 127-141.

World Health Organization. Available from https://www.who.int/news-room/fact-sheets/detail/cancer. [Accessed 5th, March, 2021]

Yuri, P., Rochadi, S., and Danarto, R. 2016. A Device for Predicting Prostate Cancer Risk: A Logistic Regression. *Journal of Prostate Cancer*, 1(2), 1-5.

Yusuff, H., Mohamad, N., Ngah, U.K., and Yahaya, A.S. 2012. Breast Cancer Analysis Using Logistic Regression. *IJRRAS*, 10(1), 14-22.

ZANCO Journal of Pure and Applied Sciences
The official scientific journal of Salahaddin University-Erbil
https://zancojournals.su.edu.krd/index.php/JPAS

ISSN (print): 2218-0230**, ISSN (online):** 2412-3986**, DOI: http://dx.doi.org/10.21271/zjpas**

RESEARCH PAPER

NONSTANDARD COMPLETION OF NON-COMPLETE METRIC SPACE

Ala O. Hassan, Ibrahim O. Hamad

Department of Mathematic, College of Science, Salahaddin University-Erbil, Kurdistan Region, Iraq

A B S T R A C T:

Our aim in this study is to establishing nonstandard foundations, definitions and theorems for completion a noncomplete metric spaces. We have a lot of space or sets X which agree with all usual properties of complete, except at a small size subset of it. In this paper, by using nonstandard analysis tools founded by A. Robinson and axiomatized by E. Nelson, we try to reformulate the definition of completion corresponding to nonstandard modified metric $\hat{d}$, and to give a nonstandard form to the classical (standard) completion theorem and to use the power of nonstandard tools to overcome the incompetence of those spaces which has deprivation at a small size subset.

KEY WORDS: Nonstandard, infinitesimal, completion, unlimited, infinitely close, non-complete spaces.
DOI: http://dx.doi.org/10.21271/ZJPAS.33.4.13
ZJPAS (2021), 33(4);129-135.

1.INTRODUCTION :

In this paper, we present a nonstandard way for constructing a complete metric space which satisfy all conditions of metric spaces and it is a completion of a non-complete metric space and to overcome the gaps of the classical treatments by introducing a new definitions compatible with our aim for giving a precise and perfect proof for completion of non-complete metric spaces. In mathematical analysis the standard complete metric space it means that every Cauchy sequences in the metric space is converge to a point in it (Macías-Díaz, 2015). Throughout this paper $\mathbb{R}^*$ is the extension of $\mathbb{R}$, includes all real numbers together with nonstandard quantities, and sometimes $\mathbb{R}^*$called it set of hyperreals.

* **Corresponding Author:**
Ala O. Hassan
E-mail: ala-omerr@hotmail.com
Article History:
Received: 07/04/2021
Accepted: 20/05/2021
Published: 18/08 /2021

2. BASIC CONCEPTS

Definition 2.1 (Keisler, 1976)
An element $x \in \mathbb{R}^*$ is
Infinitesimal if $|x| < r$ for all positive real r;
Limited if $|x| < r$ for some real r;
Unlimited if $|x| > r$ for all real r.

Definition 2.2 (Goldbring, 2014).
For $x, y \in \mathbb{R}^*$, we say x and y are infinitely close, written, $x \simeq y$, if $x - y$ is infinitesimal.
Every infinitesimal is limited

Definition 2.3 (Goldblatt, 1998)
A real number x is called ***appreciable*** if it is neither infinite nor infinitesimal.

Definition 2.4 (Keisler, 1976)
Given a hyperreal number $x \in \mathbb{R}^*$, the ***monad*** of x is the set
$$monad(x) = \{y \in \mathbb{R}^* : x \simeq y\}.$$
The ***galaxy*** of x is the set
$$galaxy(x) = \{y \in \mathbb{R}^* : x - y \text{ is limited}\}.$$

Definition 2.5 (Goldbring, 2014)

(1) The set of limited hyperreals is
$$R_{lim} := \{x \in \mathbb{R}^* \mid |x| \leq n \text{ for some } n \in N\}.$$
(2) The set of infinitesimal hyperreals is
$$R_{inf} := \{x \in \mathbb{R}^* \mid |x| \leq 1/n \text{ for all } n \in N > 0\}.$$
(3) The set of unlimited hyperreals is
$$R_{unl} := \mathbb{R}^* \setminus R_{lim}.$$

Theorem 2.6 (Existence of Standard Parts) (Goldbring, 2014)
If $r \in R_{lim}$, then there is a unique $s \in \mathbb{R}$ such that $r \simeq s$. We call s the standard part (or shadow) of r and denoted by $st(r)$ or $^\circ r$.

Corollary 2.7 (Keisler, 2011)
Let x and y be a finite
i. $x \simeq y$ if and only if $st(x) = st(y)$.
ii. $x \simeq st(x)$.
iii. If $r \in \mathbb{R}$ then $st(r) = r$.
iv. If $x \leq y$ then $st(x) \leq st(y)$.

3- MAIN RESULTS

Next we give a first results for our modification and extinction of the classical notions about complete, isometry, and dense with respect to nonstandard definitions given in previous. First we start with some new notions about ordering of sequences. All of this modifications and new notions will be necessary for nonstandard construction proof of completion of a non-complete metric space given the last.

Definition 3.18
Let (X, d) be a metric space and let C be the set of all Cauchy sequence in X, the two sequences $x = \{x_n\}, y = \{y_n\}\ in\ C\ are$ said to be:
1) In the same order and denoted by $x \simeq^{\Delta} y$, if $x_n \simeq y_n\ \forall n$.
2) Standardly in the same order denoted by $x \simeq_s y$, if $x_n \simeq y_n\ \forall^{st} n$.
3) Unlimitedly in the same order denoted by $x \simeq_\omega y$, if $x_n \simeq y_n\ \forall^{unlimited}\ n$.

Definition 3.2
Let (X, d) be a complete metric space and $Y \subseteq X$. Then we say that Y is **nearly complete** if Y is dense in X.

Definition 3.3
Let (X, d) and (Y, ρ) be metric spaces. Then by **nearly isometry** we mean a function $f: X \to Y$ where f is a bijection and for all $x, y \in X$ and
$$\rho(f(x), f(y)) \simeq d(x, y) \forall x, y \in X.$$
In general, a function $i: X \to Y$ is **nearly isometry** we can write a function h if
$$h\big(i(x), i(y)\big) \simeq h(x, y) \qquad \forall x, y \in X.$$

Definition 3.4
Let (X, d) be a matric space. A subset $S \subseteq X$ is said to be **nearly dense** if S can be nearly isometrically embedded in X.

Lemma 3.5
Let (X, d) and (Y, ρ) be two metric spaces such that X is standard. Then a function $f: X \to Y$ is nearly isometry if and only if for all $x, y \in X$ there exists $f(x), f(y) \in f(X)$ such that $^\circ\rho\big(f(x), f(y)\big) = d(x, y)$.

Proof
Let (X, d) and (Y, ρ) be two metric spaces such that $f: X \to Y$ is nearly isometry.
Then f is bijective and for all $x, y \in X$, $\rho(f(x), f(y)) \simeq d(x, y)$.
Since X is standard then $d(x, y)$ is standard.
Thus, by definition of shadow, we have $^\circ\rho\big(f(x), f(y)\big) = d(x, y)$.
Conversely, assume that X is standard and $f: X \to Y$ be a function such that $^\circ\rho\big(f(x), f(y)\big) = d(x, y)\ \forall x, y \in X$, then $\rho(f(x), f(y)) \simeq d(x, y)$.
Now we have to show that f is bijective.
If $f(x) = f(y)$, then $^\circ\rho\big(f(x), f(y)\big) = 0$.
Hence, $d(x, y) = 0$.
Therefore, $x = y$.
Thus, f is on to one and f is onto by hypothesis and $^\circ\rho\big(f(x), f(y)\big) = d(x, y)\ \forall x, y \in X$.
Therefore, f is bijective.
Hence, f is nearly isometry.

Definition 3.6
Let $\hat{X} = \{[\lambda]: \alpha_n \to \lambda;\ \alpha_n \in X\}$, X is an arbitrary metric space equipped with metric d. where
$$[\lambda] = \begin{cases} \alpha_n \in C : \alpha_n \to \lambda \in X \\ \beta_n \in C : \beta_n \to \lambda \notin X \end{cases}$$
Define
$\hat{d}: \hat{X} \to \mathbb{R}$ by: $\hat{d}([\lambda], [\mathfrak{z}]) =$
$$\begin{cases} d(\alpha_n, \beta_n) & if\ n\ is\ unlimited \\ 0 & otherwise \end{cases}$$
Where $\alpha_n, \beta_n \in C \subset X$ such that $\alpha_n \to \lambda, \beta_n \to \mathfrak{z}$, and we define equality among members of $\hat{X}$ by: $[\lambda] = [\mathfrak{z}] \equiv \lambda \simeq \mathfrak{z} \equiv \alpha_n \simeq \beta_n\ \forall^{unlimited}\ n$.

The following examples are to verify our **Definition 3.6**

Example 3.7

1. Let $X = (0,1]$ and $\lambda = 0$, then
$$\hat{X} = \{[0]: \alpha_n \to 0;\ \alpha_n \in X\},$$
And
$$[0] = \begin{cases} \alpha_n \in C:\ \alpha_n \to 0 \in X \\ \beta_n \in C:\ \beta_n \to 0 \notin X \end{cases}$$

2. Let $X = \mathbb{Q}$ and $\lambda \in \mathbb{R}$, then
$$\hat{X} = \{[\lambda]: \alpha_n \to \lambda;\ \alpha_n \in \mathbb{Q}\},$$
And
$$[\lambda] = \begin{cases} \alpha_n \in C:\ \alpha_n \to \lambda \in \mathbb{Q} \\ \beta_n \in C:\ \beta_n \to \lambda \notin \mathbb{Q} \end{cases}$$

Theorem 3.9

$(\hat{X}, \hat{d})$ is a metric space.

Proof

We have to show that $\hat{d}$ is define a metric on $\hat{X}$. From **Definition 3.6** we have
$$[\lambda] = [\mathfrak{z}] \equiv \lambda \simeq \mathfrak{z}$$
$$\equiv \alpha_n \simeq \beta_n \equiv\ d(\alpha_n, \beta_n) \simeq 0\ \forall^{unlimited}\ n.$$

Definition 3.8

Let $\hat{Y}$ be a subset of $\hat{X}$ such that $\hat{Y} = \{[S_x], x \in X\}$. Then we define S_x to be the $S_x = \{\ s_n \in C: s_n \simeq x\ \forall^{unlimited}\ n\}$.

Thus,
$$\hat{d}([\lambda],[\mathfrak{z}]) = \begin{cases} d(\alpha_n, \beta_n) = \begin{cases} c & n\ unlimited\ \ \alpha_n \not\simeq \beta_n \\ \varepsilon & n\ unlimited\ \ \alpha_n \simeq \beta_n \end{cases} \\ 0 \qquad\qquad otherwise \end{cases}$$

Where c is an appreciable real and ε is infinitesimal. Before we prove that $(\hat{X}, \hat{d})$ is a metric space, we have to prove the $\hat{d}([\lambda],[\mathfrak{z}])$ is really exists for every $\alpha_n, \beta_n \in C \subset$X. we have
$$|d(\alpha_n, \beta_n) - d(\alpha_m, \beta_m)| \le |d(\alpha_n, \beta_n) - d(\alpha_n, \beta_m)| + |d(\alpha_n, \beta_m) - d(\alpha_m, \beta_m)| \quad (1)$$
Also, for d a metric, we have
$$|d(x,y) - d(y,z)| \le d(x,z) \quad \forall x,y,z \in X \quad (2)$$
Applying (2) in (1) we obtain
$$|d(\alpha_n, \beta_n) - d(\alpha_m, \beta_m)| \le d(\beta_n, \beta_m) + d(\alpha_n, \alpha_m) \quad (3)$$
Since both α_n, β_n are Cauchy sequences in X, then
$d(\beta_n, \beta_m) \simeq 0, d(\alpha_n, \alpha_m) \simeq 0\ \forall^{unlimited}\ n, m.$
Equivalently,
$$\beta_n \simeq \beta_m, \alpha_n \simeq \alpha_m\ \forall^{unlimited} n, m \quad (4)$$
From (3), (4) we get that $|d(\alpha_n, \beta_n) - d(\alpha_m, \beta_m)| \simeq 0\ \forall^{unlimited}\ n, m.$
Equivalently,
$d(\alpha_n, \beta_n) \simeq d(\alpha_m, \beta_m)\ \forall^{unlimited}\ n, m,$
It follows that $\{d(\alpha_n, \beta_n)\}_{n \in \mathbb{N}}$ is a Cauchy sequence in $\mathbb{R}$. Since $\mathbb{R}$ is complete then $d(\alpha_n, \beta_n)$ is converge to a value in $\mathbb{R}$. That is $d(\alpha_n, \beta_n)$ is exists and since d is metric, then $d(x,y) = 0 \Leftrightarrow x = y$. Thus, if $x \simeq y \Rightarrow d(x,y) \simeq 0$.
To show that $\hat{d}$ is well defined, we have to prove that if
$[\lambda] = [\lambda^*]$ and $[\mathfrak{z}] = [\mathfrak{z}^*]$, then $\hat{d}([\lambda],[\mathfrak{z}]) = \hat{d}([\lambda^*],[\mathfrak{z}^*])$ for $\alpha_n \to \lambda, \beta_n \to \mathfrak{z}, {\alpha_n}^* \to \lambda^*$ and ${\beta_n}^* \to \mathfrak{z}^*$.
Now, for any positive integer n we have
$$d(\alpha_n, \beta_n) \le d(\alpha_n, {\alpha_n}^*) + d({\alpha_n}^*, \beta_n)$$
$$d(\alpha_n, \beta_n) \le d(\alpha_n, {\alpha_n}^*) + d({\alpha_n}^*, {\beta_n}^*) + d({\beta_n}^*, \beta_n)$$
Thus as $[\lambda] = [\lambda^*]$, then $\lambda \simeq \lambda^*$ and so as $\mathfrak{z} \simeq \mathfrak{z}^*$. Therefore, $\alpha_n \simeq {\alpha_n}^*$ and $\beta_n \simeq {\beta_n}^*$. Then
$d(\alpha_n, {\alpha_n}^*) \simeq 0\ and\ d({\beta_n}^*, \beta_n) \simeq 0$. Therefore,
$$d(\alpha_n, \beta_n) \lesssim d({\alpha_n}^*, {\beta_n}^*) \quad (5)$$
Similarly,
$$d({\alpha_n}^*, {\beta_n}^*) \lesssim d(\alpha_n, \beta_n) \quad (6)$$
From (5) and (6) we obtain that
$d(\alpha_n, \beta_n) = d({\alpha_n}^*, {\beta_n}^*)$
Thus $\hat{d}([\lambda],[\mathfrak{z}]) = \hat{d}([\lambda^*],[\mathfrak{z}^*])$.

To show that $\hat{d}$ is a metric on $\hat{X}$.

1) Since d is metric on X then $\hat{d}([\lambda],[\mathfrak{z}]) \gtrsim 0$.
2) Let $[\lambda]=[\mathfrak{z}]$ then $\forall \alpha_n,\beta_n \in C \subseteq X\ \alpha_n \simeq \lambda \simeq \mathfrak{z} \simeq \beta_n \Leftrightarrow d(\alpha_n,\beta_n) \equiv d(\lambda,\mathfrak{z}) = 0 \Leftrightarrow \hat{d}([\lambda],[\mathfrak{z}]) = 0$.
3) It is clear $\hat{d}([\lambda],[\mathfrak{z}]) = \hat{d}([\mathfrak{z}],[\lambda])$.
4) $\hat{d}([\lambda],[\mathfrak{z}]) \le \hat{d}([\lambda],[\varphi]) + \hat{d}([\varphi],[\mathfrak{z}])$ is directly from d is metric.

Theorem 3.10

$(\hat{Y},\hat{d})$ and (X,d) are nearly isometry.

Proof

We have to find a bijective function between $X\ and\ \hat{Y}$ such that

$\hat{d}(f(x),f(y)) \simeq d(x,y)$,

Where $\hat{Y} = \{[S_x], x \in X\}$, $S_x = \{\, s_n \in C : s_n \simeq x\ \forall^{unlimited} n\}$ and

$$\hat{d}([\lambda],[\mathfrak{z}]) = \begin{cases} d(\alpha_n,\beta_n) = \begin{cases} c & n\ unlimited\ \ \alpha_n \neq \beta_n \\ \varepsilon & n\ unlimited\ \ \alpha_n \simeq \beta_n \end{cases} \\ 0 \qquad\qquad otherwise \end{cases}$$

Let $f(x) = [S_x]\ \forall x \in X$.

Now, we prove that f is one to one and onto

Let $.f(x) = f(y)$ We have to show that $[x] = [y]$,

Now, since $f(x) = f(y)$, then $[S_x] = [S_y]$, where

$[S_x] = \{\, \alpha_n \in C : \alpha_n \simeq x\ \forall^{unlimited} n\}$

$[S_y] = \{\, \beta_n \in C : \beta_n \simeq y\ \forall^{unlimited} n\}$

Since $[S_x] = [S_y]$, then $[S_x] \subseteq [S_y]$ and $[S_y] \subseteq [S_x]$, In other way, we can say for all unlimited n, if $\alpha_n \in S_y$, then $\alpha_n \simeq y$ and if $\beta_n \in S_x$, then $\beta_n \simeq x\ \forall^{unlimited} n$,

Therefore,

$\alpha_n \simeq x \simeq \beta_n \simeq y\ \forall^{unlimited} n$.

That is $x \simeq y$.

In general, if $\alpha_n \simeq \beta_n$, then $[x] = [y]$.

Hence, we prove that f is one to one.

To prove that f is onto

Let $y \in \hat{Y}$. Then there exist $x \in X$ such that $y = [S_x]$

That is $y = f(x)$

Hence, f is onto.

Now, we have to show that

$$\hat{d}(f(x),f(y)) \simeq d(x,y)$$

Let $x,y \in X$ such that $f(x) = [S_x]$ and $f(y) = [S_y]$. Then,

$$\hat{d}(f(x),f(y)) = \hat{d}([S_x],[S_y]) = \begin{cases} d(\alpha_n,\beta_n) = \begin{cases} c & n\ unlimited\ \ \alpha_n \neq \beta_n \\ \varepsilon & n\ unlimited\ \ \alpha_n \simeq \beta_n \end{cases} \\ 0 \qquad\qquad otherwise \end{cases}$$

Then either $\hat{d}(f(x),f(y)) = d(\alpha_n,\beta_n)$ where $\alpha_n \to x$ and $\beta_n \to y\ \forall^{unlimited} n$.

That is $\hat{d}(f(x),f(y)) = d(\alpha_n,\beta_n) \simeq d(x,y)\ \forall^{unlimited} n$.

Or,

$\hat{d}(f(x),f(y)) = d(\alpha_n,\beta_n) = \varepsilon \simeq 0$ where $\alpha_n \to x$ and $\beta_n \to y\ \forall^{unlimited} n$.

Then

$\hat{d}(f(x),f(y)) = d(\alpha_n,\beta_n) \simeq d(x,y)\ \forall^{unlimited} n$.

In both cases we have

$$\hat{d}(f(x),f(y)) \simeq d(x,y)$$

Thus, $(\hat{Y},\hat{d})$ is nearly isometry (X,d).

Theorem 3.11

$(\hat{Y},d)$ is dense subspace of $(\hat{X},\hat{d})$.

Proof

To prove that $(\hat{Y},d)$ is dense subspace of $(\hat{X},\hat{d})$. we have to show that for all $p \in \hat{X} - \hat{Y}$, then p is a limit point of $\hat{Y}$. That is to show that for all $p \in \hat{X} - \hat{Y}$, there exists $q \in \hat{Y}$ such that $q \in mond(p)$, or we have to show that we can embedded $\hat{Y}$ into $\hat{X}$ isometrically.

Let $\hat{x} \in \hat{X} - \hat{Y}$. Then from **Definition 3.6**, we have that $\hat{x}$ is a Cauchy sequence in $\hat{X}$.

Let $\hat{x} \equiv x_n$ such that $x_n \to x$. Then by **Definition 3.6** we have either $x \in X\ or\ x \notin X$.

Now, since x_n is Cauchy sequence, then $x_n \simeq x_m\ \forall^{unlimited} n,m$.

Let $\{\, t_n\}$ be a sequence in X such that $t_n \simeq x_k$ for all fixed k, that is $\{\, t_n\}$ is a constant sequence. Then, its clear that $t_n \to x_k$. That is $t_n \simeq x_k\ \forall^{unlimited} n$.

From definition of $S_x\ and\ \hat{Y}$, we have $t_n \in \hat{Y}$ and for all unlimited n,

$\hat{d}([x],[x_k]) \equiv d(x_n,t_n) = \varepsilon \simeq 0\ \forall^{unlimited} n$ (because $x_n \simeq t_n$).

Therefore, $[x] \simeq [x_k]$. It means that $x \simeq x_k$.

Thus, $x_k \in mond(x)$.

That is $[x_k] \in [x] = \{x_n : x_n \to x\}$

Hence, $(\hat{Y}, d)$ is dense subspace of $(\hat{X}, \hat{d})$.

As a consequence of the all the previous given results in the following theorem, we will give prove of main considered problem of completion.

Theorem 3.12 (Basic Theorem)

$(\hat{X}, \hat{d})$ is complete metric space.

Proof

Since $\hat{X} = \{ [\lambda]: x_n \to \lambda \ x_n \in X\}$, where

$[\lambda] = \begin{cases} x_n \in C : x_n \to \lambda \in X \\ y_n \in C : y_n \to \lambda \notin X \end{cases}$ and

$$\hat{d}([\lambda], [\mathfrak{z}]) = \begin{cases} d(x_n, y_n) & if\ n\ is\ unlimited \\ 0 & otherwise \end{cases}$$

for $x_n, y_n \in C \subset$X such that $x_n \to \lambda, y_n \to \mathfrak{z}$, and

$[\lambda] = [\mathfrak{z}] \equiv \lambda \simeq \mathfrak{z}$.

$\equiv x_n \simeq y_n \ \forall^{unlimited}\ n$.

Also $\hat{Y} = \{[S_x], x \in X\}\ and\ \ S_x = \{ s_n \in C: s_n \simeq x \ \forall^{unlimited}\ n\}$.

We will try to follow through the prove step by step:

Step1: Let $\{ [S_{x_n}]\}$ be a Cauchy sequence in $\hat{Y}$ where $[S_{x_n}]$ is equivalence class of all Cauchy sequences. Then the metric distance between $[S_{x_m}]$ and $[S_{x_m}]$ is equivalence to

$$\hat{d}([S_{x_m}], [S_{x_m}]) \equiv \begin{cases} d(S_{x_m}, S_{x_n}) & if\ n, m\ are\ unlimited \\ 0 & otherwise \end{cases}$$
$$\equiv \begin{cases} d(x_n, x_m) & if\ n, m\ are\ unlimited \\ 0 & otherwise \end{cases}$$

Since $\{ [S_{x_n}]\}$ is a sequence of equivalent classes of Cauchy sequences in $\hat{Y}$ and $\{ [S_{x_n}]\}$ is Cauchy sequence, it follows that $\{x_n\}$ is a Cauchy sequence in X.

Hence $x_n \simeq x_m \ \forall^{unlimited}\ n, m$.

Step2: Our aim in this step is to take an element in $\hat{X}$ and show that our Cauchy sequence $\{ [S_{x_n}]\}$ in $\hat{Y}$ is converge to an element in $\hat{X}$.

Now, let $[x] \in \hat{X}$. Then

$[x] = \{x_n \in C : x_n \simeq x \in X \ \forall^{unlimited}\ n\}$, and

$$\hat{d}([x], [y]) = \begin{cases} d(x_n, y_n) & if\ n\ is\ unlimited \\ 0 & otherwise \end{cases}$$
$$\equiv \begin{cases} d(x_n, y_n) = \begin{cases} c\ \ n\ unlimited\ \ x_n \neq y_n \\ \varepsilon\ \ n\ unlimited\ \ x_n \simeq y_n \end{cases} \\ 0 \qquad otherwise \end{cases} \tag{7}$$

Without loss of generality, we can take $[y] = [S_{x_n}]$, where $[S_{x_n}] \in \hat{Y}$.

Since $\{x_n\}$ is a Cauchy sequence in X we can write $[x_m]$ as:

$[x_m] = \{\{x_k\}: x_k \simeq x_m\}$, where $m = 1, 2, 3, ...$

Now, since $[\lambda] = [\mathfrak{z}] \equiv \lambda \simeq \mathfrak{z} \equiv \alpha_n \simeq \beta_n \ \forall^{unlimited}\ n$, then

$$\hat{d}([x], [S_{x_n}]) = \begin{cases} d(x_n, x_{kn}) = \begin{cases} c\ \ n\ unlimited\ \ x_n \neq x_{kn} \\ \varepsilon\ \ n\ unlimited\ \ x_n \simeq x_{kn} \end{cases} \\ 0 \qquad otherwise \end{cases}$$

Since we have $x_n \simeq x_m \forall^{unlimited} n, m$ and $x_{kn} \simeq x_k$, then

$$\hat{d}([x], [S_{x_n}]) \equiv \hat{d}([x_m], [S_{x_{nm}}])$$
$$\equiv \begin{cases} d(x_m, x_{nm}) & m\ is\ unlimited\ and\ n\ fixed \\ 0 & otherwise \end{cases}$$
$$\equiv \begin{cases} d(x_m, x_n) & m\ is\ unlimited\ and\ n = 1,2,3, ... \\ 0 & otherwise \end{cases}$$

But we know that $x_n \simeq x_m$. Then $d(x_m, x_n) \simeq 0$.

Hence, a Cauchy sequence $\{ [S_{x_n}]\}$ in $\hat{Y}$ is converge to a point $[x] \in \hat{X}$.

Step3: the last step is to take a sequence in $\hat{X}$ and to show that it is converge to that point that belongs to $\hat{X}$.

Assume that $\{\hat{x}_n\}$ is a Cauchy sequence in $\hat{X}$, then

$$\hat{d}(\hat{x}_n, \hat{x}_m) = \begin{cases} d(x_{kn}, x_{km}) = \begin{cases} c & n\ unlimited\ \ x_{kn} \neq x_{km} \\ \varepsilon & n\ unlimited\ \ x_{kn} \simeq x_{km} \end{cases}, \\ 0 \qquad\qquad otherwise \end{cases}$$

and since $[x] \in \hat{X}$, then we have $\forall^{unlimited}\ n\ \exists \lambda \in X$ such that $\hat{x}_n = [\lambda]$. Therefore,

$$\hat{d}([\lambda],[\mathfrak{z}]) \equiv \hat{d}(\hat{x}_n, \hat{x}_m) \equiv \begin{cases} d(x_{kn}, x_{km}) = \begin{cases} c & n\ unlimited\ \ x_{kn} \neq x_{km} \\ \varepsilon & n\ unlimited\ \ x_{kn} \simeq x_{km} \end{cases} \\ 0 \qquad\qquad otherwise \end{cases}$$

$$\equiv \begin{cases} d(x_n, x_m) & \forall^{unlimited}\ n, m \\ 0 & otherwise \end{cases},$$

where $\hat{x}_m = [\mathfrak{z}]$ and $x_n \in [\lambda] = \{\hat{x}_k\}$ for fixed k.

Since $\{x_n\}$ is a Cauchy sequence in X, then $x_n \simeq x_m \forall^{unlimited}\ n, m.$ (8)

Therefore $\hat{d}(\hat{x}_n, \hat{x}_m) \equiv d(x_n, x_m) \simeq 0.$

Now, by **Theorem 3.11**, we have $(\hat{Y}, d)$ is dense subspace of $(\hat{X}, \hat{d})$.

Then $\forall^{unlimited}\ n$, there exist $[S_{y_n}] \in \hat{Y}$ such that $y_n \in [S_{y_n}] \in \hat{Y}$.

By (1) we have $x_n \simeq y_n\ \forall^{unlimited}\ n.$

(9)

Since $x_n \simeq y_n$ and $\{x_n\}$ is a Cauchy sequence in X, then $\{y_n\}$ is a Cauchy sequence in X.

Thus $x_m \simeq x_n \simeq y_n \forall^{unlimited} n, m$, in the other hand we have $x_m \simeq y_m$.

Then $y_n \simeq y_m \forall^{unlimited}\ n, m.$

Similarly, $\hat{d}(\hat{y}_n, \hat{y}_m) \equiv d(y_n, y_m) \simeq 0.$

Thus $\hat{y}_n \simeq \hat{y}_m\ \forall^{unlimited}\ n, m.$

Thus $\{\hat{y}_n\} \equiv \{[S_{y_n}]\}$ is a Cauchy sequence in $\hat{Y}$.

Again by **Theorem 3.11**, we have $\hat{Y}$ is nearly dense in $\hat{X}$.

Then there exist $\hat{y} \in \hat{X}$ such that $\hat{y}_n \simeq \hat{y}\ \forall^{unlimited}\ n.$ (10)

To complete the prove we have to prove that

$\hat{x}_n \simeq \hat{y}\ \forall^{unlimited}\ n.$ (11)

Now, by (7) and (8) we have $y_m \simeq x_n\ \forall^{unlimited} n, m.$

Returning the result to the correspond equivalent classes with respect to the metric $\hat{d}$, we obtain that

$\hat{y}_m \simeq \hat{x}_n\ \forall^{unlimited}\ n, m.$

By (10) we have $\hat{y}_m \simeq \hat{y}\ \forall^{unlimited}\ m.$

Hence, $\hat{x}_n \simeq \hat{y}\ \forall^{unlimited}\ n.$

That is a Cauchy sequence $\{\hat{x}_n\}$ in $\hat{X}$ is converges to $\hat{y}$ in $\hat{X}$. Thus $(\hat{X}, \hat{d})$ is complete metric space.

Theorem 3.13

If X is nearly complete, then $\hat{X}$ is completion of X, and either

$^{\circ}\varphi(X) = \hat{X}$ or $\varphi(X) \subseteq \hat{X}$.

Proof

Let $T = [\{t_n\}] \in \hat{X}$. Then $\{\varphi(t_k)\}_{k\in\mathbb{N}}$ is a sequence in $\varphi(X)$. We will try to prove that the sequence $\{\varphi(t_k)\}_{k\in\mathbb{N}} \simeq T \in \hat{X}$, that is to show that $\varphi(X)$ is nearly dense in $\hat{X}$.

Now,

$\hat{d}(T, \varphi(t_k)) = \hat{d}(t_n, (\varphi(t_k))_n)$

$$\equiv \begin{cases} d(t_n, \varphi(t_k)) & n\ unlimited \\ 0 & otherwise \end{cases}$$

$$\equiv \begin{cases} d(t_n, t_k) & n, k\ unlimited \\ 0 & otherwise \end{cases}$$

Since $\{t_n\}$ is Cauchy, then $t_n \simeq t_k\ \forall^{unlimited}\ n, k,$ and

$$\equiv \begin{cases} d(t_n, t_k) = \varepsilon & n, k\ unlimited \\ 0 & otherwise \end{cases}$$

It means that $d(t_n, t_k) \simeq 0\ \forall^{unlimited}\ n, k.$

Which means that $(t_k) \simeq T\ \forall^{unlimited}\ k.$

Then $\varphi(t_k) \to T \in \hat{X}$.

On the other hand, we have $\varphi(t_k) \in \varphi(X) \forall^{unlimited}\ k$

Then $\varphi(X)$ is nearly dense in $\hat{X}$. By **Lemma 3.5** we have either $^{\circ}\varphi(X) = \hat{X}$ or $\varphi(X) \subseteq \hat{X}$.

REFERENCES

Albeverio, S., Hegh-krohn, R., Lindstrm, T., 2009, *Nonstandard methods in stochastic analysis and mathematical physics*. Dover Publication.

Anderson, R. M. 1976, A non-standard representation for Brownian motion and Its integration, *Israel Journal of Mathematics* 25, 1-2, 15–46.

Andreev, P.V. and Gordon, E.I. 2001, An axiomatics for nonstandard set theory, based on von Neumann-Bernays-Gödel theory. *Journal of Symbolic Logic*, pp.1321-1341.

Cutland, N. J., Dinasso, M. and Ross, D. A. 2017, *Nonstandard methods and applications in mathematics*, *Lecture Notes in Mathematics*, 25, Association for Symbolic Logic, Cambridge University Press, Cambridge.

Davis, M. 2014, *Applied nonstandard analysis*. Courier Corporation.

Goldbring, I. 2014, *Lecture notes on nonstandard analysis*, Ucla summer school in logic.

Gordon, E. I. 1997, *Nonstandard methods in commutative harmonic analysis*, American Mathematical Society, providence, Rhode Island.

Hamad, I. O. and Pirdawood, M. A. 2020, Nonstandard Solutions for Ordinary Differential Equations near Singularity,*3rd International Conference on Recent Trends in Multi-Disciplinary Research* (ICRTMDR- 20), Maldives.

Hamad, I. O. 2016, On Some Nonstandard Development of Intermediate Value Property, Assiut University *Journal of Mathematics and Computer Science*, Vol 45(2), 35-45.

Hamad, I. O. 2011, *Generalized Curvature and Torsion in Nonstandard Analysis*, Ph.D. thesis, LAP Lambert Academic Publishing, ISBN 978-3-8443-0763-4.

Keisler, H.J. 1976, *Foundations of infinitesimal calculus* (Vol. 20). Boston: Prindle, Weber & Schmidt.

Macías-Díaz, J.E. 2015, *Complete Metric Spaces*, IX Conference on Exact Sciences Universidad Autónoma de Aguascalientes.

Ponstein, J. 2001, *Nonstandard analysis*. University of Groningen.

Robinson, A. 1996. *Non-standard analysis*. Princeton University Press.

ZANCO Journal of Pure and Applied Sciences
The official scientific journal of Salahaddin University-Erbil
https://zancojournals.su.edu.krd/index.php/JPAS

ISSN (print):2218-0230**, ISSN (online):** 2412-3986**, DOI: http://dx.doi.org/10.21271/zjpas**

RESEARCH PAPER

Estimation of Time-Dependent Delay Models at Actuated Traffic Signals in Duhok City

Millet Salim Mohammed Doski1, Aso Faiz Saeed Talabany*,2

[1] Duhok Municipality, Duhok, Kurdistan Region, Iraq
[2] Department of Civil Engineering, College of Engineering, Salahaddin University-Erbil, Kurdistan Region, Iraq

A B S T R A C T:

Duhok City, developed rapidly in recent years, leading to an increase in the traffic volume on its streets which are not sufficient for this increase resulting in traffic congestion. Therefore, this paper studied the delay as an important measure of effectiveness at traffic signals. The delay was measured and predicted (for saturated and under saturated conditions) to help in solving some underestimation problems by using the transportation system management (TSM) techniques. Five signalized intersections on Barzani major street in Duhok city was chosen. Vehicle delay was measured in these intersections directly from field, then it was calculated using the time-dependent equations recommended by three different official manuals, Highway Capacity Manual (HCM2000), Canadian Capacity Guide (ITE1995) and Australian Capacity Guide (ARRB1995). After that comparisons between the results of each theoretical method and the field result was made. Finally, the regression analysis technique was used to establish different relationships between the delay data obtained from the field and each of the theoretical methods to find the best applicable model to predict the vehicle delay at signalized intersections in Duhok City. It was proved that the logarithmic relationship between field and theoretical results obtained from the Canadian Capacity Guide is the best

KEY WORDS: Actuated Traffic Signal Delay; Time Dependent Delay Model, HCM Delay Model, Field Delay
DOI: http://dx.doi.org/10.21271/ZJPAS.33.4.14
ZJPAS (2021), 33(4);136-148.

1.INTRODUCTION :

Vehicular delay at signalized intersections in Duhok City-Kurdistan-Iraq increases the total travel time through an urban road network, resulting in a reduction in the speed, increase in environmental pollutions and cost-effectiveness of the transportation system.

The scope of control of signalized intersections can be grouped into three categories:

1. Individual (isolated) intersection control;
2. Arterial (corridor) control; and
3. Network (down town) control.

The Individual (Isolated) Intersection Control is a single traffic signal operates without affecting the operation of other traffic signals and may be controlled as:

1 - pre-timed (fixed time)
2 - actuated (partial or full), or
3 - traffic responsive mode

Vehicle-Actuated Signals require actuation by a vehicle on one or more approaches in order for certain phases or traffic movements to be serviced. They are equipped with detectors and the necessary

* **Corresponding Author:**
Aso Faiz Saeed Talabany
e-mail: aso.talabany@su.edu.krd
Article History:
Received: 12/04/2021
Accepted: 22/05/2021
Published: 18/8/2021

control logic to respond to the demands placed on them. Vehicle-actuated control uses information on current demands and operations, obtained from detectors within the intersection, to alter one or more aspects of the signal timing on a cycle-by-cycle basis. Timing of the signals is controlled by traffic demand. Actuated controllers may be programmed to accommodate variable green times for each phase and variable cycle length, caused by variable green times. Such variability allows the signal to allocate green time based on current demands and operations.

Delay in the Highway Capacity Manual (HCM 2000) context is defined as "the difference between the travel time actually experienced and the reference travel time that would result during ideal conditions; in the absence of traffic control, in the absence of geometric delay, in the absence of any incidents, and when there are no other vehicles on the road optimize the signal system to perform at a minimum delay".

Numerous equations have been developed for the estimation of delay. The use of steady state models during peak periods can introduce significant errors therefore, time dependent models are required for such periods.

The most frequently used manuals and guides for the estimation of vehicular delay using time dependent models are the American Highway Capacity Manual (HCM2000), the 1995 Australian Capacity Guide, and the 1995 Canadian Capacity Guide. The equations of these manuals and guides are a function of multiple input parameters arising from geometry, traffic and signal conditions.

Most signal intersection delay models fall into two categories, steady-state models and deterministic queuing models. the former are usually considered useful only for predicting delays at intersections with light loads, while the later do well only in the analysis of heavily loaded intersections where the volume is greater than the capacity (i.e. v/c >1). These models ignore the effect of random arrivals on queue lengths when intersections are slightly saturated. Because their assumptions are based on different v/c values, these two types of models are incompatible. However, when the load is heavy but v/c is still less than one, some good models are expected to produce excellent estimates.

The most frequently used manuals for the design of signalized intersection in developed countries assumes homogeneous and lane based traffic for analysis, which exists in those countries. But traffic flow in countries like Iraq consists of different classes of vehicles having no lane disciplined. There are no proper guidelines available to estimate saturation flow for non-lane based traffic conditions. The saturation flow has a direct great effect on the value of the capacity which has direct influence on the time dependent term (d_2) in delay equation in all theoretical methods that used in this research.

In 1958 Webster, (Webster F. V., 1958.) developed one of the fore most delay equations assuming practical distributions like Poisson (random) arrivals with uniform discharge headways. Webster introduced three terms to the delay equation: The first represents the delay when traffic is considered to arrive at a uniform rate, the second is a correction to the random nature of the arrivals and the third is empirical correction term with value of 5 to 15 percent of delay in most cases. But under some conditions Webster model may not be the right one (Gandhi Ganem Sofia, 1998).

In 1968 Miller developed an equation for delay estimation at signalized intersections. The guide developed by Miller became the basis of signalized intersection design in Australia during the 1960s and throughout the 1970s (Miller, A. S., 1968).

Time-dependent queuing models for oversaturated conditions started to interest the research field in 1977 from the work of Catling, who adopted equations of classical queuing theory for over saturated traffic conditions. He developed comprehensive queue length and delay formulas that may be used to represent the situation at the oversaturated intersections (Catling, 1977).

In 1978 Reilly, R and Gardner, C., used time- lapse photography to measure

vehicle journey time from the moment the vehicle enters the approach to the moment of passing over the stop line. Data about the percent of vehicles stopped at 10 intersections were collected. The journey time was divided into 3 parts; the first part was the approach delay. This delay was defined as the time spent while vehicle decelerate to join the queue. The authors recommended that the point sample, stopped delay may be used for field measurement of delay (Reilly R. and Gardner C., 1977).

In 1979 Kimber and Hollis, developed a sophisticated time-dependent model for the prediction of vehicle delay. This model was found to provide reasonably accurate results over a wide range of operating conditions (Kimber, RM and Erica M. Hollis, 1979).

In 1985 James M. S. and Herbert S. L. analyzed delays at signalized intersections assuming "platoon" arrival flow. They estimated the average travel time delay using graphic analysis of vehicle platoon arrivals. The delay obtained was compared with delay obtained by three conventional methods: The Webster method, May's continuum model method and the 1985 HCM method. The three conventional produced same results for v/c up to 0.75. For v/c from 0.75 to 1.0, Webster and HCM methods resulted in high values of delay than May's method (James M.S. and Herbert S. L., 1985).

In 1988 Akçelik, in Australia, further developed the delay equation by utilizing the coordinate transformation technique to obtain a time-dependent equation that is applicable to signalized intersections. A generalized delay equation was developed that embraces the Australian and Canadian delay formulas (Akcelik, R., 1988).

In 1990 Olszewski, computed delay for a pre-timed signal when the arrival rate is non-uniform by utilizing the step arrival rate model. A significant finding of his research was that the progression affects the uniform delay term and not the overflow delay term in the HCM delay equation (Olszewski, P., 1990).

In 2000 in USA the Highway Capacity Manual (HCM) time-dependent delay equation is utilized in delay computations. The HCM 2000 propounds that delay be computed using the equations (1) to (3):

$$d = d_1 PF + d_2 + d_3 \quad (1)$$

$$d_1 = \left(\frac{C}{2}\right) * \{ \frac{(1-g/C)^2}{1-[min(1,X)*\frac{g}{C}]} \quad (2)$$

$$d_2 = 900T\,[(x-1) + \sqrt{(x-1)^2 + \left(\frac{8kIx}{cT}\right)}] \quad (3)$$

Where:

d = Control delay (s/veh),
d_1= Uniform delay component (s/veh),
PF = Progression adjustment factor,
d_2= Incremental delay component (s/veh),
d_3= Delay due to pre-existing queue (s/veh),
T = Analysis period (h),
X = Volume to capacity ratio for lane group (v/c),
C = Cycle length (sec),
k = Incremental delay factor for actuated controller settings; 0.50 for pre-timed controllers,
I = Upstream filtering/metering adjustment factor; 1.0 for individual intersection analyses,
c = Capacity of lane group (veh/h), and
g = Effective green tme for lane group (sec).

In 1995 the Australian Capacity Guide developed a time-dependent delay equation for the estimation of delay at traffic signals using equations (4) to (6):

$$d = d_1 + d_2 \quad (4)$$

$$d_1 = \frac{0.5*C\,(1-g/C)^2}{1-[min(1,X)*\frac{g}{C}]} \quad (5)$$

$$d_2 = 900.T. \left[(x-1) + \sqrt{(x-1)^2 + \frac{m.(x-x_0)}{c.T}}\right] \quad (6)$$

Where:

$$X_0 = 0.67 + \left(\frac{sg}{600}\right);$$

m =12 by assuming the uniform arrivals case;
T = analysis period, h;
x = degree of saturation, v/c ;
c = capacity, veh/h;
s = saturation flow rate, veh/sg, (vehs per second of green); and
g = effective green time, sec.
C = cycle length (sec).

In 1995 the Canadian Capacity Guide developed a time-dependent delay equation

for estimation of delay at traffic signals using equations (7) to (9):

$$d = d_1 . k_f + d_2 \quad (7)$$

$$d_1 = \frac{0.5 * C\,(1-g/C)^2}{1-[min(1,X)*\frac{g}{C}]} \quad (8)$$

$$d_2 = 15.T.\left[(x-1)+\sqrt{(x-1)^2+\frac{240.x}{c.T}}\right] \quad (9)$$

Where:

T = analysis period, h;
x = degree of saturation, v/c ;
c = capacity, veh/h;
k_f = progression adjustment factor;
g = effective green time, sec; and
C = cycle length (sec).

In 2006 Francesco Viti, in Delft city in Netherland, describes the progress made in the modelling of queues and delays at traffic signals and discusses the limitations of these models in describing the stochastic and dynamic behavior of these service systems. Starting from a well-established theory in operations research, the renewal theory of Markov Chains, which has been applied in the past to investigate and analyze the dynamic behavior of overflow queues at fixed time signals, he developed and integrated within this modelling framework a probabilistic formulation also for the queue behavior within each cycle. This model enables one to deal with queues using a continuous time approach, and it describes the effect of the variability of the arrivals in the service time process, which reflects into the variability of the delay caused by the signal operation. The flexibility of this modeling framework allows its application in more sophisticated service systems (Francesco Viti, 2006).

In 2006 Fang Zhao and Zhen Ding in Florida, developed intersection delay models to estimate highway and transit travel times. The objectives to be achieved in this research include; evaluating the appropriateness of different traffic engineering software for the purpose of determining intersection delays under different combinations of traffic conditions and intersection geometry, and developing models that are capable of predicting intersection delays based on traffic conditions and simplified intersection geometry (Frang Zhao, and Zhen Ding, 2006).

It can be drawn from the reviewed literature, that the delay is affected by a number of physical and operational features of the intersection. The intersection delay may be related to other factors seems to be site specific, or at least local in nature. The driver behavior is one of the mentioned above factors. The methods currently used in calculation of delay at intersection either ignore the way in which delays vary with time (which is useless in saturated conditions) or cope with variation using mathematical applications of common sense than mathematical models of traffic signal systems. To obtain accurate results better information about traffic patterns is needed.

The main objective of this study is to compute the time-dependent delay at actuated traffic signals by using theoretical models given in different official transportation manuals and guides and also computing delay by field observation methods for different time periods, and then make comparisons between the result of each theoretical method and the result of the field method.

Finally, the most practical models were chosen for the estimation of time-dependent delay at actuated traffic signals in Duhok city using regression analysis technique.

2. METHODOLOGY

To achieve the objective of this study a methodology includes the methods and equations which had been used to obtain the necessary elements for the data analysis was followed.

2.1 Passenger Car Equivalent (PCE)

HCM 2000 tables had been used to find Passenger Car Equivalents for trucks and buses as it reports PCEs according to percent and length of grade and proportion of heavy vehicles.

The terrain in the studied segments is a combination of horizontal and vertical alignment permits heavy vehicles to maintain approximately the same speed as passenger cars. Therefore, the terrain is assumed to be

level terrain, and the value of PCE was selected as 1.5 for trucks and buses.

2.2 Link Speed

Moving vehicle method had been used to obtain average link travel speeds between intersections on the arterial streets. Also spot speed study at selected location in the mid-links were used to determine the Mid-Link spot speed using the stopwatch method, minimum necessary sample size of vehicles was usually obtained.

2.3 Traffic Volume

Traffic volume studies was conducted to determine the number, movements, and classification of roadway vehicles at study locations using Moving vehicle method to obtain link volume on arterial streets and video recording technique for the determination of intersection volumes at peak hours dividing the period of data collection into 5 minute intervals to obtain PHF.

2.4 Saturation Flow Rate

HCM2000 method was used for the determination of saturation flow rate which is used for the computation of both cycle time, capacity and traffic control delay for the signalized intersections.

2.5 Signal Timing

For the computation of delay at actuated traffic signals, the actuated signal timing was designed for each intersection. The average cycle length and effective green recommended by Highway Capacity Manual (HCM2000) was determined and used in this study.

2.6 Intersection Delay Estimations

Measurements of delays, stops, queue length etc. was done using video, and manual observations. Different theoretical and field methods for the estimation of vehicle delay at traffic signals was used.

2.6.1 Theoretical Delay

The HCM 2000, the Australian Capacity Guide (ARR 1995) and the Canadian Capacity Guide (ITE 1995) was used for the estimation of theoretical delay at studied intersections.

2.6.2 Field Delay

The travel time method is the most practical method for the determination of field delay because it accounts for the deceleration and acceleration delay times. In this study the travel time from a point in advance of the intersection to another point in or beyond the intersection was measured using the video recording technique. The travel time had been measured before the vehicle be influenced by presence of intersection and the other point at the place when the vehicle leaves the intersection and will not be influenced by presence of intersection again.

2.6.3 Time-Dependent Expressions for Field Delay

Simple regression analysis technique was used to establish different relationships between the field and the theoretical methods as it is the simplest relationship consists of a straight line.

The goal of using regression analysis is the development of statistical model that can be used to predict the value of the field (actual) delay in this research, based on the value of the theoretical delay. The models were obtained by using Statistical package for the social sciences (SPSS version 18) and Microsoft Office Excel (2007 Edition).

3. STUDY AREA AND DATA COLLECTION

The four important elements that should be considered when observing and collecting traffic data are site selection, measurement location, time of day for observation, and period of observation.

The study area selected for this study is Duhok City-Kurdistan Region-Iraq. The most important and congested arterial street in Duhok city is Barzani Street, therefore five successive intersections on this street was selected for this study as shown in Figures (1) to (6). Data collection was made by choosing different time periods from 7:30 AM to 7:30 PM according to the traffic activity in working days.

Data was collected on intersections and links geometry, approach counts, AM and PM peak hour counts, posted speed on all

links and approaches, percent of heavy vehicles, all the data required for field studies of travel time and approach delay, signal timing and phasing data was collected

The manual Method was used to collect the intersection geometry, signal timing, detectors measurements, approach speed and mid link spot speed. The moving vehicle method was used to collect the speed and volume data for the links between the studied intersections, while video camera technique was used to collect classified approach counts (AM and PM peak hour counts), travel time, approach delay and all other data. The video camera data was abstracted using a computer program named EVENT (Al-Neami, A.H.K., 1995).

Figure (1): Google image of Barzani street showing the Five studied intersecions (Directorate of Traffic, Traffic Engineering Department, Duhok City, 2009)

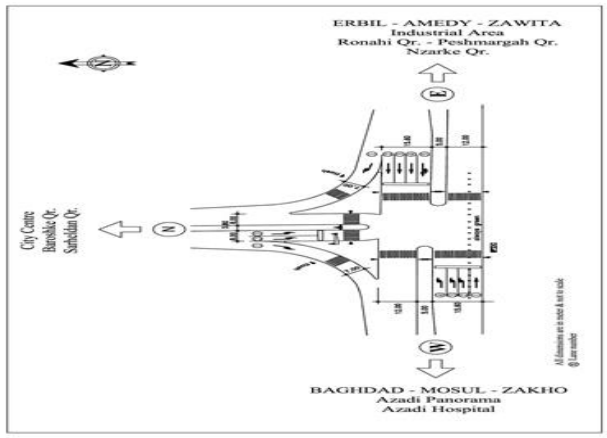

Figure (2): Peshmarga Intersection (P) Plan (Directorate of Traffic, Duhok City, 2009)

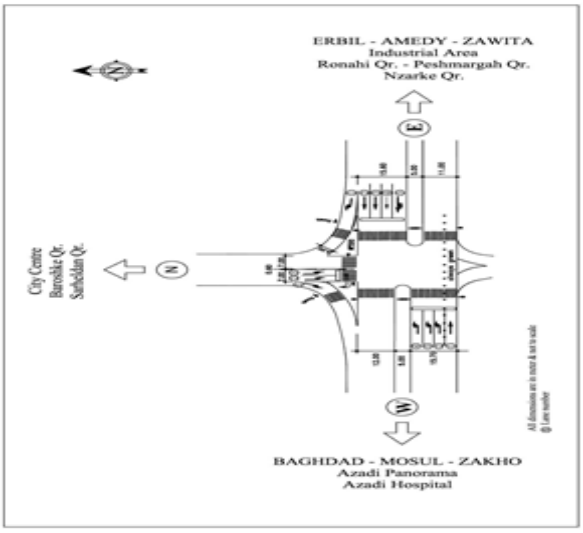

Figure (3): Sarsink Intersection (SRS) Plan (Directorate of Traffic, Duhok City, 2009)

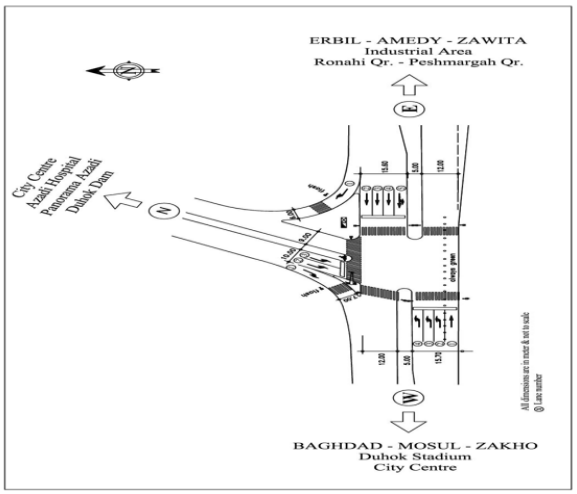

Figure (4): Silav Intersection (SIL) Plan (Directorate of Traffic, Duhok City, 2009)

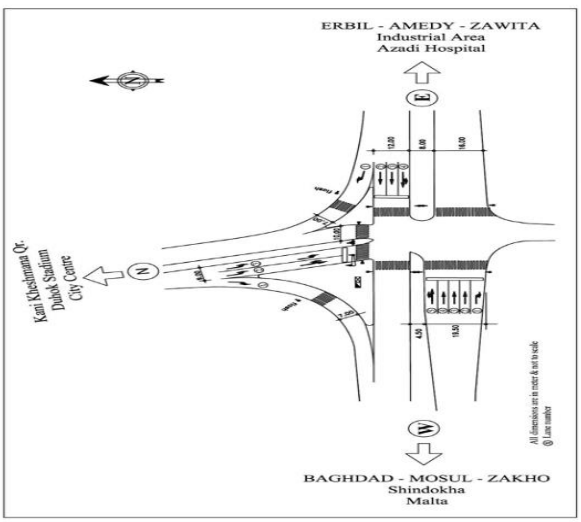

Figure (5): Raza Intersection (R) Plan (Directorate of Traffic Duhok City, 2009)

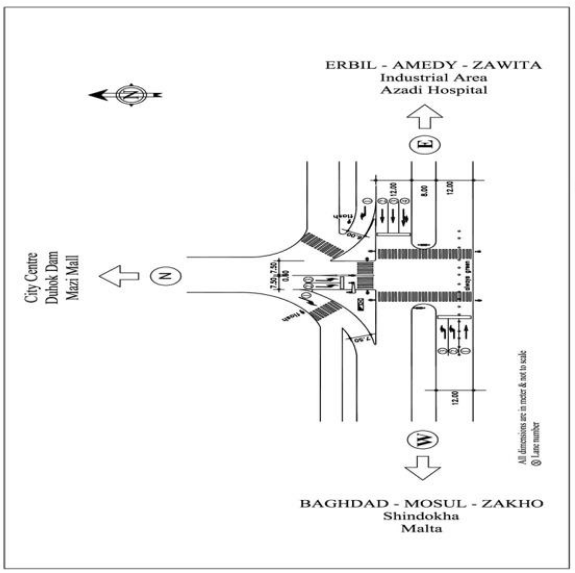

Figure (6): Sarok Intersection (SK) Plan (Directorate of Traffic, Duhok City, 2009)

4. DATA ANALYSIS

The collected data was analyzed for the determination of theoretical and field delays by using different official methods then developing time-dependent delay models for signalized intersections in Duhok City. Finally, the most practical models were chosen to use for the estimation of time-dependent delay at actuated traffic signals in Duhok city.

4.1 Link Volume and Speed

The volume and speed of each link between the intersections were counted as shown in Table (1).

Table (1): Link Speed and Volume Data on Barzani Street

Link	Link length (m)	Travel speed (km/h)	Running speed (km/h)	Mid-Link Spot Speed			Volume (vph)	Directional Distribution %
				Sample size (N)	Mean (km/h)	S.D		
P-SRS	1225	44.18	49.92	106	64.9	10.89	2492	49.90
SRS-P	1225	41.26	45.72	116	76.8	11.04	2502	50.10
SRS-SIL	1050	35.46	44.80	116	71.7	10.65	3125	50.80
SIL-SRS	1050	38.10	44.27	111	62.2	10.10	3019	49.20
SIL-R	305	13.76	28.75	105	48.4	9.33	2913	49.00
R-SIL	305	27.61	27.61	101	64.7	11.65	3024	51.00
R-SK	1100	42.20	47.96	109	78.2	11.24	2747	49.60
SK-R	1100	28.43	43.72	104	77.7	11.63	2782	50.40

4.2 Intersection Volume and Signal Timing Plan

The volume of each approach in all intersections was counted and recorded for each 15-minute interval in the peak hour. The volumes and PHF are shown in Table (2).

Table (2): Traffic Volumes, Saturation Flow Rate, Degree of Saturation and Capacity for Studied Intersections (pcph)

Intersection	Direction	Peak Hour Volume (pcph)	PHF (5 min)	Heavy Vehicle %	Degree of Saturation	Capacity (pcph)	Saturation Flow Rate(pcphg)
Peshmargah	East	2459	0.923	6.20	0.983	2502	1614
	West	1056	0.752	2.34	0.741	1424	1597
	North	504	0.841	1.94	0.684	737	1574
Sarsink	East	3191	0.844	6.91	1.091	2925	1615
	West	468	0.714	0	0.272	1720	1650
	North	60	0.433	0	0.194	309	1468
Silav	East	2592	0.797	7.90	1.237	2096	1438
	West	948	0.706	10.1	0.774	1225	1460
	North	1020	0.748	5.8	1.067	956	1708
Raza	East	2279	0.806	6.67	1.341	1700	1568
	West	2099	0.674	7.4	1.212	1733	1321
	North	1007	0.72	0	1.226	822	1746
Sarok	East	1956	0.915	9.01	1.047	1868	1607
	West	528	0.684	9.38	0.396	1332	1494
	North	540	0.733	5.14	0.775	697	1488

For the computation of delay at actuated traffic signals, the average cycle length and effective green must be used as recommended by Highway Capacity Manual (HCM2000). Therefore, the average cycle length and effective green are determined in field during peak hour period as shown in Table (3).

Table (3): Signal Timing plan for Studied Intersections

Int.	Direction	Average Cycle Length	Unit Extention	Yellow	All Red	Green Time		Average Effective Green
						Max.	Min.	
P	East	111	3	4	2	40	10	43
	West		3	4	2	30	10	33
	North		3	4	2	23	7	26
SRS	East	95	3	4	2	40	10	43
	West		3	4	2	30	10	33
	North		3	4	2	15	7	10
SIL	East	118	3	4	2	40	10	43
	West		3	4	2	30	10	33
	North		3	4	2	30	10	33
R	East	119	3	4	2	40	10	43
	West		3	4	2	36	10	39
	North		3	4	2	25	10	28
SK	East	111	3	4	2	40	10	43
	West		3	4	2	30	10	33
	North		3	4	2	23	8	26

4.3 Saturation Flow Rate and Approach Capacity

The saturation flow rate for each approach is computed and the results of all approaches are shown in Table (2).

The capacity of each approach is estimated by multiplying the saturation flow by effective green to cycle length ratio. All results are shown in Table (2).

4.4 Degree of Saturation (X)

The degree of saturation which is represented by volume to capacity ratio for each approach is computed for the peak hour as a whole, and also for each 15 minutes in peak hour separately as it's shown in Table (2) for all studied intersections.

4.5 Delay Calculations

4.5.1 Theoretical Delay Calculations

The delay for each approach are estimated using different time-dependent equations which are recommended by most frequently used manuals which are the American Highway Capacity Manual (TRB 2000), the Australian Capacity Guide (ARR 1995) and the Canadian Capacity Guide (ITE 1995).

4.5.1.1 Highway Capacity Manual (HCM 2000)

In the field analysis it can be noted that there is not large variability in arrival type in each cycle in peak hour period and its around between AT2 and AT4, therefore its assumed to be AT3 in this study as its recommended by HCM 2000 for non-coordinated traffic signals, and the value of PF will be equal to unity.

The incremental delay calibration factor (k) is determined from HCM2000 for all approaches of each intersection. The incremental delay adjustment factor (I) incorporates the effects of metering arrivals from upstream signals. For a signal analysis of an isolated intersection, the value of I is equal to unity as it is recommended by HCM2000.

The control delay was estimated for each 15 minutes' interval and also for the peak hour as a whole. All results are shown in Figure (7) for all approaches in each intersection.

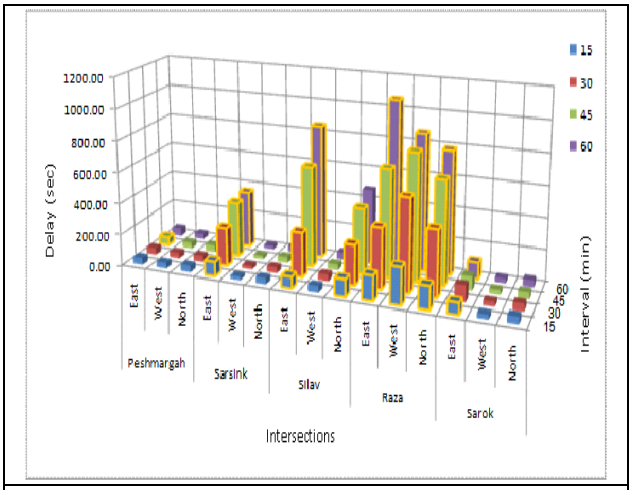

Figure (7): Approach Control Delay for All Intersections Using HCM

Note: The oversaturated intervals have yellow color in Scatter diagrams and also yellow border lines at its corners in the Histograms to be recognized from under-saturated intervals.

4.5.1.2 The Australian Capacity Guide (ARR 1995)

The Australian Capacity Guide does not consider a delay due to a positive initial queue and has the same expression for the uniform delay component d_1, but it does not consider the progression factor. The delay had been estimated for all approaches using equations of this manual. All results are shown in Figure (8) for all approaches in each intersection.

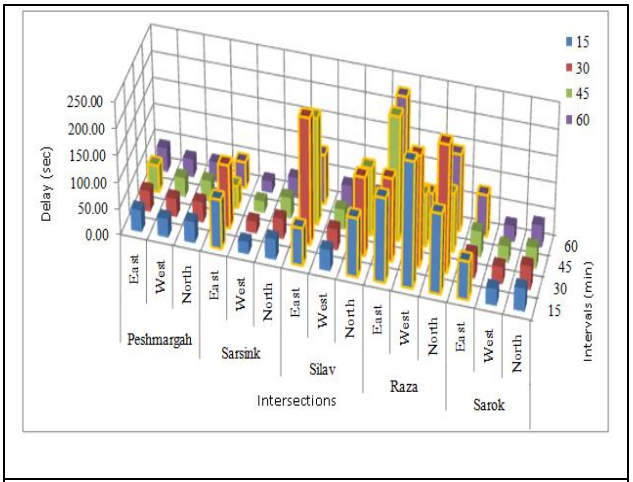

Figure (8): Approach Control Delay for All Intersections Using ARR

4.5.1.3 The Canadian Capacity Guide (ITE 1995)

Similarly, to the Australian Guide, the Canadian Capacity Guide considers only uniform and incremental delay components,

while no initial queue delay is present. Therefore, it does not consider the delay due to a positive initial queue. The delay had been estimated for all approaches using equations that are recommended by this method. Results are shown in Figure (9) for all approaches in each intersection.

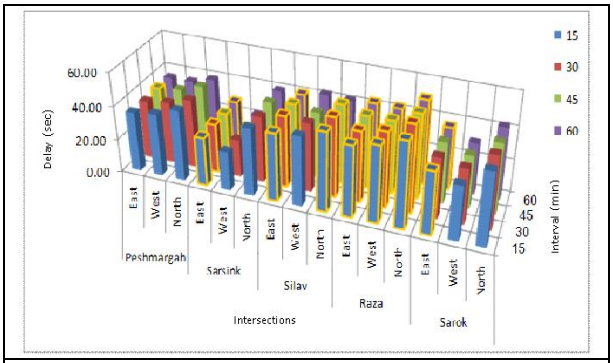

Figure (9): Approach Control Delay for All Intersections Using ITE

4.5.1.4 Field Computation of Intersection Delay

Travel times then the vehicles are crossing the intersection by free flow speed is shown in Table (4). The field measured delays in all approaches for each 15-minutes interval and for peak hour as a whole are shown in Figure (10) for all approaches in each intersection.

Table (4): Travel Times When the Vehicles are crossing the Intersection by Free Flow Speed

Intersection	Travel Time (sec)		
	East	West	North
Peshmargah	9.41	16.00	8.26
Sarsink	11.44	8.27	7.57
Silav	10.22	20.47	13.10
Raza	18.12	10.90	11.40
Sarok	5.30	14.90	6.45

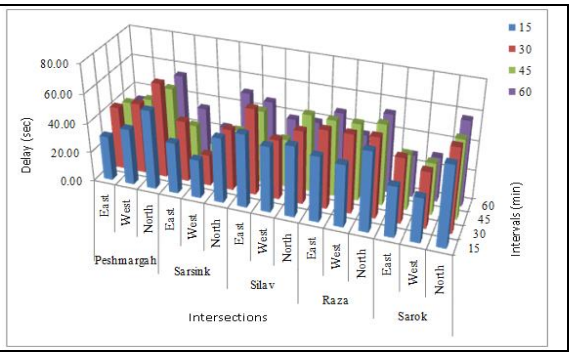

Figure (10): Field Approach Control Delay for All Intersections

4.6 Comparison Between Field Delay and Theoretical Delay

The comparison between field and theoretically computed delay using HCM2000, ARR1995 and ITE1995 manuals and also between the manuals themselves was made for one-hour design period as shown in Figure (11). Also to show the effect of the existence of initial queue at the beginning of analysis period the weighted average delay was taken between the four 15-minute intervals in the peak hour for each leg of each intersection as shown in Figure (12). All results are lower, except of the HCM value which is very higher in oversaturated cases because there is initial queue at the beginning of three intervals of these cases and the d_3 will have high value.

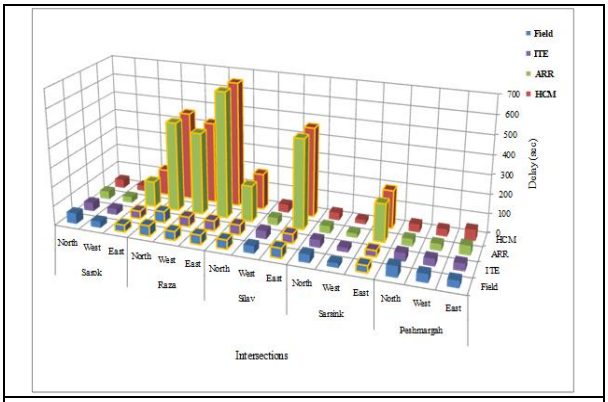

Figure (11): Comparison between Different Delays for One Hour Analysis Period

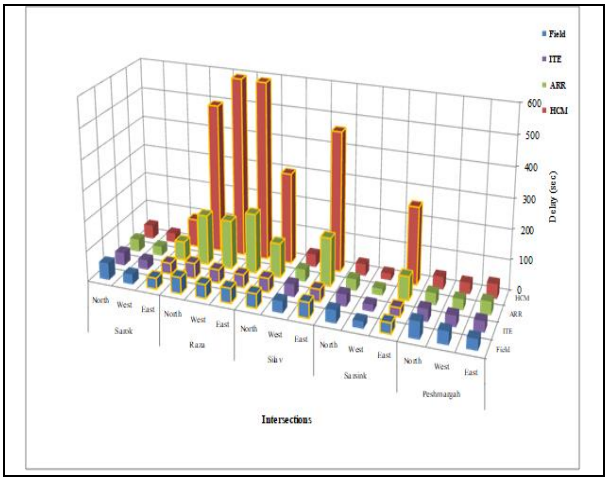

Figure (12): Comparison between Different Delays for Weighted Average Delay of four 15-Minute periods

4.6.1 HCM Method

Generally, in case of under-saturation conditions, or where the demand to capacity ratio (v/c) is smaller than 1.0 (X < 1.0), the field results of delay measurement are relatively close to that obtained theoretically from time-dependent equation in HCM2000. In such conditions the value of incremental delay (d_2) is very small because it is mainly depending on the degree of saturation value (X). The value of initial queue delay is zero in most cases of this condition because; usually there is no initial queue.

When the demand exceeds capacity, the condition changes to oversaturated (X > 1.0), the value of field measured delay will be very small compared to the theoretically estimated results, because the incremental delay (d_2) become very large due to the large value of degree of saturation. Also the initial queue delay (d_3) become very large, especially in last half of peak hour period due to the existence of initial queue and cumulative of this queue in last one or two analysis periods.

4.6.2 ARR 1995 Method

Generally, the field measured results are close to that obtained from Au
stralian Capacity Guide (ARR, 1995) when the demand is smaller than the capacity (X < 1.0). The ARR equation consist of two terms which are uniform delay term (d_1) and incremental delay term (d_2), and in case of under-saturated conditions the last term of equation have a small value when demand is near to the capacity (0.85 < X < 1.0), and negligible value when the demand is under 85 percent of capacity. The delay estimated using ARR1995 equation is very close to that estimated using HCM2000 equation in case of under-saturated conditions.

In the cases of oversaturated conditions, the ARR equation`s results are substantially overestimated field-measured values of delay, but not to the extent of HCM equation`s, because it is not including the initial queue delay term which cause extra overestimation of delay.

4.6.3 ITE 1995 Method

In general form, the field measured delay results are very close to that obtained from the Canadian capacity Guide (ITE, 1995) in all traffic conditions or when the demand is smaller, equal or higher than capacity (X ≤ 1.0, or X > 1.0).The Canadian Capacity Guide delay results are relatively close to that of Highway Capacity Manual and Australian Capacity Guide in under saturated cases only and it is very smaller in oversaturated cases, because the second term (d_2) of the ITE equation is not very sensitive to the degree of saturation.

4.7 Time-Dependent Expressions for Field Delay

Simple regression analysis technique was used to establish different relationships between the field and the theoretical methods. The simplest relationship consists of a straight line or linear relationship ($Y=B_o+B_1X$).

The goal of using regression analysis is the development of statistical models that can be used to predict the field (actual) delay based on the value of the theoretical delay, and also to select the best theoretical equation.

4.7.1 Field Delay with HCM Delay

The relationship had been determined between Field and HCM delay results using different forms of mathematical functions (linear, logarithmic, inverse, quadratic, and cubic), and then the best equation had been chosen which is the inverse form between Field and HCM. The scatter diagram and the best inverse fit is shown in Figure (13).

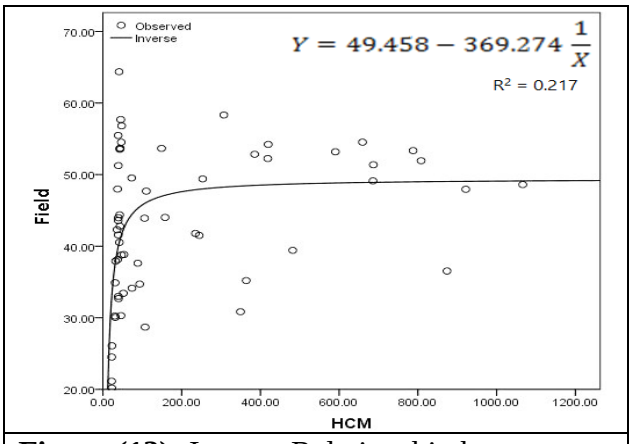

Figure (13): Inverse Relationship between

Field and HCM Delays **(sec/veh)**

The F-Test for the regression equation showed that the calculated F-Test value = 16.111 and the tabulated value at α = 0.05 and degree of freedom (df1= 1, df2=58) = 4.008. As the tabulated F-Test value is less than the calculated value for the same df1 and df2, this means that there is a statically significant Inverse relationship between the field delay and the theoretical (HCM) delay.

4.7.2 Field Delay with ARR Delay

The relationship had been determined between Field and ARR delay results using different forms of mathematical functions (linear, logarithmic, inverse, quadratic, and cubic), and then the best equation had been chosen which is the inverse form between Field and ARR. The scatter diagram and the best fit is shown in Figure (14).

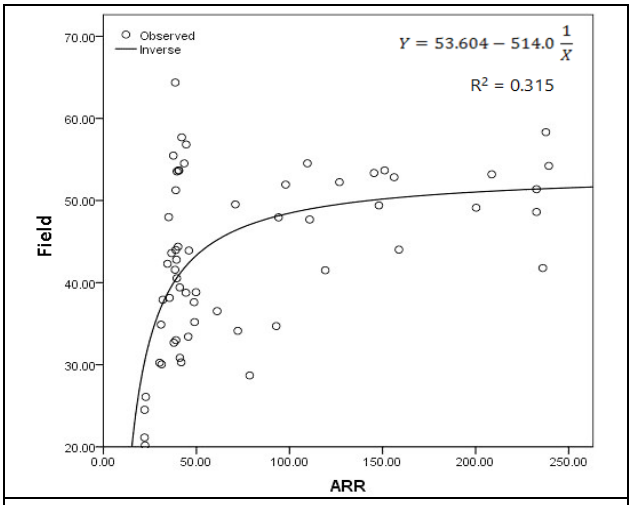

Figure (14): Inverse Relationship between Field and ARR

The F-Test for the regression equation showed that the calculated F-Test value = 26.708 and the tabulated value at α = 0.05 and degree of freedom (df1= 1, df2=58) = 4.008. As the tabulated F-Test value is less than the calculated value for the same df1 and df2, this means that there is a statically significant Inverse relationship between the field delay and the theoretical (ARR) delay.

4.7.3 Field Delay with ITE Delay

The relationship had been determined between Field and ITE delay results using different forms of mathematical functions (linear, logarithmic, inverse, quadratic, and cubic), and then the best equation had been chosen which is the logarithmic form between Field and ITE, see Figure (15).

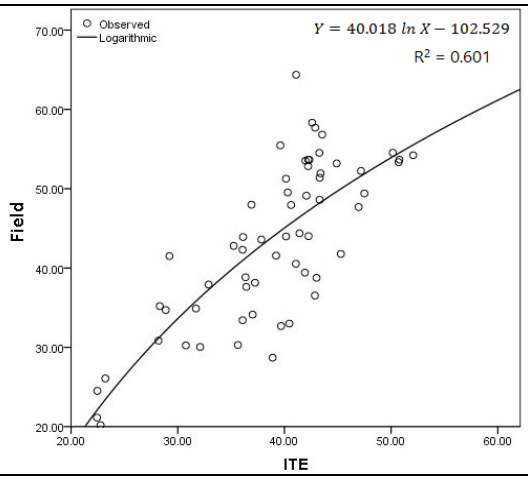

Figure (15): Logarithmic Relationship between Field and ITE

The F-Test for the regression equation showed that the calculated F-Test value = 89.644 and the tabulated value at α = 0.05 and degree of freedom (df1= 1, df2=58) = 4.008. As the tabulated F-Test value is less than the calculated value for the same df1 and df2, this means that there is a statically significant logarithmic relationship between the field delay and the theoretical (ITE) delay.

5. Conclusions

Based on the results of this study, it can be concluded that:

1. The range of intersection control delay was between (22.98) sec/veh on West approach of Sarsink Intersection and (56.79) sec/veh on North approach of Peshmargah Intersection, when the delay observed in field.
2. The range of intersection control delay was between (22.46) sec/veh on West approach of Sarsink Intersection and (594.80) sec/veh on West approach of Raza Intersection, when the delay computed by HCM equation.
3. The range of intersection control delay was between (22.38) sec/veh on West approach of Sarsink Intersection and (197.48) sec/veh on East approach of Raza

Intersection, when the delay computed by ARR equation.

4. The range of intersection control delay was between (22.75) sec/veh on West approach of Sarsink Intersection and (50.99) sec/veh on North approach of Raza Intersection, when the delay computed by ITE equation.
5. HCM has good delay results with respect to Field observed delay in under-saturated conditions but it has extra overestimate delay in oversaturation conditions.
6. ARR has good delay results with respect to Field observed delay in under-saturated conditions but it has overestimate delay in oversaturation conditions.
7. ITE has good delay results with respect to Field observed delay in under-saturated and oversaturation conditions too.
8. There was a good relationship between field measured delay and the control delay estimated by ITE equation, with (R^2=0.601) in case of logarithmic relationship.
9. There was a statically significant but relatively weak relationship between field measured delay and the control delay estimated by ARR equation, with (R^2_{adj}=0.303) in case of inverse relationship.
10. There was a statically significant but relatively very weak relationship between field measured delay and the control delay estimated by ARR equation, with (R^2_{adj}=0.204) in case of inverse relationship.

6. Recommendations

1. Due to high delay values on most approaches, there is a need to apply coordinated traffic signals for all the studied intersections in order to reduce delay, hence, reducing fuel consumption and vehicle emission.
2. HCM, ARR and ITE may be used to estimate delay for under saturated conditions because they have good delay results with respect to field observed delay.
3. The ITE may be used for the delay estimation for over saturated conditions as it has good delay results with respect to field observed delay.
4. The obtained regression equations between Field and ITE delay could be used for the prediction of field delay.

7. Further Research

Further studies on intersection delay is required for Duhok city street networks after signal coordination using ITE delay model.

Acknowledgements

As this paper is part of an MSc thesis submitted to college of engineering-Salahaddin University-Erbil, the authors acknowledge the civil department staff for their support and help during the study.

References

Transportation Research Board (TRB), "Highway Capacity Manual (HCM)", National Research Council, Washington. D. C. 2000.

The Australian Road Research Board (ARRB) Transport Research, "Australian capacity guide" 1995.

The Institute of Transportation Engineers (ITE),"Canadian capacity guide" 1995.

Francesco Viti, "The Dynamics and the Uncertainty of Delays at Signals", Ph.D. thesis, submitted to the Delft University of Technology, 2006

Webster F. V. "Traffic Signal Settings", Road Research Laboratory, Technical Paper No. 39, HMSO, London, U.K. 1958.

Gandhi Ganem Sofia, "Development of Traffic Flow Models at Networks In Mosul City", Ph.D. thesis, submitted to the College of Engineering, University of Baghdad, 1998.

Catling, "A Time-Dependent Approach to Junction Delays" traffic Engineering and Controls, Nov. 1977

Reilly R. and Gardner C. "Technique for measuring delay at instructions" Transportation Research Record, 644, 1977, pp. 1-7.

Kimber, RM and Erica M. Hollis, "Traffic Queues and Delays at Road Junctions" , Department of the Environmental and Department of the Transport,TRRL

Report LR 909. Growthorne, U.K.,1979

James M.S. and Herbert S. L., "signal Delay with Platoon Arrivals", Transportation Research Record, 1005, 1985, pp. 28-37.

Akcelik, R., "The Hoghway Capacity Manual Delay Formula for Signalized Intersections", ITE Journal, March 1988, pp 23-27

Olszewski, P., "Traffic Signal Delay Model for Non-Uniform Arrivals", Transportation Research Record 1287, TRB, National Research Council, Washington, D.C., 1990, pp. 42-53.

Frang Zhao, and Zhen Ding, "Improving Highway Travel Time Estimation in FSUTMS by Considering Intersection Delays", Department of Civil and Environmental Engineering , College of Engineering and Computing, Florida International University, August 2006.